

Battery Energy Storage System for Renewable Energy Integrated Power System Stability Enhancement

by

Ujjwal Datta

B.Sc., M.Sc.

A Dissertation Submitted in Fulfillment of the
Requirements for the Degree of

DOCTOR OF PHILOSOPHY

in the Institute for Sustainable Industries and Liveable Cities (ISILC)

College of Engineering and Science
Victoria University, Melbourne, Australia



© Ujjwal Datta, "2020" All rights reserved. Reproduction in whole or in part
requires the permission of the author.

ABSTRACT

With growing environmental concerns and sustainability movements, renewable energy source (RES) penetration is increasing and expected to have a steady growth in the coming years. Power systems have encountered several inherent technical challenges, resulting from either low inertia contribution by the increased RES or the displacement of fossil fuel generation systems within the network. The decreased system inertia and the decline in power reserve capacity are affecting the dynamic and transient stability performance of the power system adversely and this adverse impact will continue to increase due to further RES penetration in electric power systems.

In this context, this thesis contributes new knowledge to the modelling of droop controlled BESS for enhancing damping capability and transient stability of large-scale power networks with different level of RES penetration. The BESS with conventional Proportional Integral (PI), and two new PI-lead and lead-lag controlled BESS with coordinated charge control are given wider attention. In the initial stage, a wind farm is designed to perform frequency control in a microgrid. A sectional droop gain method is adopted for regulating doubly fed induction generation (DFIG) power output. It is observed that the proposed multi-gain droop control method demonstrates superior performance than the conventional approach. However, DFIG has a certain limit of providing under-frequency support as a result of inherent incapability of regulating incoming wind speed. Hence, a more reliable energy source is required to secure the stability of the system.

Realizing these facts, comprehensive simulation studies have been carried out to explore various RES penetration level and dynamic response capability of the system undergoing multiple contingencies. Simulation results demonstrate that generator control and system loading conditions have significant impact on damping capability in primary frequency control. However, results with active power regulated BESS exhibit its effectiveness in enhancing primary frequency controllability of the system regardless of generator control and system loading conditions in power grid as RES penetration increases. Furthermore, a new state of charge (SOC) adaptive charging strategy is

proposed for recovering battery SOC to ensure BESS reliability against future contingencies. The new adaptive SOC strategy defines separate levels of SOC charging limit than that of the maximum SOC limit to ensure sufficient SOC excursion for over-frequency events.

In the next stage, a droop controlled BESS is modelled and investigated to control simultaneous voltage and frequency responses of the system by regulating its active and reactive power independently. The performance of BESS is compared with the state-of-the-art technology Static Compensator (STATCOM), while the system is exporting a large amount of power across the network under various contingency studies. It is shown via simulation studies that STATCOM fails to secure voltage and frequency stability of the system in the occurrence of a single or multiple adjacent faults. On the contrary, the incorporated BESS with active and reactive regulating capability remains successful in maintaining the stability of the power system. Also, lead-lag controlled BESS has demonstrated improved performance than PI and PI-lead controlled BESS.

In the final stage of research, the effectiveness of BESS in a charging station is explored to avoid transformer overloading, provide PV smoothing and to increase the charging capacity of the station. Simulation studies showed that BESS can effectively reduce transformer overloading and as a result it prolongs its lifespan and provide grid services when charging station has no load demand.

DECLARATION OF AUTHENTICITY

I, Ujjwal Datta, declare that the PhD thesis title as "Battery Energy Storage System for Renewable Energy Integrated Power System Stability Enhancement" is no more than 100000 words excluding tables, figures, appendix, footnotes and references. The contents of this thesis, in whole or part, have not been submitted previously for the award of any other academic degree or diploma. Except otherwise mentioned, this thesis is my own work.

UJJWAL DATTA

DATE

ACKNOWLEDGMENTS

I would like to thank Professor Akhtar Kalam and Co-Supervisor Associate Professor Juan Shi for their immense support during my doctoral studies in terms of technical advices, constructive feedbacks and suggestions on this thesis and publications which helped me not only to complete the PhD degree but also to become a good researcher.

I delightedly acknowledge the continuous financial assistance of Victoria University Research Training Program during my doctoral studies. I would also like to thank Graduate Research Office and the Institute of Sustainable Industries and Liveable Cities (ISILC) for processing and supporting me financially to attend the conferences, seminar and paying article processing charges.

I would also like to thank OPAL-RT for the real time simulator OP5600 and associated on-campus trainings and technical support to carry out a part of the research work.

DEDICATION

To my beloved parents, elder brother, sister-in-law and my dear wife, Mousumi Nath,
for their support, encouragement and love.

Contents

Abstract	ii
Declaration of Authenticity	iv
Acknowledgments	v
Table of Contents	vii
List of Figures	xiii
List of Tables	xx
List of Acronyms	xxi
List of Nomenclatures	xxiii
List of Publications	xxviii
1 Introduction	1
1.1 Motivation	1
1.2 Objectives of the Thesis	3
1.3 Original Scientific Contribution	4
1.4 Thesis Outline	7
2 The Employment of BESS in Renewable Energy Integrated Power System	
- Literature Review	10
2.1 Introduction	10
2.2 Energy Storage Technologies	13
2.2.1 Storage Technologies-General Consideration	13

2.2.2	Operating Time Frame, Power and Energy Rating	14
2.3	BESS Technology and Batteries	14
2.3.1	BESS Connection Diagrams	15
2.3.2	Power Conversion System and Converter Technologies	17
2.3.3	Quantities for Battery SOC Calculation	19
2.3.4	Battery Types	21
2.3.4.1	Lead Acid	22
2.3.4.2	Lithium-Ion (Li-ion)	22
2.3.4.3	Sodium Sulfur	23
2.3.4.4	Nickel Cadmium	24
2.3.4.5	Nickel Metal Hydride	24
2.3.4.6	Zinc Hybrid Cathode	24
2.3.4.7	Vanadium Redox Battery (VRB)	25
2.3.4.8	Polysulphide Bromide	25
2.3.4.9	Zinc Bromine (ZnBr)	26
2.4	BESS Application in Renewable Energy System	27
2.4.1	Output Power Smoothing with BESS	27
2.4.2	Peak Generation/Load Shaving	30
2.4.3	Voltage Regulation	31
2.4.4	Frequency Regulation	33
2.4.5	Voltage and Frequency Regulation	35
2.4.6	PV/Wind Plant Dispatchability	36
2.4.7	Fault Ride Through (FRT)	38
2.4.8	Key Findings of BESS Application in PV-Wind-BESS Energy System	39
2.4.9	Key Challenges of BESS Application in PV-Wind-BESS Energy System	41
2.5	Shortcoming of Current Literature	43
2.6	Conclusion	44
3	Frequency regulation of an isolated MG with incorporated multi-gain droop and fuzzy regulated pitch angle control of DFIG	46

3.1	Introduction	46
3.2	Conventional Fixed Droop and Emulated Inertia Control Method	49
3.3	The Proposed Multi-gain Droop Control Method	52
3.4	Wind Energy Conversion System and Microgrid	55
3.4.1	Wind Turbine Modeling	55
3.4.2	The Control of Pitch Angle with Traditional PI	56
3.4.3	The Control of Pitch Angle with Fuzzy Logic	57
3.4.4	Depiction of the Studied Microgrid	60
3.5	Simulation Studies and Discussion	62
3.5.1	Footprint of Load Event on Frequency Performance	63
3.5.2	Alteration in Wind Speed and Frequency Response	65
3.5.3	The Impact of Wind Speed Below Rated Speed	67
3.5.4	Multiple DFIG for PFC in MG	70
3.5.5	The Influence of the Number of Fuzzy Membership Functions on Frequency Performance	74
3.6	Conclusion	77
4	The applicability of BESS in providing frequency control with the growth of wind energy penetration	79
4.1	Introduction	79
4.2	Wind Penetration and Primary Frequency Control	81
4.2.1	The Impact of Wind Penetration	81
4.2.2	Primary Frequency Control, Wind and BESS	82
4.3	The Detailed Modeling of BESS	84
4.3.1	Frequency Controller	85
4.3.2	Active Power (P) Controller	87
4.3.3	Battery Charge Controller	88
4.3.4	d-q Current Controller	89
4.3.5	Battery Model	90
4.3.6	Battery SOC Calculation	91
4.3.7	Charge/Discharge Cycle and Battery Lifetime	91
4.4	System Modeling and Case Studies	92

4.4.1	System Modeling	92
4.4.2	Case Studies	94
4.5	Result and analysis	94
4.5.1	Case-1: Wind Penetration with Single-phase-ground Fault	95
4.5.2	Case study-2: Temporary Outage of the Heavily Loaded Line	99
4.5.3	Case study-3: Load Growth Event at Load B	102
4.6	Conclusion	104
5	BESS for Reducing the Impact of PV penetration on Frequency Regulation and SOC Recovery	105
5.1	Introduction	105
5.2	Frequency Control with PV and NEM Grid Conditions for Frequency Stability	108
5.3	The Overall Modeling of BESS for Voltage and Frequency Control	110
5.3.1	Feedback Signals for BESS Regulation	110
5.3.1.1	Frequency Droop Controller	111
5.3.1.2	Voltage Droop Controller	112
5.3.1.3	PQ Controller with Lead-lag Controller	115
5.3.2	BESS Charge/Discharge Management	116
5.3.2.1	BESS With Droop-type Charging/Discharging	117
5.3.2.2	BESS Recharging with Maximum SOC	118
5.3.2.3	BESS Recharging with Adaptive SOC	119
5.3.3	Current Controller on d-q axis	120
5.4	Attributes of the Test System	120
5.4.1	Case Studies	121
5.5	Analysis of Transient Stability	122
5.5.1	Line outage with Operating Strategy 1 and 2	122
5.5.2	Load Reduction Event With Operating Strategy 1	125
5.5.3	BESS Installation Location and Converter Sizing	127
5.5.4	Battery Charging with the Proposed Approach	128
5.5.5	The Comparative Advantages of the Proposed Adaptive SOC Method	130

5.6	Conclusion	132
6	The application of BESS in Stabilizing Simultaneous Voltage and Frequency in a Transmission Network and Enhancing Power Transfer Capacity	134
6.1	Introduction	134
6.2	BESS Layout	138
6.2.1	Active/Reactive (PQ) Controller	138
6.2.1.1	PI-lead Controller	139
6.3	Studied System and Stability Criterion	140
6.3.1	System Description	140
6.3.2	STATCOM and Wind Model	142
6.3.3	Stability Criterion	143
6.4	Results and Analysis	144
6.4.1	Case 1: Permanent line outage of N-Sirttoverkko line	145
6.4.2	Case 2: Load growth and Permanent line outage of N-Sirttoverkko line	150
6.4.3	Case 3: Permanent line outage of N-Sirttoverkko line and load growth	152
6.4.4	The Performance of BESS in Other Circumstances	154
6.4.4.1	Case 4: Momentary Single-phase-to-ground Fault	155
6.4.4.2	Case 5: Permanent Single-phase-to-ground Fault	156
6.4.4.3	Case 6: Without Series Capacitors Between Two Systems	156
6.4.5	The Study of Performance Index	157
6.5	Conclusion	158
7	Coordinated control of PV and BESS in a smart EVCS for reducing the overloading of grid connecting transformer, PV smoothing and V2G	160
7.1	Introduction	160
7.2	Studied EV Charging Station	163
7.3	BESS Modeling at EVCS	165
7.3.1	Reference Power Generator $P_{BESS-ref}$	165

7.3.2	Active Power (P) Regulator	166
7.3.3	BESS Charge Controller and Current Controller	167
7.4	BESS Control in PV Combined EVCS	168
7.4.1	Control of BESS Scaling Down of Transformer Overloading	168
7.4.2	PV Output Smoothing and Transformer Overloading Reduction	169
7.4.3	The Integrated Control for B2G and Battery Recharging	171
7.4.4	Determining BESS (kW) and Transformer (kVA) Capacity	173
7.5	Results and Analysis	173
7.5.1	Reducing Transformer Loading with BESS and without PV	174
7.5.2	Integrated Control of PV & BESS to Reduce Transformer Loading and PV Smoothing	176
7.5.3	BESS for B2G Service	178
7.5.4	Battery Recharging without Violating Transformer Capacity	179
7.6	Conclusion	180
8	General Conclusions and Future Research Works	182
8.1	General Conclusions	182
8.2	Future Research Works	185
	Appendix	188
	References	191

List of Figures

Figure 1.1	Complete thesis outline	7
Figure 2.1	Typical BESS applications in renewable energy integrated system	12
Figure 2.2	Energy storage technologies capability- operating time frame . .	14
Figure 2.3	Typical BESS connection in a PV-BESS energy system; (a) PV/BESS connection through an individual converter (b) BESS connection using common DC side through DC/DC converter (c) Direct BESS connection on the DC side	16
Figure 2.4	Typical BESS connection in a wind-BESS energy system; (a) BESS through DC/AC converter (b) BESS through DC/DC and DC/AC converter (c) BESS connection on the dc side with wind turbine DC/DC	16
Figure 2.5	Typical BESS connection in a PV-wind-BESS energy system; (a) Connected to a common DC bus (b) Connected to a common AC bus	17
Figure 2.6	Various operation modes of BESS	18
Figure 2.7	Components of a lead-acid battery [21], Licensed under CC BY 4.0	22
Figure 2.8	Components of a Li-ion battery [21], Licensed under CC BY 4.0	23
Figure 2.9	Components of a Sodium Sulfur battery [21], Licensed under CC BY 4.0	23
Figure 2.10	Components of a Nickel Cadmium battery [21], Licensed under CC BY 4.0	24
Figure 2.11	Components of a Nickel Metal Hydride battery [21], Licensed under CC BY 4.0	25

Figure 2.12	Components of a Zinc Hybrid battery. Reprinted from [83] with permission from Elsevier	25
Figure 2.13	Components of a VRB battery [21], Licensed under CC BY 4.0	26
Figure 2.14	Components of a Polysulphide Bromide battery. Reprinted from [87] with permission from Elsevier	26
Figure 2.15	Components of a ZnBr battery [21], Licensed under CC BY 4.0 .	27
Figure 2.16	PV output smoothing with BESS	29
Figure 2.17	PV peak generation shaving with BESS	31
Figure 2.18	Voltage regulation with BESS in a PV integrated system	32
Figure 2.19	Voltage and frequency regulation with BESS in a wind integrated 9-bus system; (a) PCC voltage (b) Generator speed (c) BESS active/reactive power	36
Figure 2.20	Dispatched PV power with BESS	37
Figure 3.1	European Network of Transmission System Operators for Electricity (ENTSO-E) defined frequency stages [196]	50
Figure 3.2	The Combined emulated inertia and Fixed Droop Control [197] .	51
Figure 3.3	The Proposed Multi-gain Droop Control Strategy	53
Figure 3.4	DFIG power response for conventional and proposed methods with the selected parameters [197]	55
Figure 3.5	Conventional PI based pitch angle control [197]	57
Figure 3.6	FLC based pitch angle control [197]	58
Figure 3.7	FLC membership function for (a) the error of rotor speed (b) the integration of rotor speed error (c) pitch angle reference at FLC output [197]	59
Figure 3.8	The implementation of the proposed approach in Simulink [197]	61
Figure 3.9	The simple Microgrid with integrated wind farm [197]	62
Figure 3.10	The frequency response of synchronous generator [197]	63
Figure 3.11	The variation in DFIG rotor speed [197]	64
Figure 3.12	DFIG pitch angle responses with various control methods [197] .	65
Figure 3.13	The DFIG power output [197]	65
Figure 3.14	The frequency response of generator [197]	66

Figure 3.15	The variation in DFIG rotor speed [197]	67
Figure 3.16	The pitch angle responses with changing wind speed [197] . . .	67
Figure 3.17	Wind farm power output [197]	67
Figure 3.18	The frequency response with various power margin [197]	68
Figure 3.19	The control of power margin for varying wind speed value [197]	69
Figure 3.20	The frequency response with multiple power margin [197] . . .	69
Figure 3.21	The network diagram with multiple DFIGs [197]	70
Figure 3.22	The frequency response with multiple DFIGs in MG [197] . . .	71
Figure 3.23	DFIG rotor speed of both Wind Farm A (a) and Wind Farm B (b) [197]	72
Figure 3.24	DFIG pitch angle output of both wind farms [197]	73
Figure 3.25	Active power output of Wind Farm A (a) and Wind Farm B [197]	73
Figure 3.26	Inputs (a) output (b) with 5 FLC membership functions [197] . .	75
Figure 3.27	The frequency outcome with different fuzzy membership functions [197]	76
Figure 3.28	DFIG pitch angle under various fuzzy membership functions [197]	76
Figure 3.29	DFIG rotor speed under various fuzzy membership functions [197]	76
Figure 4.1	The block diagram of frequency control with BESS	83
Figure 4.2	The detailed BESS control techniques [219]	86
Figure 4.3	BESS design in DigSILENT PowerFactory	87
Figure 4.4	Block diagram of PI controller with anti-windup [220]	88
Figure 4.5	Block diagram of R_{int} equivalent battery model [48]	90
Figure 4.6	The studied 9 bus system with the installed wind and BESS [219]	93
Figure 4.7	The power output of wind farm (%) with respect to varying wind speed [219]	93
Figure 4.8	Frequency of generator G2 with single-phase-ground fault (phase-a) [219]	96
Figure 4.9	Frequency of generator G1 with single-phase-ground fault (phase-a) [219]	96

Figure 4.10	Active power output of generator G2 with single-phase-ground fault (phase-a) [219]	97
Figure 4.11	Active power output of generator G1 with single-phase-ground fault (phase-a) [219]	98
Figure 4.12	The power output of BESS [219]	98
Figure 4.13	Battery SOC [219]	98
Figure 4.14	The frequency response of generator G2 for line event [219] . . .	99
Figure 4.15	The frequency response of generator G1 for line event [219] . . .	100
Figure 4.16	Active power output of generator G1 with line outage [219] . . .	100
Figure 4.17	Active power output of generator G2 with line outage [219] . . .	101
Figure 4.18	BESS active/reactive power [219]	101
Figure 4.19	Battery SOC [219]	102
Figure 4.20	The frequency of generators G1 and G2 with temporary load growth [219]	103
Figure 4.21	BESS active/reactive power [219]	103
Figure 4.22	Battery SOC [219]	104
Figure 5.1	Primary frequency control of PV integrated system with BESS [48]	109
Figure 5.2	Frequency and voltage control with BESS [48]	111
Figure 5.3	The model of BESS in DigSILENT/PowerFactory	112
Figure 5.4	Frequency and active power control of BESS [48]	113
Figure 5.5	Voltage and reactive power control of BESS [48]	113
Figure 5.6	Frequency droop characteristics [48]	114
Figure 5.7	Voltage droop characteristics [48]	115
Figure 5.8	The block diagram of BESS charge controller, d and q axis current control [48]	117
Figure 5.9	The IEEE 9-bus system with PV and BESS location [48]	120
Figure 5.10	The frequency (pu) oscillations of generator G2 [48]	123
Figure 5.11	Active Power output (MW) of generators G1 and G2 [48]	124
Figure 5.12	Voltage at BESS connection point [48]	125
Figure 5.13	The active and reactive power of BESS and battery SOC [48] . . .	125

Figure 5.14	The frequency (pu) oscillations of generator G1 and G2 with load event	126
Figure 5.15	The active and reactive power of BESS and battery SOC [48] . . .	127
Figure 5.16	The frequency rise of G1 and G2 with BESS installed at different buses for load reduction event	128
Figure 5.17	The frequency of G2 with BESS installed at different buses for line outage [48]	129
Figure 5.18	The frequency of G1 with BESS installed at different buses for line outage	129
Figure 5.19	SOC status with different charging mechanism [48]	130
Figure 5.20	The frequency of generator G1[p.u.] with BESS (a) and voltage at bus 7 (b) [48]	131
Figure 5.21	The closer view of generator frequency G1[p.u.] (a and b) [48] .	131
Figure 5.22	Battery SOC for various adaptive SOC strategy (a), BESS power output (b) [48]	131
Figure 5.23	SOC status with different charging mechanism [48]	132
Figure 6.1	Conventional PI regulated PQ controller [220]	138
Figure 6.2	Lead-lag regulated PQ controller [220]	139
Figure 6.3	PI-lead regulated PQ controller [220]	140
Figure 6.4	The studied customized equivalent transmission grid [220] . . .	141
Figure 6.5	Voltage and frequency standards by NEM [220]	143
Figure 6.6	The frequency of generators [p.u.] (a) and bus voltages [p.u.] (b) with line outage and without STATCOM/BESS [220]	146
Figure 6.7	The frequency of generators [p.u.] (a) and bus voltages [p.u.] (b) with line outage and STATCOM [220]	147
Figure 6.8	The active and reactive power of STATCOM	147
Figure 6.9	The frequency of generator [p.u.] (a), bus voltage [p.u.] (b), the closer look of frequency (c) and voltage (d) with line outage and BESS [220]	148
Figure 6.10	BESS power output - active (a) and reactive (b) [220]	149
Figure 6.11	Battery SOC for all BESS control strategies	149

Figure 6.12	The frequency of generators [p.u.] (a), bus voltages [p.u.] (b) without STATCOM/BESS, the frequencies [p.u.] (c) and voltages [p.u.] (d) with STATCOM [220]	151
Figure 6.13	The frequency of generator [p.u.] (a) and bus voltage [p.u.] (b) with BESS [220]	152
Figure 6.14	BESS power output - active (a) and reactive (b) [220]	152
Figure 6.15	The frequency of generators [p.u.] (a), bus voltages [p.u.] (b) without STATCOM/BESS, the frequencies [p.u.] (c) and voltages [p.u.] (d) with STATCOM [220]	153
Figure 6.16	The frequency of generator [p.u.] (a) and bus voltage [p.u.] (b) with PI, PI-lead and lead-lag controlled BESS [220]	154
Figure 6.17	BESS power output - active (a) and reactive (b) [220]	154
Figure 6.18	The frequency of generator [p.u.] (a) and bus voltage [p.u.] (b) [220]	155
Figure 6.19	The power output of BESS - active [MW] (a) and reactive [MVar] (b) [220]	155
Figure 6.20	The frequency of generator [p.u.] (a) and bus voltage [p.u.] with permanent single-phase-ground fault (b) [220]	156
Figure 6.21	BESS power output - active (a) and reactive (b)	157
Figure 6.22	The frequency of generator [p.u.] (a) and voltage [p.u.] (b) without series capacitors and with [220]	157
Figure 7.1	Studied EVCS with EVs, PV and BESS [313]	164
Figure 7.2	Load profile of EVCS in food center ($P_{EV,1}$) and residential area ($P_{EV,2}$) [313]	164
Figure 7.3	Active power (P) regulator with $P_{BESS-ref}$ generator [313]	166
Figure 7.4	BESS charge/discharge control and d-q axis current controller [313]	167
Figure 7.5	Flow diagram for transformer overloading reduction with BESS [313]	169
Figure 7.6	Coordinated control of transformer overloading reduction and PV smoothing with BESS [313]	170

Figure 7.7	Coordinated control of reducing transformer overloading, smoothing PV output and B2G at EVCS with BESS [313]	172
Figure 7.8	Flowchart of the proposed energy management scheme [313] . .	174
Figure 7.9	EV charging load demand (a) and transformer overloading in different operation modes (b) [313]	175
Figure 7.10	BESS active power output (a) and battery SOC during transformer overloading period (b) [313]	176
Figure 7.11	BESS active power output (a) Transformer loading during overloading reduction with constant PV output (b) [313]	177
Figure 7.12	PV output variation (a) and BESS active power output during PV smoothing with no transformer overloading action (b) [313] .	177
Figure 7.13	BESS active power (a) Transformer loading and during integrated control (b) [313]	178
Figure 7.14	Fluctuation of PV output (a) and BESS active power response (b) [313]	178
Figure 7.15	BESS active power (a) and battery SOC (b) during B2G with and without designed constraint [313]	179
Figure 7.16	BESS active power (a) and battery SOC (b) during battery recharging [313]	180

List of Tables

Table 2.1	Advantages and disadvantages of available battery technologies.	28
Table 3.1	Rule table of the proposed FLC	60
Table 3.2	The relative frequency responses with load growth event	64
Table 3.3	The relative frequency response with wind speed deviation . . .	66
Table 3.4	The performance of frequency responses for varying wind speed level	69
Table 3.5	The relative performance analysis of frequency variation	71
Table 3.6	Rule table of the proposed FLC with 5 membership functions . .	74
Table 5.1	The power output of generators and loads in MW for both strategies	121
Table 5.2	Frequency deviation for various operating strategies and network conditions	123
Table 5.3	Maximum frequency deviation for load reduction event	126
Table 6.1	The comparative performance of controllers based on SSE analysis	158
Table B2.1	Load parameter	189
Table B2.2	Generator active and reactive power parameters:	190

LIST OF ACRONYMS

AEMO	=	Australian Energy Market Operator
BESS	=	Battery Energy Storage System
B2G	=	Battery to Grid
CD	=	Conventional Droop
CDFP	=	Conventional Droop with the Proposed FLC Pitch Control
CDPP	=	Conventional Droop with PI Pitch Control
DFIG	=	Doubly Fed Induction Generator (DFIG)
DOD	=	Depth-of-Discharge
EV	=	Electric Vehicle
EVCS	=	EV Charging Station
FACTS	=	Flexible AC Transmission System
FLC	=	Fuzzy Logic Controller
FRT	=	Fault Ride Through
LiFePO ₄	=	Lithium Iron Phosphate
MG	=	Microgrid
MPP	=	Maximum Power Point
MPPT	=	Maximum Power Point Tracking
NEM	=	National Electricity Market
NOFB	=	Non-Operating Frequency Boundary
P	=	Proportional
PEC	=	Power Electronic Converter
PCC	=	Point of Common Coupling
PCS	=	Power Conversion System
PFC	=	Primary frequency Control
PI	=	Proportional-Integral
PID	=	Proportional-Integral-Derivative
PLL	=	Phase-Locked-Loop
PMR	=	Peak-to-mean Ratio

PSS	=	Power System Stabilizer
PV	=	Photovoltaic
PWM	=	Pulse Width Modulation
RES	=	Renewable Energy Sources
RNN	=	Recurrent Neural Networks
ROCOF	=	Rate-of-Change-of-Frequency
ROCOP	=	Rate of Change of Power
RTDS	=	Real Time Digital Simulator
SA	=	South-Australia
SD	=	Sectional Droop
SDFP	=	Sectional Droop with FLC Pitch Control
SDPP	=	Sectional Droop with PI Pitch Control
SGs	=	Synchronous Generators
SMs	=	Submodules
SOC	=	State of Charge
SOH	=	State-of-Health
SSE	=	Sum of Squared Errors
STATCOM	=	Static compensator
VRB	=	Vanadium Redox Battery
VRLA	=	Valve Regulated Lead Acid
VSC	=	Voltage Source Converter
ZnBr	=	Zinc Bromine

LIST OF NOMENCLATURES

df	Frequency deviation
P	BESS active power output
ΔP_{IE}	Inertial power of wind turbine
R_{P-f}	Droop value for BESS active power regulation
$P-f$	Power-frequency droop
H_G	Inertia gain
P_{W-MPPT}	DFIG MPPT power reference
ΔP_{PFC}	Active power reference of DFIG for frequency control
H_G	Inertia gain
f_{grid}	Grid frequency
f_{ref}	Reference frequency
P_{W-MPPT}	DFIG MPPT power reference
P_w^{ref}	Updated power reference
ΔP_{PFC}	Active power reference of DFIG for frequency control
Δf_{Ml}	Medium low
Δf_{Mh}	Medium high
Δf_h	Maximum frequency deviation
Δf_l	Minimum frequency deviation
P_{WTmh}	Power reference in high sensitive positive region
$-P_{WTml}$	Power reference in high sensitive negative region
Δf_l	Low limit
Δf_h	High limit
ΔP_{MX}	Maximum power contribution of DFIG in the positive region
ΔP_{MN}	Maximum power contribution of DFIG in the negative region
P_1+P_{WTh}	Power reference in low sensitive positive regions
$-(P_3+P_{WTl})$	Power reference in low sensitive negative region
P_{wtm}	Wind turbine mechanical power
C_p	Power coefficient

λ	Tip speed ratio
β	Pitch angle
ρ	Air density
A	Turbine blade's sweep area
β_{ref}	Pitch angle reference
τ_1	Time constant
β_{max}	Maximum pitch angle value
β_{min}	Minimum pitch angle value
τ_2	Filter time constant
ω_{ref}	Rotor speed reference value
ω_{ra}	Actual rotor speed values
$\Delta\omega_{ra}$	Error signal
G_{Δ} and $G_{f\Delta}$	Gain for FLC inputs
ω_{ref}	Rotor speed reference value
ω_{ra}	Actual rotor speed values
$\Delta\omega_{ra}$	error signal
f_{min}	minimum frequency
f_{max}	maximum frequency
X_p and Y_p	Fuzzy subsets
Z_p	Singleton FLC output
P and W_a	Rule weighting factor
β_{o1}	Output of FLC
P_{max}	Maximum power margin
P_{min}	Minimum power margin
P_{RES}	Aggregated power output of any RES generating units
P_{SG}	Aggregated power output of SG units
P_L	Load power demand
P_{Gen}	Generated power
ΔP_d	Error between P_{Gen} and P_L
H_n	Total system inertia constant

H_B	BESS inertia constant
D_1 and D_2	Droop coefficient of generators SG_1 and SG_2
P_{ref}	Power references without frequency control
P_{ref-1}	Power references with frequency control
f_{nom}	Nominal frequency (pu)
f_{error}	Frequency error
K_{BESS}	Droop gain for BESS regulation
P_{in}	Output at BESS AC side
Δi_d	Difference between charge controller input and output on d axis
$y_{mn} = i_{d-min}$	Minimum d-axis current
$y_{mx} = i_{d-max}$	Maximum d-axis current
$V_{oc}(s, SOC)$	Internal voltage (voltage source)
$R_{int}(s, SOC)$	Internal resistance
U_{DC}	Terminal voltage
U_{max}	Fully charged battery voltage
U_{min}	Fully discharged battery voltage
I_b	Battery current
C_b	Battery capacity (Ah)
η	Coulomb efficiency
Δk	Change of period
L_b	Lifetime of a battery
NC_m	Number of cycles at a DOD
CFd_n	Cycles to failure at a DOD
f_{disch}	Discharging frequency
f_{ch}	Charging frequency
df_{max}	Maximum frequency deviation
df_{min}	Minimum frequency drop
P_{ch-max}	Maximum BESS power consumption
$P_{disch-max}$	Maximum BESS power discharging

v_{bus}	Actual bus voltage
dv	Error between v_{bus} and v_{ref}
v_{ref}	Nominal reference voltage
dv	Voltage error
dp_{ref}	Active power reference signal from frequency controller
dq_{ref}	Reactive power reference signal from voltage controller
R_{Q-v}	Droop value for BESS reactive power regulation
Q_{max}	Maximum reactive power injection
$-Q_{max}$	Maximum reactive power consumption
dv_{max}	Maximum voltage deviation
dv_{min}	Minimum voltage deviation
dv_{min}	Minimum voltage deviation
Δi_q	Difference between charge controller input and output on d axis
SOC_{min}	Lowest SOC limit
SOC_{max}	Highest SOC limit
i_{ch-A}	Charging current
$SOC_{adaptive}$	Adaptive SOC
$i_{ch-threshold}$	Charging threshold value
$i_{d-ref-out}$	Active power signal from d axis
$i_{q-ref-out}$	Reactive power signal from q axis
p_{md}	Modulation index in d axis
p_{mq}	Modulation index in q axis
$P_{meas(s)}$	Measured reference for regulating BESS active power
T_1 and T_2	First order filter time constant
k	Time in hour
P_{TR}	Total power demand by the transformer
P_{EV}	Total EV load demand
P_{TR-nom}	Nominal transformer rating
$P_{BESS-ref}$	Active power reference for regulating BESS power output
$P_{meas(s)}$	Measured power for BESS regulation

P_{PV}	PV output
P_{BESS1}	Amount of BESS power output for transformer overloading reduction
P_{PV-lim}	Predefined PV output value
$P_{BESS/PV}$	Power reference for BESS for PV lower than the predefined value
$P_{PV/S}$	PV status
$P_{BESS/PV0}$	BESS power reference for PV smoothing
$P_{BESS-ref/OLS}$	BESS power reference for overloading reduction and PV smoothing
$P_{BESS-ref1}$	BESS power output reference
$P_{TR-B2G-lim}$	The boundary for B2G operation
$P_{TR-V2G-lim}$	Limit of BESS active power output for V2G
P_{TR-nom}	Transformer nominal capacity
$P_{V2G/S1}$	BESS power limit for transformer overloading reduction and PV smoothing
$P_{BESS-nom}$	Nominal capacity of BESS
$P_{BESS/ch}$	Recharging power of BESS
$P_{V2G/S}$	Signal for V2G mode
P_{EV-max}	Peak EV charging demand
$P_{BESS-req}$	Required BESS size

LIST OF PUBLICATIONS

Journal articles-published:

1. U. Datta, A. Kalam and J. Shi, "The economic prospect of rooftop photovoltaic (PV) system in the commercial buildings in Bangladesh: A case study," *Clean Technologies and Environmental Policy* (Q2), Accepted-November 2020.
2. U. Datta, A. Kalam and J. Shi, "Battery Energy Storage System for Aggregated Inertia-Droop Control and a Novel Frequency Dependent State-of-Charge Recovery," *Energies*, vol. 13, pp. 2003, 2020 (h-index=78, Q2, IF=2.702).
3. U. Datta, A. Kalam and J. Shi, "Smart control of PV and BESS in EV charging station for reducing transformer overloading and providing grid ancillary service," *Journal of Energy Storage*, vol. 28, pp. 101224, 2020 (h-index=29, Q1, IF=3.762).
4. U. Datta, J. Shi and A. Kalam, "Primary frequency control of an islanded microgrid using integrated dynamic sectional droop and fuzzy based pitch angle control for wind farm," *Journal of Electrical Power and Energy Systems*, vol. 111, pp. 248-259, 2019 (h-index=116, Q1, IF=3.588).
5. U. Datta, A. Kalam and J. Shi, "Battery Energy Storage System Design for Mitigating PV Penetration Impact on Power System Primary Frequency Control," *IEEE Transaction on Sustainable Energy*, vol. 11, pp. 746-757, 2020 (h-index=101, Q1, IF=7.44).
6. U. Datta, A. Kalam and J. Shi, "Frequency Performance Analysis of Multi-gain Droop Controlled DFIG in an Isolated Microgrid Using Real-Time Digital Simulator," *Engineering Science and Technology, an International Journal*, Accepted-December 2019 (h-index=39, Q1, IF=3.219).
7. U. Datta, A. Kalam and J. Shi, "The relevance of large-scale Battery Energy Storage (BES) application in providing primary frequency control with increased wind energy penetration," *Journal of Energy Storage*, vol. 23, pp. 9-18, 2019 (h-index=29, Q2, IF=3.762).

8. U. Datta, A. Kalam and J. Shi, "Battery Energy Storage System to Stabilize Transient Voltage and Frequency and Enhance Power Export Capability," *IEEE Transaction on Power System*, vol. 34, pp. 1845-1857, 2019 (h-index=242, Q1, IF=6.074).
9. U. Datta, N. Saiprasad, A. Kalam, J. Shi, and A. Zayegh, "A Price Regulated Electric Vehicle Charge-Discharge Strategy for G2V, V2H and V2G", *International Journal of Energy Research*, vol. 43, pp. 1032–1042, 2019 (h-index=88, Q2, IF=3.741).
10. U. Datta, A. Kalam and J. Shi, "Electric Vehicle (EV) in Home Energy Management to Reduce Daily Electricity Costs of Residential Customer, *Journal of Scientific and Industrial Research (JSIR)*, vol. 77, pp. 559-565, 2018 (h-index=49, Q2, IF=0.729).

Book chapters-published:

1. U. Datta, A. Kalam and J. Shi, "The Strategies of EV Charge/ Discharge Management in Smart Grid Vehicle-to-Everything (V2X) Communication Networks," *Advanced Communication and Control Methods for Future Smart grids*, 1st ed., London, Intechopen, 2019.
2. U. Datta, A. Kalam and J. Shi, "Hybrid Renewable Energy Sources for Microgrid application- An Overview," in *Hybrid-Renewable Energy Systems in Microgrids*, 1st ed., Woodhead Publishing, 2018, pp. 1-22.

Conference articles-published:

1. U. Datta, J. Shi, A. Kalam and J. Li, "DFIG Pitch Angle Control with PID-type Fuzzy Logic Controller in a Microgrid ", *ICIEA 2020*, Norway.
2. U. Datta, A. Kalam and J. Shi, "Battery Energy Storage System for Improving Primary Frequency Control with Increased Level of Photovoltaic Penetration", *2019 29th Australasian Universities Power Engineering Conference (AUPEC)*, Nadi, Fiji, 2019, pp. 1-6.

3. U. Datta, A. Kalam and J. Shi, "Electric Vehicle Charging Station for Providing Primary Frequency Response in Microgrid," 2019 14th IEEE Conference on Industrial Electronics and Applications (ICIEA), Xi'an, China, 2019, pp. 2440-2444.
4. U. Datta, A. Kalam and J. Shi, "Power system transient stability with aggregated and dispersed penetration of hybrid distributed generation," 2018 Chinese Control and Decision Conference (CCDC), Shenyang, 2018, pp. 4217-4222.
5. U. Datta, A. Kalam and J. Shi, "An approach in dual-control of battery energy storage systems in windfarm output power smoothing," 2017 Australasian Universities Power Engineering Conference (AUPEC), Melbourne, Australia, VIC, 2017, pp. 1-5.
6. U. Datta, A. Kalam and J. Shi, "Battery energy storage system for transient frequency stability enhancement of a large-scale power system," 2017 Australasian Universities Power Engineering Conference (AUPEC), Melbourne, VIC, Australia, 2017, pp. 1-5.

The part of published/submitted article contents and figures have been adopted in the chapters. The specific information of the article adopted in each chapter is given in the table as follows:

Chapter	Article Title	Publication Info	Publication Status
3	Primary frequency control of a microgrid with integrated dynamic sectional droop and fuzzy based pitch angle control	International Journal of Electrical Power & Energy Systems, vol. 111, pp. 248-259, 2019	Published
4	The relevance of large-scale battery energy storage (BES) application in providing primary frequency control with increased wind energy penetration	Journal of Energy Storage, vol. 23, pp. 9-18, 2019	Published
5	Battery Energy Storage System Control for Mitigating PV Penetration Impact on Primary Frequency Control and State-of-Charge Recovery	IEEE Transactions on Sustainable Energy, vol. 11, pp. 746-757, 2020	Published
6	Battery Energy Storage System to Stabilize Transient Voltage and Frequency and Enhance Power Export Capability	IEEE Transactions on Power Systems, vol. 34, pp. 1845-1857, 2019	Published
7	Smart control of BESS in PV integrated EV charging station for reducing transformer overloading and providing battery-to-grid service	Journal of Energy Storage, vol. 28, pp. 101224, 2020	Published

Chapter 1

Introduction

1.1 Motivation

Continual growth in energy demand and intensified sustainability concern of fossil fuel-based electricity generation has thrust the escalation of renewable energy sources (RES), mainly photovoltaic (PV) and wind energy penetration, into the existing power system. The government policy, social movement, advancement in renewable energy technologies, present-day installation scenarios, academic and industry research portfolios are indicating the focus on an emission free future electricity industry. Due to such resolutions, a similar momentum of RES penetration is expected to be maintained in the years to come.

Regarding the realm of this work, incorporating the large-scale RES of alternating nature has brought an additional dynamic and transient stability challenges in the existing electric grid. RES with different degrees of operational characteristics than the conventional synchronous generators and inherent fluctuating behavior has increased the complexity of power system operation. Moreover, with RES penetration, the main electric grid encounters several technical difficulties such as violation of voltage limits, transmission congestions, peak generation-peak demand imbalance, the higher need of load-generation balance (spinning reserve) etc. In addition, reduction of system inertial

capability due to low inertial RES penetration is an increased area of concern, mainly their impact on power oscillation damping following a disturbance. Therefore, RES can provide clean energy but with the expense of stability distress. Moreover, weather dependency of RES will result in power export within the network to maintain generation-demand balances and this situation will force certain transmission lines to be operated near their maximum capacity. With already aged power grid infrastructures, the stability of the system is often at great risk while the highly loaded lines encounter disturbance. The accomplishment of sustainable electricity industry would require the amalgamation of state-of-the-art technologies, operational practices and sophisticated tools. The target would be to incorporate the highest possible electricity generation from renewable energies, without raising stability and reliability concern in the power system. The collective global efforts on rehabilitating critical grid infrastructures, advancing electrical equipment design and control technology, simulating tools and embracing artificial intelligence are essential to achieve a major shift towards the future sustainable and smarter electric grid.

The custom of power electronics devices to facilitate the higher amount of renewable energy throughputs and enhance power system stability are a common practice in many countries; mainly by means of different energy storage technologies. The advancement in power electronics technology associated with an energy storage system has the ability to respond promptly. Present electric grid with added RES faces many technical challenges and all of the understanding and problems are yet to be resolved. Credible efforts have been put in the modelling of energy storage system for utility-scale power system simulation in minimizing the adverse impact of RES [1–7]. Among many energy storage technologies, Battery Energy Storage System (BESS) has been used in dealing with the challenges of high penetration of RES in electric power grid by enhancing power system stability. BESS is at the forefront mainly because of the technological advancement and reduction of battery costs in the last few years [8]. In addition, the services that can be offered by a BESS have increased in the past decades. The first-hand concept of BESS applications on grid level has been presented in this research.

This research work enhances the vicinity of BESS application on the grid level aimed at providing transient stability support and increasing the penetration level of RES in the existing electric grid. The detailed modelling of BESS with independent active and reactive power control mechanism is addressed in this research. The modelling is developed keeping in mind the operational requirements by the electric grid that differs in accordance with the rationale of BESS employment. Considering transient stability support, activating maximum power of BESS is given paramount importance. The control design and application that are proposed in this study signifies an exemplary shift in the capacity this auxiliary device is traditionally been used to support the stability of the power system. It is established in this research work that the use of "application-based modeling" retains the important characteristics in determining BESS performance to enhance the stability of the connected electric grid.

1.2 Objectives of the Thesis

The key objective of this thesis is to design and develop a BESS model with independent active and reactive power control features that are suitable for multiple power system applications. The competency and performance of BESS are investigated in the context of the capability for dynamic and transient stability enhancement of large-scale power system integrated with different level of RES penetration. To utilize the fast regulation capability of BESS, this study has explored dynamic and transient stability benefits offered by the incorporated BESS in power system under various contingencies for improving power system damping performance and thus enhancing system stability. To the author's best knowledge, no earlier researches are available in this paradigm of transient stability studies with the incorporated BESS in power system. Undeniably, with fast dynamic response competency, ample opportunities are available for BESS application in grid level. It is worth noting that this study considers purely the technical aspects of BESS.

In summary, the research objectives are as follows:

- To regulate the active power output of DFIG and participate in frequency control of the grid using OPAL-RT - a real-time digital simulator (RTDS).
- To facilitate the higher level of PV and wind energy penetration in the existing electric grid considering the perspective of transient stability phenomena.
- To provide flexible SOC management depending on network requirement without affecting the existing SOC strategy.
- To alleviate transient stability under numerous contingencies and enhance power export capability of the power system.
- To reduce the overloading of a grid-coupling transformer in a charging station and maintaining transformer capacity limit while providing grid service to the grid and recharging the battery.

1.3 Original Scientific Contribution

In this research work, BESS controls are coordinated to regulate system frequency using active power and voltage using reactive power. However, the preferences of active and reactive power are planned depending on their particular application in the power system. In contrast, to design an individual BESS model for separate application with major modification in control techniques, this model reduces adjustment complexity and provides the flexibility to be used in different environment with minimum amendments in it. In this research, BESS contributions are addressed in minimizing the adverse impact of RES, improving power system damping and transient stability and thereby facilitating cleaner energy penetration that will benefit industry and community. Furthermore, simultaneous transient voltage and frequency stability support from BESS is considered and this can provide added value over Static Synchronous Compensator (STATCOM) in relation to the voltage and frequency stability. This ensures a better economic value of BESS for power system application. Moreover, incorporating BESS in charging station, it is able to reduce transformer rated capacity and overloading

during a specific period of operation, which would be able to bring down the cost. It is also possible to obtain other grid services that provide an additional benefit of using BESS.

The original scientific contributions of this thesis may be encapsulated as follows:

- A sectional droop control method associated with fuzzy logic regulated pitch angle adjustment for real-time frequency regulation in an isolated microgrid (MG) using doubly-fed induction generator (DFIG) type wind turbine. The remarkable outcome is visible for both the conventional PI and fuzzy logic controller regulated pitch angle controls.
- A comprehensive analysis of the application of BESS in reducing distresses related to the penetration of low/zero inertial wind and PV energy system and supporting better frequency oscillation damping and increasing renewable energy penetration. The new models originating from this research encapsulate the dynamic characteristics of the network. Considering various application scenarios, BESS modelling ranges from voltage and/or frequency feedback control to the active/reactive power controllers. This has led to the selection of feedback signals and the adoption of different control loops to regulate BESS responses to the changes in system dynamics according to BESS capacity and design constraints.
- An adaptive battery state-of-charge (SOC) recovery strategy for flexible BESS operation according to the network planning without compromising the total battery capacity for network events. The charging limit can be easily adjusted according to the BESS operator planning by simply varying the value of charging current.
- BESS modelling with simultaneous active and reactive power regulation and stabilizing transient voltage and frequency stability and enhancing power export capability of the power system. In addition, comparative studies are carried out to evaluate the performance of different

controllers, namely PI, PI-lead and lead-lag controllers to regulate BESS active and reactive power for power system stabilization.

- The development of BESS control technique in reducing transformer overloading in a grid-integrated electric vehicle charging station (EVCS). Moreover, this will increase the overall capacity of charging station and BESS can be utilized for providing battery-to-grid (B2G) service and charging from the grid without violating the transformer limit depending on the rated capacity of transformer and battery. The active power at charging station output acts as feedback signal to regulate BESS power flow. In emergency situation or during low charging demand periods, BESS can be used to provide grid services to the network and also to be charged to maintain sufficient battery SOC. However, it is necessary that transformer capacity limit is not violated while providing grid services or recharging.

1.4 Thesis Outline

Organization of the complete thesis can be summarized in a flowchart as follows:

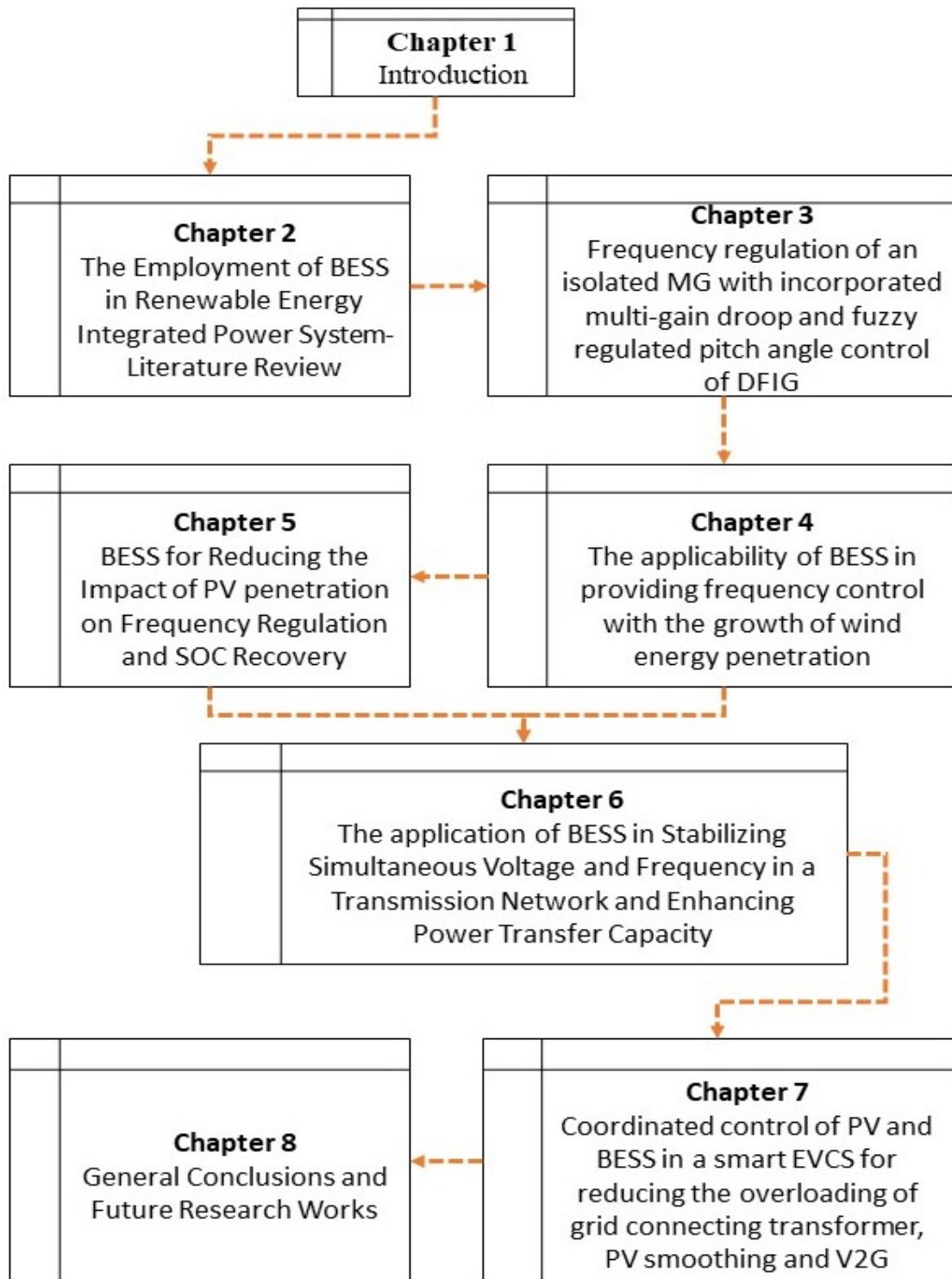


Fig. 1.1 Complete thesis outline

In **Chapter 1**, motivation of the study, research objectives and the original scientific contributions are discussed. The complete thesis outline and a brief description of each of the chapters are also highlighted in this chapter.

In **Chapter 2**, comprehensive research on BESS is presented, emphasizing on early endeavors on modelling BESS to deal with uncertainties of RES. Presently, BESS is one of the widely installed energy storage devices to deal with intermittent phenomena from RES. In this regard, wide-range of research studies have already been carried out in academia and industry and will be given further attention considering multi-dimensioning applicability of BESS. It discusses and analyses the array of BESS application in mitigating the alternating nature of RES, converters topologies in BESS, confronts key challenges of the earlier research works and possible research directions.

Chapter 3 depicts the frequency control of an isolated MG by taking advantage of DFIG based wind turbine regulation capability. The integrated control of sectional droop and inertia emulation is employed along with proportional-integral (PI) and fuzzy logic controller (FLC) regulated pitch angle control for regulating system frequency. The simulation is carried out in real-time using OPAL-RT.

Chapter 4 presents the damping performance of the power grid with various level of wind energy penetration compared to without wind energy. In order to improve system damping capacity, BESS is incorporated in the network. The efficacy of BESS is demonstrated to improve the system's damping capability and diminish over-frequency or under-frequency excursion resulting from contingencies events with increased wind energy penetration. It is shown that when BESS is incorporated in the grid, the inertial impact of increased wind energy penetration can be minimized. The BESS design is modified and used in later chapters according to their purpose and operation in the grid.

Chapter 5 demonstrates the impact of PV penetration on power system damping performance in primary frequency control. More importantly, it is demonstrated at which point the electric system fails to comply with the grid requirements as PV penetration increases. Generator control and system loading have a significant influence on the dynamic behavior of the system and hence, special consideration is given to

determine network operating condition for evaluating PV penetration. BESS is incorporated to provide additional system damping and enhance primary frequency controllability of the system. In addition, the generator's control and system loading influence on damping performance of the grid is further investigated with the growth of PV penetration. Simulation results illustrate that BESS efficiently improves the damping capability of the system in responding to primary frequency control undergoing contingencies. Therefore, BESS reduces inertia related difficulties with increased PV penetration and support the provision of increasing PV growth in the electric grid. The efficacy of the proposed SOC recovery strategy is substantiated through simulations.

Chapter 6 illustrates the applicability of BESS and Static Compensator (STATCOM) in enhancing voltage and frequency stability of a large-scale power system and improving power export capability within two large interconnected power systems. STATCOM and BESS technologies are at the forefront in the future electric grid where aging transmission lines, intermittent RES, complex electricity market are the dominant factors in power system stability. To demonstrate their comparative performance, various single/multiple network/load events are applied while exporting power in an equivalent transmission network. In addition, few other network events are also considered to illustrate the efficacy of BESS and STATCOM. Through simulation studies, it is demonstrated that STATCOM fails to maintain voltage and frequency stability when the system is exporting 44% higher than the normal operating limit and encounters permanent network faults. However, the incorporated BESS delivers needed damping to the system and BESS competently withstands single/multiple network/load contingencies and temporary/permanent single-phase-to-ground fault.

Chapter 7 presents the capability of BESS in reducing transformer overloading and improving the charging station's capacity. BESS modelling is developed according to active power feedback-controlled strategy. BESS is also designed for PV smoothing and providing grid services. The simulation studies are carried out to validate BESS efficacy in the designed charging station.

Chapter 8 encapsulates the overall conclusions of the thesis and provides future research direction based on the studies in this thesis.

Chapter 2

The Employment of BESS in Renewable Energy Integrated Power System - Literature Review

2.1 Introduction

The installation of RES have grown remarkably and is foreseen to expand expeditiously in upcoming years. Integrating RES in power network can minimize grid losses and reduce carbon footprint. However, with inconsistent and little predictable nature, RES can generate serious lapse that may create difficulty in maintaining normal grid balance i.e. load and generation equilibrium [9, 10]. Rapid fluctuations, especially from large-scale PV and wind farms put more stress in power system [11] such as voltage fluctuations, reverse power flow, frequency deviations, etc. In extreme cases, these phenomena can lead to catastrophic collapse of the entire system i.e. “a complete blackout”. The adverse impact of RES farm originates from variable solar radiation and wind speed that changes seasonally, monthly, daily, hourly and even in seconds.

Harmonic distortions and voltage flickering are few of the other problems that arise with the large-scale penetration of PV and wind generating plants [12, 13]. As the level

of RES penetration increases, frequent fluctuations in RES power output may impose additional stress on conventional generation units in order to maintain voltage and frequency within the acceptable limit. This will minimize the lifespan of conventional generation units and also increase operational cost in conventional generation unit [12]. Moreover, an increment in RES penetration reduces accessible inertia in the system that increases the need for additional spinning reserves and eventually imposes extra costs.

In order to minimize the harmful effects of RES in the grid, many countries are already maintaining compulsory grid codes guideline considering such unpredicted situations to ensure controlled fluctuations and reliable renewable energy operation within the acceptable operating range [14, 15]. The grid codes range from limits in ramp-rate, fault-ride-through (FRT) capability, voltage and frequency regulation capability, dispatchability, etc. Few countries like Italy [16], Germany [17] and UK [18] have already imposed financial penalties in the case of RES farms do not maintain the promised output power schedule. If auxiliary power reserves are not arranged as RES penetration increases, the power system may encounter severe system failure i.e. blackout can be more frequent in the future.

Energy storage technologies have the capability to regulate its output and thus minimize the adverse impact of RES indeterminacy. Among many existing energy storage technologies, such as flywheel, pump hydro, capacitor, super-capacitor and compressed air energy storage, BESS offers better flexibility in terms of capacity, siting facility and fast response to fulfill the requirements of storage system application [1]. BESS can store energy and is able to control active and reactive power flow independently at the point of common coupling (PCC) and provides various services as shown in Fig. 2.1. The BESS services may include transient frequency stability [2], enhanced reliability [3], peak shaving [4], transmission congestion management [19], output power leveling [20], ramp rate control [6] and dispatchability [7]. The mitigation of output power fluctuation, frequency regulation, peak shaving and plant dispatchability can be improved by regulating BESS active power output. Conversely, reactive power reinforcement, voltage regulation and Low Voltage Ride-Through can be realized by regulating BESS reactive power output.

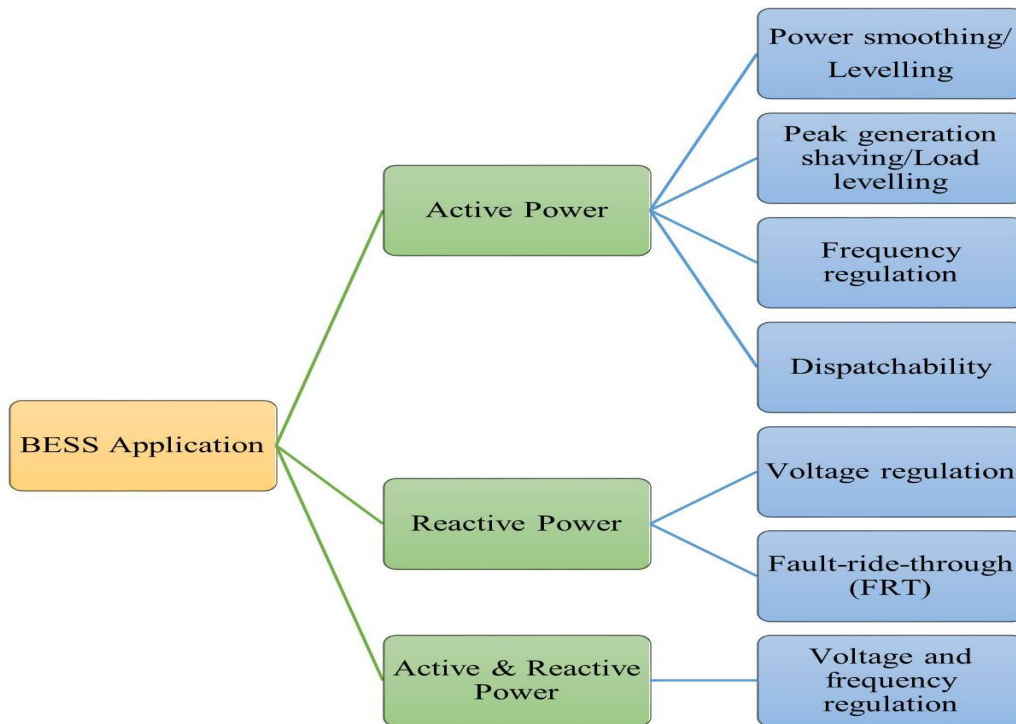


Fig. 2.1 Typical BESS applications in renewable energy integrated system

In this chapter, the main objective is to provide a comprehensive review of various applications of BESS in renewable energy integrated power systems as shown in Fig. 2.1. Initially, common BESS connection diagrams in PV/wind integrated system and associated converter technologies are discussed. Then a brief discussion on different battery technologies and their relevant advantages/disadvantages are summarized. The applications of BESS are classified in active/reactive or simultaneous active and reactive power regulation. It was found that either the active or simultaneous active and reactive power from BESS are widely studied by the researcher in grid application whereas BESS application study for reactive power regulation is limited. The main reason is due to the capability of BESS for regulating active and reactive power and also related cost-benefit aspect of utilizing BESS. Furthermore, general findings of the study are summarized for providing an overview of existing BESS application and their relevance in grid application. The key challenges and their viable reasons are identified and discussed in order to present the existing challenges of integrating BESS in the grid. This also provides the idea of future research opportunity on BESS for integrating into the grid.

2.2 Energy Storage Technologies

Energy storage technology is subjected to the type of storages, short-term and long-term operating time frame, power and energy ratings and applications [21,22].

2.2.1 Storage Technologies-General Consideration

The available energy is possible to be stored for later use in various energy forms including mechanical, magnetic and electrical natures which can be summarized as follows [21–23]:

- Electric type storage, which can be further divided into two types
 - Electro-chemical batteries
 - * Electrolyte type batteries- Lithium-ion, Lead-acid, etc.
 - * Flow batteries-Vanadium Redox
 - Capacitors and super-capacitors
- Magnetic type storage
 - Superconducting magnetic energy storage
- Mechanical type storage
 - Flywheels energy storage
 - Compressed air energy storage
 - Pumped hydro storage
- Thermal type storage
 - Sensible heat storage
 - Latent heat storage

2.2.2 Operating Time Frame, Power and Energy Rating

The application of energy storage technologies in power industry has existed for more than 150 years. Many storage technologies with high potential have been advanced and further research is ongoing for their application to large-scale power systems. The application of available energy storage technologies can be classified in terms of short-term and long-term period as shown in Fig. 2.2.

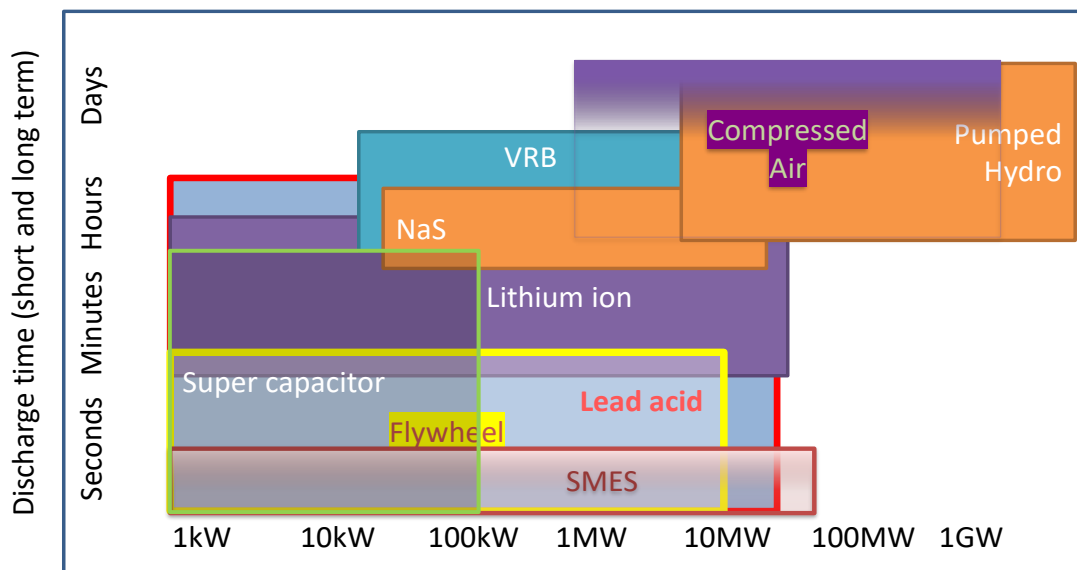


Fig. 2.2 Energy storage technologies capability- operating time frame

As indicated in Fig. 2.2, several battery storage technologies are available in MW power and MWh energy capacity. However, mechanical storage systems are still at the forefront in the course of higher power and energy rating. Recent technical advancement in battery technologies are set in motion for large scale battery storage installation ever than before.

2.3 BESS Technology and Batteries

The battery technologies have been in practice for more than 100 years. However, only rechargeable or secondary batteries are preferred in power system application. The battery technologies are gaining popularity in power system application due to their

ability of providing operational flexibility, rapid response, reduction in price/kWh [24] and technological advancement in recent battery technologies. The batteries are widely used at all voltage levels in power systems [25]. Their application can ensure operational flexibility and environmental benefits. However, large-scale application of battery storage systems are not widely used because of their low energy density and power capacity. Nevertheless, recent advancement in battery technologies, especially in lithium-ion batteries have increased the interests for their application to large-scale power systems.

2.3.1 BESS Connection Diagrams

The basic structure of BESS mainly depends on voltage level it is intended to be connected. A typical BESS structure may consists of battery banks (typically stacks of batteries in parallel), DC/AC power conversion system. A transformer might be needed to convert BESS output voltage level to the grid voltage level if BESS is planned to be connected with local distribution or transmission system. Very often, BESS absorbs and delivers power to and from the grid which requires a bi-directional Voltage Source Converter (VSC) [26, 27], current-source converter [28], with its choice mainly depending on the purpose of BESS in that particular case study. Commonly used BESS-PV configurations are shown in Fig. 2.3. Each configuration has its own advantages and disadvantages. In the case of Fig. 2.3(a), an additional DC/AC converter will increase system cost. In addition, as BESS is directly connected to the PCC, it requires added circuit protection system that further increases costs to the system. However, the main advantage is that BESS can be regulated as a separate storage system for grid service. The intermediate DC-DC inverter with BESS in Fig. 2.3(b) provides the flexibility to be connected with various DC-link voltage level as it allows to increase the battery voltage to the high DC-link voltage. The block diagram in Fig. 2.3(c) eliminates the need of a DC-DC converter. This architecture is only suitable for a battery voltage equal to the DC-link voltage. The battery cannot be controlled and this requires proper inverter control with the varying DC-link voltage as battery SOC varies for grid synchronicity.

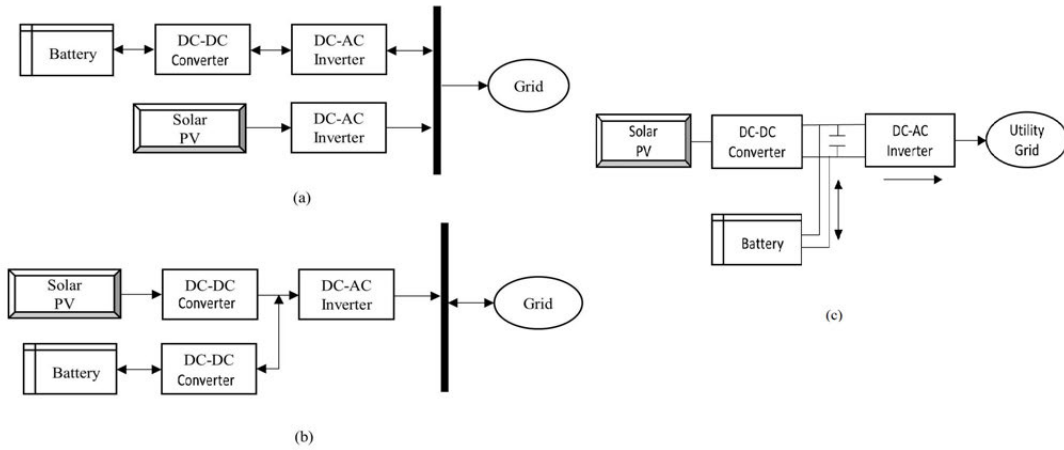


Fig. 2.3 Typical BESS connection in a PV-BESS energy system; (a) PV/BESS connection through an individual converter (b) BESS connection using common DC side through DC/DC converter (c) Direct BESS connection on the DC side

The classical BESS structure in a wind farm comprises a very similar structure as employed in a solar PV system; a battery bank, power conversion system and a transformer, if needed. Most importantly, BESS application in wind farm is to store excess energy from wind power and deliver it during low or no wind period. General schematic diagrams of wind-BESS combination are shown in Fig. 2.4. The battery is connected in such a way that BESS can be regulated as an independent storage system as shown in Figs. 2.4 (a) and (b) whereas battery can be connected to the DC-link in some cases as shown in Fig. 2.4(c).

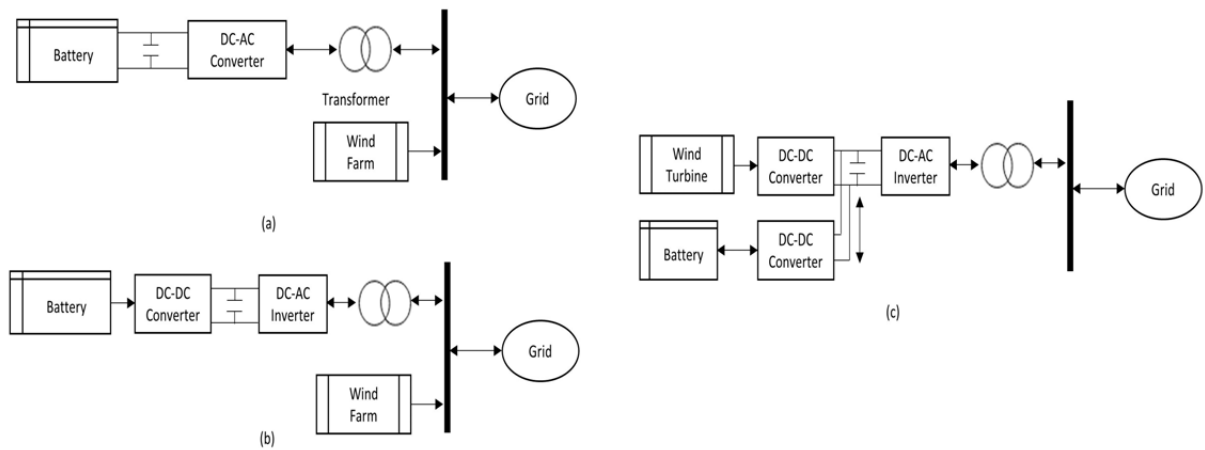


Fig. 2.4 Typical BESS connection in a wind-BESS energy system; (a) BESS through DC/AC converter (b) BESS through DC/DC and DC/AC converter (c) BESS connection on the dc side with wind turbine DC/DC

In the case of hybrid energy system, battery can be coupled either to DC or AC bus,

depending on design constraints and preferences. The battery banks may be integrated directly [27, 29, 30] or with a DC-DC power conversion system to DC bus [31–33]. Another option for BESS connection is a battery bank with a DC/AC power conversion system to be connected with AC bus. A transformer can be installed at BESS output before local AC bus [34–37] or after local AC bus [38, 39] to finally being connected with the grid. A few possible PV-wind-BESS structures are shown in Fig. 2.5.

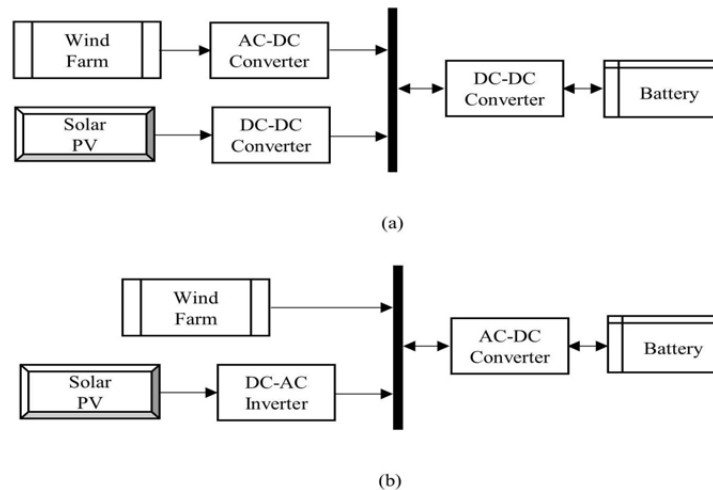


Fig. 2.5 Typical BESS connection in a PV-wind-BESS energy system; (a) Connected to a common DC bus (b) Connected to a common AC bus

2.3.2 Power Conversion System and Converter Technologies

Power conversion system (PCS) is a power electronics based interface to connect storage system with AC. As battery storage system employs DC interface, battery can be incorporated with DC terminal of PV, sharing the same DC bus. However, in a wind farm terminal, such possibility do not exists. Therefore, PCS is necessary to connect a BESS with AC grid. With high efficiency, fast response and control design, PCS performs both instantaneous active and reactive power regulation, as demanded in the present day grid applications. The PCS comprises of two level control- primary and secondary control [40]. Primary control generates gate drive signals to control power converter depending on reference charging mode and state of the system. The secondary control receives active and reactive power command and select appropriate operation mode based on the SOC, electricity tariff etc..

- Most trivial primary control approach is:
 - Proportional-Integral (PI) control.
- Secondary control determines the operation mode of the power converters. Three frequent practices are:
 - Charge mode
 - Discharge mode
 - Standby mode.

The direction of power flow denotes BESS power output i.e charging (negative) and discharging (positive) as shown in Fig. 2.6. In ideal condition, BESS output is zero. However, there will be a small amount of power flow in BESS in reality due to the self discharge of batteries and converter losses.

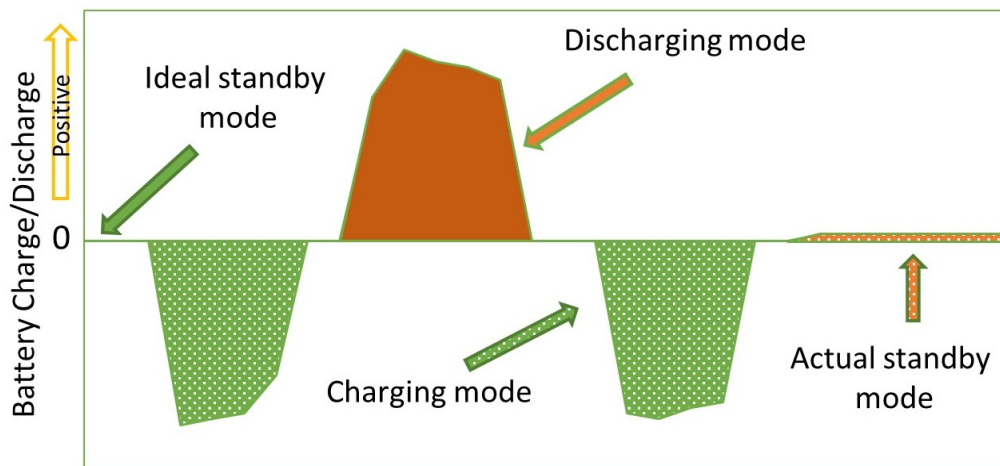


Fig. 2.6 Various operation modes of BESS

Most common power conversion system design topologies are-

1. Single stage converter (DC/AC)
2. Dual stage converter (DC/DC & DC/AC)
3. Single/dual stage multi-port converter (multiple DC/DC or DC/AC converters in parallel).

Single-stage converter (DC/AC) is one of the less complex power electronics technologies for converting battery DC voltage into a three-phase AC voltage [41].

Many batteries are connected in parallel and series for high voltage-high power application. The addition of medium frequency transformer isolated AC/AC converter with BESS DC/AC converter eliminates the need of DC-link capacitors, reduces the size of grid filter [42]. However, this increases the total harmonic distortion in the output voltage resulting from the non-idealistic nature of switching.

A limitation of direct battery connection to DC-link voltage is the wide operating range of DC-link voltage as battery voltage alters according to its SOC status and so as the DC-link voltage. Therefore, to accommodate this broad voltage operating ranges, semiconductors need to be over-sized for safe operation. The DC-link voltage can be controlled by incorporating a DC/DC converter between the battery and DC/AC converter that allows maintaining a constant DC bus voltage regardless of battery SOC status [43]. In contrast to a non-isolated DC/DC converter [43], an isolated bidirectional DC/DC converter enhances converter efficiency, provides smoother power flow control and reduces costs [44].

In order to connect BESS to the medium voltage grid without a step-up transformer, the modular converter can be designed in cascaded order. In single-stage cascaded H-bridge converter type connection, each series connected cells can contain equally distributed battery modules with smaller battery strings (distributed) and each full bridge converter can control battery modules to regulate the power flow [45]. In the modular multilevel converter, long battery strings can be connected to the common DC-link (centralized) with submodules (SMs) in series to form converter arms. However, a centralized battery connection hinders the advantage of cascaded structure [46]. In dual-stage multi-port converter, each SM consists of DC converter with battery and DC/AC converter [47].

2.3.3 Quantities for Battery SOC Calculation

The SOC is the accessible battery capacity to participate in charging/discharging cycles that is possible to define from the perspective of power and energy application. The measurable quantities for battery SOC estimated calculation are as follows:

- Cell/electrolyte Temperature
- Ambient temperature
- Ampere-hour counting
- Battery age
- Cell voltage
- Concentration of the electrolyte.

In model free approach, Coulomb Counting Method [48] and Open Circuit Voltage [49] methods are the reasonable ways to determine a battery SOC but the accuracy is debatable as the estimation results are dependent on initial error and accumulated noise in voltage and current measurements. An intelligent Recurrent Neural Networks (RNN) method based on battery voltage/current and ambient temperature is another way of estimating SOC [50]. Nevertheless, RNN is a training dependent method which may not perform satisfactorily for unseen data sets and also as this ignores the internal parameters of battery, the error may persist in SOC estimation.

On the contrary, model based method comprises of closed loop approach that uses estimation algorithms for correcting SOC error regularly from the voltage, current and temperature measurements to provide more accurate SOC calculation. A dual fractional-order extended Kalman filter [51] or other types of Kalman filter has been one of the most preferred algorithms for estimating SOC. Battery surface temperature often varies by a great number than the battery internal temperature and hence battery shell temperature is added for better SOC estimation [52]. Nevertheless, as the battery parameters change with battery aging and operating conditions, model based approach still faces difficulties in providing reliable SOC estimation [53]. Few adaptive estimation approaches are available in the literature for estimating SOC accurately and reliably [54, 55]. The errors in measurement and model result in incorrect SOC estimation [56] and it can be said that there are ample space for developing an accurate, robust and reliable SOC estimation technique.

2.3.4 Battery Types

Generally, batteries are categorized in two different battery technologies:

- Primary (non-rechargeable); and
- Secondary (rechargeable).

Rechargeable batteries are the most mature method of energy storage [57, 58] as chemical energy [59] and is preferred in power system application. A battery comprises of numerous electrochemical cells coupled in series and/or in parallel based on appropriate voltage and capacity requirement [60]. Individual cell is composed of positive and negative electrode, separated by liquid, paste or solid electrolyte [61, 62]. The important characteristics of rechargeable batteries are that transformation of electrical energy to chemical energy (charge) and vice versa (discharge) should be energy efficient and of minimal physical changes [63].

Rechargeable or secondary batteries can respond very quickly ($<s$) [64] which allows BESS to be popular and widely used option for steady-state and dynamic stability enhancement in power systems. Some important features or performance characteristics of batteries [61, 65] that are intended for power system applications comprise of the following:

- Power and energy capacity;
- Battery efficiency level;
- Battery life span;
- Battery temperature;
- State of charge (SOC);
- Depth of discharge (DOD);
- Battery self-discharge;
- Battery sizing;
- Operation and maintenance requirements.

The duration of energy storage ranges from hours to months [62]. Various battery

technologies [63, 66, 67] used in renewable energy system are briefly discussed in the following subsections.

2.3.4.1 Lead Acid

Since the beginning of the practical application of lead-acid batteries in 1860, it has been the most sophisticated and frequently adopted rechargeable battery technology in power system. Lead-acid cell comprises of a lead oxide positive electrode and a sponge lead negative electrode- which are isolated by a micro-porous substance as shown in Fig. 2.7 [21]. It has 70-90% efficiency but limited life cycle span (5-15 years) which restrict its large-scale storage application [62, 68]. Flooded battery and valve regulated (VRLA) [69] types are the most common types of lead-acid battery.

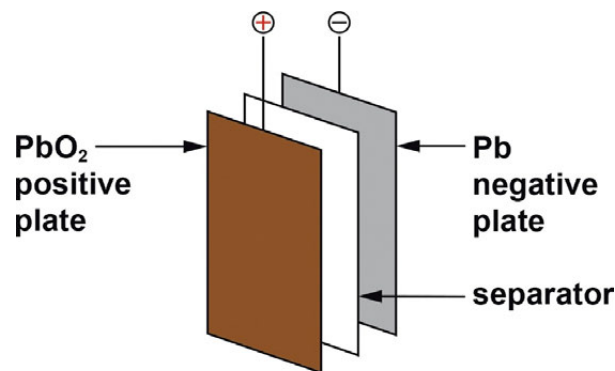


Fig. 2.7 Components of a lead-acid battery [21], Licensed under CC BY 4.0

2.3.4.2 Lithium-Ion (Li-ion)

With nearly 50 years technology development, Li-ion is well recognized in hybrid electric vehicle or Plug-in hybrid vehicle and in power grid application [70]. The anode of Li-ion batteries is comprised of a lithiated graphite or Lititanate and the cathode is Li metal oxide or a Li metal phosphate separated by electrolyte made of lithium salts as illustrated in Fig. 2.8 [21, 71]. With an efficiency of nearly 100% [62, 68], this technology is lucrative for 3Cs (computer, communication, consumer) market applications. However, the problem with Li-ion batteries is its high capital cost (\$)/kWh. With slightly distorted O₂ atoms, lithium iron phosphate (LiFePO₄) forms an

orthorhombic olivine-type structure [72]. It shows lower heat generation but it has lower energy density [73]. LiFePO_4 is most valued material in electric vehicle(EV) application [74]. In Li-ion polymer batteries, electrodes are separated by microporous poly-olefin [75]. These batteries are becoming more attractive in renewable energy and EV as a result of higher power and energy density and less memory effect [75, 76].

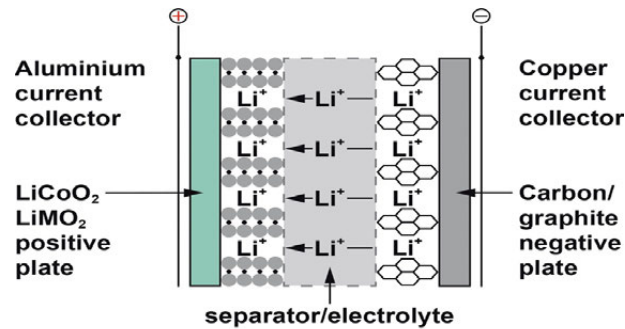


Fig. 2.8 Components of a Li-ion battery [21], Licensed under CC BY 4.0

2.3.4.3 Sodium Sulfur

Sodium sulfur has four times higher power and energy density compare to lead-acid battery with nearly a similar energy efficiency [77]. The electrodes are composed of molten sulfur (positive), molten sodium (negative) and separated by a strong ceramic electrolyte, sodium alumina as depicted in Fig. 2.9 [21]. A study in [78] shows that expensive NaS is more economical compare to cheap lead-acid for a long-term period.

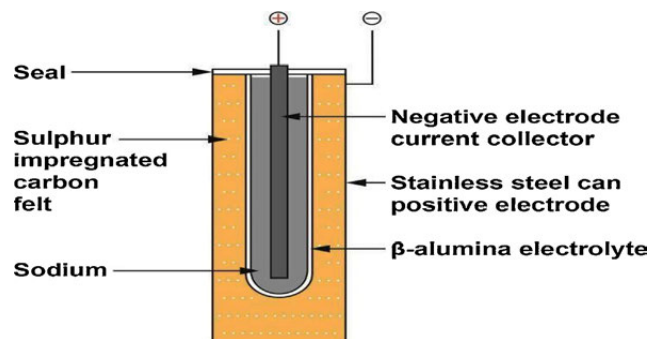


Fig. 2.9 Components of a Sodium Sulfur battery [21], Licensed under CC BY 4.0

2.3.4.4 Nickel Cadmium

Nickel cadmium batteries have over 100 years matured technology. Nickel hydroxide is used as cathode and metallic cadmium is used as anode, separated by an alkaline electrolyte as exhibited in Fig. 2.10 [21]. Nevertheless, NiCd is a robust alternative to lead-acid batteries, with higher energy density (2 times) and power density (6-7 times) [77].

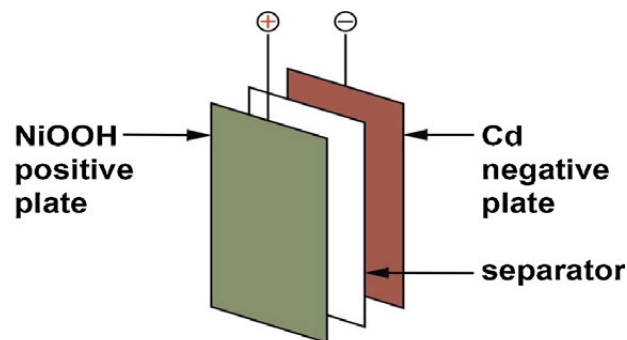


Fig. 2.10 Components of a Nickel Cadmium battery [21], Licensed under CC BY 4.0

2.3.4.5 Nickel Metal Hydride

Nickel-metal-hydride as shown in Fig. 2.11 [21] has nearly 50 years battery technology and preferably used in EVs. They possess higher power and energy density than that of a NiCd batteries [77] but with a nearly 40% lower cost/kWh [79]. As a low cost battery technology, they have replaced toxic NiCd in many applications mostly in transportation industries [80]. Nonetheless, limited service life and high self-discharge has limited their application in power system.

2.3.4.6 Zinc Hybrid Cathode

With a development of 13 years, zinc hybrid cathode battery technology by Eos Znyth® technology, is a low cost DC battery system with a price of \$160/kWh which is almost 50% cheaper than that of current lithium-ion battery technology [79,81,82]. Components of Zinc Hybrid battery is shown in Fig. 2.12 [83].

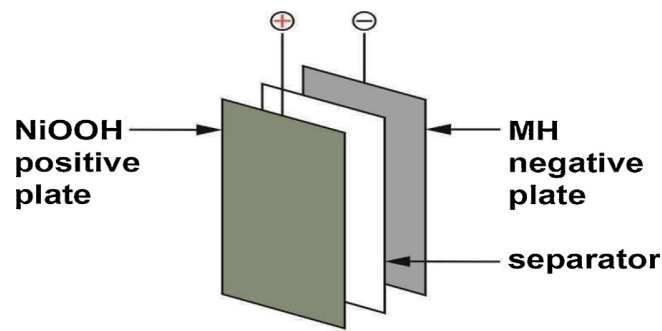


Fig. 2.11 Components of a Nickel Metal Hydride battery [21], Licensed under CC BY 4.0

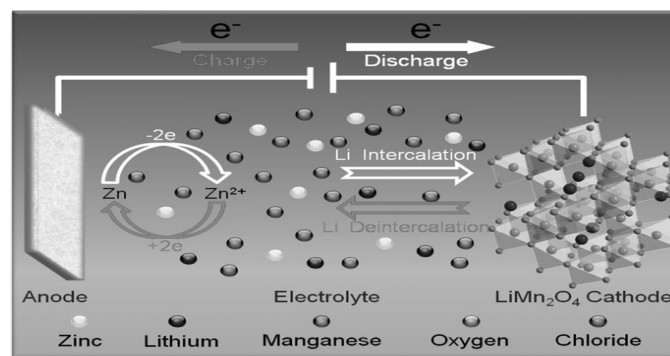


Fig. 2.12 Components of a Zinc Hybrid battery. Reprinted from [83] with permission from Elsevier

2.3.4.7 Vanadium Redox Battery (VRB)

VRB as portrayed in Fig. 2.13 [21] accumulates energy by exchanging (accepting/donating) electron between electrolytes during the charging/discharging process. They have really large cell voltage which is beneficial to acquire large power and energy than that of other redox flow battery [84]. The fast responsive VRB [85] has a round trip efficiency, including several losses, of 75% in their life time [86].

2.3.4.8 Polysulphide Bromide

Polysulphide Bromide technology is a regenerative reversible electrochemical reaction between sodium bromide and sodium polysulphide electrolytes, a polymer membrane that works as a separator between electrolytes as illustrated in Fig. 2.14 [87]. Positive

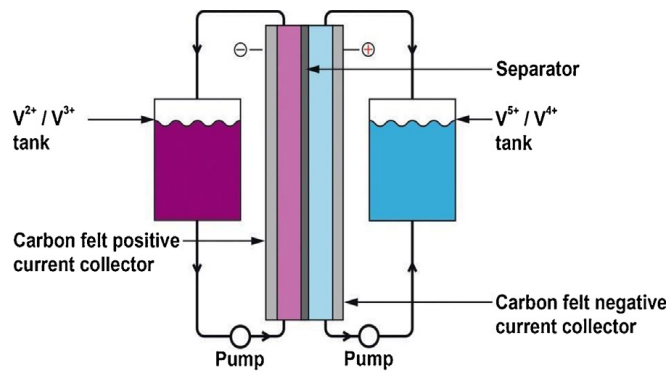


Fig. 2.13 Components of a VRB battery [21], Licensed under CC BY 4.0

sodium is allowed to pass through and the efficiency of this battery is about 75% [62].

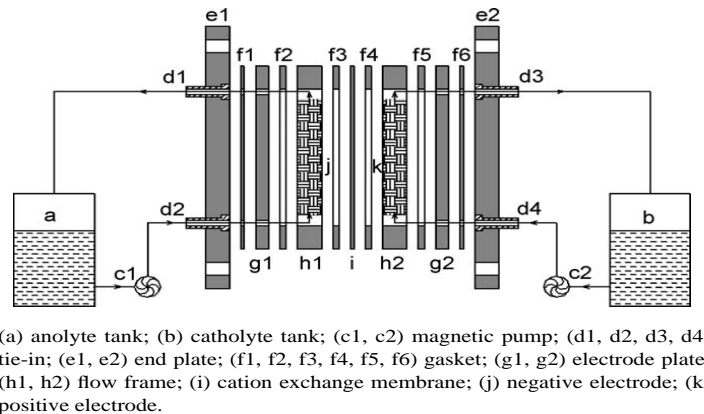


Fig. 2.14 Components of a Polysulphide Bromide battery. Reprinted from [87] with permission from Elsevier

2.3.4.9 Zinc Bromine (ZnBr)

ZnBr is of hybrid form as shown in Fig. 2.15 [21], a combination of Zinc and Bromine, two electrolytes flow through two electrodes, microporous polyolefin membrane as a separator and a efficiency of about 75% [62]. With a high energy density and low cost, ZnBr is pondered as striking for large scale application [86].

Advantages and disadvantages of different types of battery are summarized in Table 2.1.

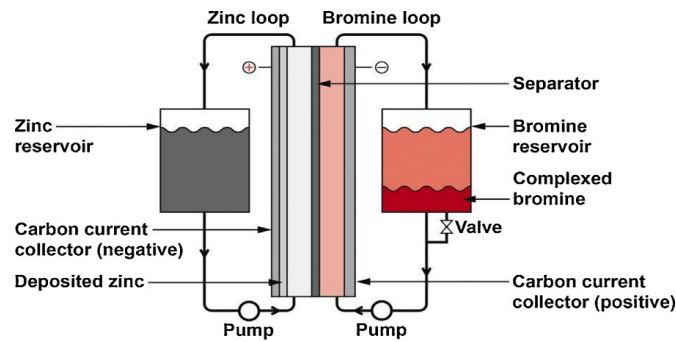


Fig. 2.15 Components of a ZnBr battery [21], Licensed under CC BY 4.0

2.4 BESS Application in Renewable Energy System

The application of BESS in the electric grid has started several decades ago. However, with the growing level of intermittent RES penetration, BESS is becoming one of the dominant energy storage technologies in the modern power system application. BESS improves reliability and provides operational adaptability to wind/PV farm. Owing to complementary behavior, a hybrid combination of solar PV and wind has drawn much broader attention globally in recent years. However, regardless of an interconnected system or hybrid islanded system, the stable operation requires support from auxiliary energy sources. A comprehensive study of existing researches on different types of BESS application in PV, wind and hybrid (PV-wind) integrated power system are analyzed and summarized in this section.

2.4.1 Output Power Smoothing with BESS

PV generation is mainly affected by solar radiation, ambient temperature, panel temperature, cloud coverage and operating characteristics. A consistent power flow to the grid from PV is always desirable and certainly it is possible to attain such expected stable power output [88]. However, this can result in rapid charging and discharging of batteries, thereby, affecting battery life cycle. In some occasion, battery storage energy management strategy allows to purchase/sell electricity to and from the grid [39]. However, this does not reduce peak-to-mean ratio (PMR) and hence an optimized

Table 2.1
Advantages and disadvantages of available battery technologies.

Battery Type	Advantage	Disadvantage
Lead-Acid	<ul style="list-style-type: none"> -Most widely used industrial battery during the past 140 years. -Batteries available in sealed and maintenance-free structures. -They are economical and yield the prime benefit for power and energy per kilowatt-hour. -They possess the longest life cycle and are recycled at an exceptionally high percentage. 	<ul style="list-style-type: none"> -Lead-acid battery is heavier compared to some of the other alternatives or types
Lithium-ion	<ul style="list-style-type: none"> -They have high specific energy. -Widely used in mobile and notebook computer applications. 	<ul style="list-style-type: none"> -Costlier than lead-acid battery. -In addition, recycling system for large lithium-ion batteries is not yet well-established
Sodium-sulfur	<ul style="list-style-type: none"> -With nearly same efficiency as lead-acid, this battery has three to four times higher specific energy. 	<ul style="list-style-type: none"> -Does not have too many commercial application.
Nickel-cadmium	<ul style="list-style-type: none"> -This battery is dependable and able to operate in a range of temperatures. -Great tolerant to abuses. - Behaves competently following long durations of storage. 	<ul style="list-style-type: none"> -This battery is three to five times costlier than lead-acid. -Its substance are lethal. -The recycling infrastructure for large nickel-cadmium batteries is mostly defined.
Nickel-metal hydride	<ul style="list-style-type: none"> -This battery is reliable and lightweight. 	<ul style="list-style-type: none"> -The alloys in the Nickel-metal hydride battery are 25 times costlier than lead acid battery. -Nickel has been classified as a carcinogenic and no significant recycling capability exists.
Vanadium redox battery (VRB)	<ul style="list-style-type: none"> -Provide fast response. -It has higher power and energy density than that of other available redox flow batteries. 	<ul style="list-style-type: none"> -Relatively low energy density has limited the development in stationary application only.
Polysulphide bromide	<ul style="list-style-type: none"> -Practically zero self-discharge makes suitable for long term use. 	<ul style="list-style-type: none"> -Large-scale practical application is limited by technical difficulties in storage technology.
Zinc bromine (ZnBr)	<ul style="list-style-type: none"> -This battery has high energy density than that of lead acid type batteries. 	<ul style="list-style-type: none"> -Low efficiencies compared to the other traditional battery technology.

energy management strategy is suggested in [89] that reduces PMR in accordance with the variable sizes of integrated battery capacity. Moving average method determines the average generation of system, compensates the error with less storage capacity and ensures better load supply [90]. However, this method has a memory effect that results

in frequency switching of BESS producing an increased energy losses and thus reduces battery life cycle compared to ramp-rate control method [91]. The value of window size defines the degree of smoother output (ramp-rate in Watt/min) i.e. longer window size reduces the change of ramp/min. An approach for PV output smoothing with BESS is shown in Fig. 2.16. BESS operates in charging or discharging mode depending on the surplus or shortfall in PV energy to smooth out PV power and meet the desired load demand. One of the main drawback with this kind of approach is that BESS undergoes huge number of charging/discharging cycle that affects lifespan of a battery.

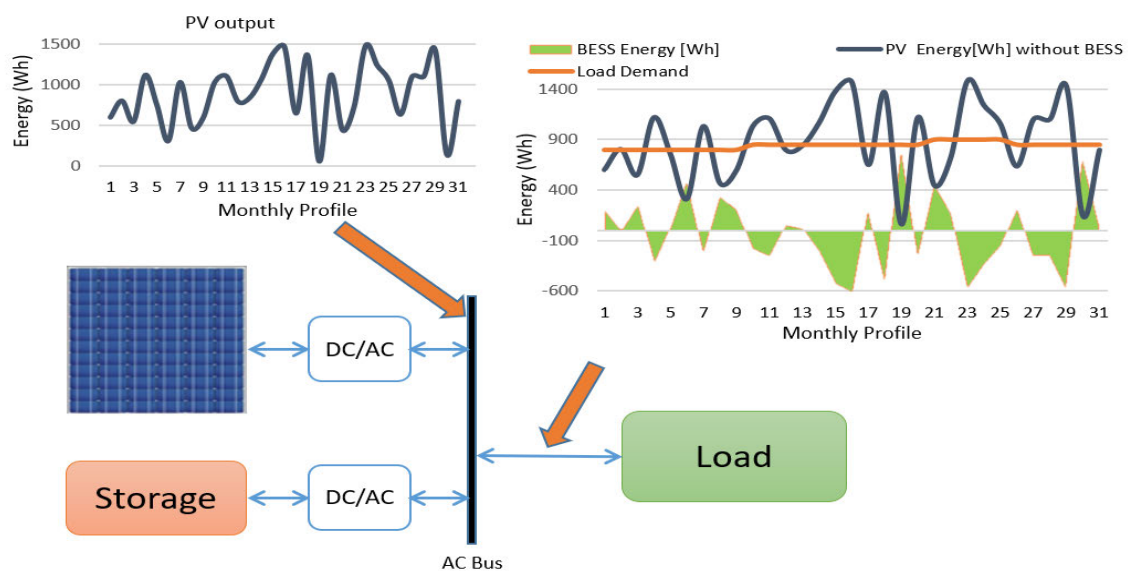


Fig. 2.16 PV output smoothing with BESS

Battery storage plays the foremost role to secure power leveling following wind variations. SOC status of battery is a crucial measure of providing the capability of output power smoothing at desired level and duration. While providing fluctuation smoothing service, a SOC feedback method is presented in [92] to avoid overcharging/discharging. In favor of maintaining a constant wind power output at its terminal, battery storage system can store/supply surplus/shortfall in wind power system [38]. In order to maintain proportionate economic expenditure and smoothing performance, an optimal sized and fuzzy controlled charging/discharging strategy for BESS is proposed in [8] that concluded BESS as a cost-effective solution for wind farm owners. A constrained charging/discharging of multiple battery sets can prolong battery's lifespan [93], however, the actual implementation is essential for validating the

proposed method.

A discrete Kalman filter is incorporated for eliminating the bias errors and predicting the actual power of PV and wind that reduces the requirement of BESS power for providing smoothing service [94]. Battery state-of-health (SOH) can also be incorporated for improved battery health while smoothing output with the coordinated regulation of battery power output [95]. In a SOC-based adaptive power control strategy, the study of initial SOC (such as 10-90%) variation demonstrates detail battery performance in a different SOC (overcharge/over-discharge) situation [96].

2.4.2 Peak Generation/Load Shaving

Peak generation and peak load demand in industry, commercial and residential buildings do not often coincide. Battery storage system can store excess energy during peak generation and supply the stored energy throughout peak demand period at later time of the day. Additionally, battery can further be charged from the grid following low price period.

BESS installation facilitates the maximum use of available PV generation by peak demand smoothening [4]. BESS can store excess energy during the day time and utilize stored energy in the evening to support peak load demand [97] and significantly reduce the peak power flows in the network [98]. The battery charging/discharging rate is updated in response to the actual SOC with the desired SOC level [99] and with minimized cost and power loss [100]. In some cases, peak load demand in a feeder may not align with the utility-wide peak demand and customer owned BESS can perform satisfactory peak reduction if sufficient battery capacity is available [101]. A typical BESS operation for peak generation shaving is illustrated in Fig. 2.17. BESS can store the surplus PV energy during the daytime that can be used later on in the evening to facilitate peak load demand reduction.

Demand peak-cutting is extremely important to reduce a definite point of peak power consumption in commercial buildings, factories and in residential buildings that might

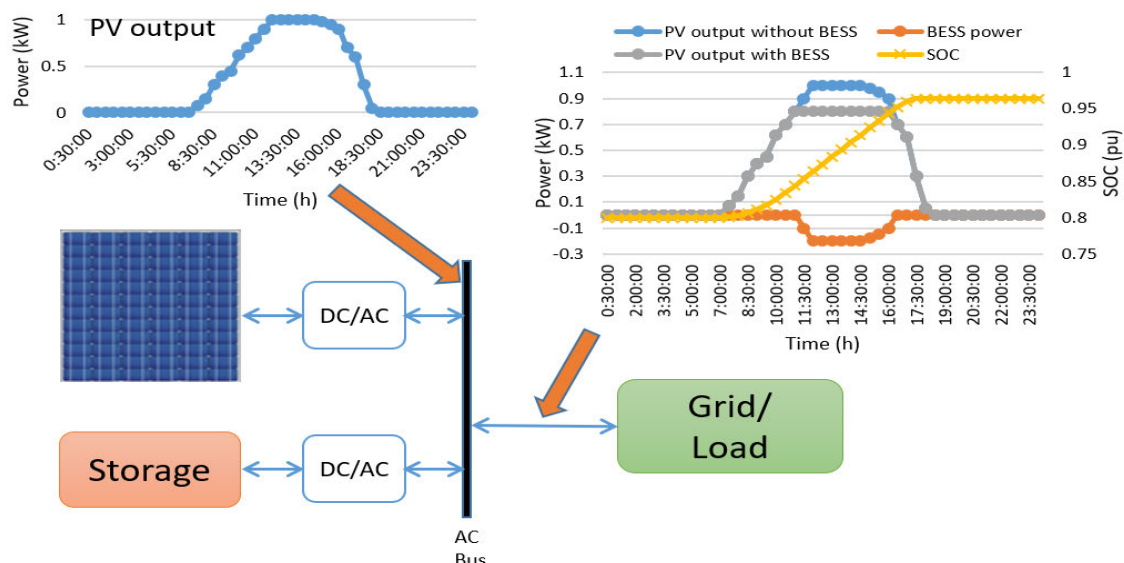


Fig. 2.17 PV peak generation shaving with BESS

cause an extra cost to consumers and the adoption of BESS can considerably reduce users electricity bill [102]. However, in response to deregulated and competitive electricity distribution system, peak time energy price may not be much higher than that of regulated price, thereby affecting the economic benefit of battery storage system in such cases.

2.4.3 Voltage Regulation

To ensure nominal voltage remains within the operating limit, fluctuating renewable energy generations must follow strict voltage regulation rules. Battery storage responds quickly by charging/discharging the battery by following voltage sags/swells and taking the initiative of maintaining steady voltage source in power system. Voltage surge arises during PV peak generation periods with little or no load demands resulting in a power flow in reverse direction to the network. However, a large-scale distributed generation unit at a single connection point can also result in voltage violation [103]. A variety of solutions have been proposed to overcome such undesirable effect of large PV infiltration in low voltage distribution network [104–108]. PV curtailment can be one of the solutions but this will reduce maximum use of PV generation capacity with the consequent of minimizing financial benefit [104]. Other adopted solutions are: PV converter reactive power compensation [105], installation of voltage regulator [106] and

transformer tap adjustment [107]. Grid reinforcement may be another solution that can reduce feeder losses but it is a costlier solution [108]. BESS can be used to consume surplus PV energy during the peak generation and thus reducing the voltage rise impact of PV in the grid as shown in Fig. 2.18. According to the network requirement, BESS can be designed to regulate grid voltage within the allowable limit by consuming surplus energy or regulating reactive power.

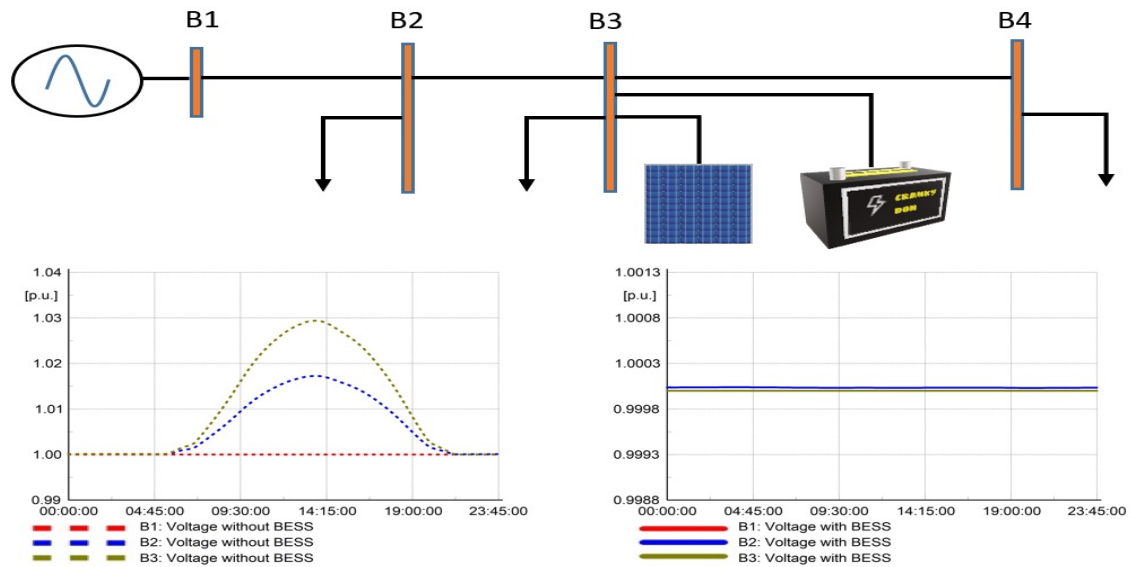


Fig. 2.18 Voltage regulation with BESS in a PV integrated system

To deal with voltage rise/drop that emerges at peak PV generation or peak load demand, battery storage system plays an important role [109–115]. Battery charging/discharging can be controlled by local droop method in regard to battery SOC [109], monitoring PCC voltage [110] and using measurements from distributed controllers [111]. Battery storage system may support increased PV penetration while maintaining allowable voltage limit [112], reducing transformer operational stress and resistive power losses [113] and to achieve the most functional combination of PV and BESS in mitigating voltage regulation constraints [114]. BESS active power [111] or priority on BESS reactive power coordinated with BESS active power can be designed for providing voltage regulation [115].

The overvoltage is possible to be controlled considering wind power operation below maximum power point (MPP) but this will incur unwanted energy loss. Few research is available in wind farm voltage support utilizing a battery storage system.

Battery charge/discharge is regulated to control DC-link voltage in a wind farm at varying wind speed conditions while maintaining overall system efficiency and increase the lifespan of battery [116]. Voltage regulation is achieved by controlling both real and reactive power [117] and SOC based active power and dead band based reactive power control [118].

Peak generation associated with PV during day time and wind at night time may create voltage stability issues (voltage rise/drop) for outreaching the power limit. Typically battery system is integrated with a separate conversion system to store and supply energy. However, in a PV-wind-BESS hybrid system, based on the configuration, PV inverter can be utilized to charge/discharge battery at night to control voltage rise issue that arise from wind farm surplus energy [119]. An optimum placement and size of BESS is imperative for improved voltage regulation and prolonged life of the battery [120].

2.4.4 Frequency Regulation

The power system inertia decreases reciprocally with increased share of renewable energies. Hence, renewable power plants must adjust their output power proportionally to respond against frequency deviation. The PV controller can be exploited in order to provide frequency control which is subjected to over-frequency support through PV curtailment [121]. Under-frequency support is possible to carry out but this requires PV to be operated at a point other than the maximum power point (MPP) [122]. Since, PV output is intermittent in nature and weather dependent, PV plants need to arrange dispatchable auxiliary energy source to support system frequency whenever needed. Batteries are widely studied storage arrangement to support system frequency in a PV plant. The battery can be charged during peak generation and power can be supplied back to the system whenever low PV output is available. Battery storage system reduces power fluctuation and provides fast response to frequency deviation [41]. The combined control of PV and BESS can also be an alternative for frequency regulation in which BESS injects active power in the case of PV power deficit [123]. The power-frequency

droop (P/f) characteristics as in (2.1) can be fixed type [123] or adaptive type, nevertheless, an adaptive P-f demonstrates smoother transitions in various control strategies [124]. Coordinated optimized control of frequency control and self-consumption for battery recharge can be technically and economically demanding which requires a trade-off between them [125]. The amount of active power regulation of BESS (P) is determined by the droop value R_{P-f} with respect to the changes in frequency deviation (df) from the nominal set point as in (2.1).

$$P = \frac{df}{R_{P-f}} \quad (2.1)$$

BESS not only reduces the frequency drop but also diminishes frequency oscillation compared to without a BESS. Conventional generators are getting replaced by large-scale wind power plants and therefore wind power plants must commence the duty of frequency regulation support in future. The participation of Wind farm in frequency regulation has been evidenced via inertial control [126] and pitch control [127]. Mainly, low frequency support is controlled by integrating pitch control mechanism and high frequency support is controlled by battery charging/discharging accordingly [128]. Battery storage system can provide system frequency support on the basis of power imbalances [129] for severe under-frequency situation [130]. To regulate system frequency, battery stores surplus energy thereby providing peak shaving facility, supplying stored energy throughout the low wind period [36]. However, it is argued in [131] that the coordinated control provides better frequency regulation compared to individual BESS or wind turbine control due to the need for large power in a short-term. Nevertheless, in a coordinated control approach, the wind farm can regulate its output for regulating frequency and battery storage will compensate if regulation demand is not satisfied [132]. The effective utilization of BESS allows reducing the amount of unexpected energy consumption while preventing wind fluctuations and provide additional regulation services without affecting the lifespan of the battery. However, extra benefits and economic advantages are subjected to accuracy in wind power estimation, market price and battery technology [133].

The shortcoming associated with wind and PV are dependent on unpredicted wind speed and irregular solar radiation. Thus intermittent nature renewable generation often result in difficulty to meet load demand that greatly affects system frequency. In addition, rapid oscillation in hybrid power output might lead the system to instability. Frequency is possible to be controlled by sliding mode regulated wind turbine pitch control and battery system [134]. Battery storage (over/under-frequency) and PV (over-frequency) may provide primary frequency support and diesel generator can be used to provide secondary frequency support for long term frequency regulation service [135]. Adaptive SOC can be incorporated in the feedback control for regulating high frequency oscillations where generators provide low frequency oscillations that minimizes stress on the conventional generators providing frequency control [136].

2.4.5 Voltage and Frequency Regulation

Referring to temporary or permanent island operation, following a fault in the system and passing clouds, BESS, as an active and reactive power contributor is much more reliable compared to other available conventional energy sources, for instance, diesel power source, to satisfy generation-load balance. An optimized operating scheme [137], single master operation master/slave control [138] and PI controller based control [139] strategy is suggested to support ancillary services such as voltage and frequency to a PV system considering dynamic behavior of the network and connected loads [137, 139]. The batteries can be charged either from PV surplus energy [137, 139] or grid following a low energy price period [137].

In a grid connected mode, MG operation might be needed in case of a grid fault. Therefore, an isolated system must be able to maintain nominal voltage and frequency to guarantee reliable operation. Battery storage system improves dynamic performance by scaling down system voltage and frequency fluctuation [140]. VSC tracks the active and reactive power following the grid demand, the available battery energy [141] and wind speed changes to regulate voltage and frequency of the studied network [142]. In some cases, an additional dump load might be useful to dump excess energy beyond the battery

capacity to be stored [143]. BESS for voltage and frequency regulation in 9-bus system are shown in Fig. 2.19(a-b) which demonstrates that BESS can improve grid voltage and frequency by regulating its active and reactive power as illustrated in Fig. 2.19 (c).

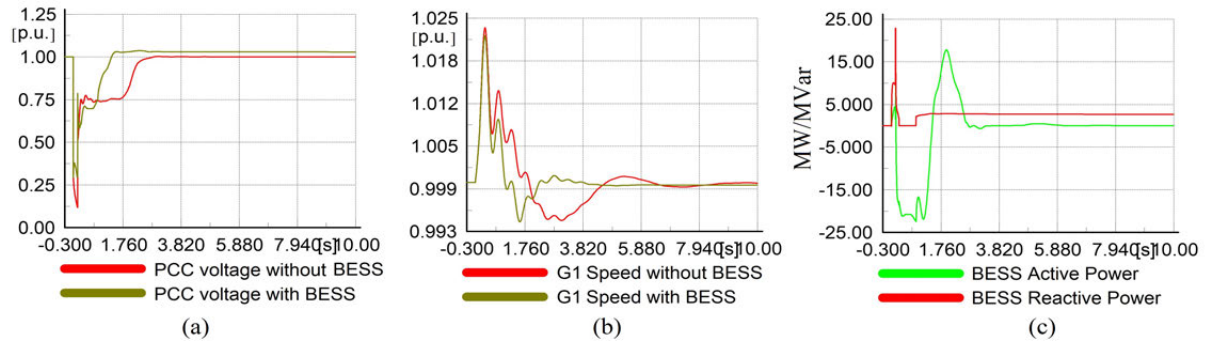


Fig. 2.19 Voltage and frequency regulation with BESS in a wind integrated 9-bus system; (a) PCC voltage (b) Generator speed (c) BESS active/reactive power

Intentional or unintentional islanding operation requires voltage and frequency stability to serve the loads continuously. Considering intermittent nature of PV/wind in an islanded hybrid system, fluctuation in voltage and frequency in response to load-generation imbalances, a battery storage system may enhance power quality of the system. The controller will detect the power deficit and control the battery to maintain DC-link voltage and system frequency by providing required power [144]. A combination of frequency control by BESS and reactive power control by the PV/wind converter is an alternative to maximize BESS use for frequency regulation and PV/wind regulated voltage control in a MG [145]. Different controller may have technical benefit over another such as fuzzy controller may outperform PI controller under different scenarios with advanced dynamic response and minimum overshoot [146]. However, rigorous assessment of operational complexity, technical benefits etc. need to be addressed clearly to draw any conclusion.

2.4.6 PV/Wind Plant Dispatchability

Non-dispatchability of RES in comparison to dispatchable conventional power plants; acts as the main hurdle for RES to be integrated in a large scale. RES dispatching ability influences estimated power production to manage load demand in real time. RES plant

output power is estimated from weather forecast on intra-hour to upto 39hrs [147]. RES should have sufficient feasibility of dispatchability due to forecasting error and storage systems are recognized as the utmost solution in such circumstance. Moreover, electricity authorities in some countries, such as in California in the US [148], UK [149] and Italy [150] are impelling incentives and obligatory specifications to ensure RES penetration without impacting system reliability by means of encouraging storage system establishment.

Battery storage improves PV plant dispatchability by facilitating peak demand management, minimizing losses and charge/discharge cycles of battery [7]. Dispatchability schedule to determine battery charging/discharging operation at a minimum cost may be based on forecasts generated one day ahead [7] or 1h ahead [151] which largely depends on the dispatch period and renewable generation types. Large size of BESS capacity is required in order to minimize the error between the forecasted PV and actual PV power dispatch. BESS can be dispatched to constrain PV output within the allowable maximum and minimum limit as shown in Fig. 2.20.

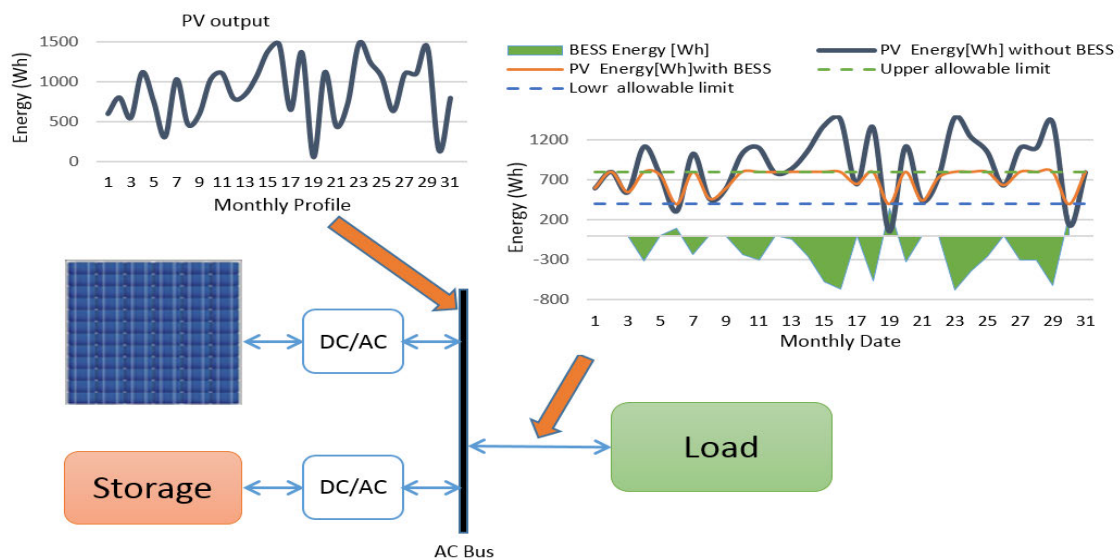


Fig. 2.20 Dispatched PV power with BESS

Battery storage system, as a simple charging/discharging scheme, provides the flexibility to store surplus energy that can reduce forecast error in real time wind power and contribute in dispatchability improvement of wind farm [152]. Dual BESS can provide added safety to BESS operation [153]. However, dual BESS may bring

additional costs compared to single BESS topology. Optimal coordinated planning provides efficacious handling of non-Gaussian wind power unpredictability [154] and economic dispatch opposed to battery cost through an effective coordination and optimization [155]. BESS not only can minimize overall costs but also contributes to reducing carbon emissions from the conventional generation units by supporting higher wind penetrations without raising the stability concern [156].

The ultimate purpose of BESS usage in wind farm dispatchability improvement is to smoothen wind farm output power at a given dispatch period i.e. 30min or hourly dispatch etc. [157]. Battery SOC plays key role in power mismatch compensation by using battery storage to improve the dispatchability of wind farm [158]. When SOC is the primary objective for dispatch scheduling, dispatchability is largely reliant on battery capacity. Battery charging/discharging efficiency also acts as major determinant of dispatchability improvement [159]. To match load demand by hybrid system output, BESS contributes in increasing dispatchability of the hybrid system, reduce the spillage rate of PV/wind energy when participating in dispatching event and thus reducing the costs of the system [160].

2.4.7 Fault Ride Through (FRT)

Typically, following a grid faults, DG units are removed for safe operation but removal of large size PV plants will affect negatively to system stability in such situation. Therefore, PV generation plants need to have an adequate FRT or Low Voltage Ride-Through capability to remain connected during faults period and provide active power immediately following fault clearance. Unlike in a wind power plant, a few studies are available on PV FRT capability because of small capacity of PV and thereby neglecting the negative impact on the grid.

In order to provide FRT service during fault period, battery storage is designed to consume surplus active power during the fault and possibility to contribute in reactive power support to control DC-link voltage [161]. The DC/DC converter operates in buck mode to charge battery from available extra charge at DC-link [162]. However, if DC-link

voltage exceeds the DC bus threshold or if SOC limits exceeds allowable limit, battery system should stop functioning [163].

With the increment of large-scale DG units, disconnection of DG units tend to increase the vulnerability of electric grid. Therefore, recent grid codes considered such conditions and included FRT requirements for wind farm to be connected in existing electric grid. To enhance the response of faults in wind turbine, the coordination of battery storage system and wind turbine is essential [164]. Battery storage reduces over-current during a transient fault in the system and supports DC-link voltage converters to improve dynamic stability [165].

Following a transient disturbance in the system, distributed renewable energy should remain connected to avoid catastrophic failure of the system. Thereby, PV and wind farm must ensure fault ride through capability to avoid possible instability in the system. Fault ride through capability improves the overall system stability [166].

2.4.8 Key Findings of BESS Application in PV-Wind-BESS Energy System

Thorough review of existing literatures unfolds the importance of BESS application in renewable energy system to provide required active and reactive power support. The key finding of these studies are summarized as follows:

- The damping of active power oscillation is generally provided by tracking output power as a reference and BESS supplies the required power imbalances. In other cases, voltage/frequency or both is used as an error signal for BESS contribution.
- The most commonly used battery technologies are lithium-ion, lead-acid, sodium-sulfur and flow batteries because of their technical advancement and accessibility in MW range capacity.
- Direct integration of batteries on DC side of DFIG back-to-back converter or on DC converter terminal of a PV may eliminate the necessity of an additional PCS,

associated losses and thus minimize related costs. However this may require complex design to improve converter's robustness with high power/energy transfer capability.

- The adoption of battery storage system to reduce forecast error may not be always a cost effective approach [147]. The main determinants of cost-benefit are the investment costs of battery, round trip efficiency and service life.
- A large capacity of BESS is essential for reducing the error between the forecasted and the actual generation from RES which requires techno-economic justification for the mandatory investment [151].
- The performance of smoothing is ameliorated by battery charging/discharging rates and thereby smoothing of high ramp rates may result better output profile but at a cost of quicker battery aging.
- Several minutes/hourly based dispatch strategy improves the charging/discharging profile of batteries than that of a constant output power smoothing and thus improves the life span of battery.
- An appropriate control of battery charging/discharging is able to maintain a stable SOC at the end of the day and increase the life-cycles of batteries [137].
- Dual-BESS combination may significantly improves battery charging/discharging management and is capable of reducing the number of charge/discharge cycle, however this will incur more cost due to additional battery set to maintain enough capacity of BESS [153].
- SOC based battery control design is crucial to avoid battery overcharging/discharging and adversely affecting battery lifespan [96]. However, with high forecast error, SOC feedback based control strategy could be unsuccessful in maintaining desired smoothing performance [92] over the long period.
- In general, the improvement in power quality, stability, reliability, dispatchability and fluctuation reduction is limited by the battery capacity.

- Coordinated and adaptive control algorithms always provide more robust performance and better power tracking [154].
- VRB can be economically more viable for the same level of smoothing service than the lead-acid battery owing to their longer life span, lower maintenance costs and suitability for frequent alteration due to non-constraint characteristics of charge/discharge switch [8].

2.4.9 Key Challenges of BESS Application in PV-Wind-BESS Energy System

Comprehensive study of BESS application in renewable energy system reveals the potential challenges associated with BESS installation, efficiency of BESS components and energy regulation policy. The key challenges are summarized as follows:

- Optimal sizing of battery in PV smoothing is greatly affected by the maximum level of ramp-up and minimum ramp-down boundary. This often results in difficulty in finding an appropriate size specially when the occurrence and level of both ramp-up and ramp-down events differs by a large margin [6].
- Battery energy efficiency and lifespan plays an enormous role in optimal sizing of BESS. Thus, an improvement in battery technology is imperative to bring down battery costs.
- Sometimes a simple control approach can be effective for smoother PV output but it may be subjected to memory effect and result in reduced life cycle due to persistent battery switching [91].
- The constraint charging/discharging of an individual battery can be economically advantageous but the actual implementation of the proposed method through a single power conversion system is a demanding and complex task which requires validation [93].

- The inaccuracy between the forecast and real-time production of RES power output varies by a large margin in 24h ahead market than 1h ahead market. This results in the commitment for large BESS capacity in a day-ahead market that increases the capital cost for installation and hence, techno-economic feasibility is demanding for participating in such dispatchable market [151].
- Complex business contracts between small scale consumers and power distributors often retards small scale RES penetration on the grid. Hence, an interactive and friendly negotiation between the network operators and customers are imperative for supporting small scale RES generation.
- The installation cost of BESS is quite high so far which impedes the attraction of BESS adoption by RES farm owner. Therefore, a cost-efficient and high efficient BESS technology is required to minimize the impediment of BESS implementation.
- BESS can be directly connected to the DC-link but this lacks the control of battery. To provide the regulation capability, battery can be coupled to the desired bus via DC/DC or DC/AC converter. However, this will add the converter's cost.
- An appropriate selection of DC-DC converter (unidirectional/ bidirectional) is needed to handle the required power conversion (low/high-power/energy capacity) efficiently.
- In the case of multiple BESS structure, a proper power allocation between individual batteries is always a demanding and complex task. Decentralized battery sets with multiple SMs provide better operational flexibility than the centralized converter module with long battery strings. Nevertheless, an array of converters will incur higher costs.
- Wind turbines/PV panels are connected through power electronic converter (PEC) to the grid, therefore improvement in PEC control techniques may facilitate efficient power management and reduce converter losses.
- Accurate forecasting is able to alleviate proper planning of battery charging/discharging to ensure an achievable unit commitment to the grid with

economical battery operation. However, it is often difficult to predict accurately and hence, improvement in predicting irradiance and wind speed is essential for BESS management.

- The requirement of battery power is highly unpredictable than that of battery energy which causes troublesome in real-time BESS operation.
- Potential dynamic features of wind turbines are often ignored to reduce complexity in calculation, but this may hinder rigorous output therefore both slow and fast dynamics need to be considered during designing stage.
- Dynamic impact of battery conversion efficiency to the grid support is often ignored. There is a need to consider converter's conversion efficiency including variable charging/discharging resistance with respect to battery SOC in real-time.
- Most commonly used controllers in a BESS control are PI, Proportional (P) and Fuzzy Logic Controller. Comparative study of these available controllers or new controller techniques need to be explored to find the better output response of the grid.
- The impact from the failure or disturbances in battery storage systems to the connected network is open for investigation.
- A convenient battery SOC recovery is pivotal for ensuring sufficient battery capacity for participating in the energy market or stability enhancement. This is particularly challenging in terms of stability performance requirement versus the economical charging of battery.

2.5 Shortcoming of Current Literature

Disregard of progressive research in this field, ample opportunities are available to accomplish further research in the applications of BESS in renewable energy systems. BESS can be adapted for various applications by modifying its closed loop feedback control strategy and incorporating a suitable battery SOC management and SOC

recovery strategy. These demands further research concentration for improving the performance of battery integrated grid. BESS in an EV charging station can also be a part of energy management that may allow to reduce transformer overloading and provide grid services.

2.6 Conclusion

With the proliferating nature of RES penetration, the urgency of minimizing the adverse impact of RES has drawn significant consideration in recent years. Considering this, an attempt has been put forward to present BESS application in RES integrated power system and how they have been adapted for diminishing the adverse impact of RES.

The literature survey points out that BESS is widely used to regulate active power or simultaneous active and reactive power while participating in minimization RES impact in grid voltage and frequency regulation. In addition, as compared to smaller window size for smoothing, the larger window provides better ramp profile per minute but this requires larger battery capacity to be installed. On the contrary, BESS employment for reactive power management is not yet widely acknowledged both in practice and academic research. The concern arises due to the fact that the fractional use of BESS (reactive power can be provided by any other shunt devices with lower cost) is not economical as compared to the use for active and reactive power.

Integrating battery to the DC-link of DFIG generator/PV can be a cost-effective solution to control active/reactive power supply. However, this has a shortcoming of DC-link voltage to be regulated by battery SOC that needs to be large-sized or limited SOC operating range for safe operation. A separate DC/DC converter can provide better operational flexibility but this will incur an additional cost.

In this thesis, various applications of BESS for grid stability enhancement with the incorporated RES and in the EV charging station (EVCS) will be investigated. However, at first, the frequency regulation capability of wind turbine technology needs to be

investigated to identify the potential of RES for stability support. Therefore, the next chapter is focused on regulating the power output of the wind turbine in frequency regulation under multiple contingencies. The pivotal point is to improve the control technique of wind turbine regulation for stability enhancement.

Chapter 3

Frequency regulation of an isolated MG with incorporated multi-gain droop and fuzzy regulated pitch angle control of DFIG

This chapter contains the following publication - U. Datta, J. Shi and A. Kalam, “Primary frequency control of an islanded microgrid using integrated dynamic sectional droop and fuzzy based pitch angle control for wind farm,” *Journal of Electrical Power and Energy Systems*, vol. 111, pp. 248-259, 2019.

3.1 Introduction

In the 21st century, a soaring tendency in wind energy penetration can be found in power systems, essentially due to the advancement in wind technologies, the reduction of costs related to wind generation and renewable friendly legislations by the government [167]. In the midst of many wind technology, DFIG is the most prevailing technology due to their active and reactive power regulation capability [168]. The

variable nature of wind turbine output creates several challenges to the security and reliability of power systems. In addition, base-load units experience rapid power fluctuations in order to minimize the influence of power deviation of wind turbine and maintain stable frequency. At a wind speed of lower than the rated speed, DFIG works in maximum power point tracking (MPPT) [169] and the pitch angle control regulates wind power output at rated wind speed. DFIGs are linked to the grid via power electronics interface which restricts the provision of built-in inertia support by the DFIGs to the grid. This causes critical complication when there is a temporary power imbalances in the grid. Large synchronous machines usually fulfill any power imbalances but in an isolated MG, such arrangement is often limited to get in order to maintain stable grid operation. Hence, necessary actions needs to be taken for wind farms for contributing to the grid frequency control.

Involuntary P-f regulation is available in many countries. However, the prerequisites of p-f regulation varies according to the country and transmission system operator. For instance, Canadian Independent Electricity System Operator requires 10% increment of wind farm power output during a frequency drop event [170] whereas Danish grid requires a 10%-100% regulation of wind farm capacity for p-f control [171].

Many research works have proposed various droop and inertia control techniques to provide frequency support to the grid by the wind turbines. Emulated inertia is recognized to be a potential method of wind turbine control for regulating frequency that can significantly minimize the rate-of-change-of-frequency (ROCOF) value [172]. In addition, smaller frequency drop and the faster restoration of grid frequency can be achieved with the utilization of wind turbine's emulated inertia capability [173]. However, it is found in [174] that emulated inertia is not effective in improving frequency response. In some cases, droop control can be a competent alternative to emulated inertia and reduce frequency drop and ROCOF [175]. The comparative performance analysis of emulated inertia and droop in [176] concluded that emulated inertia is able to provide reduced frequency drop but droop can contribute in faster recovery and less steady state error. In order to maximize the benefit of individual control approach, researchers have suggested the combination of emulated inertia and

droop method for participating in frequency control [177]. The combined control contributes to lower ROCOF, faster recovery of system frequency and improved steady-state value [178].

Frequency regulation can be accomplished by curtailing or increasing the stored kinetic energy of wind turbine temporarily and hence it needs to be operated at a point other than the MPPT. This phenomena is known as deloaded operation and suggested by many researchers [179, 180]. Various pitch angle control approaches have been recommended in enhancing DFIG performance such as proportional [181], PI [182], proportional-integral-derivative (PID) and non-linear H_∞ [183] for tracking the expected power output and enhance the stability in the case of contingencies event. Fuzzy logic based FLC [184], fuzzy-P and fuzzy-PID [185] controllers are presented for regulating and smoothing power output. The authors in [186] suggested that torque control provides faster response than the pitch angle control. Understanding the comparative advantages of pitch angle and torque control, a coordinated control is found to provide better stability performance as demonstrated in [187]. Also, the combined control of emulated inertia and pitch angle control [188], droop, emulated inertia and pitch angle control [189] are found to minimize frequency variation and exhibit enhanced output response.

Several studies have pointed out that conventional linear droop gain has a certain level of limitation in term of providing better system performance. Hence, variable gain scheme such as online tuned droop gain and PI controlled pitch angle control [190] and ROCOF adapted droop gain [191] are a few of the many suggested methods to minimize frequency drop and avoid the risks of vulnerability of the grid. A combined droop and emulated inertia [192] and time varying droop-inertia gain [193] are recommended for providing frequency support. Nevertheless, any information on pitch angle control mechanism is not available. On the contrary, a time reliant variable droop gain proposed in [194] may not perform satisfactorily in variable network operating conditions. Two separate droop gains in the case of wind speed below and above the rated speed are proposed in [195]. However, all the aforementioned studies of primary frequency control (PFC) with wind turbine lack the coordinated control of dynamic droop and

emulated inertia for power control and FLC regulated pitch angle control.

This chapter proposes a multi-gain droop with emulated inertia control for producing power reference and FLC controlled pitch angle control which is unique in the sense that the intensity of power margin is regulated with the level of frequency deviation. The objective of this chapter is on the design of a coordinated sectional (multi-gain) droop control with emulated inertia of a DFIG based wind turbine for providing frequency control in an isolated MG. The sectional-droop gain is split into multiple regions i.e. high and low sensitive regions depending on the sensitivity of frequency alteration from the nominal value. The coordinated control is then inspected with the conventional PI and the proposed FLC governed pitch angle control mechanism. In addition, a high power margin of 25% for the wind speed of above or equal to the rated speed and 15% for the wind speed of lower than the rated value are selected to avoid undesired higher fluctuations during lower wind speed.

OPAL-RT, a Real Time Digital Simulator (RTDS) based real time simulation is executed to validate the efficacy of the recommended multi-gain and FLC control methods. It is shown that the suggested sectional droop gain method demonstrates remarkable performance than the traditional fixed droop gain approach. Not only the smaller frequency drop and rise but also the improved frequency oscillation damping is achieved by the proposed method. Moreover, the suggested sectional droop gain performs equally better regardless of PI or FLC regulated pitch angle control control than with the fixed droop gain. The same robust performance capability of the proposed control approach can be claimed for a wind speed of lower or equal to the rated value.

3.2 Conventional Fixed Droop and Emulated Inertia Control Method

Large synchronous generators (SGs) usually take care of the temporary power imbalances and maintain the grid frequency. With the existence of physical inertia of the machine, SGs is able to provide inertia response and followed by primary, secondary and tertiary

frequency control as shown in Fig. 3.1 depending on their droop settings and available capacity.

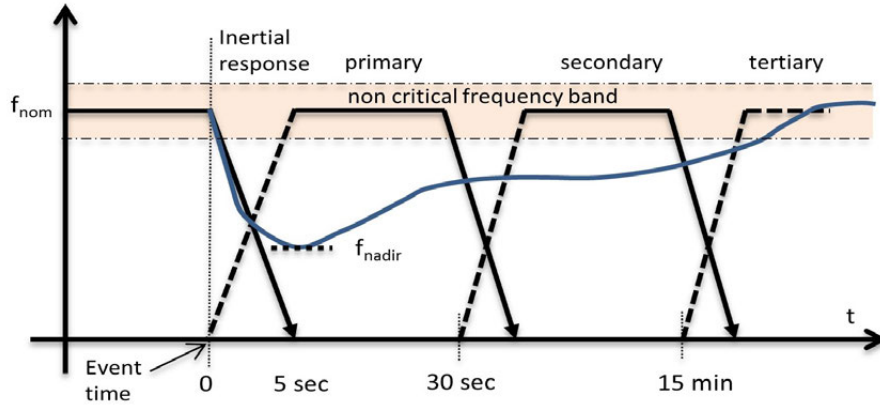


Fig. 3.1 European Network of Transmission System Operators for Electricity (ENTSO-E) defined frequency stages [196]

The advancement in power electronics interface of wind turbine with the grid lets to the modification of the DFIG controller to integrate droop-inertial control loop and regulate DFIG power output accordingly. This provides DFIG to emulate the characteristics of a SG and contribute in frequency regulation. In order to regulate grid frequency, DFIG power needs to be adjusted and this is known as deloading. The inertial power of wind turbine ΔP_{IE} can be written as in (3.1):

$$\Delta P_{IE} = 2H_G \frac{d}{dt} (f_{grid} - f_{ref}) \quad (3.1)$$

where, H_G is the inertia gain, f_{grid} is the grid frequency and f_{ref} is the reference frequency. To avoid unwanted variation of DFIG power output during emulated inertia support, a ± 0.001 pu of deadband is added in the emulated inertia loop as shown in Fig. 3.2 [197]. The contribution of emulated inertia power is regulated by the positive and negative value of frequency error and limited by the inertia gain of 0.2pu. The emulated inertia has large impact at the beginning of the fault event but has less contribution with increasing post fault time. The droop control has larger impact on PFC and to avail this option in the DFIG control, droop control loop is integrated with the emulated inertia control loop as illustrated in Fig. 3.2. The droop control is activated beyond the operating limit of ± 0.002 pu from the nominal value and this can be

calculate as in (3.2):

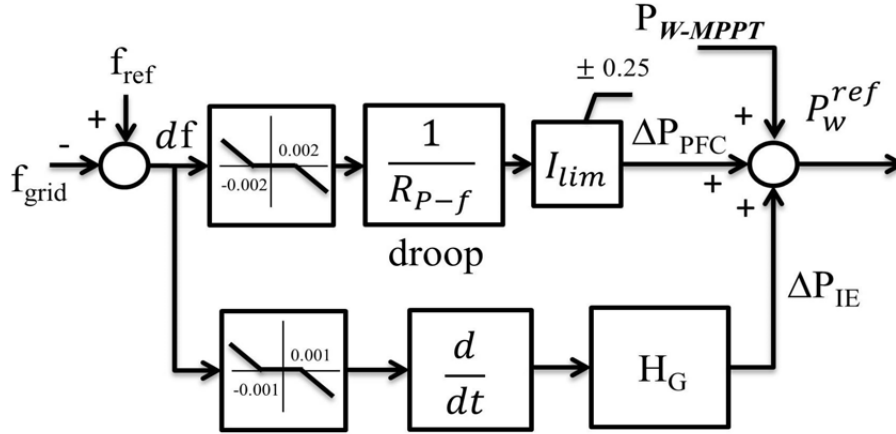


Fig. 3.2 The Combined emulated inertia and Fixed Droop Control [197]

$$\Delta P_{PFC} = \frac{1}{R_{P-f}} df \quad (3.2)$$

where, the droop gain is defined by $\frac{1}{R_{P-f}}$, df is the variation between the actual and the reference frequency. Since the droop gain has large influence on regulating power output, it is limited to $\pm 25\%$. The combined power reference is amalgamated with the DFIG MPPT power reference P_{W-MPPT} for generating the updated power reference P_w^{ref} . Hence, the updated reference for DFIG power output to the rotor side converter can be written as in (3.3)

$$P_w^{ref} = P_{W-MPPT} + \Delta P_{PFC} + \Delta P_{IE} \quad (3.3)$$

If the grid frequency is greater than the nominal plus deadband value, ΔP_{PFC} and ΔP_{IE} values become negative and thus reducing DFIG power output from the P_{W-MPPT} value and vice versa. The fixed droop gain is picked as 31.25 to show 25% power margin with a frequency deviation df of 0.008pu. A limit (I_{lim}) is added to restrict the droop power variation within 25%.

However, linear droop gain may have negative impact on frequency, mainly it can cause high oscillations with a high droop gain if frequency variation is small and system

is lightly loaded. On the contrary, small droop gain will lower the addition/subtraction of DFIG power output in frequency control which will limit the improvement in frequency response. Hence, to avoid this sort of undesirable performance, a sophisticated approach needs to be incorporated for ensuring reliable, smoother and desirable frequency control without compromising the stability performance.

3.3 The Proposed Multi-gain Droop Control Method

A large droop gain will result in higher contribution from DFIG output in frequency regulation but this can cause higher oscillation, especially near the edge of deadband regions i.e. low-frequency oscillations. Therefore, this chapter provides a new control method that addresses this problem. The first sectional droop control is presented in [198] which is adopted and redesigned for this particular stability analysis.

The proposed sectional droop intended to regulate DFIG power output in accordance with the changes in frequency while adjusting the droop gain into two different levels associated with two separate frequency ranges i.e. low and high frequency boundary as illustrated in Fig. 3.3. The sectional droop gain is adjusted according to the intensity of df rather than the wind speed as in [191, 199]. The controller is inactive when the value of grid frequency is within the NOFB i.e. the active power reference of DFIG for frequency control ΔP_{PFC} is zero i.e. $P_s = 0$ as shown in Fig. 3.3. The deadband boundaries for both the conventional and the proposed droop control is the same. The low and high frequency boundary is designated as high and low sensitive region. The purpose of selecting sensitivity region is to adjust active power participation in frequency control.

The boundary between medium low Δf_{Ml} and deadband low limit and medium high Δf_{Mh} and deadband high limit indicate smaller frequency alteration and it is defined as high sensitive region. The droop gain is small in this region which reduces considerably the participation of DFIG power output in frequency regulation. This is to avoid unexpected large oscillation with high droop gain and ensure smoother frequency

response compare to the conventional approach. The reduced power references for DFIG participation in the proposed method are P_3 and P_1 rather than P_4 and P_2 as in the conventional approach. This can assure smaller changes in DFIG power output for a smaller frequency variations and achieve smoother frequency response. The value of droop gain is increased to raise DFIG participation in frequency control when frequency increases and drops beyond Δf_{Ml} and Δf_{Mh} . The power reference in high sensitive positive and negative regions are P_{WTmh} and $-P_{WTml}$. The proposed multi-gain droop control method can be mathematically written as in (3.4):

$$\Delta P_{PFC} = \begin{cases} P_{MX} & \text{if } df \geq \Delta f_h \\ P_1 + P_{WT_h} & \text{if } \Delta f_{Mh} < df < \Delta f_h \\ P_{WTmh} & \text{if } \Delta f_h < df < \Delta f_{Mh} \\ 0 & \text{if } \Delta f_l \leq df \leq \Delta f_h \\ -P_{WTml} & \text{if } \Delta f_{Ml} < df < \Delta f_l \\ -P_3 - P_{WTl} & \text{if } \Delta f_l < df < \Delta f_{Ml} \\ P_{MN} & \text{if } df \leq \Delta f_l \end{cases} \quad (3.4)$$

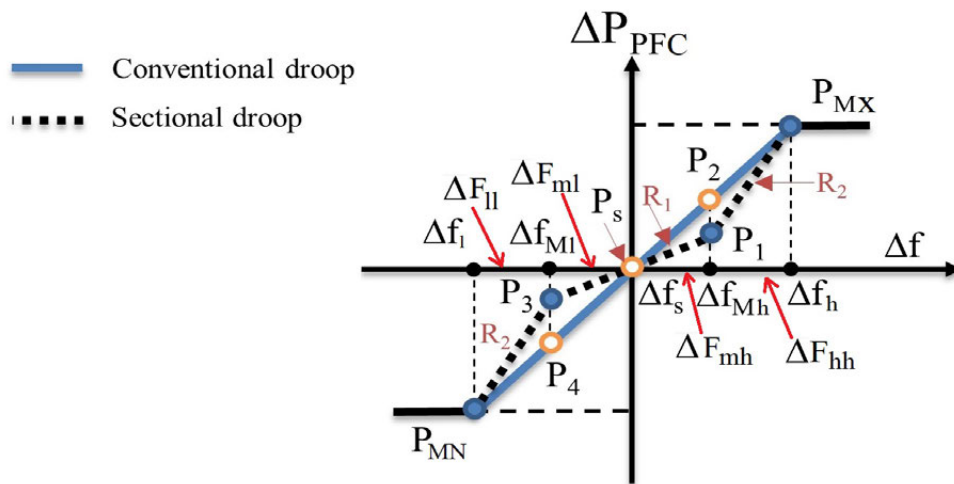


Fig. 3.3 The Proposed Multi-gain Droop Control Strategy

The associated power coefficient values are:

$$\begin{aligned}
 P_{WT_h} &= \frac{P_{MX} - P_{Mh}}{\Delta f_h - \Delta f_{Mh}} (\Delta F_{hh}) \\
 P_{WT_{mh}} &= \frac{P_1}{\Delta f_{Mh}} (\Delta F_{mh}) \\
 P_{WT_{ml}} &= \frac{P_{Ml}}{\Delta f_{Ml}} (\Delta F_{ml}) \\
 P_{WT_l} &= \frac{P_{Min} - P_{ML}}{\Delta f_{ML} - \Delta f_L} (\Delta f_{ll}) \tag{3.5}
 \end{aligned}$$

The region between medium low Δf_{Ml} and low limit Δf_l and medium high Δf_{Mh} and high limit Δf_h indicates higher frequency deviation and it is defined as low sensitive region. Hence, the droop gain is high in this region which defines the higher participation of DFIG power output. The maximum power contribution of DFIG in the positive and negative regions are $(\Delta P_{MX}$ and $\Delta P_{MN})$ respectively, which are supposed to be accelerated for the corresponding high Δf_h and low Δf_l frequency. The maximum power intensity for frequency control is the same as in the conventional droop. The power reference in low sensitive positive and negative regions are $P_{Mh} + P_{WT_h}$ and $-(P_3 + P_{WT_l})$, respectively. The proposed and conventional droop gain settings are plotted in Fig. 3.4. The various levels of power margin are proposed in the literatures such as 10-20% in [192, 199] and 28% in [200]. However, a fixed power margin may not be effective with the changing wind speed which has a dominant impact on the available power output at DFIG terminal. Considering such phenomena, two separate levels of power margin are selected; 15% if the wind speed is lower than the rated speed for the frequency deviation of $df=0.008$ pu and 25% if the wind speed is at the rated value for the same frequency deviation.

The power reference for the median droop is $\Delta P_{PFC}=0.056$ pu when the frequency deviation Δf_{Mh} and $|\Delta f_{Ml}|$ is within 0.004pu. This defines the updated droop gain of 14 between Δf_l and Δf_{Ml} instead of 31.25 in the case of traditional fixed droop gain. The purpose of lower gain is to reduce possible high oscillations during contingencies. The sectional droop gain and associated time are determined on trial and error basis and

hence the optimal tuning of p-f setting will be considered in the future study.

If wind farm contributes in frequency control, the net power of wind farm may be decreased based on the total volume of energy exchanged for providing under/over-frequency control. The reduction in net power transfer to the grid will incur financial losses and this can affect wind farm owner to decide whether they are interested in providing such services or not. Nevertheless, considering stability concern and the mandatory grid requirements will push wind farms to participate in frequency control and they must oblige regardless of the economic performance. As such, techno-economic analysis also needs to be considered and further study can be carried out in this area to evaluate the benefit of the grid and wind farm owner while providing frequency control services.

3.4 Wind Energy Conversion System and Microgrid

3.4.1 Wind Turbine Modeling

The DFIG type wind turbine is selected for the studied MG and a brief discussion on wind turbine modeling is given in this subsection. The wind turbine mechanical power can be written as in (3.6):

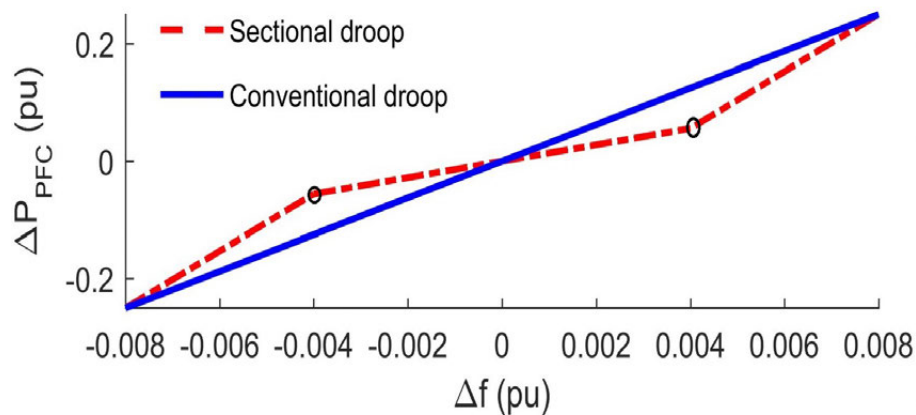


Fig. 3.4 DFIG power response for conventional and proposed methods with the selected parameters [197]

$$P_{wtm} = 0.5 \rho A C_p(\lambda, \beta) v_w^3 \quad (3.6)$$

where C_p is the power coefficient and a function of λ which is the tip speed ratio and β is the pitch angle, ρ is the air density, A is the turbine blade's sweep area.

With a constant wind speed, the DFIG power is defined by the power coefficient C_p . At a constant pitch angle, the maximum power for a specific wind speed is regulated by the optimum tip speed ratio. DFIG operates in MPPT during normal operation to maximize the power generation. However, to provide frequency regulation services, DFIG needs to be operated to the deloaded point. DFIG provides under-frequency support by utilizing its stored kinetic energy which can be attained by various approaches. Among various proposed methods, changing rotor speed is one of the solutions to vary DFIG power output by altering rotor speed and forming momentary power margin. This provides the opportunity to regulate DFIG power output and in turn improving the frequency response of the MG.

3.4.2 The Control of Pitch Angle with Traditional PI

The pitch angle control with conventional PI controller is briefly discussed in this subsection. The pitch angle control constraints DFIG power output within the rated capacity when the wind speed is above the rated value and thus protecting the turbine blade from any mechanical damages. The conventional PI pitch angle controller with the integrated pitch compensation is illustrated in Fig. 3.5.

For a wind speed of below the rated value, pitch angle reference β_{ref} is usually disabled and DFIG operates at MPPT to maximize DFIG power output. In the case of other conditions, pitch angle control is regulated to maintain the rated DFIG power output. The pitch angle control mechanism includes a PI controller, pitch servomechanism and the rate of change of pitch. The time constant τ_1 characterizes the dynamic response of pitch servo. The pitch servo requires a certain time to respond and thus a value of $\tau_1=0.25s$ is selected. The reference of pitch compensation is then

combined with the change of pitch. The rate of pitch change is regulated between the maximum (β_{max}) and minimum (β_{min}) value which is rated as 10 degree per second. The combined pitch reference is limited by the maximum pitch of 27 degree. The pitch output is then passed through a first-order filter and the filter time constant τ_2 is 0.012s which generates pitch angle reference for controlling wind power output.

3.4.3 The Control of Pitch Angle with Fuzzy Logic

The proposed FLC for pitch angle control is a PI type FLC that replaces the conventional PI type pitch angle control and pitch compensation blocks as shown in Fig. 3.6. The FLC output for pitch angle is dictated by the fuzzy inputs, a set of IF-THEN rules. Sugeno type mechanism is used to obtain FLC output and then finally de-fuzzification operation is put in place to obtain the output signal. The thorough discussion of the proposed FLC controlled pitch angle control is provided in here.

The error between the rotor speed reference value (ω_{ref}) and the actual rotor speed values (ω_{ra}) generates error signal ($\Delta\omega_{ra}$). This error and the integration of error are the inputs to the FLC. The two inputs of FLC can be written as in (3.7) and (3.8):

$$\Delta\omega_{ra}(p) = \omega_{ra}(p) - \omega_{ref}(p) \tag{3.7}$$

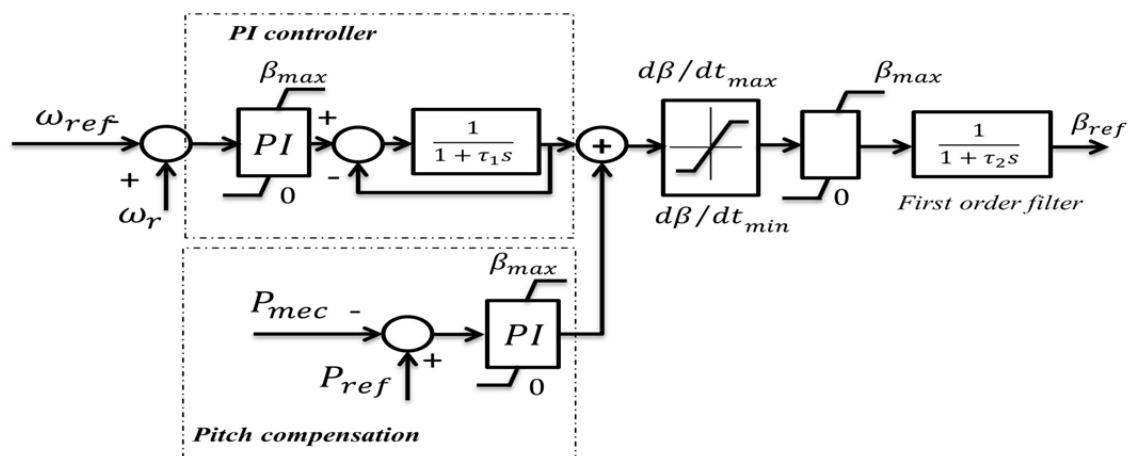


Fig. 3.5 Conventional PI based pitch angle control [197]

$$\int \Delta\omega_{ra}(p) = \int \Delta\omega_{ra}(p - 1) + T_s \Delta\omega_{ra}(p - 1) \tag{3.8}$$

The alternation of rotor speed changes is calculated by Forward Euler integration method as shown in (3.8). The gain for FLC inputs are the same as in PI controller i.e. $G_{\Delta}=3$ and $G_{f\Delta}=0.6$. The membership function of FLC inputs are Gaussian-type and the FLC output is singletons as illustrated in Fig. 3.7. In FLC system, the input membership functions performs the conversion of a crisp set of inputs into a fuzzy set with the use of fuzzy linguistic variables. The output membership functions generate crisp output. Although a large membership functions in FLC inputs and output may result robust performance of the system, a large amount of rules can be computationally demanding while implementing FLC operation. On the contrary, few set of rules may result less computation burden but may end up with poor performance of the system. The use of 7 membership functions for FLC inputs and outputs are widely been used in the earlier literature studies [184,201]. In this study, 7 membership functions are chosen. The linguistic values can be defined as Negative Big (NB), Negative Medium (NM), Negative Small (NS), Zero(ZE), Positive Small (PS), Positive Medium(PM), Positive Big(PB).

The set of FLC rules are determined based on experience and knowledge. The composition of FLC rules for inputs and output can be outlined as in (3.9):

$$RL_p : \begin{cases} IF \Delta\omega_r(n) \text{ is } X_p \text{ and } \int \Delta\omega_r(n) \text{ is } Y_p \\ THEN \beta_o \text{ is } Z_p \end{cases} \tag{3.9}$$

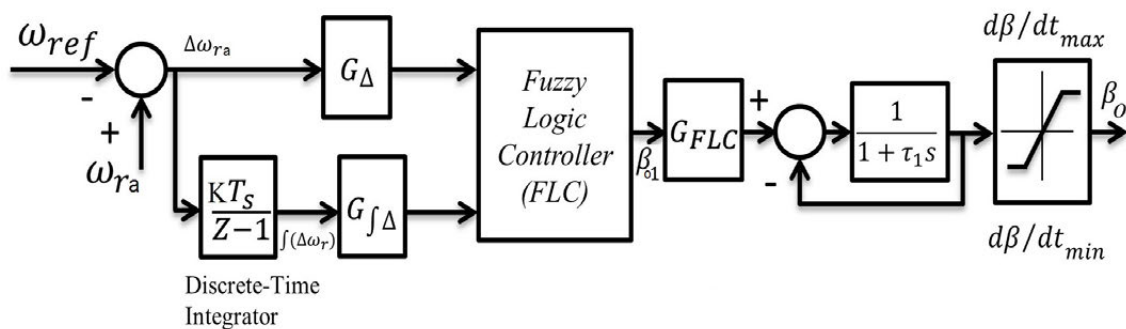


Fig. 3.6 FLC based pitch angle control [197]

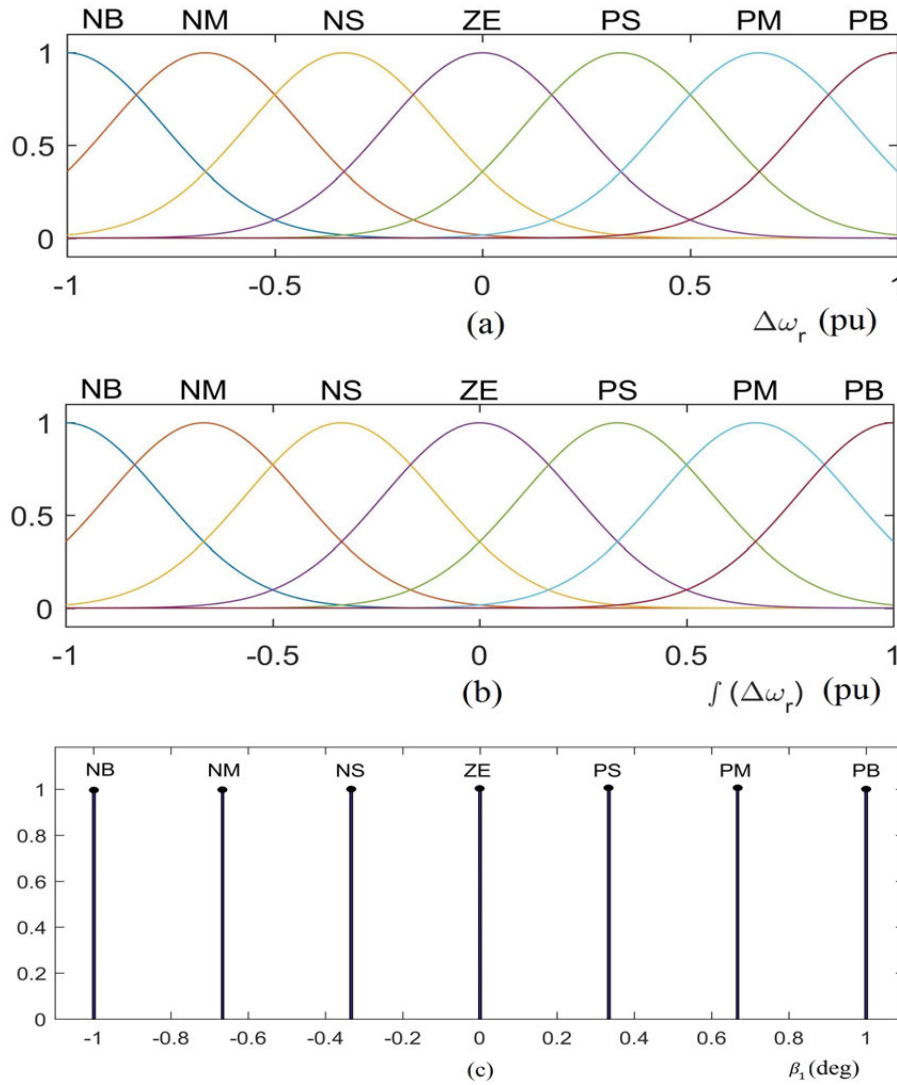


Fig. 3.7 FLC membership function for (a) the error of rotor speed (b) the integration of rotor speed error (c) pitch angle reference at FLC output [197]

where, X_p and Y_p are the fuzzy subsets, Z_p is the singleton FLC output. The fuzzy rules with 7x7 linguistic values i.e. a total of 49 rules for the FLC are provided in Table 3.1.

The output of FLC pitch angle can be determined as in (3.10).

$$\beta_1(P) = \frac{\sum_{a=1}^P W_a Z_a}{\sum_{a=1}^P W_a} \quad (3.10)$$

where, the total number of rules and the rule weighting factor are denoted by P and W_a , respectively and W_a is taken from IF segment of the rules. The output of FLC is

Table 3.1 Rule table of the proposed FLC

$\int \Delta\omega_r$		NB	NM	NS	ZE	PS	PM	PB
$\Delta\omega_r$	NB	NB	NB	NB	NB	NM	NS	ZE
	NM	NB	NB	NB	NM	NS	ZE	PS
	NS	NB	NB	NM	NS	ZE	PS	PM
	ZE	NB	NM	NS	ZE	PS	PM	PB
	PS	NM	NS	ZE	PS	PM	PB	PB
	PM	NS	ZE	PS	PM	PB	PB	PB
	PB	ZE	PS	PM	PB	PB	PB	PB

β_{o1} which is then multiplied with a gain G_{FLC} of 2. Finally, the pitch angle reference is calculated as β_1 .

The sectional droop control is incorporated in the DFIG torque control reference and FLC is integrated for regulating pitch angle. The p-f response of DFIG is managed by the droop and emulated inertia controller gains. Fig. 3.8 illustrates the combined control diagram of DFIG with the proposed droop-emulated inertia control and FLC regulated pitch angle control in MATLAB/Simulink. The p-f characteristics can be tuned by changing the parameters of maximum/minimum power margin (P_{MX} , P_{MI}), the change of maximum/minimum frequency deviation (Δf_H , Δf_L) and the midpoint of frequency deviation (Δf_{Mh} , Δf_{MI}).

3.4.4 Depiction of the Studied Microgrid

The isolated MG is shown in Fig. 3.9. The conventional generation source of 40MW and an aggregated wind farm of 10.5MW are the energy sources in the MG. The load demand of the connected loads are as follows:

- a Load A: 25.8MW and 4MVA_r and
- b Load B: 20.5MW and 5MVA_r.

Load A is 10kms away from the synchronous generation source whereas Load B is 20kms away. The wind farm is 10kms away from the central generation source. With the

increased penetration of low inertial wind energy, central generation source may fail to ensure stable grid frequency support and hence, it is important that the integrated wind farm participate in frequency control and improve security and reliability of the MG. The wind farm produces the rated power at a wind speed of 15m/s. The nominal speed of DFIG rotor is 1.2pu at 15m/s of wind speed and the typical allowed operating range is 0.7-1.3pu. The central generator is equipped with a 6th order machine model and IEEE type-1 voltage regulator, turbines and PID governor system.

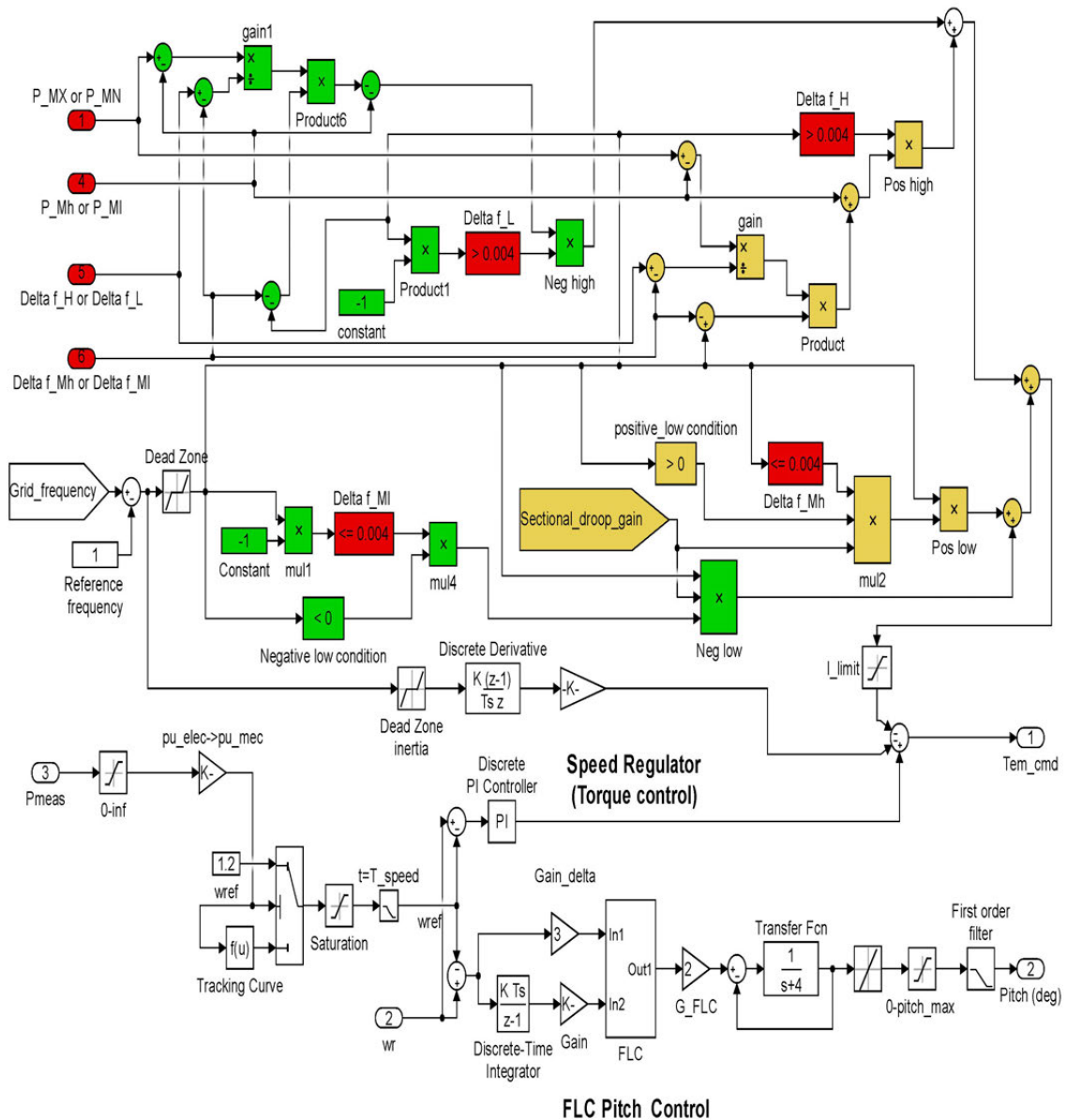


Fig. 3.8 The implementation of the proposed approach in Simulink [197]

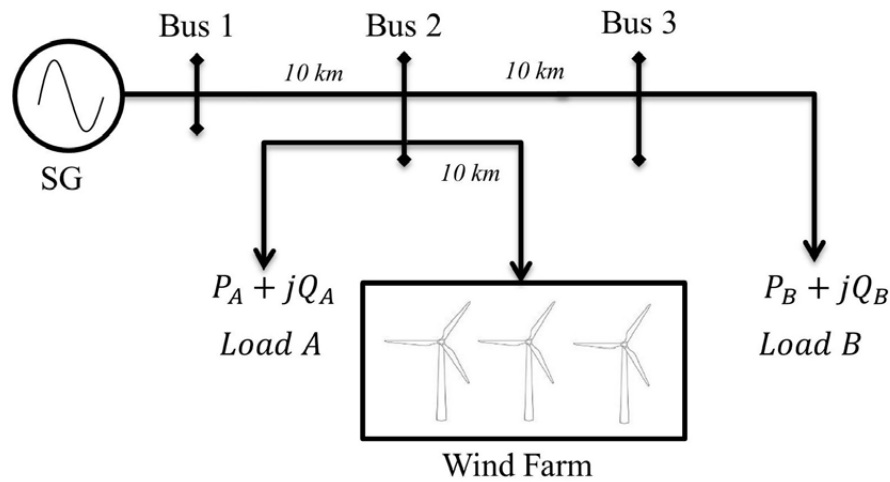


Fig. 3.9 The simple Microgrid with integrated wind farm [197]

3.5 Simulation Studies and Discussion

MATLAB/Simulink based simulations have been executed for verifying the performance of the proposed coordinated control approach. The simulation studies is executed using OPAL-RT, a RTDS and the performance is assessed between various approaches. The equations solving capacity of RTDS is sufficiently fast enough that can practically mimic the physical properties and this is why it is extensively used for design and testing purposes in the study of power system operation and control [202, 203]. Five case studies have been simulated for analyzing the accomplishment of the suggested approach.

The first two case studies discuss the impact of load event and the alteration of wind speed on frequency response. The performance of the proposed control when the wind speed is lower than the rated value is discussed in the third case study. A system with multiple DFIGs participating in frequency control is presented in the fourth case study. Finally, the influence of the number of fuzzy membership functions on frequency outcome is addressed. The following acronyms are used to define the studied various control strategies: traditional droop with PI pitch control (CDPP), traditional droop with the proposed FLC pitch control (CDFP), the proposed sectional droop with PI pitch control (SDPP) and the proposed sectional droop with FLC pitch control (SDFP).

3.5.1 Footprint of Load Event on Frequency Performance

A transitory load growth of 5MW at Load A is enforced for the duration of 1-1.45s and this will disturb grid frequency. The comparative dynamic frequency performances of various control approaches are depicted in Fig. 3.10. For the load scenario, wind speed is assumed as 15m/s and the selected value of droop intensity I_{lim} is 0.25pu.

The momentary load event results the change of frequency i.e. the value of df changes to a new value. The frequency control activates when df is beyond the deadband limit and DFIG power output operates at a different point than its MPPT position. It can be noticed that, grid experiences the maximum drop in frequency with fuzzy (FLC) (0.9888pu) or PI (0.9845pu) regulated pitch control as depicted in Table 3.2. It is interesting to observe that the proposed FLC only provides better frequency regulation than the conventional PI pitch angle control only. The proposed SDFP obtains lesser drop (0.9915pu) and smaller rise (1.0084pu) in frequency and hence demonstrates the best outcome regarding maximum (f_{max}) and minimum frequency (f_{min}) value. In addition, SDFP attains slightly better oscillation damping than the other control approaches over the period of post fault condition. A comparative discussion, illustrated in Fig. 3.10 and Table 3.2 reveals the remarkable outcome of the suggested method compared to the traditional fixed droop gain with both the PI and FLC types pitch angle control method.

As there is no droop-emulated inertia control with fuzzy pitch only and PI pitch

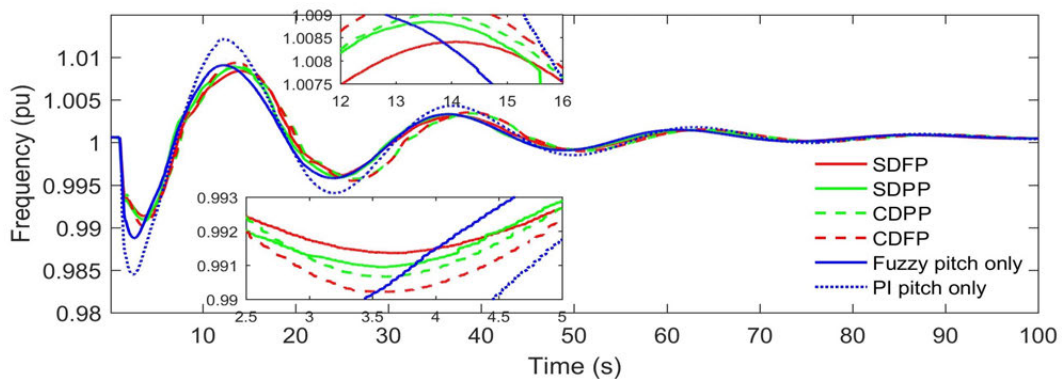


Fig. 3.10 The frequency response of synchronous generator [197]

Table 3.2 The relative frequency responses with load growth event

Control Approach	$f_{min}(pu)$	$f_{max}(pu)$
SDFP	0.9915	1.0084
SDPP	0.991	1.0088
CDFP	0.9902	1.0094
CDPP	0.9907	1.0089
Fuzzy (FLC) pitch only	0.9888	1.009
PI pitch only	0.9845	1.012

only, the change in rotor speed deviation is minimum as shown in Fig. 3.11. The impact of this minimum change of rotor speed is reflected as demonstrating poor frequency response. DFIG participates in frequency control by temporary creating a power margin through under/over-speeding. Fig. 3.11 manifests that SDFP has better regulation of rotor speed which is reflected in the outcome of frequency response. The proposed SDFP has smoother regulation as power margin is reduced close to the low frequency boundary. In the case of conventional droop with fixed gain, DFIG rotor speed has higher oscillations. Therefore SDFP shows lower fluctuations compared to the conventional method.

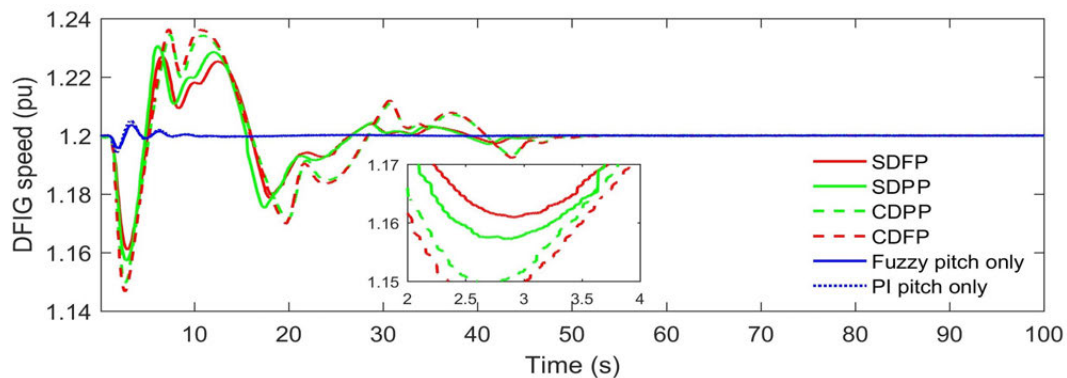


Fig. 3.11 The variation in DFIG rotor speed [197]

The combined output of conventional control i.e. CDPP and CDFP result in higher fluctuated pitch angle as illustrated in Fig. 3.12. On the contrary, SDFP and SDPP demonstrates smooth and minimum frequency acceleration and deceleration. The comparative analysis validates the superior performance of the propose control method. This ensures better power regulation as shown in Fig. 3.13 which in turn provides better grid frequency control. In addition, Fuzzy (FLC) pitch control possesses better

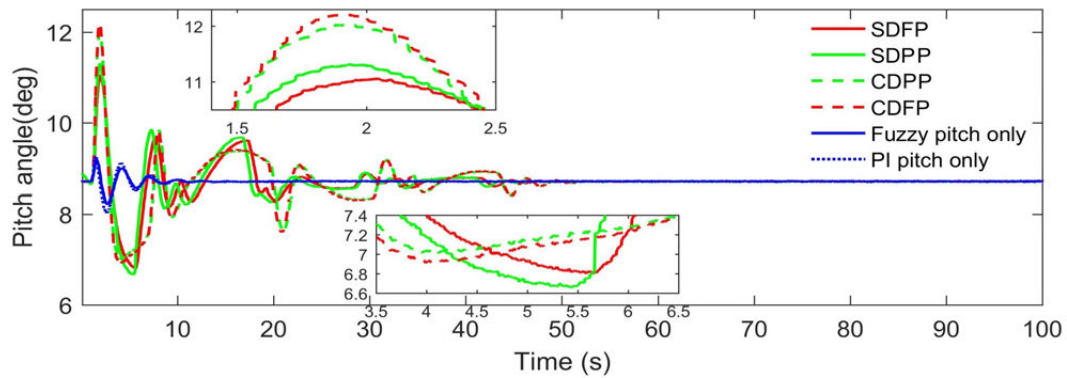


Fig. 3.12 DFIG pitch angle responses with various control methods [197]

frequency outcome than PI regulated pitch angle control.

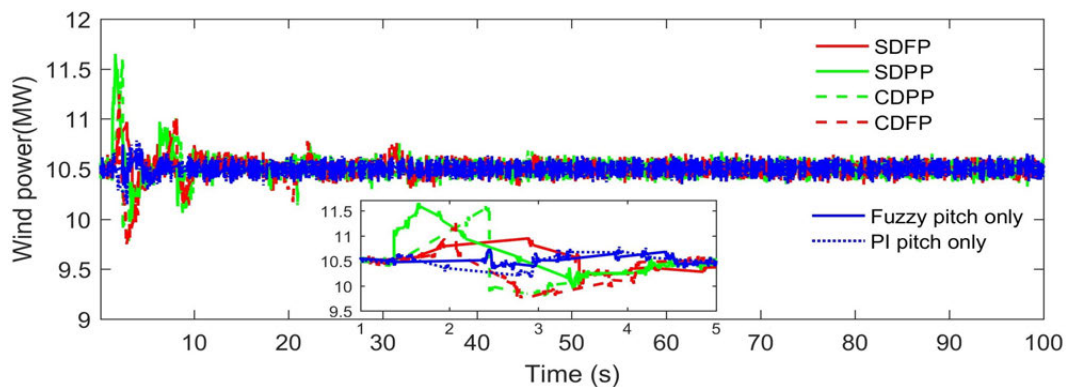


Fig. 3.13 The DFIG power output [197]

3.5.2 Alteration in Wind Speed and Frequency Response

In order to further analyze the performance of the proposed control method, the impact of wind speed variation is carried out and the frequency outcome associated with various control approaches are observed. A reduction of wind speed is applied at $t=1$ s from 15m/s to 13m/s, then an increment from 13m/s to 15m/s at $t=3$ s, further increment to 17m/s from 15m/s at $t=5$ s and finally reduced to 15m/s at $t=8$ s. The comparative performance analysis is demonstrated in Fig. 3.14 and Table 3.3. Similar to the previous case study, the grid frequency experiences large frequency fluctuation without any frequency regulation and also Fuzzy pitch control demonstrates an improved performance than the PI pitch control only. Although conventional droop control indicates exceptional performance in terms of smaller frequency drop but the proposed sectional droop manifests improved frequency

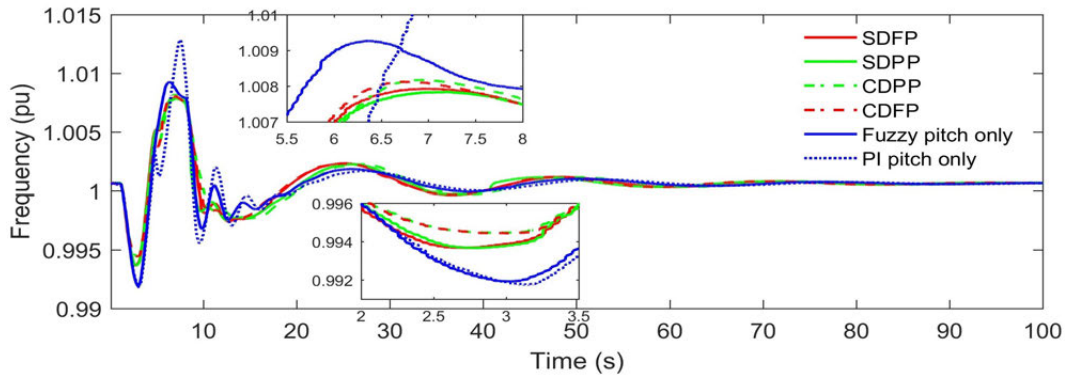


Fig. 3.14 The frequency response of generator [197]

response in terms of lower frequency rise. Overall, PI and FLC based pitch control with conventional and sectional droop performs almost identical to one another.

Table 3.3 The relative frequency response with wind speed deviation

Control method	$f_{min}(pu)$	$f_{max}(pu)$
SDFP	0.9937	1.0078
SDPP	0.9937	1.0079
CDFP	0.9944	1.0081
CDPP	0.9944	1.0082
Fuzzy pitch only	0.992	1.009
PI pitch only	0.9918	1.012

The conventional droop control demonstrates smaller frequency drop by creating less power margin and thus minimizing the reduction of DFIG power output than the sectional droop as depicted in Fig. 3.15. On the contrary, during the rise of frequency, sectional droop control possesses lower power margin, providing less power output than the conventional droop and hence results in lower frequency rise compared to the conventional droop.

Fig 3.16 indicates that the pitch angle control with PI pitch only control has the highest fluctuations which is also reflected in the frequency outcome. Comparatively, Fuzzy pitch control outperforms PI pitch control only. The conventional droop has higher pitch regulation at the initial stage of frequency drop and sectional droop has very limited contribution during the frequency rise. These phenomena supports the frequency response in regard to wind speed variation and change in DFIG power output as shown in Fig. 3.17.

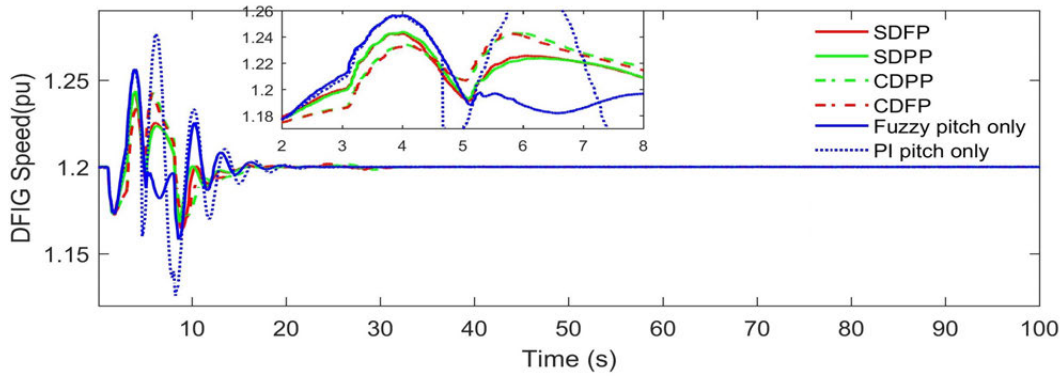


Fig. 3.15 The variation in DFIG rotor speed [197]

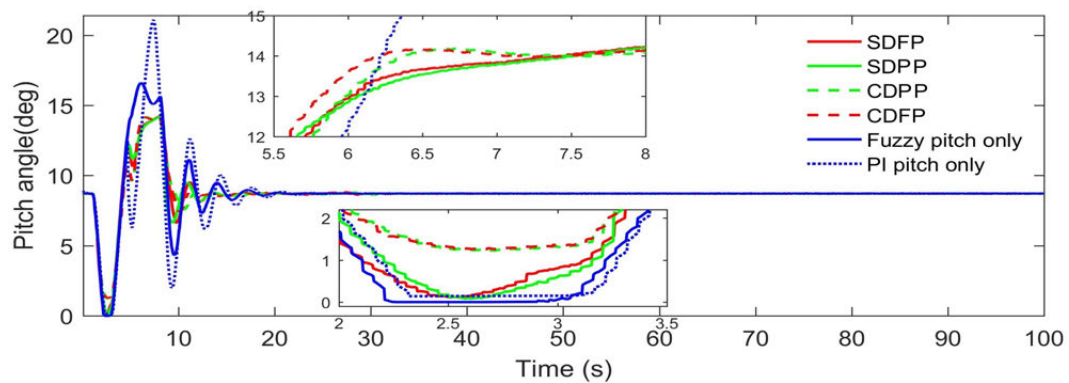


Fig. 3.16 The pitch angle responses with changing wind speed [197]

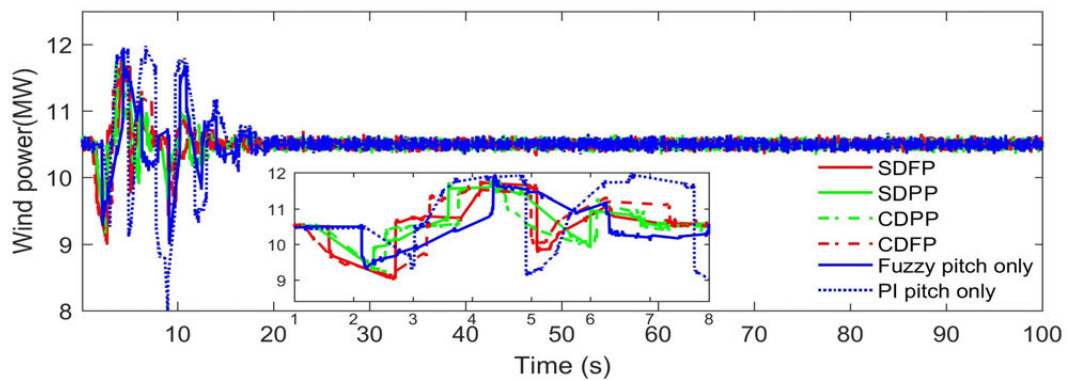


Fig. 3.17 Wind farm power output [197]

3.5.3 The Impact of Wind Speed Below Rated Speed

When the wind speed is lower than the rated speed, pitch angle control is disabled and DFIG operates at MPPT to provide maximum power output with the available wind speed. The change of wind speed is applied from the initial value of 10m/s and the various levels of power margin are investigated for performance analysis. The wind

speed is reduced to 9m/s from 10m/s at $t=1$ s, then increased at $t=3$ s to 10m/s from 9m/s, further it is increased to 11m/s at $t=5$ s from 10m/s and finally reduced to the initial speed of 10m/s at $t=8$ s. The frequency response for the aforementioned wind speed variation is depicted in Fig. 3.18 in which sectional and conventional droop is defined by SD and CD, respectively.

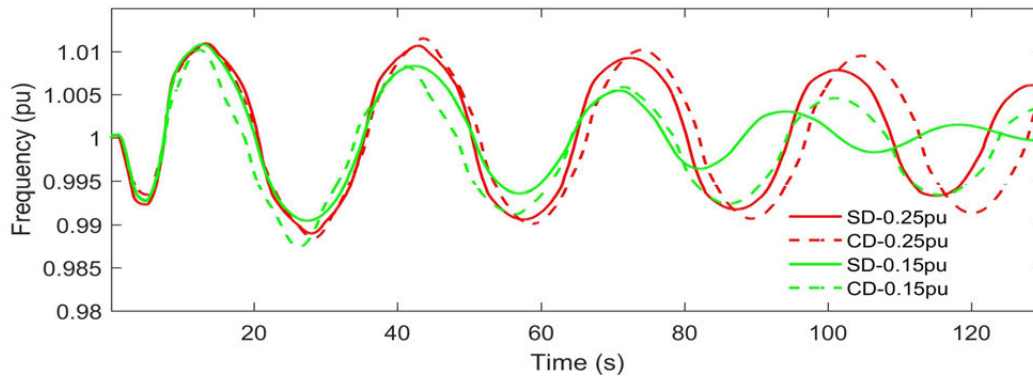


Fig. 3.18 The frequency response with various power margin [197]

The frequency response manifests that with the enforced changes in wind speed and 25% power margin, the grid struggles to achieve enhanced oscillation damping throughout the studied simulation period. This is caused due to the fact that DFIG power output is now less with lower wind speed and a high power margin originates a high fluctuation in DFIG power output, resulting in huge acceleration and deceleration. However, a very interesting observation can be made that even if 25% power margin results large oscillations in frequency, the sectional droop comparatively performs better than the conventional droop and thus shows the effectiveness of the proposed sectional droop in regulating DFIG power output. In order to minimize large oscillation during lower wind speed, a reduced order of 15% power margin is selected for a wind speed of lower than 11m/s and 25% power margin for a wind speed greater than the rated value as shown in Fig. 3.19.

The frequency response with the adapted 15% power margin is illustrated in Fig. 3.18 suggests that large frequency oscillations are reduced significantly in the case of conventional droop with 15% power margin. However, the sectional droop with the coordinated power margin of 15% demonstrates faster oscillation damping, smoother frequency response and thus validates its effectiveness compared to other control

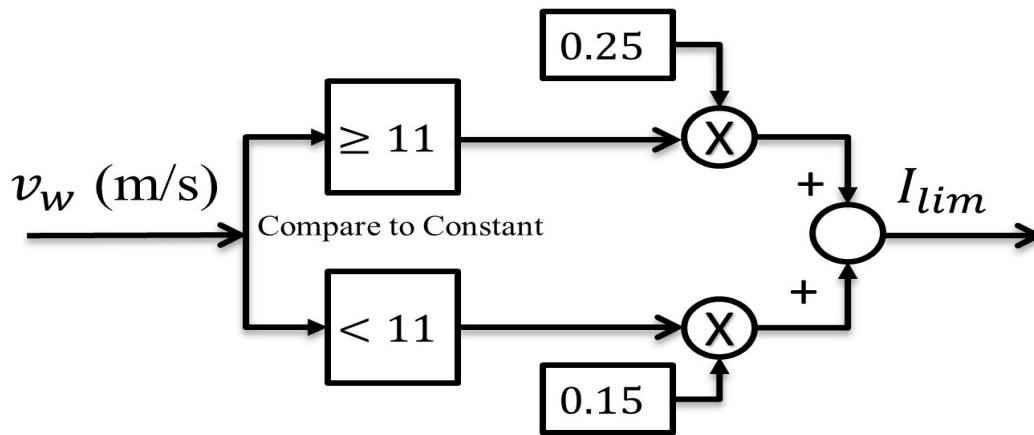


Fig. 3.19 The control of power margin for varying wind speed value [197]

approaches and power margin. The maximum and minimum frequency values for both power margin are outlined in Table 3.4.

Table 3.4 The performance of frequency responses for varying wind speed level

Power margin (right)		0.25pu		0.15pu	
Event	frequency (pu)	SD	CD	SD	CD
Wind speed variation	f_{min}	0.9876	0.9882	0.992	0.9875
	f_{max}	1.011	1.0114	1.011	1.0102
Load decrease event	f_{min}	0.9872	0.9888	0.9851	0.9888
	f_{max}	1.01102	1.01102	1.012	1.01102

On the contrary, a 5MW of temporary load growth is applied as in Section 3.5.1 and the frequency outcome is highlighted in Fig. 3.20. The figure reveals that in the event of conventional droop, frequency experiences poor oscillation damping for both types of power margin. However, the proposed sectional droop control shows decaying oscillations which substantiates the remarkable outcome of sectional droop gain over the

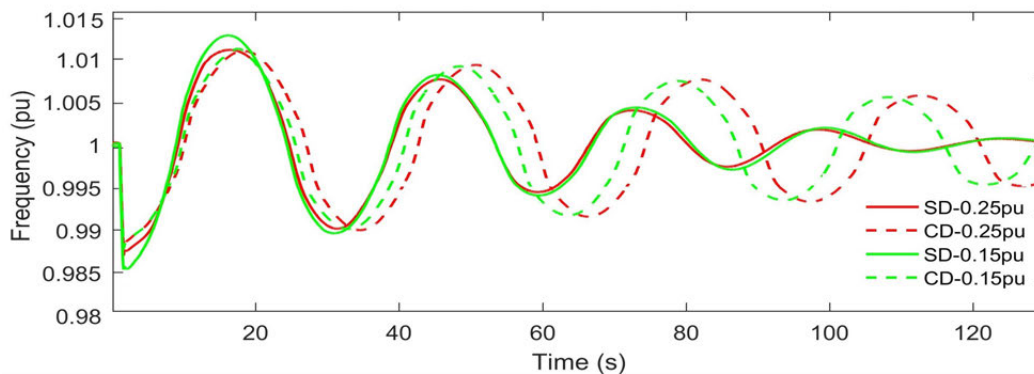


Fig. 3.20 The frequency response with multiple power margin [197]

conventional fixed droop gain. A closer look affirms that reduced power margin of 15% provides better frequency regulation during the initial stages of load event.

3.5.4 Multiple DFIG for PFC in MG

A complex MG is further investigated for analyzing the efficacy of the proposed multi-gain droop control as displayed in Fig. 3.21. An additional 10.5MW of wind farm is installed at 30km away from the central generation source and 10km away from the other wind farm. The Wind Farm B is also designed to participate in frequency control and the same control settings and parameters as in Wind Farm A are used for performing frequency regulation as in Fig. 3.9. The corresponding load demands are highlighted in Fig. 3.21. The central generation capacity is the same as in the previous studied MG in Fig. 3.9.

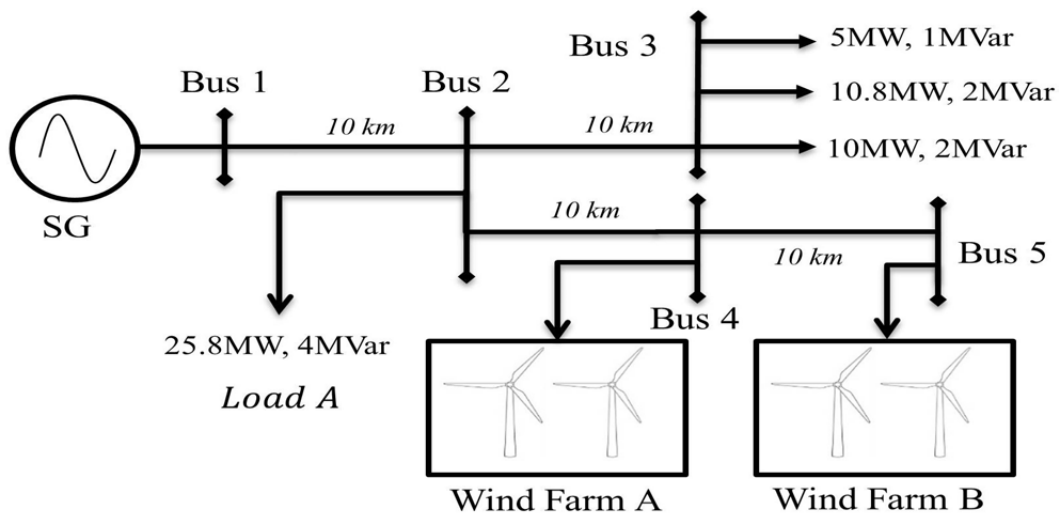


Fig. 3.21 The network diagram with multiple DFIGs [197]

A momentary load reduction of 5MW is applied at Load A during $t=1-1.5$ s and the frequency responses with various control approaches are shown in Fig. 3.22. The Fuzzy pitch control shows similar improved performance as in the previous case studies i.e. smaller frequency rise and lesser frequency drop than the PI based pitch control. The proposed sectional droop method demonstrates an improved frequency response compared to the conventional droop control with both types of pitch angle controllers.

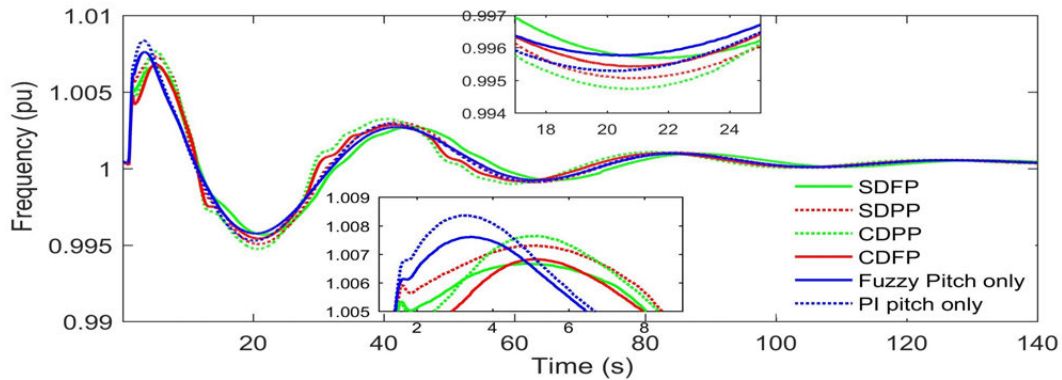


Fig. 3.22 The frequency response with multiple DFIGs in MG [197]

Table 3.5 outlines the comparative analysis of minimum frequency drop and maximum frequency rise for different types of controllers that indicates the superiority of the proposed SDFP in frequency regulation. The SDFP has higher frequency nadir and lower frequency rise than any other studied control methods. It can also be realized that the SDPP provides better frequency outcome than the CDPP which justifies the effectiveness of the sectional droop control than the traditional droop gain irrespective of the categories of pitch angle controllers.

Table 3.5 The relative performance analysis of frequency variation

Control method	$f_{min}(Hz)$	$f_{max}(Hz)$
SDFP	0.9957	1.0066
SDPP	0.9951	1.0073
CDFP	0.9954	1.0068
CDPP	0.9947	1.0076
Fuzzy pitch only	0.9958	1.0076
PI pitch only	0.9953	1.0084

The rotor speed of Wind Farms A and B are illustrated in Fig. 3.23 (a and b). The proposed sectional droop control SDFP exhibits an optimal regulation of power margin which substantiates its efficacy in regulating frequency compared to other control methods. Since the control settings and parameters are the same for both wind farms, the regulation of DFIG rotor speed in Wind Farm A shown in Fig. 3.23 (a) are fairly identical to rotor speed deviation in Fig. 3.23 (b).

The pitch angle responses for both wind farms with all the control approaches are shown in Fig. 3.24 (a and b) which display that SDFP provides an optimal regulation of

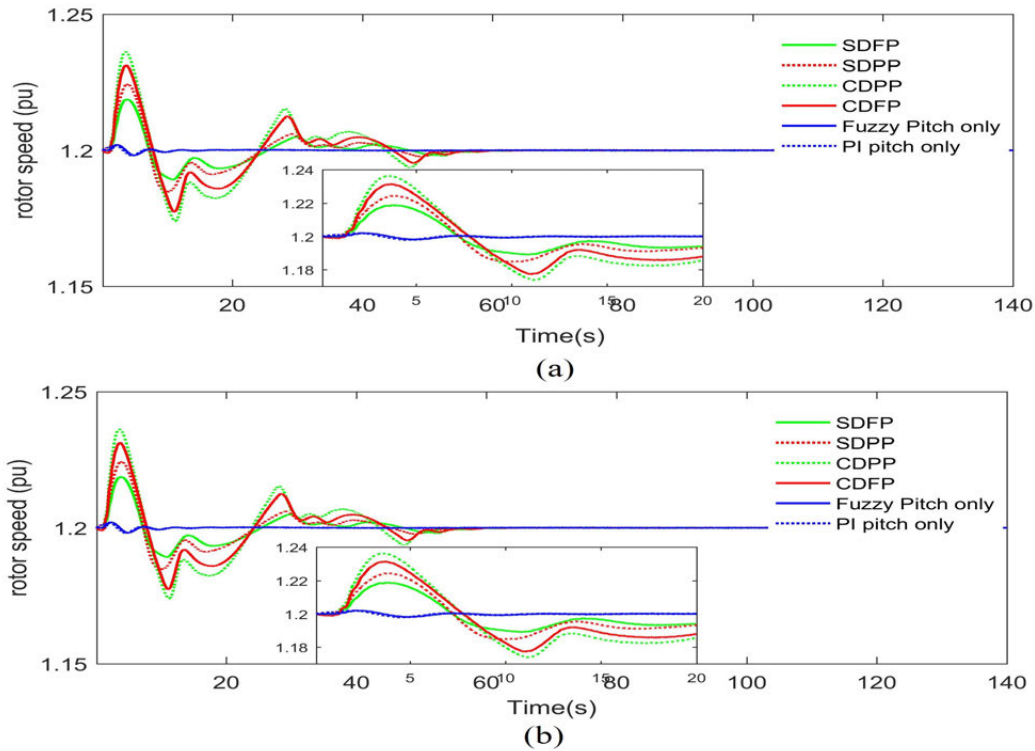
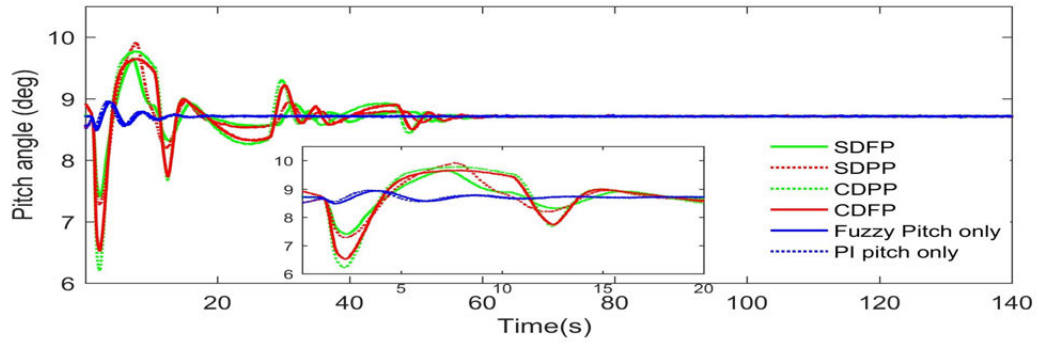


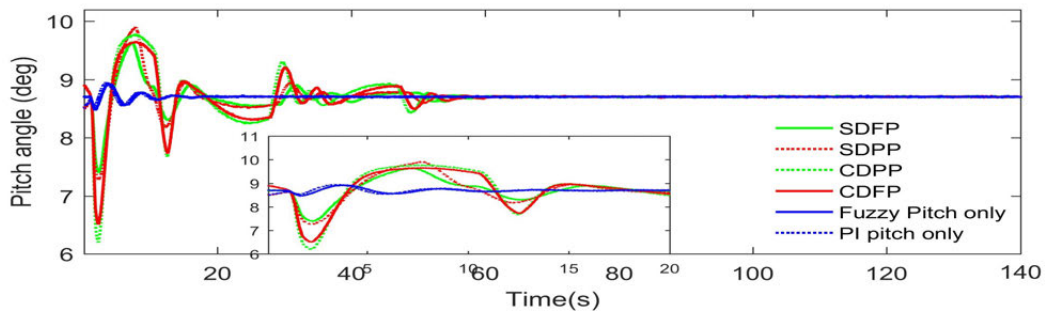
Fig. 3.23 DFIG rotor speed of both Wind Farm A (a) and Wind Farm B (b) [197]

pitch control compared to all other methods. Moreover, SDPP performs better than the CDPP as also observed in other case studies. The optimal regulation of power margin and pitch angle are reflected in a favorable outcome of DFIG power output as depicted in Fig. 3.25 (a and b). Hence, it can be said that the proposed sectional droop demonstrates equally superior performance in the case of simple and complex MG system.

Wind turbine is unable to participate in rapid acceleration and deceleration due to its inherent physical inertia. Hence, a linear p-f droop characteristics put wind turbine in stress with high droop gain [204]. The situation can be even worse for low order frequency oscillations. The simulation results in real time validates that large droop gain in the interim of low frequency fluctuation or low wind speed creates a large frequency oscillations due to the physical inertia of wind turbine. A very large fluctuation may result in system instability. On the contrary, smaller droop gain can reduce such large oscillations, but this will eventually lessen DFIG contribution in frequency regulation and thus the improvement in frequency will be compromised. The proposed multi-gain control is able to maintain a complementary trade-off between large oscillations and

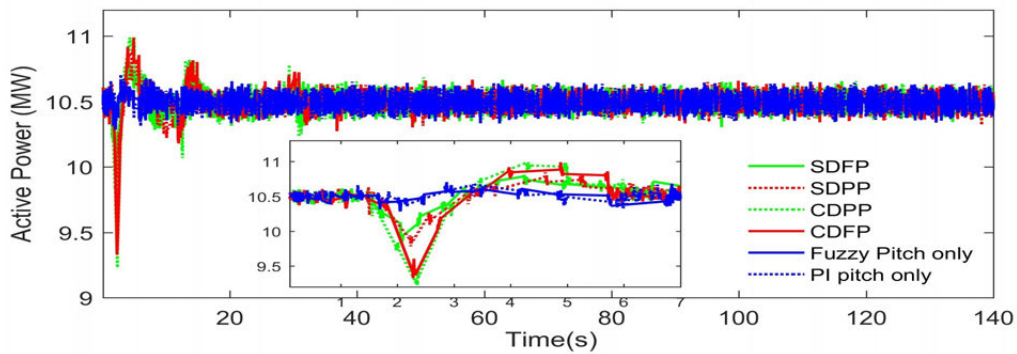


(a)

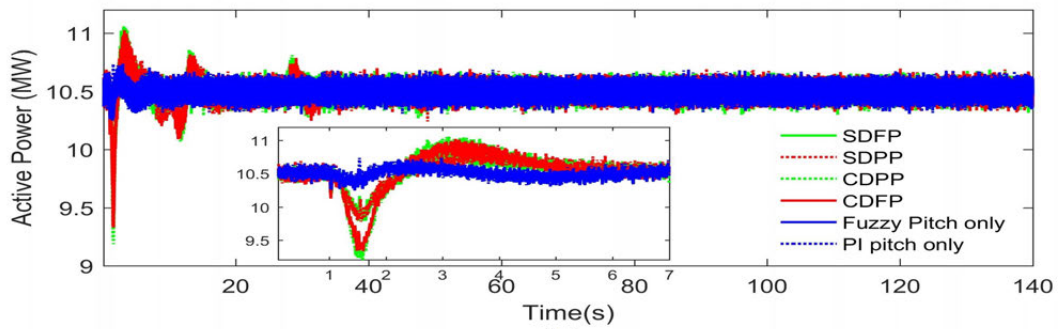


(b)

Fig. 3.24 DFIG pitch angle output of both wind farms [197]



(a)



(b)

Fig. 3.25 Active power output of Wind Farm A (a) and Wind Farm B [197]

increased power margin following various levels of frequency deviations. The proposed method allows to achieve maximum power margin for frequency control as in the conventional fixed droop gain but minimizes the droop gain at the time of low frequency fluctuations.

Real time simulation results in Figs. 3.10, 3.14, 3.18 and 3.22 reveals that the proposed sectional droop successfully reduces droop gain at the time of low frequency oscillations without minimizing the maximum amount of power margin. The frequency outcome exhibits improved maximum and minimum frequency oscillations and enhanced oscillation damping. This validates better frequency regulation with less complexity in DFIG control with the proposed control approach.

3.5.5 The Influence of the Number of Fuzzy Membership Functions on Frequency Performance

Another case study is carried out for realizing the impression of fuzzy membership functions on frequency response. FLC with 5 membership functions instead of 7 are designed for rotor speed error and the integration of rotor speed error and 5 singleton membership functions for the output of the FLC. The updated linguistic values are Negative Big (NB), Negative Small (NS), Zero (ZE), Positive Small (PS) and Positive Big (PB). The FLC rules are outlined in Table. 3.6 and FLC membership functions are illustrated in Fig. 3.26 .

Table 3.6 Rule table of the proposed FLC with 5 membership functions

$\int \Delta\omega_r$		NB	NS	ZE	PS	PB
$\Delta\omega_r$	NB	NB	NB	NS	NS	ZE
	NS	NB	NS	NS	ZE	PS
	ZE	NS	NS	ZE	PS	PS
	PS	NS	ZE	PS	PS	PB
	PB	ZE	PS	PS	PB	PB

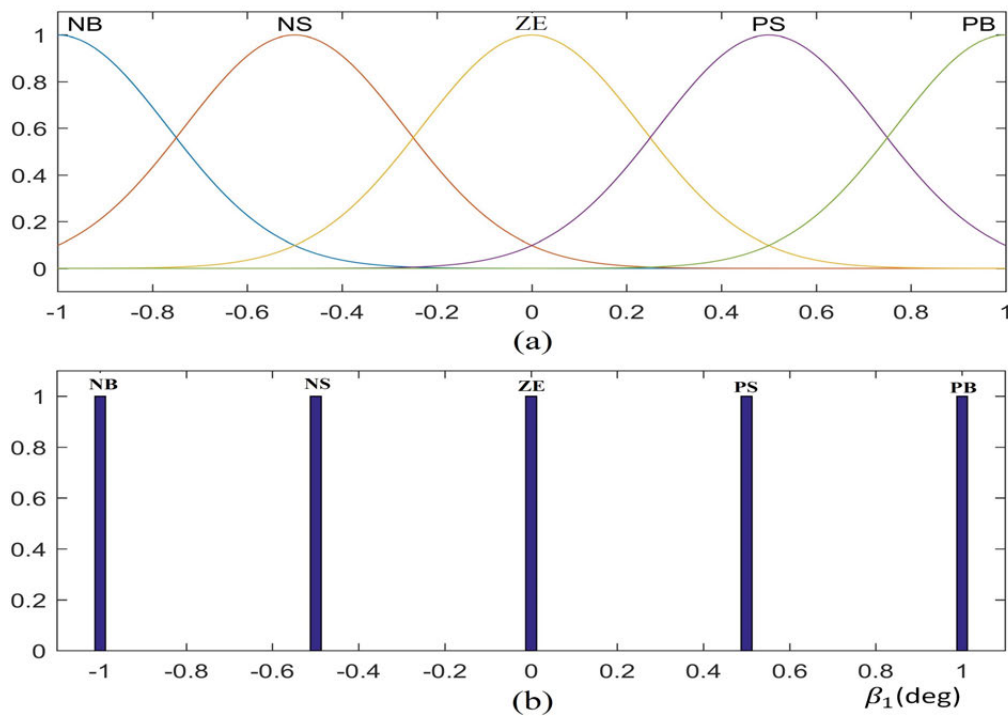


Fig. 3.26 Inputs (a) output (b) with 5 FLC membership functions [197]

In order to perform comparative performance analysis, an equivalent increase in load demand of 5MW at load A is tested during $t=1-1.45s$. The dynamic frequency outcome with 5 and 7 FLC membership functions are manifested in Fig. 3.27. A modest improvement with 5 membership functions is visible during frequency drop compared to 7 membership functions in the case of conventional droop whereas they have the same amount of rise in frequency. On the contrary, the opposite scenario is visible in the case of sectional droop. However, 7 membership functions demonstrate an improved oscillation damping over the simulation periods. The enhanced damping performance is the result of enough FLC rules to provide smoother output response.

The superior performance of 7 membership function can further be explained in Figs. 3.28 and 3.29. The DFIG pitch angle response illustrates that CDFP and SDFP with 7 membership functions provide better pitch angle regulation than that of with 5 membership functions mainly after $t=10s$. The same phenomena is also visible in optimal rotor speed deviation as shown in Fig. 3.29 to create power margin for frequency control and this substantiates the efficacy of the higher membership functions compared with lower values. In summary, more membership functions and fuzzy rules

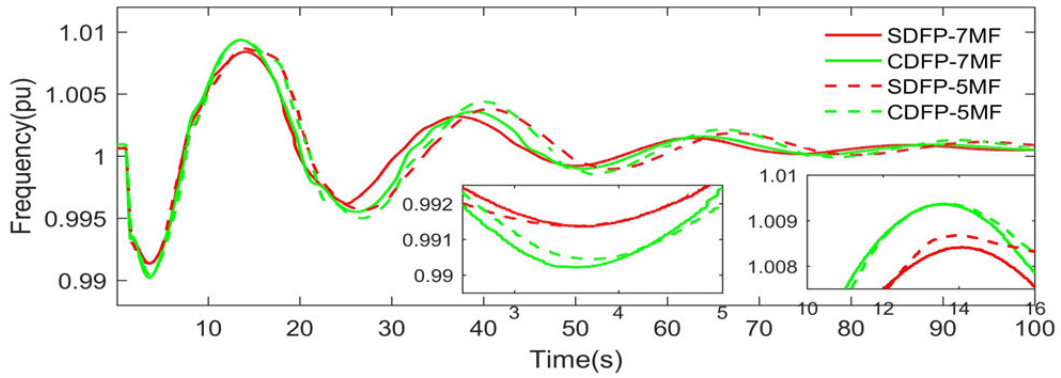


Fig. 3.27 The frequency outcome with different fuzzy membership functions [197]

can provide reasonably smoother response. However, computational complication must be examined before selecting the fixed set of membership functions and FLC rules.

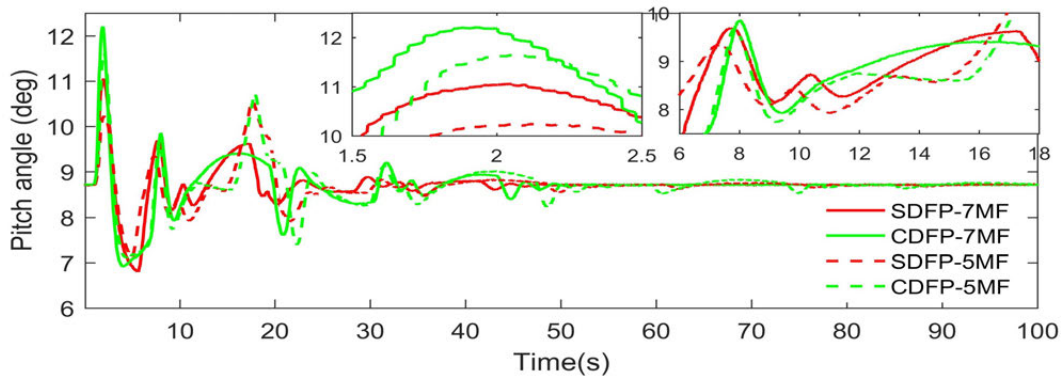


Fig. 3.28 DFIG pitch angle under various fuzzy membership functions [197]

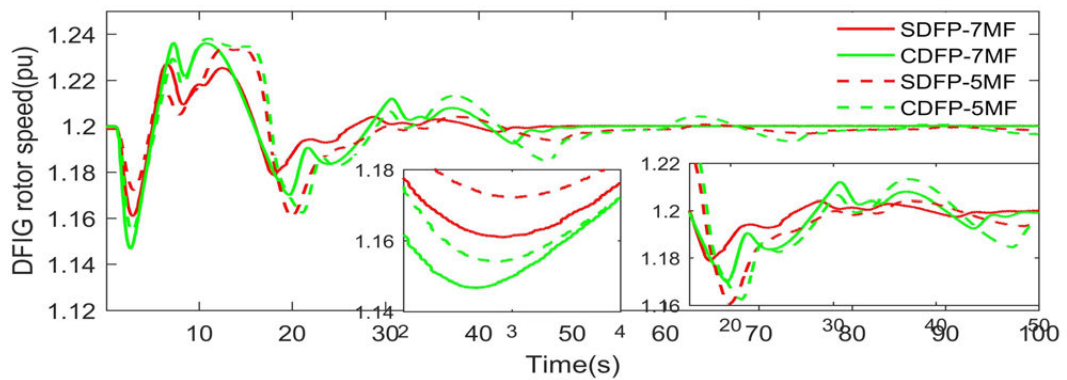


Fig. 3.29 DFIG rotor speed under various fuzzy membership functions [197]

3.6 Conclusion

This chapter has introduced a coordinated sectional droop control of DFIG for engaging in frequency regulation in a MG. The multi-gain droop is accommodated with two different types of pitch angle controllers i.e PI and FLC. The conventional droop gain is regulated by splitting into two sections having low and high gain during low and high frequency oscillations, respectively. The simulation results are carried out in real time and the main finding of simulation studies can be encapsulated as follows:

- The conventional fixed droop gain results lower frequency nadir and increased frequency rise following the studied contingencies. Moreover, high droop gain causes poor oscillation damping of the system.
- Compared to conventional droop method, the proposed sectional droop control approach contributes in higher frequency nadir and lower frequency rise. Moreover, the reduction of gain during low frequencies results in improved oscillation damping which validates its efficacy over the conventional control method.
- In addition, the sectional droop performs better when coordinated with FLC controlled pitch angle control that reveals the efficacy of FLC compared to the conventional PI regulated pitch angle control.
- A high power margin may result in higher contribution of DFIG power output in frequency control and manifest improved frequency response. However, this can create rapid acceleration and deceleration resulting in higher oscillations, mainly during lower wind speed than the rated value.
- An adapted lower power margin at the time of a wind speed of less than the rated speed results lower oscillations compared to higher power margin. This ensures better regulation of DFIG power output and thereby illustrating an improved frequency control.

It is simulated that wind farm can provide a certain amount of frequency control in the grid. In the case of over-frequency, the DFIG response can be adjusted by curtailing wind power output. The amount of power reduction can be significant [205] and this will greatly reduce the income of wind farmers. On the contrary, the wind farm can be overloaded for a few seconds only in order to respond to an under-frequency event. Moreover, the amount of power variation is highly dependent on the less reliable weather condition; from a power system security and stability point of view. In addition, considering the future energy market of 100% renewable generation sources, the total inclination on intermittent wind power for frequency control is unreliable as the wind technology itself is dependable on unpredictable weather conditions. In such a case, the system will be exposed to a greater risk of instability which requires the urgency of more reliable and dependable energy sources. This arrangement is necessary to ensure a higher level of renewable penetration in the power system has less stability concern.

Chapter 4

The applicability of BESS in providing frequency control with the growth of wind energy penetration

This chapter contains the following publication - U. Datta, A. Kalam and J. Shi, “The relevance of large-scale Battery Energy Storage (BES) application in providing primary frequency control with increased wind energy penetration,” *Journal of Energy Storage*, vol. 23, pp. 9-18, 2019.

4.1 Introduction

BESS, as a quick responsive storage device is an important and universally studied alternative energy source to provide various grid ancillary services. The up-to-date application and research information on the types of services that a BESS can provide is extensively reviewed in Chapter 2. In particular, frequency stability is one of the main technical challenges that a power system experiences with the increasing penetration of RES. BESS with fast acting capability is an outstanding alternative for providing frequency regulation and minimizing the adverse impacts of RES. Extensive research

works [206–209] have been carried out on the application of BESS in regulating grid frequency. The study in [206] presented that integrating a BESS provides significant improvement in the transient response of the MG compared to without a BESS. In another study [207], authors have shown that with the various levels of RES penetration and disturbance occurrence, the deviation of rotor speed increases significantly and incorporating a BESS reduces the deviation and therefore improves the system stability. The response of the grid with various BESS operation modes are analyzed in [208] when BESS is incorporated to contribute in frequency control. The study in [209] discussed that BESS can contribute in reducing environmental impact while providing frequency control as BESS enables the grid to allow RES penetration without affecting grid stability. Nevertheless, the earlier studies did not consider the possibility of BESS in minimizing frequency deviation and supporting the growth of RES penetration without raising stability concern.

This chapter proposes and discusses the improvement in power system stability with the use of BESS to support the growth of wind penetration in the grid. The aim is to restrict the frequency variation within $\pm 1\%$ of the nominal frequency to satisfy the grid requirements of Australian National Electricity Market (NEM) [210]. Particularly, the primary interest is to observe the changes in transient stability performance with the increased penetration level of wind. This arrangement can be of great interest for the future grid with the integrated RES as lower system inertia will result higher power oscillations. The replacement of the existing synchronous generating unit with the wind penetration is considered to somewhat predict a future generation scenario. Furthermore, the need of BESS power versus energy is also analyzed in this chapter. Multiple case studies have been performed to demonstrate the performance of BESS in the grid. It is shown that with the increased penetration of wind, frequency deviation increases and for a certain level of wind penetration, the frequency response violates the grid requirements. The level of wind penetration within the grid requirement varies according to the type and location of a disturbance event. However, BESS successfully alleviates such problem and maintains grid stability with the increased penetration of wind power.

4.2 Wind Penetration and Primary Frequency Control

The primary concern of wind integration is its low or zero inertia which predominantly influences system's capability in responding to any temporary power imbalances in the grid. This section discusses the impact of wind penetration and the primary frequency control capability of the grid.

4.2.1 The Impact of Wind Penetration

The penetration level of RES/wind can be defined as in [211]:

$$\%RES = \frac{\sum P_{RES}}{\sum P_{RES} + \sum P_{SG}} \quad (4.1)$$

where, the aggregated power output of any RES generating and SG units are represented by P_{RES} and P_{SG} , respectively. The typical impact of RES penetration can be determined by three major factors which are highlighted as follows:

- Existing fossil fuel based SGs are in operation
- Existing fossil fuel based SGs are permanently dismantles as the RES penetration increases.
- The reduced installation of new large-scale SGs based generating plants.

It is most likely the case that environment friendly generation units such as hydro, biomass, geothermal etc. will remain in operation in the future. However, existing fossil fuel based generating units will possibly be shut down permanently or will be dismantled once they reach their end of service life.

In this chapter, it is considered that the existing fossil fuel based generating units are replaced with the wind penetration. The main objective is to integrate higher amount of wind power in the power system with the utilization of BESS. BESS can regulate

frequency by absorbing excess energy or providing the energy deficit during the contingency period by altering BESS power output P_{BESS} .

4.2.2 Primary Frequency Control, Wind and BESS

SGs contribute in any temporary power imbalances for maintaining the nominal frequency within the grid defined operating region by taking the advantage of its stored kinetic energy. Thus, the governor response corresponding to the variation in frequency can be written as in (4.2):

$$\frac{df}{dt} = \frac{f_{ref}}{2 \sum H_n} \Delta P_d \quad (4.2)$$

where, the change of power demand is defined by ΔP_d which is the error between the generated power P_{Gen} and the load power demand P_L . The total system inertia constant is H_n and the nominal frequency is f_{ref} .

As the growth of RES increases, the installation of conventional generation units reduces and in some cases, they are being shut down for environmental/economical reason. This will negatively impact on the overall inertia of the system. In this situation, existing governor system may not be capable enough to compensate power imbalances resulting from varying RES generation or network disturbance events. Therefore, an alternative measure need to be considered in order to overcome the challenges of reduced system inertia. A BESS can be incorporated in the grid to minimize the threats related to the inertia and participate in frequency regulation as shown in Fig 4.1.

The frequency control with RES penetration and integrated BESS can be defined as in (4.3) [212]:

$$\frac{df}{dt} = \frac{f_{ref}}{H_B + 2 \sum H_n} \Delta P_d \quad (4.3)$$

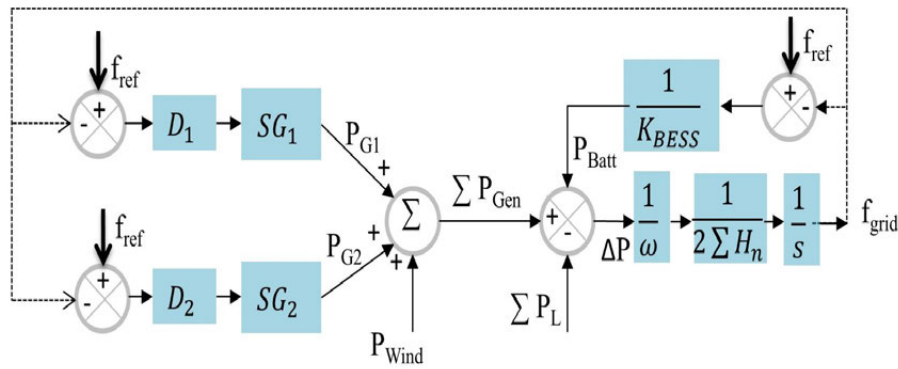


Fig. 4.1 The block diagram of frequency control with BESS

where, H_B is BESS inertia constant, the droop coefficient of SGs are D_1 and D_2 of generators SG_1 and SG_2 , respectively.

When BESS is designed to provide inertia control, BESS power reference is regulated according to the existing capacity of the grid and available BESS capacity which can be written as in (4.4) [213]:

$$P_{ref-1} = P_{ref} - H_n f_{nom} \frac{df}{dt} \tag{4.4}$$

where, the power references with and without frequency control are P_{ref-1} and P_{ref} , respectively. The nominal frequency (pu) and inertia constant (s) of the system are denoted by f_{nom} and H_n . The rate-of-change-of-frequency (pu/s) is defined by df/dt . BESS can be designed to provide such frequency regulation via inertia control or droop control. The study in [214] suggested that droop control performs better than the inertia control. Hence in this chapter, BESS is designed to be regulated via droop control method which can be written as in (4.5):

$$P_{ref-1} = P_{ref} + K_{BESS} df \tag{4.5}$$

where, the droop gain for BESS regulation is K_{BESS} , df is the frequency deviation between the reference and the actual frequency value. The amount of BESS power activation in frequency control is determined by the droop gain of BESS. In addition,

the types of controller and parameters play crucial role in regulating BESS response.

4.3 The Detailed Modeling of BESS

The BESS model typically includes a battery bank, a three-phase bi-directional DC/AC converter and a three-phase step up transformer connecting BESS into the system. However, the regulation of BESS differs significantly depending on their particular application. In research works, several BESS operation control techniques have been adopted depending on their function [138, 141, 215–217]. The main difference in BESS control technique is whether BESS is planned to support active or reactive power or both. A very common approach in BESS control is to regulate BESS active power in response to frequency deviation [138]. However, the facility to interchange reactive power with the grid is not accessible in such circumstance. In certain case, both the active and reactive power exchange is considered to regulate frequency and voltage, nevertheless active power is typically given priority over reactive power [215, 216]. With increasing PV penetration, BESS can reduce the voltage rise/drop by regulating active and reactive power without any priority given in providing BESS active and reactive power [141] or regulating active power only [217]. Another control approach is in PV/wind output power smoothing/implementing dispatch strategy/peak shaving/load leveling where the sole purpose of BESS is to regulate active power only. considering the variation in active power output of PV/wind energy system [153, 218]. Hence, it can be summarized that BESS controlling is mainly depends on their particular purpose in power system. In this thesis, the modeling and application of BESS for both the active power priority over reactive power case and equal priority of active and reactive power cases are presented. Associated simulation studies will be carried out to demonstrate the performance of an individual BESS control techniques. In this chapter, the detail modeling of BESS and its control techniques will be elaborately presented. The detailed control mechanism of BESS is illustrated in Fig. 4.2. Fig. 4.2 illustrates BESS structure used in this study. The active and reactive power in a BESS with IGBT-based PWM converter is controlled by two individual current parameters in d and q axis. The amount

of active power in controlling frequency is defined by the rated battery capacity. On the contrary, the volume of reactive power is defined by the BESS converter size. BESS can participate in voltage and frequency control as long as the total power demand remains within the converter capacity. However, this chapter discusses only the active power control of BESS. The key components of the designed BESS are as follows:

- Frequency controller
- Active Power (P) controller
- Charge controller
- Current controller on direct (d) and quadrature (q) axis.

4.3.1 Frequency Controller

This controller as shown in Fig. 4.2 triggers active power reference based on frequency error (f_{error}) between the actual grid frequency (f_{grid}) and the nominal reference value (f_{ref}) as per the expression in (4.6):

$$df = f_{ref} - f_{grid} \quad (4.6)$$

If the grid frequency differs from 1pu value plus deadband limit, BESS is designed to absorb or inject active power to recover system frequency. If “ df ” is positive, BESS will supply active power (discharging) and if “ df ” is negative, reverse current will flow to allow BESS to consume surplus power (charging).

A small deadband is incorporated in order to avoid BESS operation according to the grid defined non-operating frequency boundary (NOFB). In response to grid frequency deviation, droop defines the amount of active power to be injected or absorbed by BESS. The full capacity of BESS for active power is activated at the defined value of “P-f droop”. At steady state condition, the value of “ df ” is zero and therefore the active power reference signal value “ P_{ref} ” is also zero. The droop value is regulated as per the expression in (4.7):

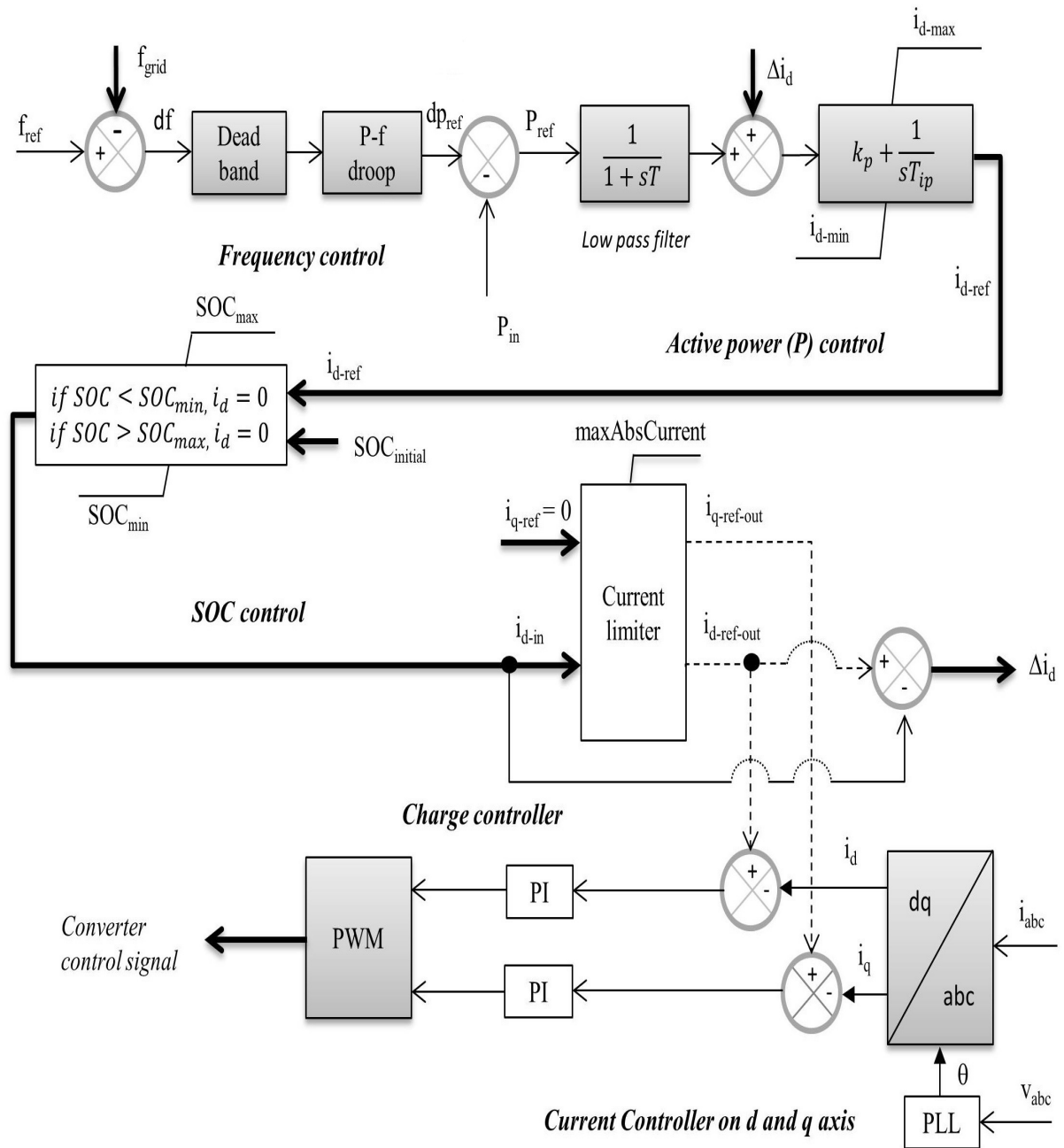


Fig. 4.2 The detailed BESS control techniques [219]

$$dp_{ref} = \pm df / droop(R_{P-f}) \tag{4.7}$$

The BESS diagram in DigSILENT/PowerFactory is shown in Fig. 4.3. The feedback signals can be adjusted according to the purpose of BESS application in the grid.

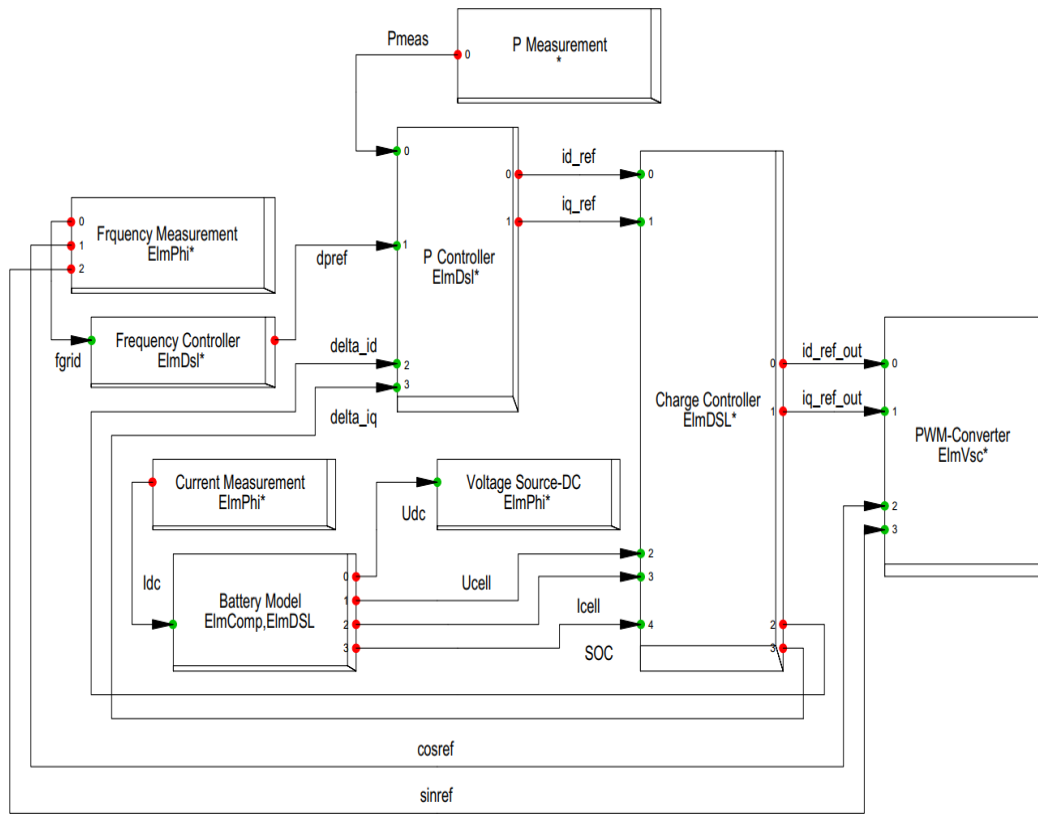


Fig. 4.3 BESS design in DigSILENT PowerFactory

4.3.2 Active Power (P) Controller

Active power (P) controller regulates BESS power output according to the power reference from frequency controller (df). The output at BESS AC side (P_{in}) is measured and taken as a feedback to the P controller to calculate the error. This error provides the updated power reference P_{ref} which is passed through a low pass filter for smoothing purpose. The filter time constant delineates the dynamic response of the output and hence, a large value may result in slower transient response. The difference between the current limiter's input and output is defined as Δi_d which is then added with P_{ref} . It is then passed through a PI controller to generate the reference for d-axis current regulation.

An anti-windup limiter is incorporated with PI controller in order to avoid integrator windup which is shown in Fig. 4.4 where x . can be written as in (4.8):

$$x_i = K_i/T_i \quad (4.8)$$

where, $y_o = i_{d-ref}$, y_{mn} and y_{mx} are the minimum and maximum d-axis current which are defined as i_{d-min} and i_{d-max} .

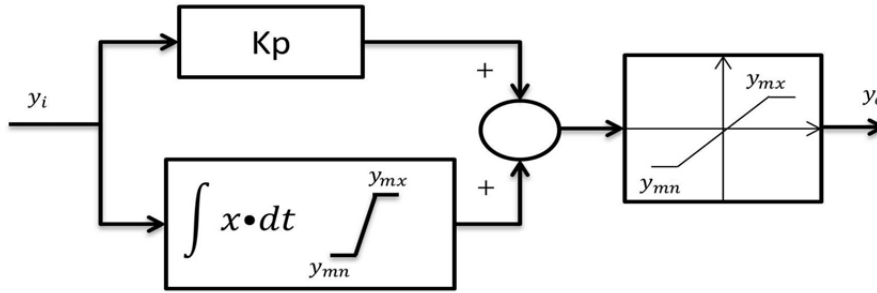


Fig. 4.4 Block diagram of PI controller with anti-windup [220]

The PI controller output can be calculated as:

$$y_o = \left(K_p * y_i + \frac{K_i}{T_i} \int_{y_{mn}}^{y_{mx}} y_i dt \right) \begin{matrix} y_{mx} \\ y_{mn} \end{matrix} \quad (4.9)$$

The PI controller output is regulated within the maximum and minimum d-axis value. The PI parameters are tuned on a trial and error basis. The main goal is to minimize frequency drop/rise and settling time. The rate of change of power (ROCOP) is not studied in this chapter, nevertheless, a ROCOP limiter can be incorporated to limit active power. The associated PI parameters are given in Appendix A.

4.3.3 Battery Charge Controller

Battery charge controller regulates BESS output (charging/discharging) according to the value and polarity of d-axis reference and depending on the accessible battery SOC. BESS injects/absorbs active power if SOC capacity remains within the designated operating boundaries. The SOC operating regions are defined in (4.10). The current limiter regulates and restrains current flow in order to avoid BESS overloading. This is

particularly applicable when BESS is designed to regulate active and reactive power. As BESS is designed to contribute in active power regulation only and d-axis reference is already restricted to the minimum and maximum value, current limiter does not play much role in this chapter. The parameters of battery SOC and charge controller are given in Appendix A. The d-axis current output is subjected to SOC control strategy which can be defined as in (4.10):

$$i_{d-in} = \begin{cases} i_{d-ref} & SOC \geq SOC_{min} \\ -i_{d-ref} & SOC \leq SOC_{max} \\ 0 & otherwise \end{cases} \quad (4.10)$$

The above condition defines that battery can consume energy (charge) if SOC is less/equal to the maximum SOC denoted as SOC_{max} and provides energy if SOC is greater/equal to the minimum SOC which is defined as SOC_{min} . Battery is not possible to be charged or discharged if SOC is outside of these maximum and minimum limits. In addition, battery can be charged when BESS is not operating and according to the defined charging strategy. The detailed discussion on battery charging strategy will be discussed in Chapter 5. The amount of maximum and minimum active power output can be adjusted separately according to the designer preferences.

4.3.4 d-q Current Controller

The current controller in d-q axis regulates BESS active/reactive current reference with respect to the grid in d-q frame of reference. BESS is synchronized with the network by Phase-locked-loop (PLL). The d-q axis error is then passed through PI controller for regulating BESS power output. The Pulse width modulation (PWM) is controlled by the modulation index of d-q axis and the reference is characterized by the cosine and sin functions. The associated PI values are given in Appendix A.

4.3.5 Battery Model

Electrical equivalent representation of chemical reaction based battery is the most challenging task in establishing a suitable battery model. Various modeling methods have been progressed over the decades [221, 222]. A typical battery is demonstrated by terminal voltage which is a function of battery SOC [223] and an internal resistance which is a function of battery SOC, temperature and the aging of battery cell [224]. The selected battery model is a simple equivalent model which is known as simple R_{int} circuit [225–229] as shown in Fig. 4.5. The voltage source is battery SOC dependent where $V_{oc}(s, SOC)$ is the internal voltage (voltage source), $R_{int}(s, SOC)$ is the internal resistance and U_{DC} is the terminal voltage. The terminal voltage can be defined as in (4.11):

$$U_{DC} = U_{max} * SOC + U_{min} * (1 - SOC) - I_b * R_{int} \quad (4.11)$$

where,

U_{max} = Fully charged battery voltage

U_{min} = Fully discharged battery voltage

I_b = Battery current

R_{int} = Internal resistance

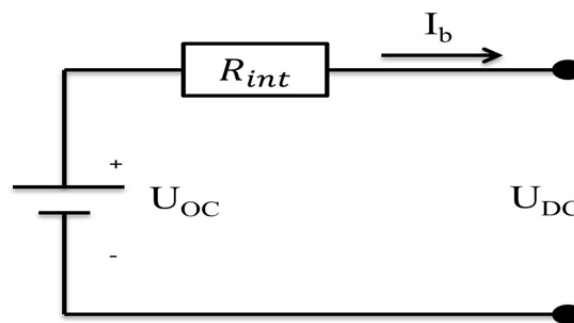


Fig. 4.5 Block diagram of R_{int} equivalent battery model [48]

4.3.6 Battery SOC Calculation

There are many SOC calculation methods that have widely been used. In this work, Coulomb counting method is used to calculate battery SOC as in (4.12):

$$SOC_k = SOC_{k-1} + \int_{k-1}^k \frac{\eta I_b}{3600 C_b} dt \quad (4.12)$$

where, I_b and C_b are the battery charge/discharge current and given battery capacity (Ah), respectively. The Coulomb efficiency is defined by η , k is the current period. The charging/discharging efficiency of the battery and converter efficiency vary in real time and lossless assumption is not accurate enough. However, many research works consider 100% efficiency for simplicity [225,227,228,230,231] in dynamic studies. Typically, this work has considered 100% efficiency for the battery and the converter, unless otherwise mentioned.

The DC terminal voltage of the BESS is 0.9kV. The maximum and minimum voltage of each battery cell are considered as 13.8V and 12V, respectively. There are 65 batteries in series to form 0.9kV at fully charged condition. The AC terminal voltage of the BESS converter is 0.4kV. BESS is integrated to the grid via 0.4/230kV transformer.

4.3.7 Charge/Discharge Cycle and Battery Lifetime

There are various factors that affect battery lifetime such as cell temperature, SOC etc. The DOD which is determined as the charge/discharge cycle of battery significantly affects battery lifetime [232]. The DOD can be written as in (4.13) [233]:

$$DOD(k) = DOD(k_o) + \frac{I_b \Delta k}{C_b} 100\% \quad (4.13)$$

where, Δk is change of period. The increased charge/discharge current will raise the change of DOD and thus adversely affects battery lifetime. The lifetime of a battery L_b

can be calculated as in (4.14) [234]:

$$L_b = \frac{1}{\sum_{m=1}^N \frac{NC_m}{CFd_n}} \quad (4.14)$$

where, NC_m and CFd_n are the number of cycles and cycles to failure at a DOD. The DOD period is defined by m which ranges from 1 to N . The equation as in (4.14) points out that battery lifetime reduces with the increase in the number of cycle with large DOD. The detailed discussion on lifetime calculation can be found in [226, 228].

4.4 System Modeling and Case Studies

This section briefly discusses the selected system modeling. In addition, the simulated case studies are also highlighted in this subsection.

4.4.1 System Modeling

The studied power system is an IEEE 9 buses system which is also known as P.M. Anderson network which is shown in Fig. 4.6 [235]. The default network comprises of 3 SGs. An IEEE Type AC1 exciter and automatic voltage regulator models are included with all the SGs. The SGs G1, G2 and G3 are equipped with gas, hydro and coal type turbine system model, respectively. The G1 is conceded as the reference machine.

The consolidated wind farm of varying capacity is incorporated at bus 9. The terminal voltage of wind farm is 0.69kV and connected to the grid via a 0.69/230kV transformer. The capacity of each wind turbine is 2.2MW. Doubly fed induction generation (DFIG) type wind power system is considered and the wind turbine is modeled with FRT facility. More details on the system modeling can be found in [236]. The rated capacity of G1 and G2 is 250MVA and 300MVA with total steady state load demand of 315 MW.

In general, the amount of wind power output varies according to the available wind

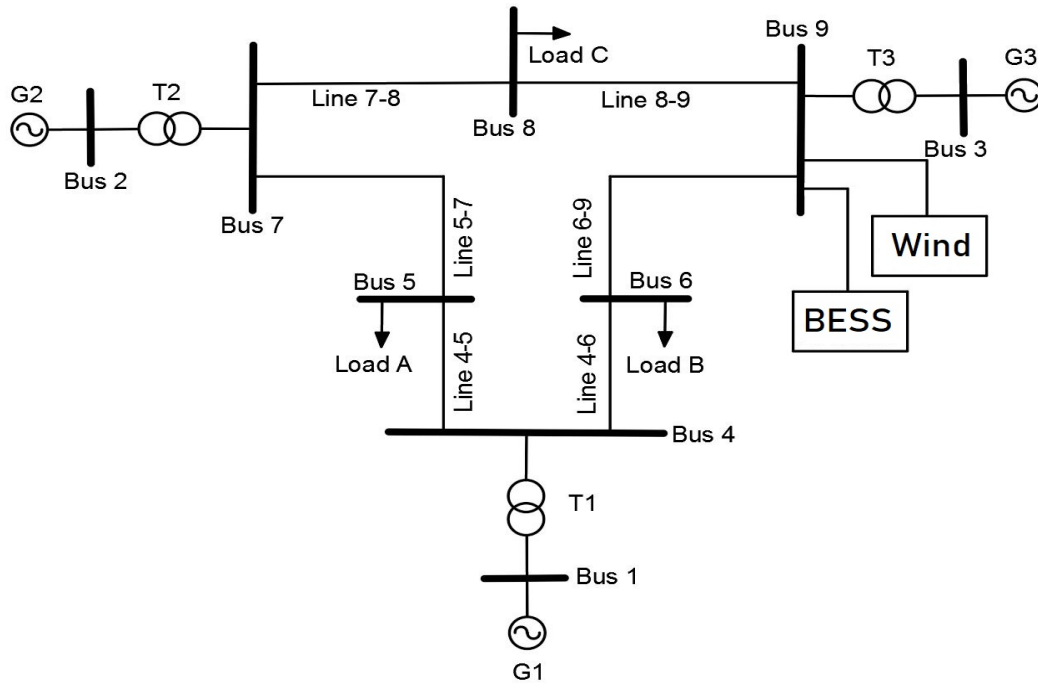


Fig. 4.6 The studied 9 bus system with the installed wind and BESS [219]

speed. Since the primary objective of this study is to analyze the transient performance of the grid with the different penetration levels of wind power, it is assumed that wind farm is producing the maximum power output at the time of transient periods. Fig. 4.7 shows a typical plot for wind speed *vs.* power output level in percentage. The maximum power output shows the impact of maximum wind power penetration and thus less power output during lower wind speed has minimum impact on transient behavior of the network.

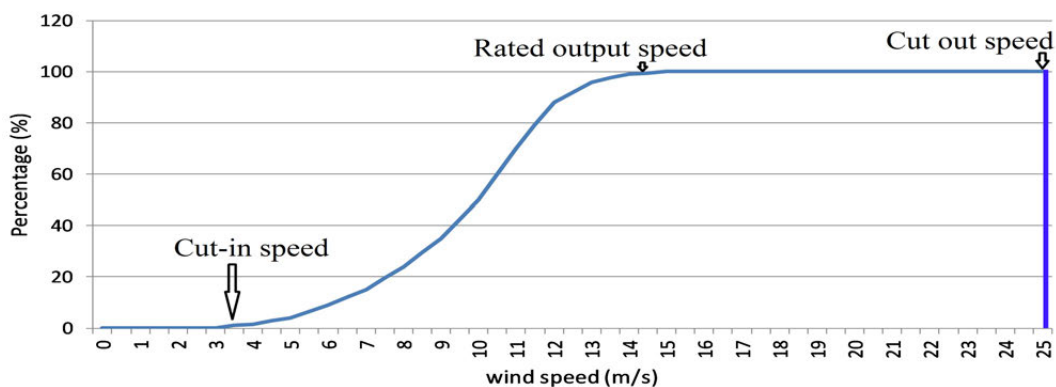


Fig. 4.7 The power output of wind farm (%) with respect to varying wind speed [219]

4.4.2 Case Studies

The impact of wind penetration depends on the installation location, FRT capability and whether they are designed to participate in frequency control or not. In addition, the types of contingencies and faults duration also determines the intensity of the impact. This chapter analyzes three case studies for demonstrating the impact of wind penetration and they are as follows:

- *Case-1*: Single phase to ground fault
- *Case-2*: Temporary outage of the heavily loaded line
- *Case-3*: Load growth event at load B.

The case studies are carried out considering four operating scenarios which are as follows:

- Base case; no wind penetration
- Wind penetration limit and the shutdown of G3 plant
- Larger wind penetration without BESS
- Larger wind penetration with BESS.

4.5 Result and analysis

The detailed analysis and discussion of the simulation studies are also presented in this section. Simulation studies are carried out in DigSILENT/PowerFactory for verifying the potential of BESS in enhancing oscillation damping with the increased penetration of wind power. The primary objective is to permanently shutdown G3 unit and install the wind power of equal or high capacity. This will put more stress on the grid compared to when the G3 unit remains connected to the grid. As wind farm is equipped with FRT capability, the wind farm will remain connected to the grid during the fault periods. The

penetration level of wind power varies for the various case studies to identify allowed penetration following the studied contingencies.

4.5.1 Case-1: Wind Penetration with Single-phase-ground Fault

The network performance is evaluated with the various levels of wind penetration following a single phase to ground fault. The point at which wind penetration violates the grid defined limits is identified and then BESS is incorporated to contribute in oscillation damping. The fault is applied at phase-a for the duration of $t=0-0.15s$ at bus 6. Figs. 4.8 and 4.9 show that when G3 unit is permanently removed from the network, 92MW (14.33%) is the maximum allowed wind penetration, considering the mandatory grid required frequency variation of $\pm 1\%$ from the nominal value for both the G1 and G2 units. However, it can be seen that the frequency drops by 9.54% as compared to the base case of no wind penetration. This clearly indicates the negative inertial impact of wind penetration in the grid. Considering the study of increasing wind power penetration, further wind power is incorporated in the grid.

Fig. 4.8 depicts that with 120MW (17.91%) of wind power integration and without a BESS, the maximum frequency of G2 reaches beyond the grid allowed limit following the applied fault. This defines system violation of the grid requirements with the 3.58% increased penetration of wind power. Nevertheless, G1 shows a satisfactory outcome as it does not violate the grid limits for both operating conditions as shown in Fig. 4.9.

When a BESS is integrated with 120MW wind penetration, the frequency rise reduces to 1.009pu which is smaller than the required grid limit. BESS reduces frequency rise and drop. In addition, it is also visible that BESS reduces frequency oscillations and achieves faster steady state value for both generators G1 and G2 compared to without a BESS condition. The grid is capable of handling the system most of the time of its operation. But, it is only during the very short period of time which requires additional inertia support and BESS is one of the most competitive option to serve this purpose.

Furthermore, the contribution of BESS is also visible in reducing the oscillation of

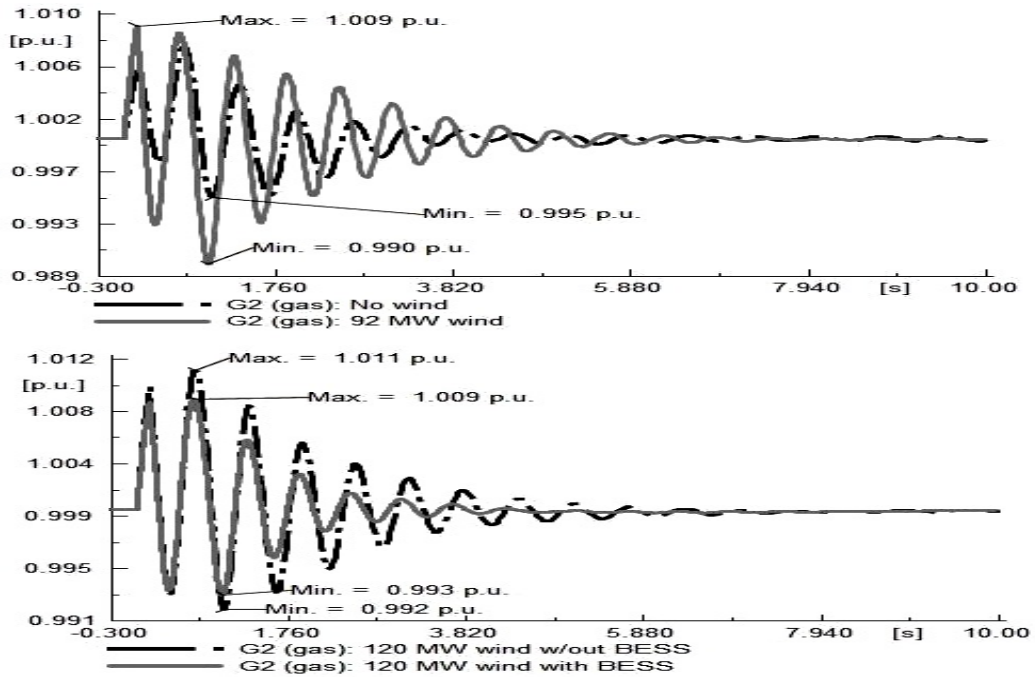


Fig. 4.8 Frequency of generator G2 with single-phase-ground fault (phase-a) [219]

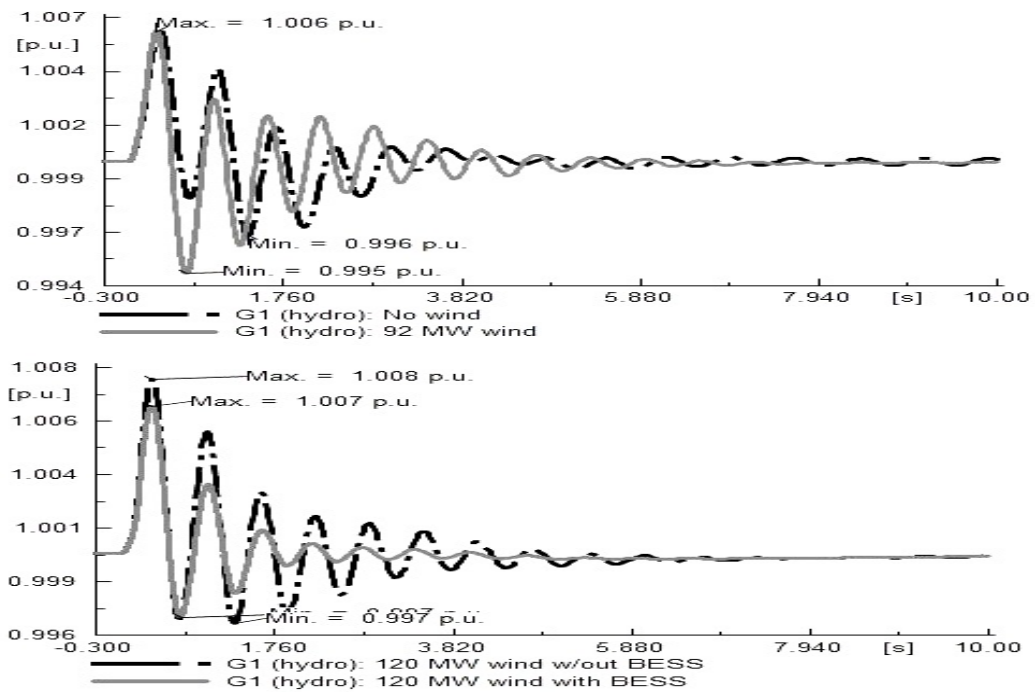


Fig. 4.9 Frequency of generator G1 with single-phase-ground fault (phase-a) [219]

generator’s power output as illustrated in Figs. 4.10 and 4.11. BESS supports in faster damping of power oscillations which are manifested in the frequency outcome. The maximum power oscillations of G1 and G2 increase by approximately 30% and 21% with 92MW wind power compared to without any wind power. Similarly, the lowest frequency

drop is also visible with the penetration of wind power in the grid. With 120MW wind power and without a BESS, the power oscillation of G2 reaches to 240MW (maximum) and 42.9MW (minimum). The same operating condition for G1 results maximum and minimum power oscillations of 180.7MW and -57.7MW, respectively. BESS results in the reduction of maximum oscillation for G2 to 237.1MW and the minimum value of 57.9MW. A similar level of performance is visible in the case of generator G1.

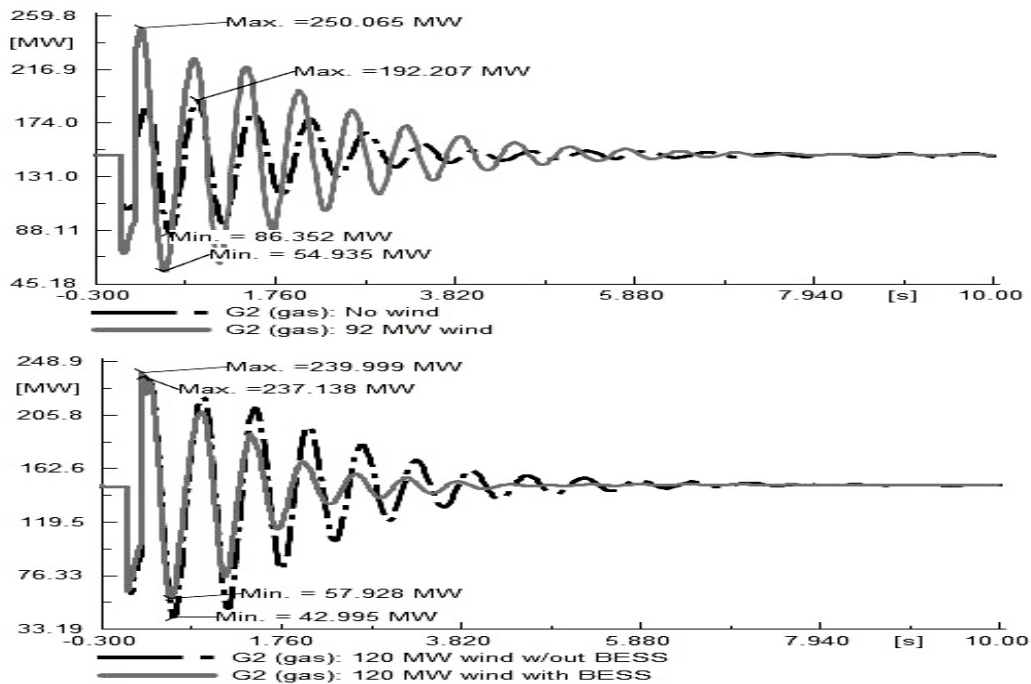


Fig. 4.10 Active power output of generator G2 with single-phase-ground fault (phase-a) [219]

The output power of BESS is illustrated in Fig. 4.12. BESS supplies approximately a maximum power of 38MW and consumes 37.5MW during the contingency periods. As no reactive power control is implemented, the reactive power output of BESS is zero. The change of battery SOC is shown in Fig. 4.13. It shows that the battery SOC has barely changed during its operation. This also indicates the importance of high BESS power output than the energy output considering temporary contingency events.

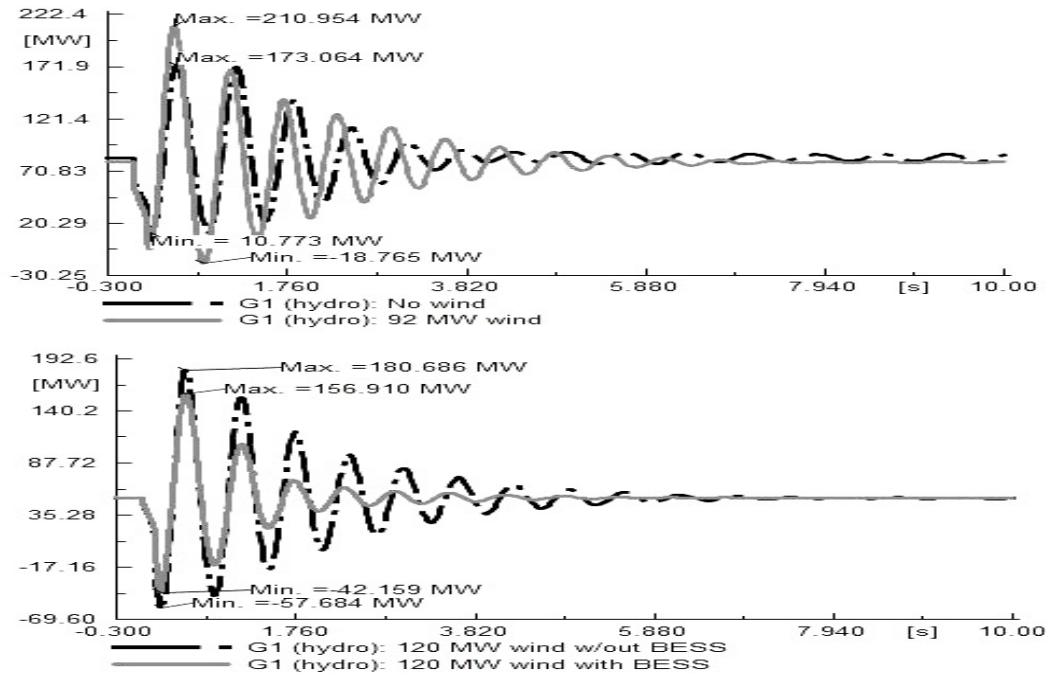


Fig. 4.11 Active power output of generator G1 with single-phase-ground fault (phase-a) [219]

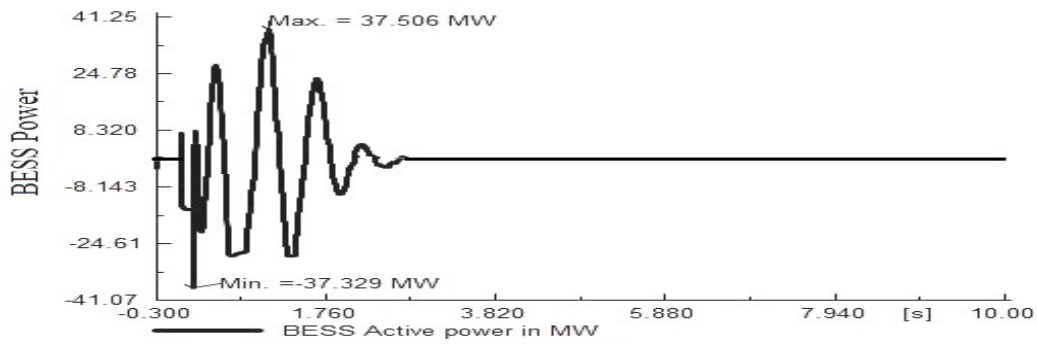


Fig. 4.12 The power output of BESS [219]

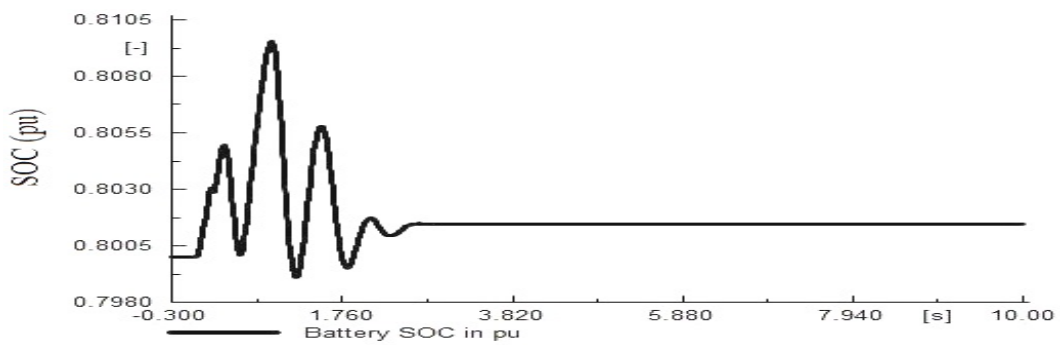


Fig. 4.13 Battery SOC [219]

4.5.2 Case study-2: Temporary Outage of the Heavily Loaded Line

Out of the many network event, line outage is often experienced by the power system mainly due to various weather dependent and natural conditions such as collapsed electric poles, broken conductors, etc.. In order to analyze the substantial impact, the heavily loaded line *Line 5-7* is selected for the event of temporary outage. The applied duration of line outage is 0-0.24s and the line is restored after 240ms.

The frequency output of generators G2 and G1 are shown in Figs. 4.14 and Fig. 4.15. Simulation results exhibit that in the case of generator G2, the grid limit allows 80MW (12.7%) of wind penetration. In order to analyze the impact of BESS, the penetration of wind power is increased to 106MW. The increased wind penetration results in the frequency of generator G2 to violate the grid allowed operational requirements. On the contrary, the integrated BESS reduces the frequency rise within the acceptable limit which justifies the influence of BESS with the increased penetration of wind power in the grid. However, the impact of the same level of wind penetration is still minimal in the case of generator G1 because generator G1 has more headroom available than G2. The impact of generator loading condition will be further discussed in Chapter 5.

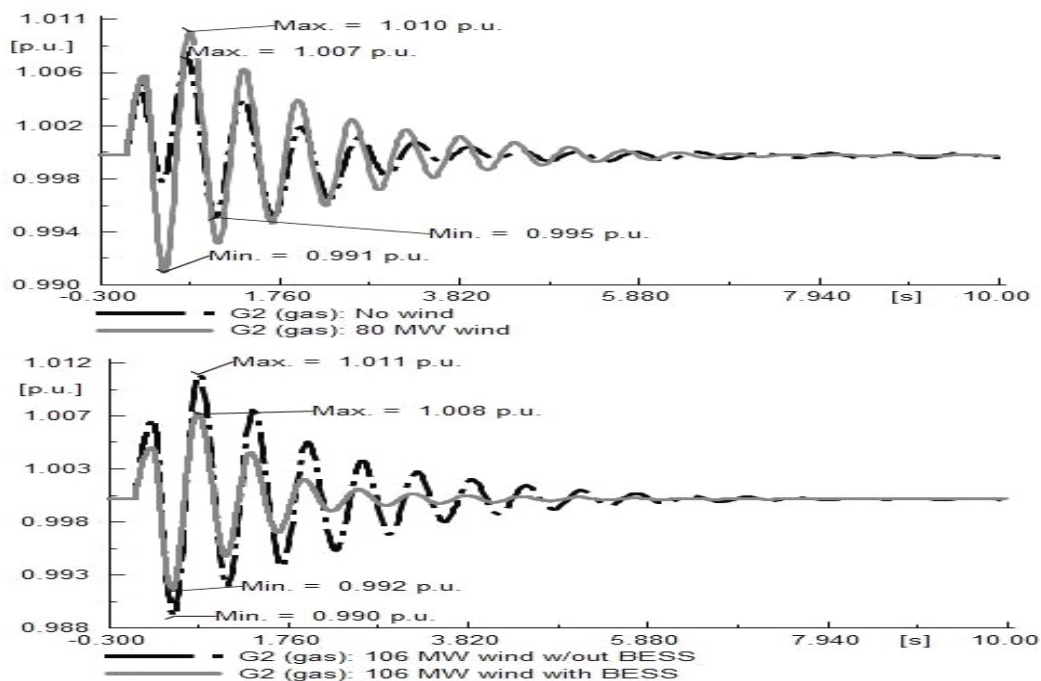


Fig. 4.14 The frequency response of generator G2 for line event [219]

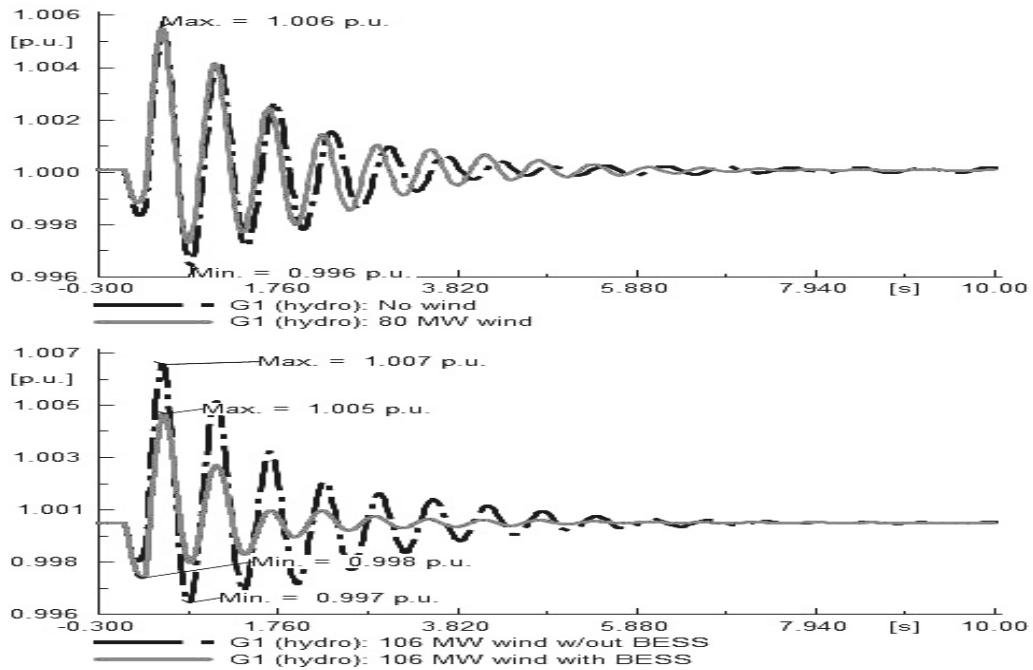


Fig. 4.15 The frequency response of generator G1 for line event [219]

BESS significantly diminishes active power oscillation in comparison to without a BESS as illustrated in Figs. 4.16 and 4.17. Moreover, the maximum and minimum oscillations of generators with a BESS reduce to lower values than the case of without a BESS. These observations demonstrate the efficacy of BESS in enhancing frequency regulation capability of the grid with increased penetration on wind power.

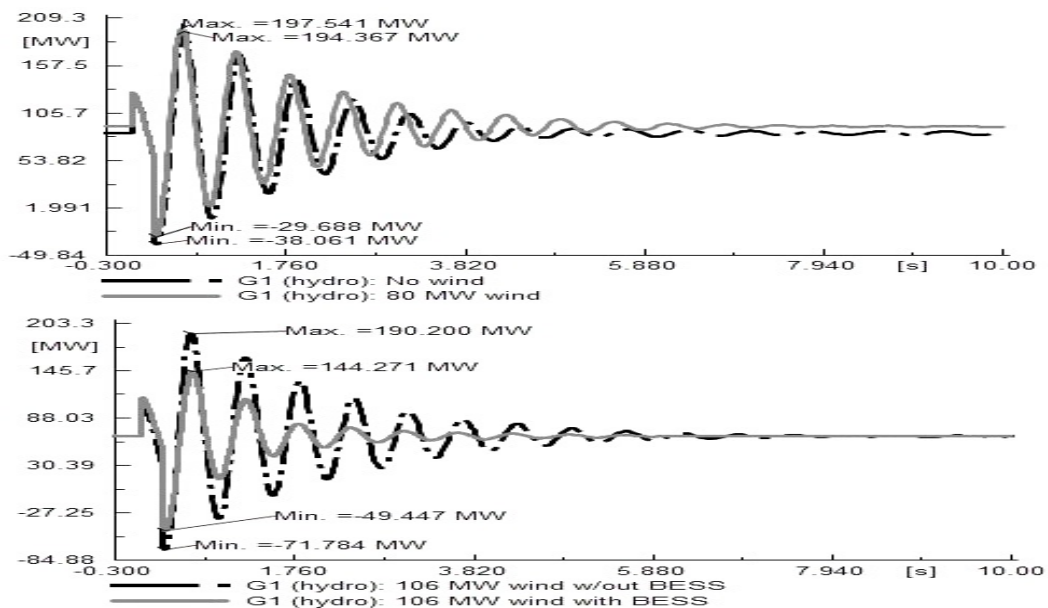


Fig. 4.16 Active power output of generator G1 with line outage [219]

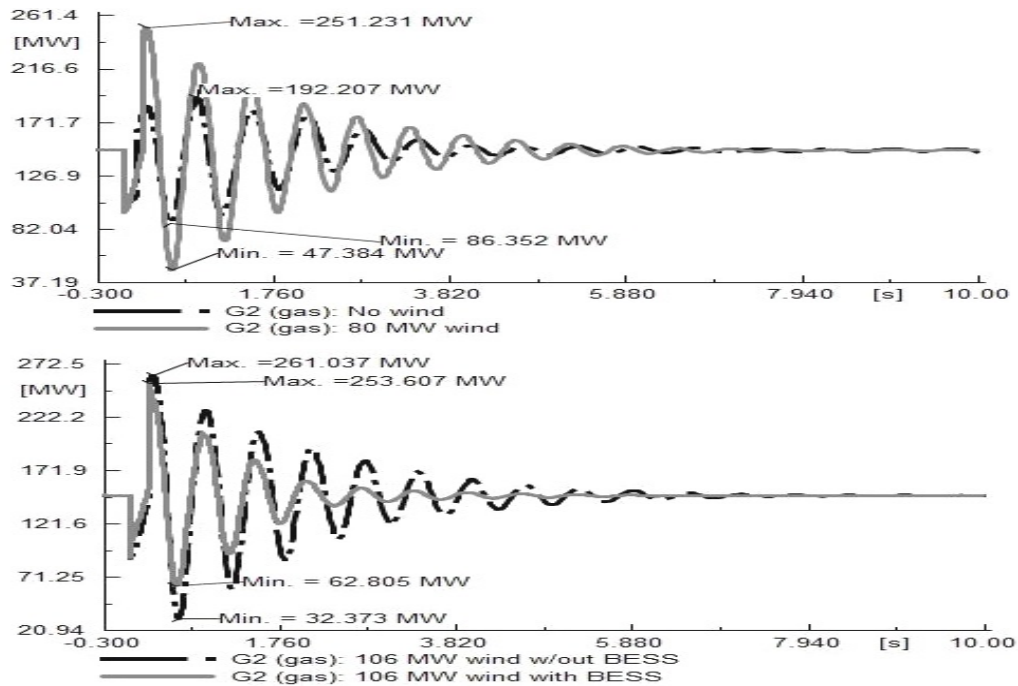


Fig. 4.17 Active power output of generator G2 with line outage [219]

The response of BESS is illustrated in Fig. 4.18. BESS consumes the excess energy during over-frequency and supplies energy during under-frequency beyond the deadband. The maximum and minimum value of d axis defines the amount of BESS power output. In order to demonstrate how these values regulate BESS power output, the minimum active power limit is selected as -70% which is reflected in the BESS power output as 28MW of the total 40MW capacity. These limits can be adjusted to various values depending on the energy management policy by the operator. Fig. 4.19 depicts that battery SOC does not show significant change. Nevertheless, this depends on the rated capacity and can be significant in the case of smaller battery size.

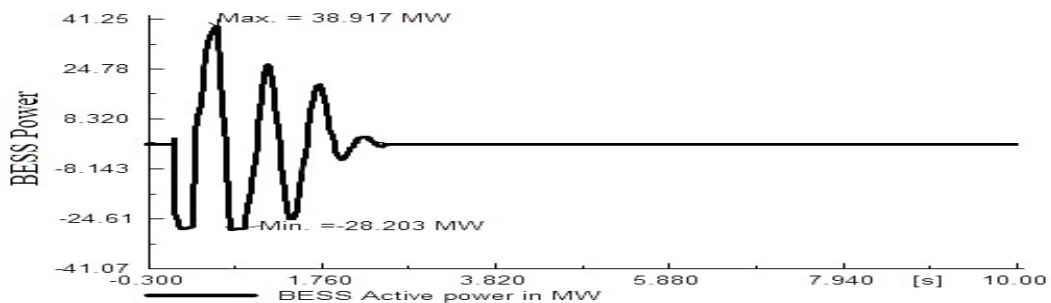


Fig. 4.18 BESS active/reactive power [219]

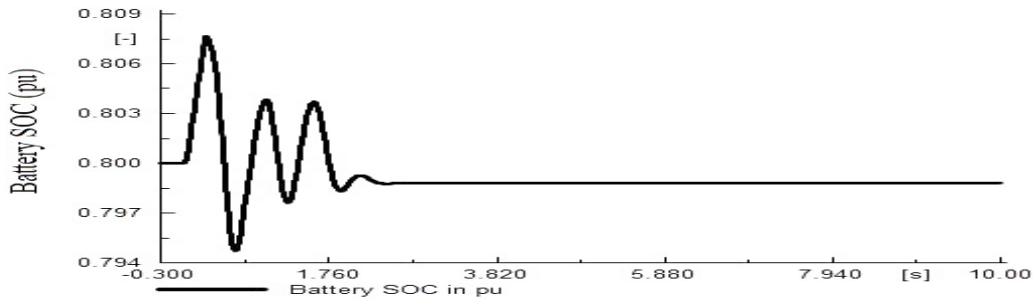


Fig. 4.19 Battery SOC [219]

4.5.3 Case study-3: Load Growth Event at Load B

An abrupt load changing event is studied for further investigating BESS performance in enhancing the stability of the grid. The load event is applied for the case of 120MW wind penetration. A temporary load growth of 50% at load A is triggered during $t=1-1.5$ s and the frequency performance is monitored for different operating conditions. The simulation results as shown in Fig. 4.20 portrays that when there is no wind penetration, the grid can successfully maintain the lower frequency boundary within the grid code requirements following the applied temporary load growth. However, with 120MW of wind penetration and same load increase event, the frequency drops to 0.989pu i.e. the grid fails to satisfy grid requirements. This phenomenon clearly indicates the negative impact of low inertial wind power in the grid.

Conversely, grid frequency is maintained within the $\pm 1\%$ of the nominal value when BESS is incorporated in the grid. BESS provides sufficient energy during the under-frequency event and pulls back the frequency closer to the nominal value. BESS is placed at two different buses to see how the grid response varies. The comparative frequency responses demonstrate that the lowest drop in frequency is moderately better when BESS is installed at bus 4. This is due to the fact that BESS is closer to the load event center when placed at bus 4. BESS manifests superior frequency performance by reducing the error and minimizes the power oscillations of both generators.

The power output of BESS is displayed in Fig. 4.21. It can be seen that BESS provides a similar level of power response following the load event. However, when it is installed at bus 4, it provides slightly higher power which in turn results in marginally

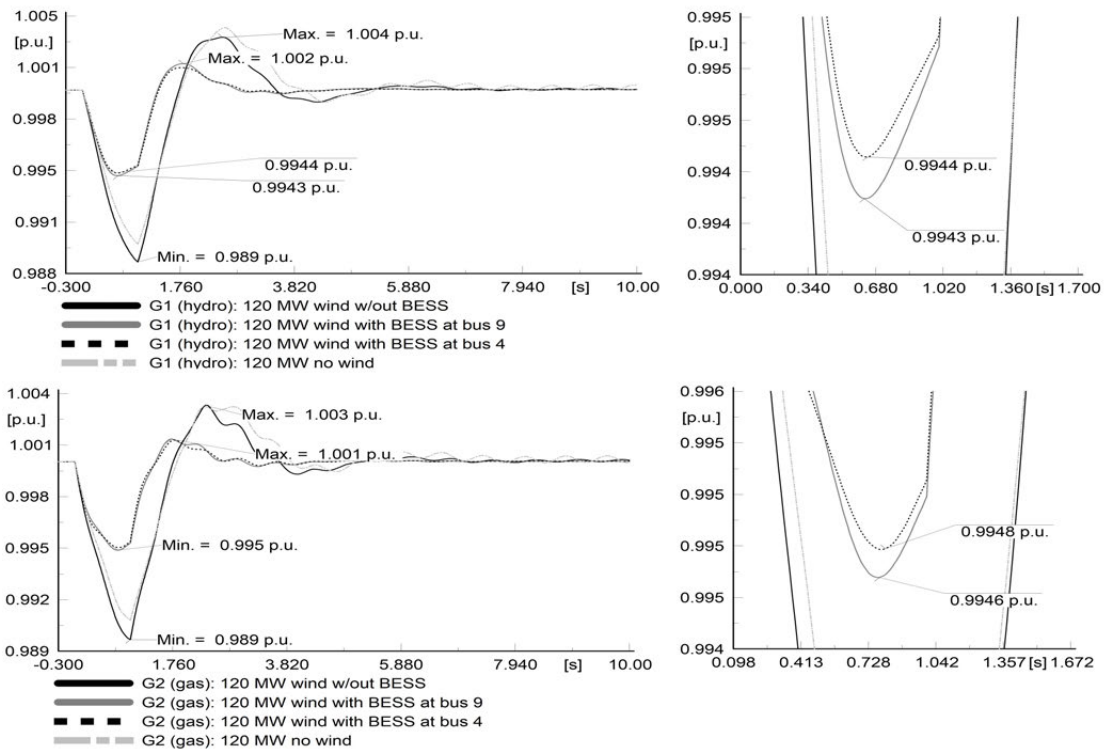


Fig. 4.20 The frequency of generators G1 and G2 with temporary load growth [219]

better frequency response. This is also due to the fact that BESS closer to the contingency location results in lower losses compared to when it is installed at a far distance. BESS active power settles to zero once the frequency is recovered within the NOFB at approximately $t=2.8s$. As the amount of power at BESS output is nearly the same for both location, battery SOC values are very close to each other as illustrated in Fig. 4.22.

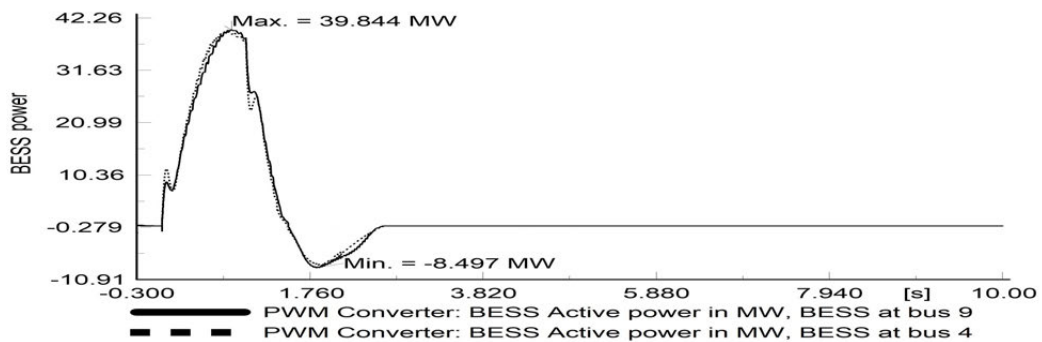


Fig. 4.21 BESS active/reactive power [219]

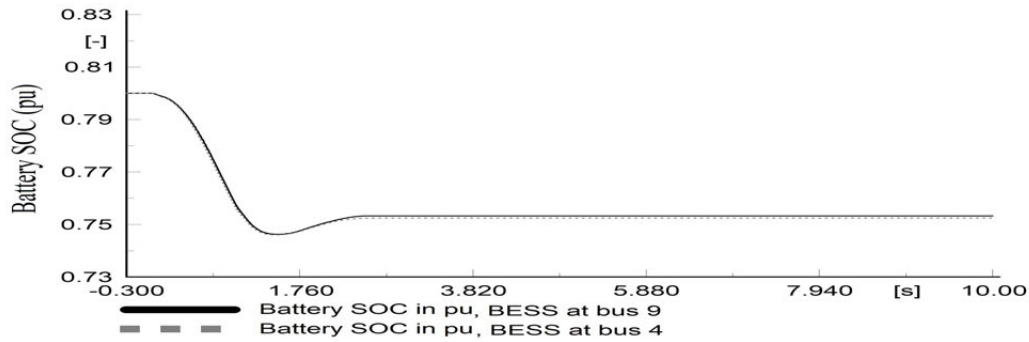


Fig. 4.22 Battery SOC [219]

4.6 Conclusion

BESS is capable of providing prompt responses to the changing grid conditions and therefore, it is foreseen as a remarkable alternative in the renewable energy integrated power grid. The impact of wind penetration level is largely affected by the types and location of the faults in the grid. A BESS in enhancing the grid stability with the increased penetration of wind power is presented in this chapter.

In order to verify the applicability of BESS, three case studies have been simulated. The simulation results exhibit that with the increase in wind penetration, the frequency of the grid is significantly affected due to the reduction in overall grid inertia. Beyond a certain limit, wind penetration results in violating the mandatory grid code requirements which will impact the stability of the grid. When BESS is installed, the grid stability is accomplished within the grid allowed boundary. This validates the important application of BESS in the grid with the focus of increasing wind penetration level. BESS not only regulates frequency within the limit but also reduces the power oscillations in the grid. Moreover, the change of BESS output power and battery SOC indicates the importance of total BESS power instead of BESS energy from the perspective of transient stability.

While BESS can provide a rapid and robust response to the grid, the type of controller for BESS output regulation plays a significant role in its performance. Furthermore, an adjustable battery SOC management is essential to provide greater flexibility of BESS operation and improve its potential. These require further investigation to ensure better regulation and performance evaluation of BESS.

Chapter 5

BESS for Reducing the Impact of PV penetration on Frequency Regulation and SOC Recovery

This chapter contains the following publication - Battery Energy Storage System Design for Mitigating PV Penetration Impact on Power System Primary Frequency Control,” IEEE Transactions on Sustainable Energy, vol. 11, pp. 746-757, 2020.

5.1 Introduction

In comparison to wind power, PV was given less attention due to their level of penetration in the grid. However, it is expected that PV penetration will have approximately 59.6% increase from their present installation scale by 2022 mainly due to the lower prices of technologies related to PV generation [237]. Hence, the dynamic influence of PV can no longer be neglected and thorough analysis on the impact of PV penetration needs to be considered.

Unlike wind turbine, PV system does not contain any moving parts which defines that there is no stored kinetic energy that can be used during a contingency event mainly

during an under-frequency event. Therefore, PV penetration will significantly reduce system inertia and this may raise severe concern for the stability of the grid. Several research works have argued that reduced inertia increases the deviation of frequency in the grid [238–240]. With the higher penetration of PV, the induced frequency oscillations can violate the grid operating requirements which can probably threaten the security and stability of the grid [240].

Various control approaches such as power oscillation damper [241], synchronous power controller [242] and adaptive controller [243] are proposed with PV system for oscillations damping resulted from any momentary imbalances between the generation and load demand. In order to regulate PV output, droop control [244], inertia control [245] and operating at deloaded point [122] are presented for regulating the power output and participating in frequency regulation. A comparative performance analysis in [121] indicated that the combined droop and inertia control provides superior system performance during over-frequency regulation than their individual control method. Nevertheless, the PV output is curtailed roughly by 50% for participating in over-frequency regulation. As mentioned earlier, PV does not have any stored kinetic energy and hence under-frequency response is not possible to incur from PV farm. In order to avoid the penalty by the transmission system operator, auxiliary energy sources are essential for participating in frequency control and satisfy the regulatory requirements.

As discussed in the previous chapter, BESS is an effective alternative energy source in providing frequency regulation and satisfying grid requirements. The study in [246] presented that the damping performance of the grid can be improved by the use of BESS. However, battery sizing and SOC calculation are not considered in the study. In addition, the penetration of PV is very low (1%) and thus does not provide any insight on the severe impact of PV penetration in a large-scale. A small-scale power system is considered in [41, 212] for demonstrating the performance of BESS in regulating frequency control of the grid. A lead-lag regulated BESS is incorporated in [220, 247] for frequency regulation and enhanced oscillation damping. However, any SOC recovery strategy is not considered in the study.

A major portion of the aforementioned studies did not present any strategy to recover battery SOC which is an incomplete technical solution for BESS integration. A SOC recovery approach is able to reduce regulation failure and minimize any accumulated costs related to penalty [248]. The studies in [225, 228, 249] have proposed a SOC recovery strategy which are studied in a MG. However, SOC is recovered to the nominal value only which lacks the flexibility of BESS operation considering the variable nature of the grid or renewable generation. On the contrary, an adaptable SOC recovery strategy is proposed in [212] but, this reduces the overall capacity of battery as the maximum and minimum SOC is limited to the adjustable SOC value.

In this chapter, a lead-lag regulated BESS with droop-type mechanism is presented for contributing to frequency control and satisfying the grid requirements as defined by the Australian NEM. The purpose of the proposed BESS is to regulate the frequency within the grid defined regions following the contingencies and avoid any relevant penalties by the network operator. In addition, BESS is also regulated to participate in voltage control, given that sufficient battery capacity is available to provide both the voltage and frequency support. Energy exchange while participating in frequency control may reduce the battery SOC significantly. Therefore, a new adaptive SOC recovery method is also presented in this study that can be adjusted according to operation requirement. The proposed design allows regulating BESS SOC to be regulated to the maximum value during the network event and to the adjustable SOC value without affecting the maximum SOC (SOC_{max}).

A medium-sized power system is chosen to analyze the performance of the proposed BESS with 18.18% of PV penetration. In the absence of any real data, the installation location and converter size of BESS is presented on a trial and error basis. It is shown that operation strategy i.e. the loading of generators at pre-disturbance condition plays a predominant role on the frequency response of the generators. Moreover as expected, an increase in PV penetration results in higher frequency oscillations and violates grid requirements when generators are heavily loaded. However, the integrated BESS successfully mitigates adverse inertia impact of PV or generator loading conditions and regulates the frequency that satisfies the grid operating requirements. The proposed

SOC recovery strategy demonstrates the superiority compared to the conventional approach in terms of responding to the network events and recharging to a level defined by the BESS operator.

5.2 Frequency Control with PV and NEM Grid Conditions for Frequency Stability

The system must have adequate energy reserve in order to provide damping support to the grid following any contingency event. The energy reserve can be arranged through the accessible generator's output or any other forms of energy storages.

The steady-state frequency should be maintained within the NOFB. The generator should provide any temporary imbalances between the load demand and the generation to maintain the nominal frequency or compensate any under/over-frequency action. Hence, the governor response to the changes in frequency with n numbers of generation systems can be written as in (5.1):

$$\frac{df}{dt} = \frac{f_{ref}}{2 \sum H_n} \Delta P_d \quad (5.1)$$

where, the change of power demand is defined by ΔP_d which is the error between the generated power P_{Gen} and the load power demand P_L . The total system inertia constant is H_n and the nominal frequency is f_{ref} .

As the growth of PV penetration increases, the system inertia will be reduced regardless of fossil-fueled power plants are connected or dismantled permanently from the existing network. In addition, with the reduced inertia and varying PV output/network operating conditions, the grid may fail to compensate for any power imbalances. A BESS can be an alternative energy storage device to provide frequency control and minimize the negative impact of PV as illustrated in Fig 5.1. Therefore, the system response with the BESS to the changes in grid frequency can be written as

in (5.2) [212]:

$$\frac{df}{dt} = \frac{f_{ref}}{H_B + 2 \sum H_n} \Delta P_d \tag{5.2}$$

where, H_B is BESS inertia constant, the droop coefficient of SGs are D_1 and D_2 of generators SG_1 and SG_2 , respectively.

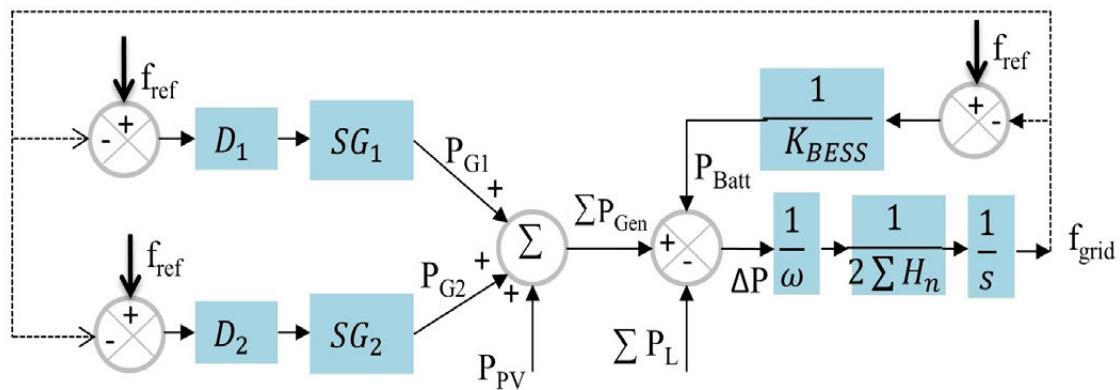


Fig. 5.1 Primary frequency control of PV integrated system with BESS [48]

The stability criteria for frequency varies with countries, grid operators, generation types and the nature of contingency events. In this chapter, the Australian NEM standards [210, 250] are considered for assessing the grid performance following the studied contingencies. It is worth noting that, these standards are applicable for the Australian Mainland only and Western Australia is not included and these standards are different for Tasmania or for an islanded/isolated grid. In the normal operation time, the frequency must be maintained within the NOFB of 0.997-1.003pu. The NEM standards allow the frequency to be maintained within 0.99-1.01pu for 15s in the case of generation or load changing event [210]. On the contrary, the frequency must be regulated within 0.98-1.02pu for 15s following a load growth/reduction event [210]. The non-operating region for voltage is 0.9-1.1pu [250].

The aforesaid frequency standards are considered as the references for designing and identifying the location and converter sizing of BESS, providing necessary oscillation damping and enhancing the capability of the grid to be compatible with the NEM grid code requirements.

5.3 The Overall Modeling of BESS for Voltage and Frequency Control

The generic design of BESS is illustrated in Fig. 5.2 which consists of a set of batteries, power conversion system and if needed, a step up transformer for connecting to the grid. BESS regulates its active and reactive power output based on the reference signals generated by the voltage and frequency controller, given that the battery SOC constraints are satisfied. The key components of BESS are as follows:

- Frequency controller
- Voltage controller
- Active/reactive Power (PQ) controller
- Charge controller
- Current controller on direct (d) and quadrature (q) axis.

The design of BESS in DigSILENT/PowerFactory is shown in Fig 5.3. The detailed discussion of each of the controllers will be presented in the coming subsection.

5.3.1 Feedback Signals for BESS Regulation

In response to any unwanted transient events, a considerable amount of damping assistance is needed to reduce oscillations of the grid. The frequency and voltage control loops initiate the needed reference for the active and reactive power regulation of BESS as illustrated in Figs. 5.4 and 5.5. The measurements are taken locally, at the BESS connection point. However, using wide area measurement technique, global frequency and voltage measurements can be considered, if needed.

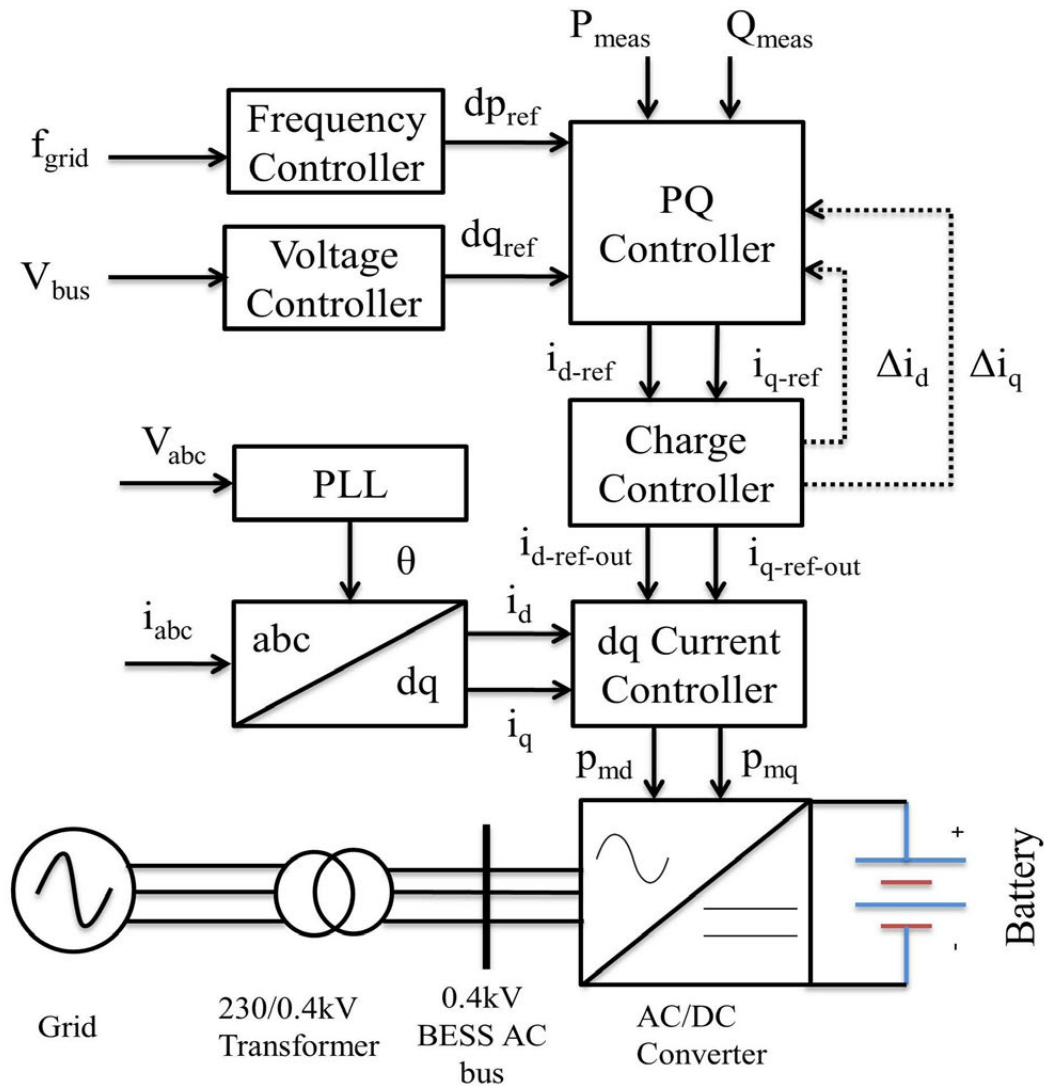


Fig. 5.2 Frequency and voltage control with BESS [48]

5.3.1.1 Frequency Droop Controller

The droop control for power-frequency regulation can be written as in (4.6). The typical characteristics for “p-f” droop can be explained in three operating zones as demonstrated in Fig. 5.6.

NOFB defines the area in which the BESS should remain inactive. The battery should operate in discharging mode when grid frequency f_{grid} is lower than the discharging frequency f_{disch} and in charging mode if f_{grid} is higher than the charging frequency f_{ch} . However, this is only possible to take place as long as the battery SOC satisfies the defined operating constraints. The NOFB regions, according to NEM, range between f_{ch}

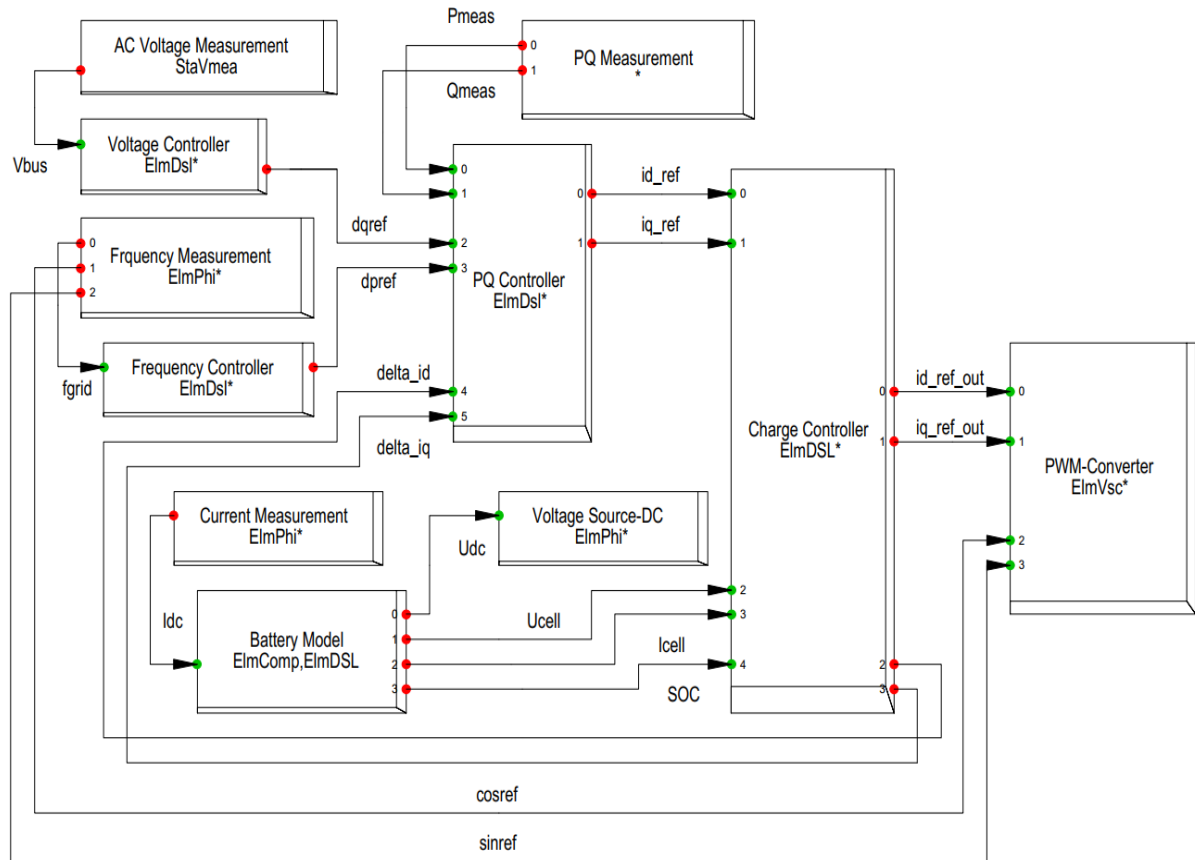


Fig. 5.3 The model of BESS in DigSILENT/PowerFactory

(1.003pu) and f_{disch} (0.997pu). The maximum frequency deviation df_{max} activates the maximum BESS power consumption (P_{ch-max}) from the grid if battery SOC stays below or equal the maxSOC. On the contrary, the minimum frequency drop df_{min} activates the maximum BESS power discharging ($P_{disch-max}$) to the grid as long as battery SOC stays above or equal to the minimum SOC.

5.3.1.2 Voltage Droop Controller

The voltage controller generates reactive power control signal reference depending on voltage error (dv) between the actual bus (v_{bus}) and the nominal reference voltage (v_{ref}) as per expression in (5.3):

$$dv = v_{ref} - v_{bus} \tag{5.3}$$

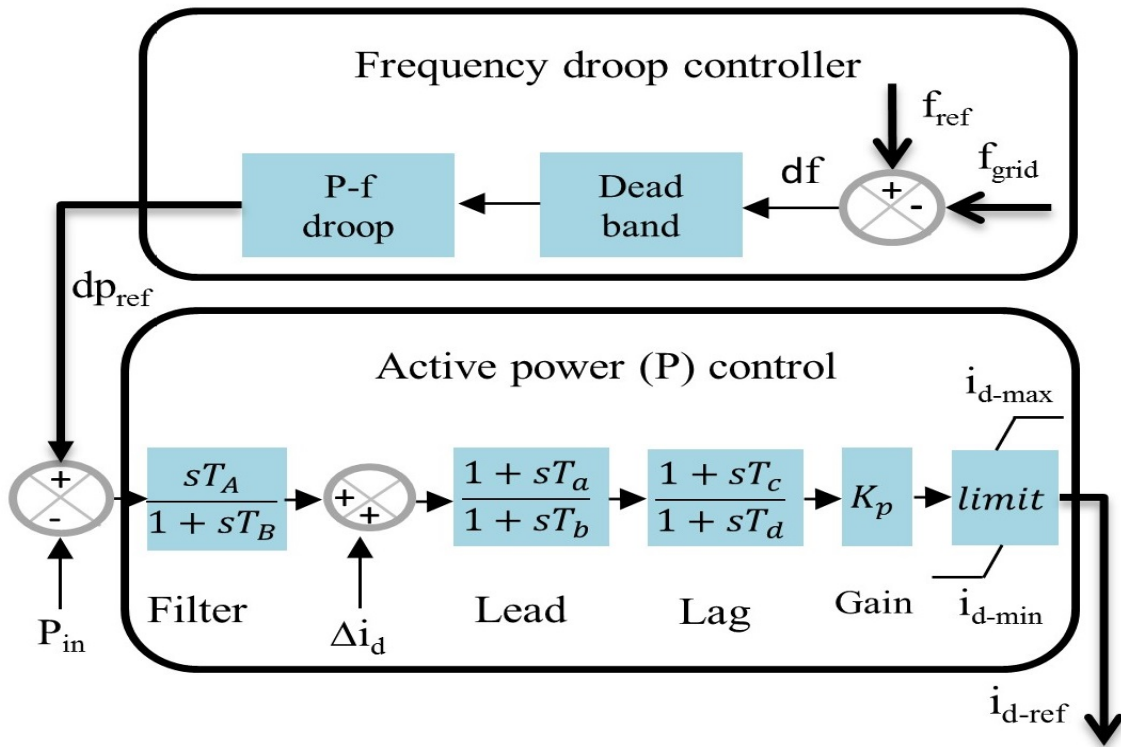


Fig. 5.4 Frequency and active power control of BESS [48]

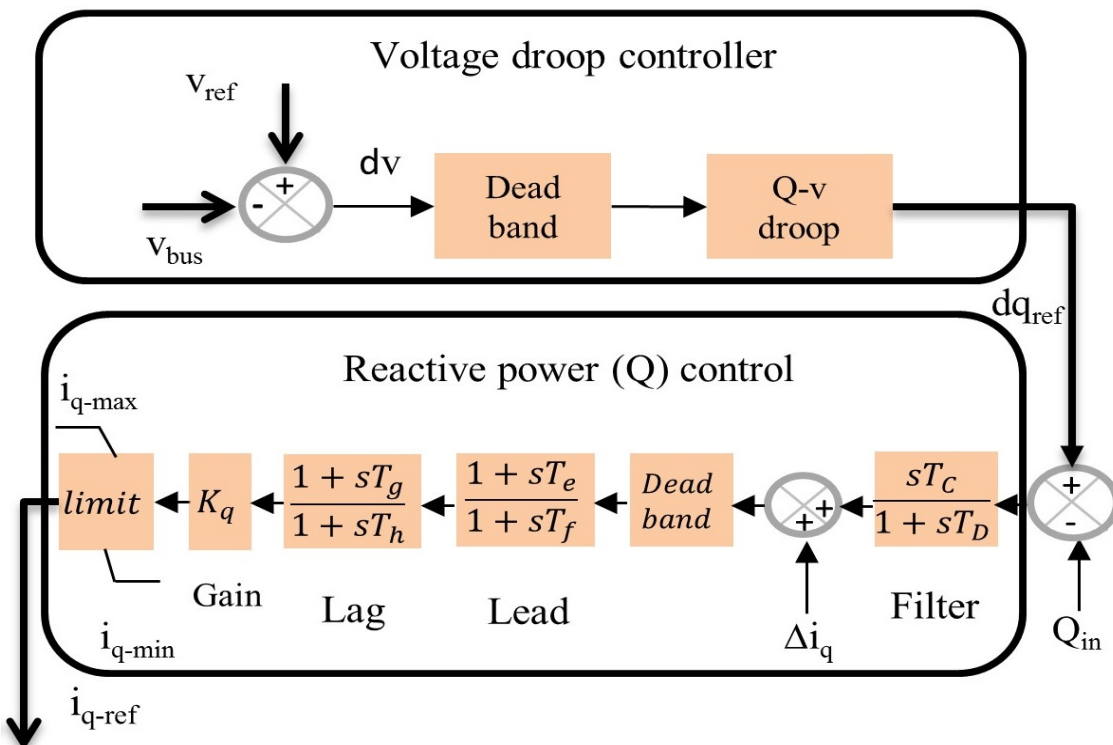


Fig. 5.5 Voltage and reactive power control of BESS [48]

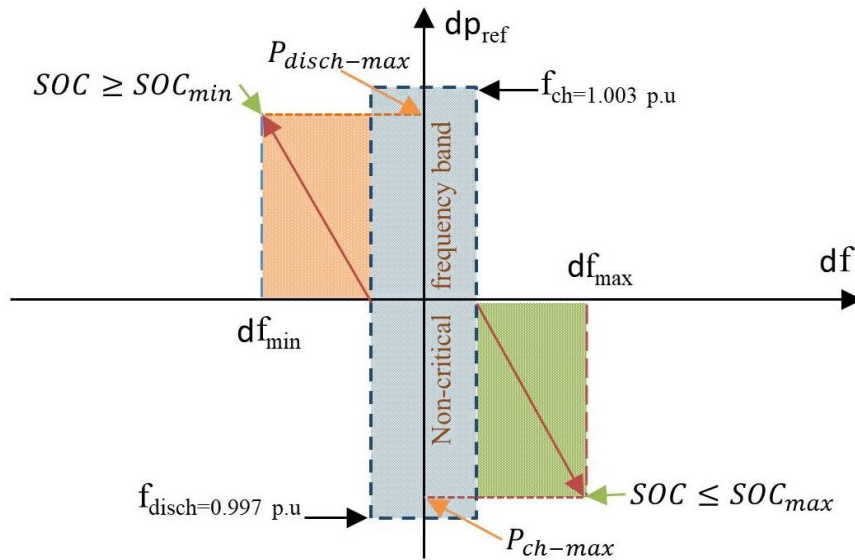


Fig. 5.6 Frequency droop characteristics [48]

The amount of full reactive power activation is defined by droop if the system voltage deviates from the nominal value. Full reactive power capacity of BESS converter is activated at the defined value of “Q-v droop” (R_{Q-v}). However, the reactive power activation depends on whether the BESS is designed to support frequency or voltage or both. At steady state condition, the value of dv and reactive power reference value dq_{ref} is zero. BESS should absorb reactive power if dv is negative and provide reactive power if dv is positive. The droop defines the ceiling for activating the full reactive power in regard to the changes in voltage from the reference value as defined in (5.4):

$$dq_{ref} = \pm dv / droop(R_{Q-v}) \quad (5.4)$$

BESS injects and absorbs reactive power for a positive and negative value of dv , respectively as presented in Fig. 5.7. The maximum reactive power injection (Q_{max}) is triggered for a minimum voltage deviation of dv_{min} . The maximum reactive power consumption ($-Q_{max}$) is triggered for a maximum voltage deviation of dv_{max} . The amount of reactive power consumption or supply depends on the remaining BESS capacity after providing the frequency regulation.

5.3.1.3 PQ Controller with Lead-lag Controller

Once the frequency and voltage controller generates the respective reference signals, they are passed to the PQ controller for further processing. The deviation between the power reference generated by the frequency controller and power output at BESS AC terminal is passed through a first-order low-pass filter. The purpose of feedback from the BESS output is to track the power output at BESS terminal and update the reference. The difference between the charge controller input and output in d-axis Δi_d is added with the filter output. It is then passed through a lead-lag controller to regulate active power output within the maximum and minimum rated capacity of BESS converter. In the case of reactive power, the charge controller output in q-axis Δi_q is added with the reactive current reference for regulating voltage.

The lead-lag controller provides the required signal magnitude and phase shift in PQ controller. The combination of lead-lag controller allows the integration of the added benefit of the individual controller and improve the steady-state performance and transient performance of the output response. The limiter restricts the regulation of power reference within the BESS converter capacity. The detailed discussion on the determination of poles/zeros of the controller can be found in [251, 252]. The associated

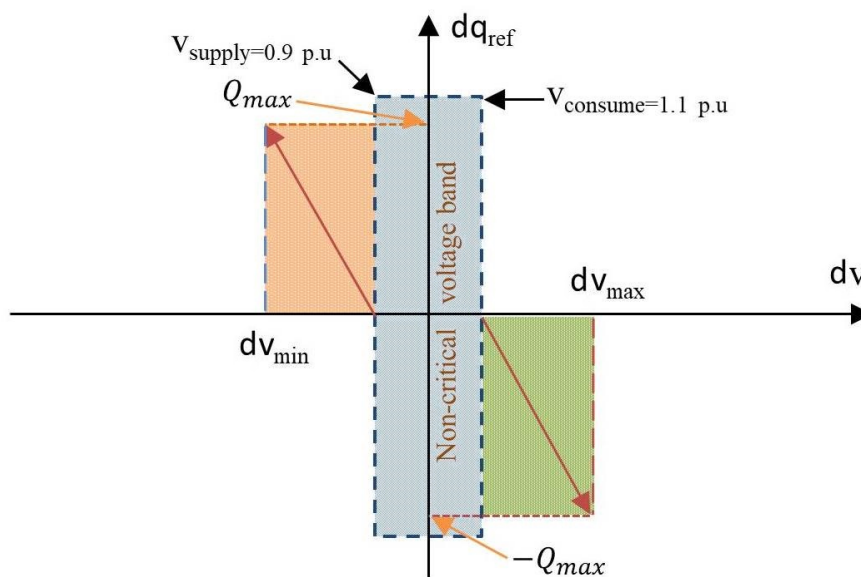


Fig. 5.7 Voltage droop characteristics [48]

transfer functions of the d-axis lead-lag controller can be defined as in (5.5):

$$K_d(s) = \frac{T_a (s + 1/T_a) T_c (s + 1/T_c)}{T_b (s + 1/T_b) T_d (s + 1/T_d)} \quad (5.5)$$

where DC gain is 1. $T_a > T_b$ (lead) and $T_d > T_c$ (lag). The associated transfer functions of the q-axis lead-lag controller can be defined as in (5.6):

$$K_q(s) = \frac{T_e (s + 1/T_e) T_g (s + 1/T_g)}{T_f (s + 1/T_f) T_h (s + 1/T_h)} \quad (5.6)$$

5.3.2 BESS Charge/Discharge Management

BESS absorbs excess energy or supplies energy shortage and thus provides oscillation damping for mitigating temporary power imbalance. The NOFB boundary varies between $df = \pm 150\text{mHz}$. The droop gain of 5 defines that the maximum BESS capacity is triggered for a frequency variation of 0.2Hz in a 50Hz system. The P-f droop maintains a linear relation as manifested in (4.7). Battery current flows in reverse order of the changes in frequency as long as the battery SOC satisfies the given conditions as illustrates in Fig. 5.8. An effective charge/discharge management strategy plays a significant role in providing the flexibility of BESS operation according to the requirement by the BESS operator.

A conventional specific maximum/minimum SOC ceiling is proposed in [212]. In contrast to the existing study, an innovative two-level adaptive SOC charging method is proposed in this chapter. The adaptive charging method is a combination of traditional maximum/minimum SOC level and an adaptive SOC limit. The main benefit of the proposed approach is that the value of (SOC_{max} or adaptive SOC) can be chosen easily by picking the appropriate charging current as defined in the control algorithm and this can be easily adjusted if it is required. Thus, the proposed method provides extra flexibility to the operator planning in the changing network conditions.

5.3.2.1 BESS With Droop-type Charging/Discharging

The simple battery charging/discharging is regulated linearly to the maximum/minimum SOC limit. BESS can inject active power if battery SOC is higher or equal to the lowest SOC limit SOC_{min} of 0.2pu and consume active power if battery SOC is lower or equal to the highest SOC limit SOC_{max} of 1pu. Hence, the droop type charging/discharging approach can be written as in (5.7):

$$i_{d-in} = \begin{cases} i_{d-ref} & SOC \geq SOC_{min} \\ -i_{d-ref} & SOC \leq SOC_{max} \\ 0 & \text{otherwise} \end{cases} \quad (5.7)$$

The current limiter as shown in Fig. 5.8 calculates the active and reactive power reference and limits the total amount of output current to avoid the overloading of BESS converter. The maximum absolute current from the input current references can be determined as in (5.8) and (5.9):

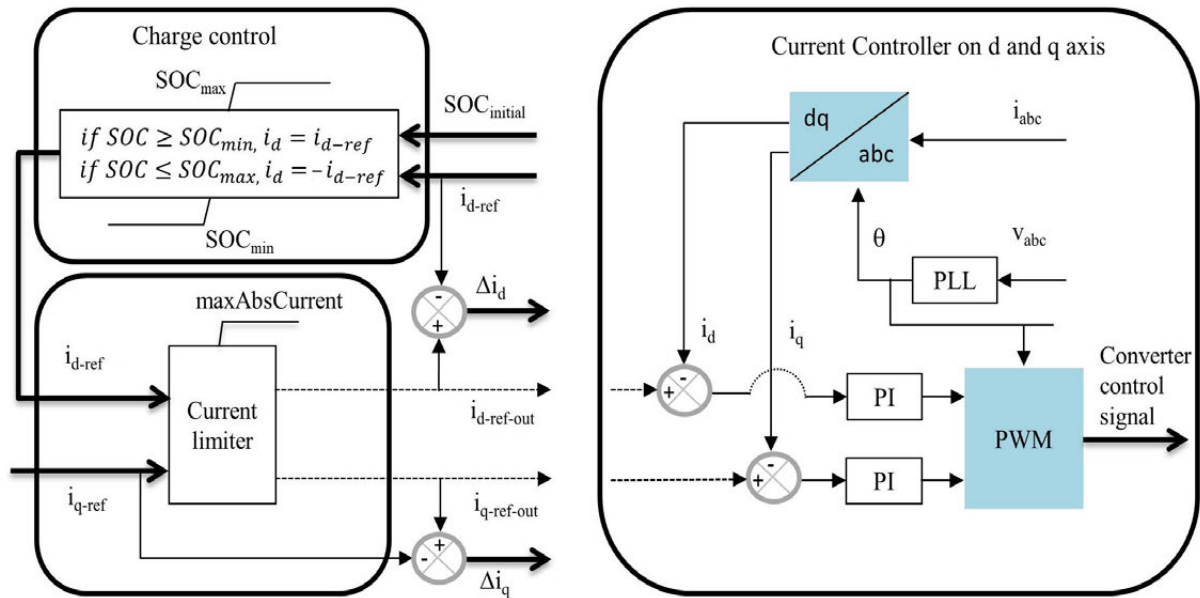


Fig. 5.8 The block diagram of BESS charge controller, d and q axis current control [48]

$$i_{d-ref-out} = \int_{-|maxVal|}^{|maxVal|} i_{d-ref} dt \quad (5.8)$$

$$i_{q-ref-out} = \int_{-y_{val}}^{y_{val}} i_{q-ref} dt \quad (5.9)$$

$$\text{where, } y_{val} = \sqrt{\left| \int_0^{|maxVal|^2} |maxVal|^2 - i_{d-in}^2 \right|} \text{ and } maxVal=1.$$

Battery charging/discharging results the change in battery SOC and depending on the amount of active power exchange during transient periods, battery SOC will increase or decrease. Moreover, the self-discharge of battery will also reduce battery SOC. These reduce the available battery capacity for responding to future events. To avoid lower SOC or relatively over-sizing the BESS capacity, an effective recharging strategy needs to be adopted that can potentially improve the system reliability and reduce the associated expenses.

5.3.2.2 BESS Recharging with Maximum SOC

Battery can be fully recharged when SOC is lower or equal to the minimum SOC or any other value other than the maxSOC when BESS is inactive. This assures that sufficient BESS capacity is accessible for participating in the future contingencies. The conventional charging method to the maxSOC can be written as in (5.10):

$$i_{d-in} = \begin{cases} i_{ch-A} & \text{if } SOC \leq (SOC_{min} + SOC_{max})/2 \text{ or} \\ & SOC \leq SOC_{min} \text{ and } i_{d-ref-in} < 0.0001 \\ 0 & \text{else} \end{cases} \quad (5.10)$$

where, the charging current can be defined as i_{ch-A} which is activated when d-axis current reference is lower than 0.0001pu and SOC is lower or equal to the minimum

SOC SOC_{min} or 0.5pu. In practice, there is always a small amount of current flows due to the self-discharge of battery or losses of the converter. Hence, d-axis current will never be completely zero and the recharging current is activated at a value of 0.0001pu. The recharging current flows until the battery reached to the maxSOC value of 1pu.

5.3.2.3 BESS Recharging with Adaptive SOC

The main drawback of charging to the SOC_{max} is that BESS is no longer able to participate in an over-frequency event and to consume the excess energy from the grid. This will affect the grid stability regardless of the available energy storage devices but mainly due to the improper management of battery SOC. Hence, a different SOC level than the maxSOC i.e. an adaptive charging method is proposed in this chapter. This allows providing a certain power margin for over-frequency event without changing the maximum charging/discharging limit in the case of a conventional method. The recharging with adaptive SOC starts for the same SOC starting conditions as in (5.3.2.2). The maximum charging limit with adaptive SOC can be regulated by selecting the value of charging current. The swapping logic of adaptive SOC or maxSOC can be defined as in (5.11):

$$SOC_{max} = \begin{cases} SOC_{adaptive} & \text{if } i_{ch-A} > i_{ch-threshold} \\ SOC_{max} & \text{if } i_{ch-A} \leq i_{ch-threshold} \end{cases} \quad (5.11)$$

It can be observed from the given conditions that the maximum charging SOC limit (SOC_{max}) is the adaptive SOC ($SOC_{adaptive}$) if the charging current is greater than the threshold and the maxSOC for a charging current of smaller or equal to the threshold value. The charging threshold value $i_{ch-threshold}$ is selected as 0.1pu. Hence, for a recharging current of 0-0.1pu, the maxSOC value is 1pu. The charging current of higher than 0.1pu will select the adaptive SOC value and the maxSOC limit for adaptive SOC is selected as 0.8pu. It is worth noting that, the maximum adaptive SOC limit and charging threshold can be always adjusted according to the strategy of BESS operator.

5.3.3 Current Controller on d-q axis

The current controller on d-q axis are shown in Fig. 5.8. The current controller inputs are the d-q references output from the active and reactive power signal ($i_{d-ref-out}$ and $i_{q-ref-out}$) and the measured d-q axis value at BESS converter's output. The PWM index in d axis (p_{md}) and q axis (p_{mq}) are converted using PLL to provide the referenced phase angle to control the converter.

5.4 Attributes of the Test System

The PV penetration, operating strategies and the proposed BESS charging technique are studied on IEEE 9-bus system (50Hz) as shown in Fig. 5.9 [253]. The detailed modeling of the generators and governors used are explained in (4.4.1). The PV output is considered as an aggregated output and the PV farm is connected to the grid via a 0.6/230kV transformer at bus 9. Further modeling information on PV farm can be found

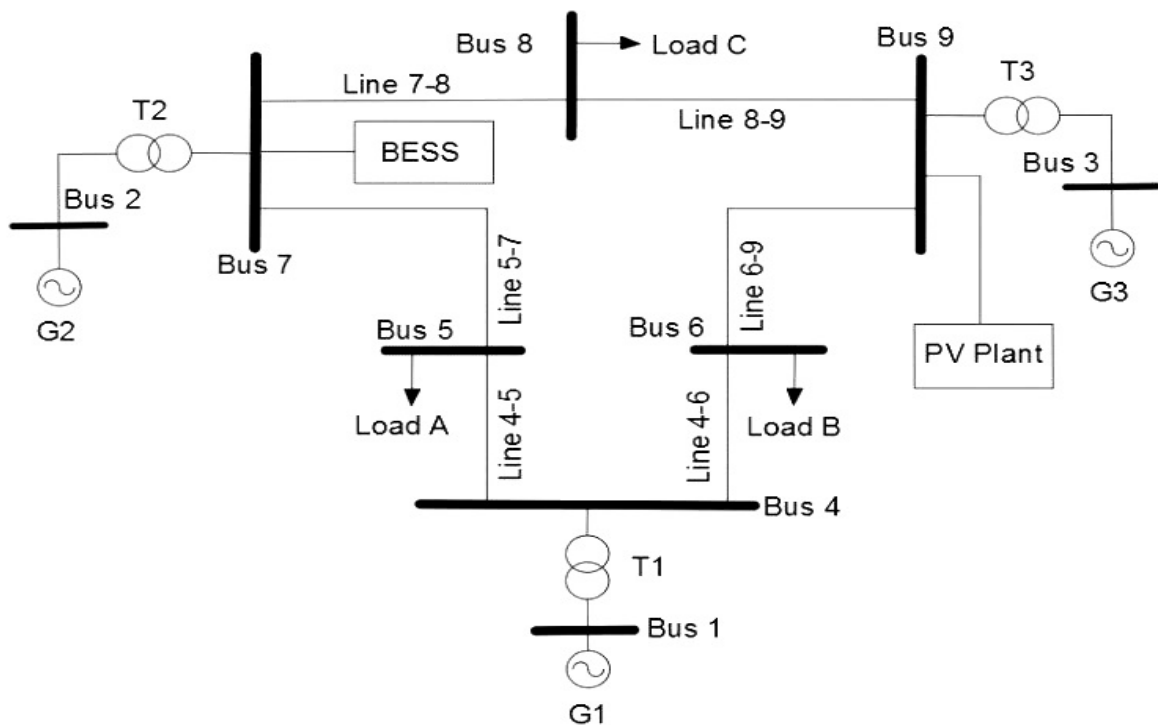


Fig. 5.9 The IEEE 9-bus system with PV and BESS location [48]

in [254]. The fossil-fueled G3 unit is completely shut down with the PV penetration. The aim of incorporating BESS is to provide damping to the grid, improve transient performance and satisfy the grid requirements. The detailed discussion on BESS installation location and sizing is presented in (5.5.3).

The value of filter time constants are selected as 5 whereas the gain K_p and K_q are 2.1 and 0.1, respectively. The controller with the selected poles/zeros locations can be written as in (5.12):

$$K_d(s) = K_q(s) = \frac{40 (s + 1/40) 13 (s + 1/13)}{38 (s + 1/38) 35 (s + 1/35)} \quad (5.12)$$

5.4.1 Case Studies

In the first case, two various operating strategies of generators are investigated to analyze the impact of PV penetration and network operating conditions and these are:

- Strategy 1: This defines the low load case.
- Strategy 2: This delineates the increment in generator G1 and G2 output due to load growth at Load A and B. Strategy 2 somewhat replicates a situation where existing SGs can be loaded during the peak periods or reduction in RES power output.

The PV output is 100MW for both operating strategies. The power output of different generators is outlined in Table 5.1.

Table 5.1 The power output of generators and loads in MW for both strategies

Strategy	SG1	SG2	PV	Load A	Load B	Load C
Strategy 1	86	140	100	125	90	100
Strategy 2	107	165	100	150	110	100

In order to analyze and understand various aspects of demanding stability phenomena, three case studies have been investigated. The proposed BESS charging method and its

comparative advantages over the conventional approach are discussed in case studies four and five. All the case studies are listed as follows:

- Case 1: Line outage with operating strategy 1 and 2
- Case 2: Load reduction event with operating strategy 1
- Case 3: BESS installation location and Converter sizing
 - (a) Operating strategy 2 with line outage
 - (b) Operating strategy 1 with load event
- Case 4: Battery charging with the proposed approach
- Case 5: The comparative advantages of the proposed adaptive SOC method.

5.5 Analysis of Transient Stability

Two contingency events i.e. line outage and load event are carried out for investigating the inertial impact of PV penetration and the performance of various operating strategies of SGs in maintaining grid standards with and without a BESS. In addition, the location for installing and sizing of BESS is also presented while maintaining grid defined frequency standards.

5.5.1 Line outage with Operating Strategy 1 and 2

Line outage is one of the common network events that occur often in power system primarily due to fallen trees or broken electric poles. A temporary line outage of line 5-7 and permanent outage of line 8-9 are taken into account for analyzing the transient performance of the grid. A single-phase-to-ground fault is applied on the lines 5-7 and 8-9 at $t=0s$. The temporary line fault on line 5-7 is cleared and restored at $t=0.24s$. The permanent fault on line 8-9 is cleared by removing the line permanently at $t=0.24s$. The line outage may threaten the grid stability if the generators are not able to provide sufficient damping to the grid. Often a power system stabilizer (PSS) may be equipped at

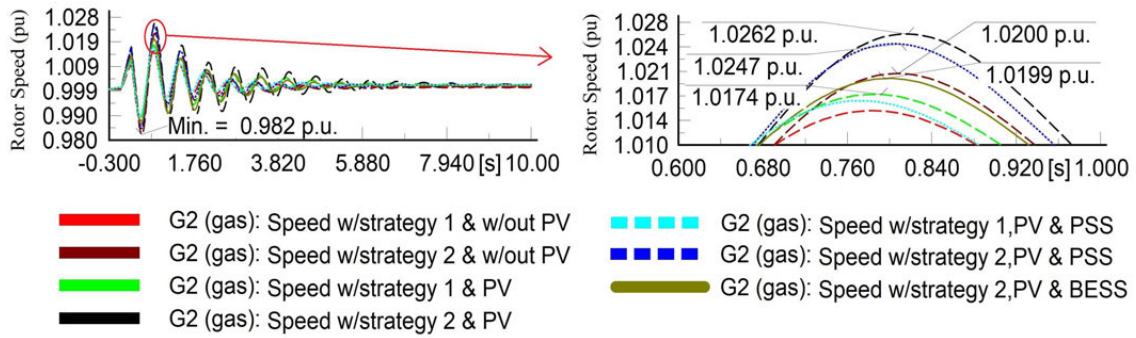


Fig. 5.10 The frequency (pu) oscillations of generator G2 [48]

the generator terminal to contribute in system damping and minimize the concern related to instability.

The performance of the grid with various network operating conditions are illustrated in Fig. 5.10. It can be observed that for operating strategy 1 and 2 and with no PV penetration (w/strategy 1 & w/out PV and w/strategy 2 & w/out PV), the frequency oscillations of G2 stay within $\pm 2\%$ of the nominal value as defined by the NEM grid code. With 100MW of PV generation and operating strategy 1 (w/strategy 1 & PV), an increase in frequency deviation can be seen but it stays within the grid limit. When generators are operating with lower power output (operating strategy 1), they have a higher margin to regulate their output which provides the capability for contributing to oscillation damping. However, the frequency deviation increases by 0.22Hz for G1 and 0.115Hz for G2 with 100MW of PV generation as outlined in Table 5.2. As the frequency variation stays within the grid allowed limit, there is no need of an energy storage device for the grid with operating strategy 1.

Table 5.2 Frequency deviation for various operating strategies and network conditions

Operating Strategy	W/out PV (Hz)	With PV (Hz)	PV & PSS (Hz)	PV & BESS (Hz)	Generator
Strategy 1	50.45	50.67	50.645	-	G1
Strategy 2	50.47	51.015	50.98	50.775	
Strategy 1	50.755	50.87	50.825	-	G2
Strategy 2	51	51.31	51.235	50.995	

On the contrary, for operating strategy 2 and the same amount of PV generation (w/strategy 2 & PV), frequency deviations of G1 and G2 are highly oscillatory and

reach to 1.0203 (G1) and 1.0262pu (G2) which violate the mandatory grid limit. However, in the case of “operating strategy 2”, power margin of the generators is reduced and hence the generators fail to provide sufficient damping to maintain the grid defined operating standards. Table 5.2 shows the increment in frequency deviation with PV penetration and operating strategy 2. The use of PSS (w/strategy 1,PV & PSS and w/strategy 2,PV & PSS) shows a slight improvement in the frequency oscillations compared to without a PSS. However, PSS fails to achieve the system stability at the expected level with operating strategy (w/strategy 2,PV & PSS).

Hence, a 35MW BESS (216 kWh) is incorporated in the grid for providing supplementary oscillation damping and maintaining frequency deviations within the mandatory grid constraints. The grid response as shown in Fig. 5.10 manifests that the integrated BESS (w/strategy 2,PV & BESS) reduces the maximum frequency rise to 1.0199pu which satisfies the grid constraints. Moreover, BESS integrated operating condition shows better oscillation damping and faster reduction of steady-state error at post-fault condition compared to without a BESS or with a PSS controller. This evidence suggests the essential of BESS in minimizing PV penetration impact and satisfying obligatory grid constraints. Furthermore, BESS also reduces the active power oscillations of generators as compared to without a BESS as shown in Fig. 5.11.

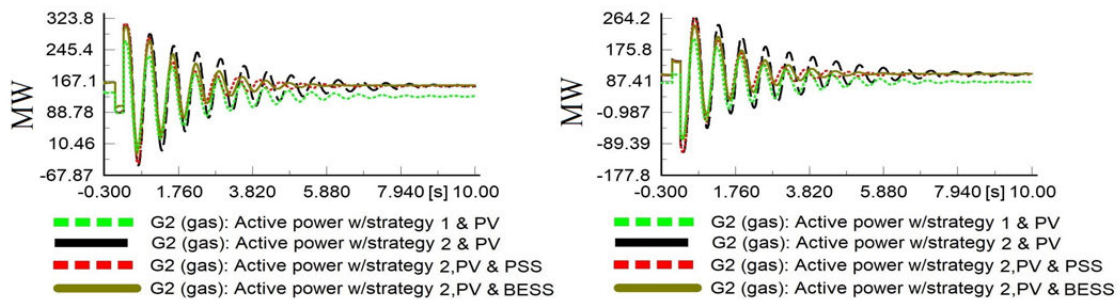


Fig. 5.11 Active Power output (MW) of generators G1 and G2 [48]

The voltages at bus 7 for different operating conditions are shown in Fig. 5.12. It can be observed that with PV penetration and operating strategy 2, the voltage drop is the highest as compared to without PV or operating strategy 1. It can also be noticed that PSS slightly improves the voltage profile following the contingencies than with a PSS condition. Nevertheless, BESS significantly improves the voltage profile as it injects

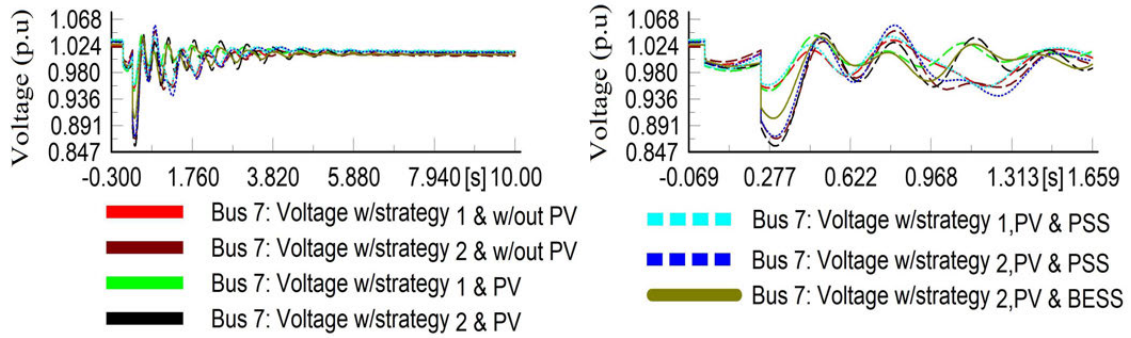


Fig. 5.12 Voltage at BESS connection point [48]

reactive power to the grid during the voltage drop and diminishes oscillations at a faster rate than the other operating conditions.

The active and reactive power of BESS are shown in Fig. 5.13(a). A large amount of active power as compared to reactive power can be seen to participate in frequency regulation as the boundary for frequency regulation is smaller and active power is given priority over the reactive power. Fig. 5.13(b) manifests the changes in battery SOC during contingency periods. It can be summarized that BESS power plays a greater role than BESS energy from the perspective of transient frequency stability circumstance. A battery capacity of 180kWh is selected for the case study, nevertheless, it is worth mentioning that this is not an optimal BESS energy size.

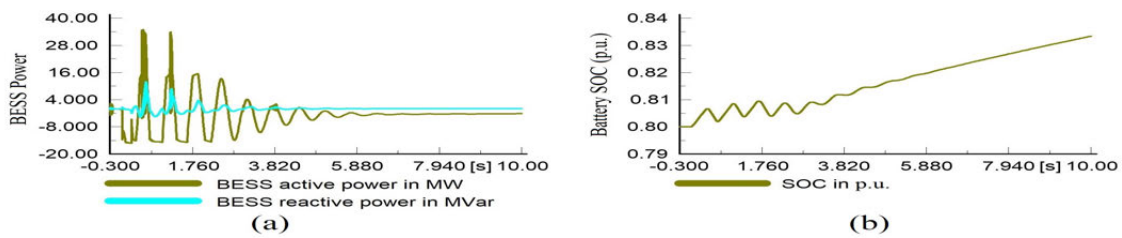


Fig. 5.13 The active and reactive power of BESS and battery SOC [48]

5.5.2 Load Reduction Event With Operating Strategy 1

A change in load demand may initiate transients in the power system which can have large impact on stability if sufficient damping is not available in the system. Case study 1 indicates that with operating strategy 1, the system is able to damp out the oscillations successfully and hence the same strategy is further investigated if the frequency

constraints are maintained according to the grid requirements with load changing event. A 50% load reduction at load A is applied for the duration of $t=0-0.6s$ with operating strategy 1 is in operation.

Simulation results as shown in Fig. 5.14 illustrates that without PV generation (w/strategy 1 & w/out PV), the existing generators successfully regulate the frequency within the $\pm 1\%$ of the nominal frequency following the load reduction event. With 100MW PV generation, the frequency of both generators oscillates beyond the allowed limit (w/strategy 1 & w/PV) as outlined in Table 5.3. It can also be seen that although PSS provides a small contribution in reducing oscillations (w/strategy 1,PV & PSS), nevertheless, the system fails to achieve the expected frequency outcome at the post-fault condition. PSS provides lesser frequency drop and better oscillation damping as compared to without a PSS at the generator terminal.

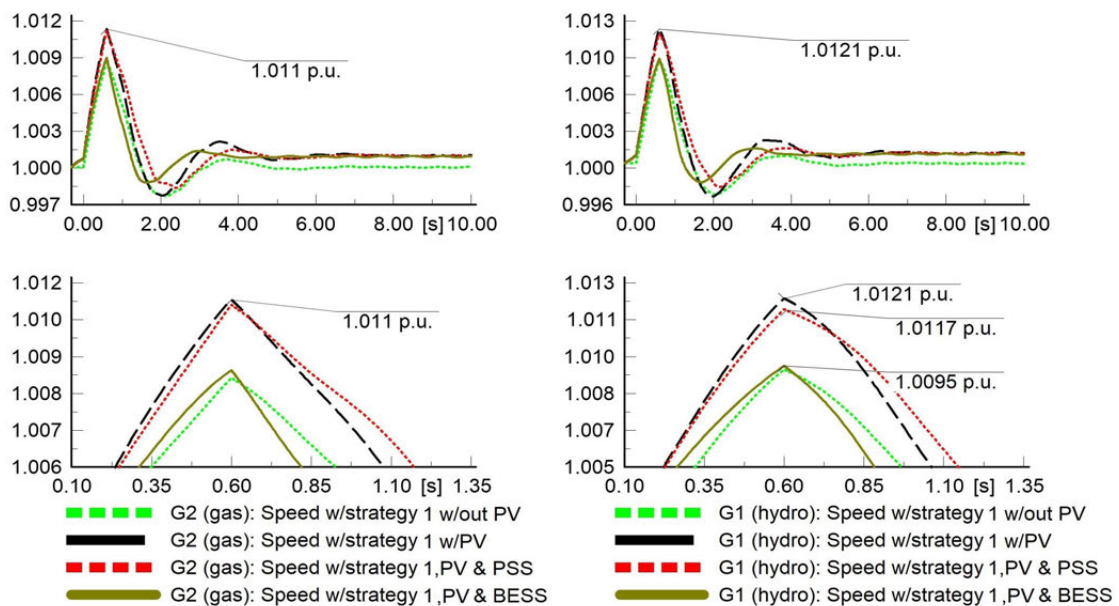


Fig. 5.14 The frequency (pu) oscillations of generator G1 and G2 with load event

Table 5.3 Maximum frequency deviation for load reduction event

Operating Strategy	W/out PV (Hz)	With PV (Hz)	PV & PSS (Hz)	PV & BESS (Hz)	Generator
Strategy 1	50.425	50.605	50.585	50.475	G1
Strategy 1	50.415	50.525	50.55	50.435	G2

Hence, a 35MW BESS is incorporated in the grid for providing supplementary damping and minimizing frequency oscillations. The response of generators as shown in

Fig. 5.14 illustrates that BESS constraints the frequency deviations within the grid defined limit (w/strategy 1,PV & BESS). Also, BESS provides a lesser drop in frequency and faster recovery of the frequency transients to the steady-state value.

The active and reactive power output of BESS and battery SOC are illustrated in Fig. 5.15 which manifests the importance of large power output for a short period of time. This signifies the need for BESS power instead of BESS energy in term of transient stability studies as also seen in the previous case study.

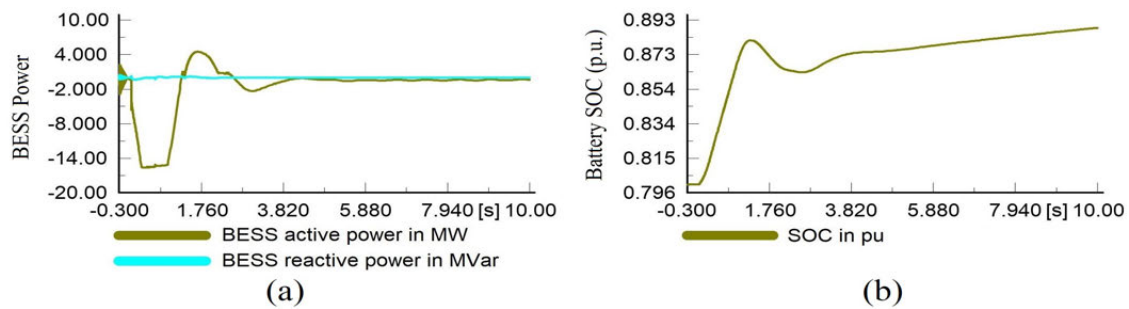


Fig. 5.15 The active and reactive power of BESS and battery SOC [48]

5.5.3 BESS Installation Location and Converter Sizing

The placement of BESS plays a significant role in order to provide the best-expected outcome with the minimum size of BESS converter and energy capacity which can help in reducing losses and the overall costs of BESS. Hence, the incorporated BESS is installed at different buses in the network to analyze the performance of BESS under both studied contingency events. The approach to finding the most suitable location for installing BESS and converter size is to carry out comparative performance study by installing BESS at various buses in the high-voltage side of the network. The studied contingency events are line outage when operating strategy 2 is in operation and load event when operating strategy 1 is in operation. The size of BESS converter is estimated in terms of minimum MW rating of BESS and the fulfillment of frequency oscillations according to grid constraints during the studied contingencies. This approach is based on trial and error, however, in the case of a large-scale system, this may not be a time-effective approach. Considering the small scale system, this chapter is limited to the trial and error

method for finding the optimal installation location and converter size of BESS.

The simulation results of load event when operating strategy 1 is selected are shown in Fig. 5.16 (w/strategy 1,PV & BESS). It can be seen that the frequency responses of both generators fulfill the grid requirement. It is difficult to draw any conclusion which is the best location for installing BESS. Hence, further simulation study for other contingency event is investigated.

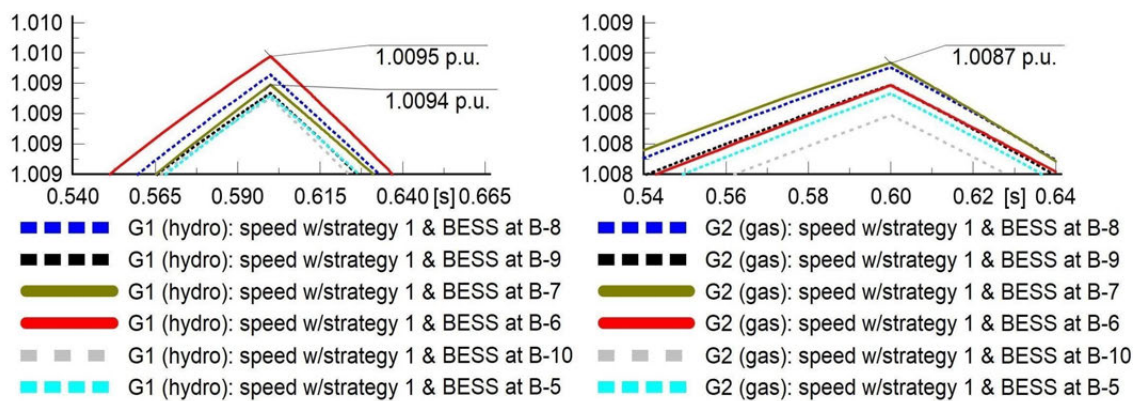


Fig. 5.16 The frequency rise of G1 and G2 with BESS installed at different buses for load reduction event

The frequency responses of generator G1 and G2 are shown in Figs. 5.17 and 5.18 following the line outage event and 35MW BESS. It can be found that not all locations are suitable for installing BESS as with the rated BESS capacity, grid fails to maintain frequency oscillations within the grid defined periphery. Although the frequency of generator G1 stays within the limit when BESS is installed anywhere in the network but, in the case of G1, only the location at bus 7 satisfies the grid requirements. Hence, it can be concluded that bus 7 is the most suitable location for installing BESS considering the line outage and load event.

5.5.4 Battery Charging with the Proposed Approach

An original multi-level battery charging approach is presented in this chapter. The maxSOC limit can be regulated according to the plan for adaptive charging. In order to carry out battery charging with the conventional and the proposed method, a 42% load

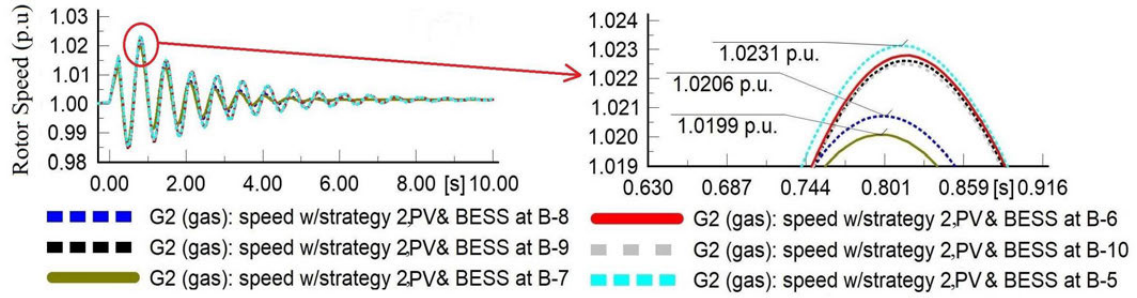


Fig. 5.17 The frequency of G2 with BESS installed at different buses for line outage [48]

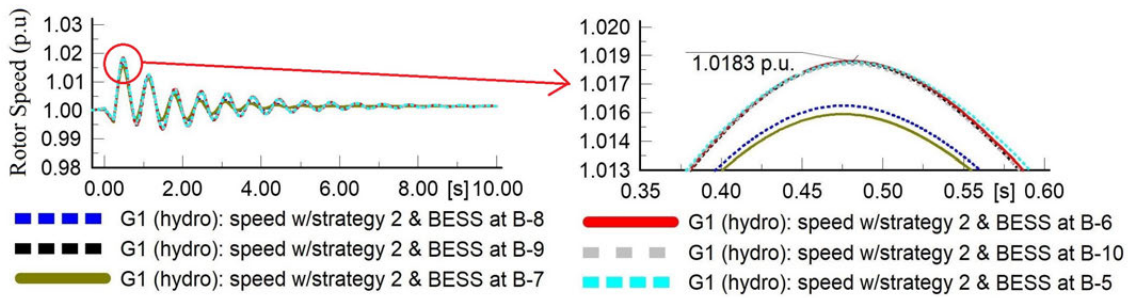


Fig. 5.18 The frequency of G1 with BESS installed at different buses for line outage

growth event is activated for $t=0-0.8s$ at load A under operating strategy 1. The battery is rated as 20Ah and initial SOC is 0.8pu. The simulation results with different charging strategy are shown in Fig. 5.19 (a and b). It can be seen in Fig. 5.19 (a) that the final SOC value is 0.494pu which is lower than the charging SOC limit of 0.6pu and battery needs to be recharged in accordance with the designed SOC control strategy as defined in (5.10). When the charging current is selected as 0.015pu, the maxSOC limit is 1pu and when the charging current is selected as 0.010pu, the maxSOC limit is adjusted to 0.8pu as defined in (5.11). This manifests the efficacy of the proposed adaptive SOC charging strategy.

Fig. 5.19 (b) shows that battery charging current i_{ch-A} takes place when the active current reference is lower than 0.0001pu as defined in (5.10). This validates that BESS satisfies the designed conditions in (5.10) and (5.11) and charges the battery effectively according to the plan of BESS operator. The total discharging duration lasts for $t=0-30.5s$. The charging to the maxSOC lasts for roughly 62.1s ($t=30.5-92.6s$) and adaptive SOC for 18.6s ($t=30.5-49.1s$). However, this duration will vary depending on the charging current, battery capacity and available SOC prior to the charging.

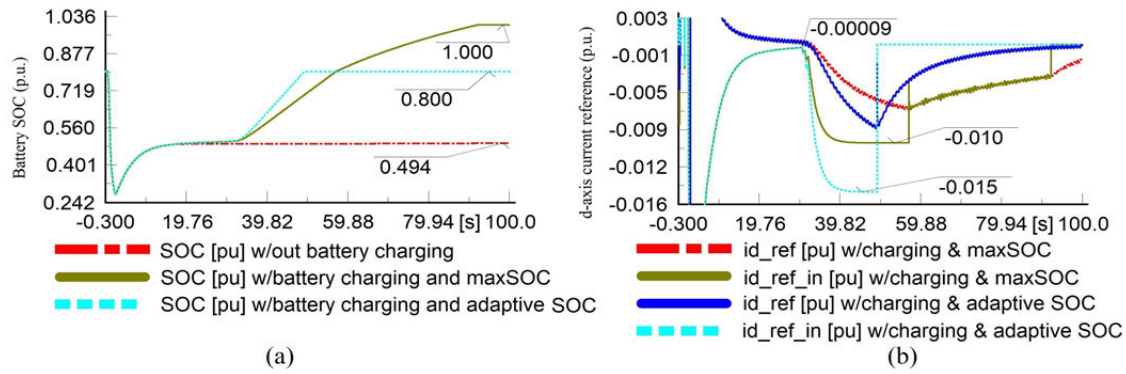


Fig. 5.19 SOC status with different charging mechanism [48]

5.5.5 The Comparative Advantages of the Proposed Adaptive SOC Method

In order to further demonstrate the comparative advantage of the proposed adaptive charging method, a 45% load growth event is activated for $t=0-0.8s$ at load A when the network is operating under operating strategy 2. The purpose of load growth event is to reduce the battery SOC to a value that requires to be charged. The ratings of battery are 7.8Ah and 0.9kV for this case study. The adaptive SOC allows the operator to maintain battery SOC value according to the weather forecast to the maxSOC or adaptive SOC. A simple weather forecast of reduced PV generation is estimated and BESS needs to be recharged to the maxSOC in order to maximize BESS reserve. A series of PV variation event is applied; reduction from 100MW to 90MW at $t=42s$, further reduction to 73MW at $t=50s$ and 68.3MW at $t=60s$ and finally restored to 100MW at $t=70s$. Fig. 5.20 (a) illustrates the total frequency response of G1 and Fig. 5.20 (b) shows the voltage at bus 7 which illustrates BESS contribution in enhancing voltage profile of the grid under the load and PV generation event. Figs. 5.21 (a and b) manifest the closer frequency response of generator G1 and it shows that BESS improves the frequency response of G1 compared to without a BESS and battery SOC does not have a visible impact on the performance as sufficient SOC is available.

Fig. 5.22 (a) demonstrates that Battery is required to be charged as SOC is lower than 0.6pu and battery is charged during its inactive periods of $t=31-39s$. The active and reactive power output of BESS are shown in Fig. 5.22 (b). The value of adaptive

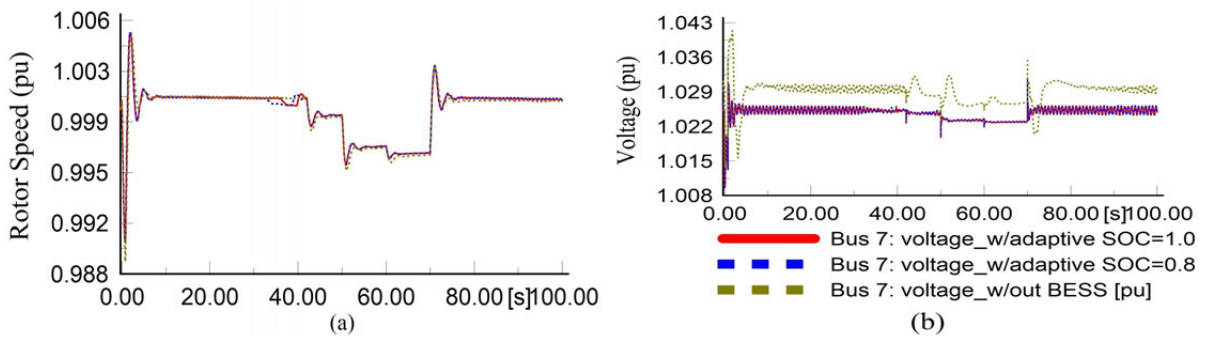


Fig. 5.20 The frequency of generator G1[p.u.] with BESS (a) and voltage at bus 7 (b) [48]

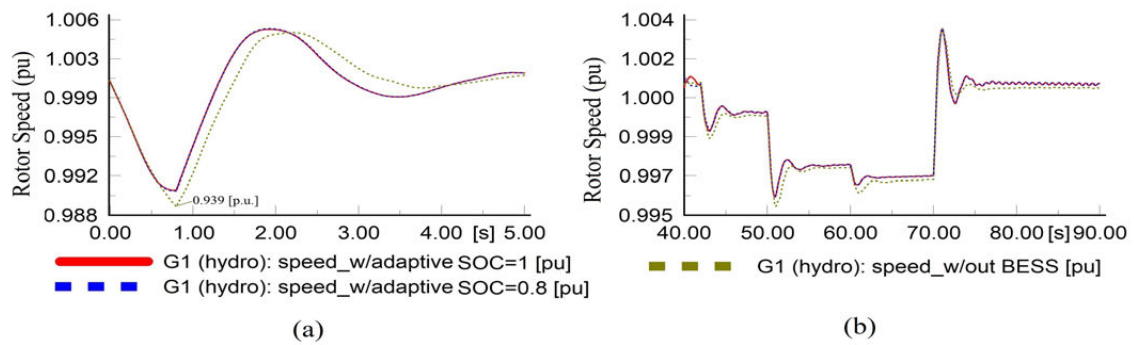


Fig. 5.21 The closer view of generator frequency G1[p.u.] (a and b) [48]

SOC is adjusted in this case study to demonstrate the wider flexibility of the proposed adaptive SOC strategy. Charging to 1pu requires larger time (6.32s for a charging current of 0.012pu) as compared to 0.8pu which takes 3.95s with a charging current of 0.10pu. It can also be seen that SOC at the end of contingency periods remains higher if it is charged at the maxSOC. With the adaptive SOC strategy, BESS can be charged to 0.8pu or 1pu or any other level depending on the expected forecast of PV generation.

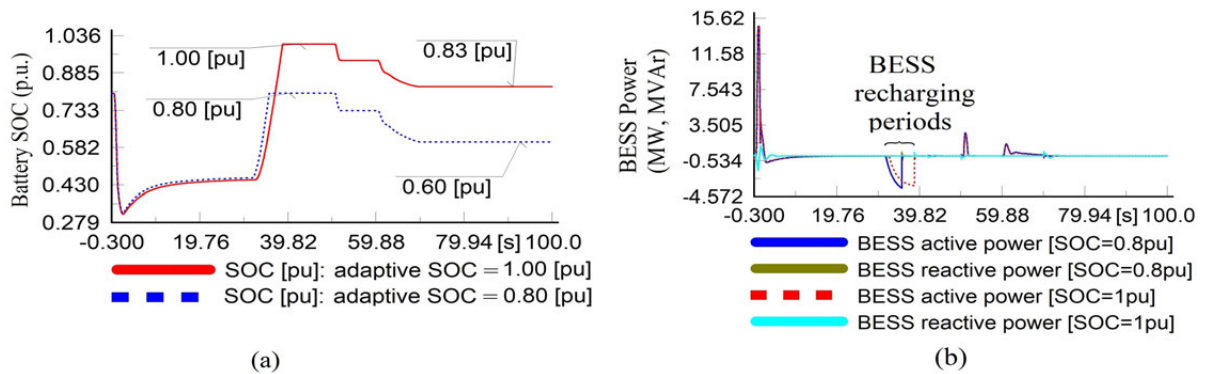


Fig. 5.22 Battery SOC for various adaptive SOC strategy (a), BESS power output (b) [48]

The comparative advantage of the proposed adaptive SOC method is further demonstrated in Fig. 5.23. A momentary decrease of 25% at load A is applied for the duration of $t=0-0.8$ s with operating strategy 2. Reduction of the load increases the frequency and BESS consumes the surplus energy until SOC reaches to 1pu. This allows using the maximum capacity for responding to the network event. However, the battery is charged to the adaptive SOC level of 0.8pu without affecting the maximum capacity for any network event. This provides the flexibility and advantage of the proposed adaptive SOC method compared to the conventional SOC regulation approach [212].

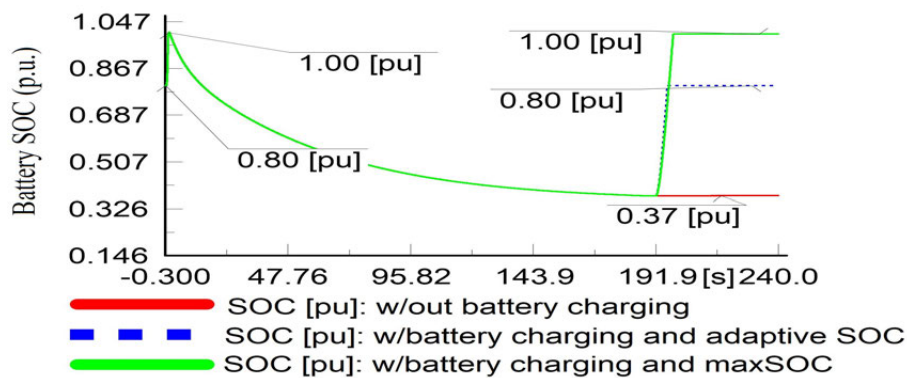


Fig. 5.23 SOC status with different charging mechanism [48]

5.6 Conclusion

In this chapter, a lead-lag regulated BESS with a new adaptive SOC recovery method is presented in order to contribute to oscillation damping and enhance frequency response of the grid. The aim of the adaptive SOC approach is to provide operational flexibility to the BESS user according to weather forecast and planning for energy management. In order to verify the proposed method, five case studies have been carried out. In summary, the study can be encapsulated as follows:

- The study of two operating strategies indicates that the power reserve of the generators at pre-fault condition plays a crucial role in maintaining frequency

within the grid defined periphery. However, generators are forced to operate at larger output during peak periods or lower PV outputs due to low sunlight.

- With 100MW of PV penetration, grid fails to maintain NEM criteria. A PSS can slightly improve the grid response but still fails to accomplish the expected outcome.
- When a 35MW BESS is installed at bus 7, the frequency responses of the generators regulate within the grid allowed boundary. BESS injects/absorbs active/reactive power to damp out frequency and voltage oscillations and thus enhances the transient profile of the grid.
- Simulation results indicate that BESS power is imperative than BESS energy as the supporting periods are very small in term of frequency transients.
- Moreover, the proposed SOC recovery approach shows that BESS can be easily managed to different SOC level without affecting the maximum battery capacity for the network event. This yields better flexibility in BESS regulation in accordance with the forecast of PV generation.

This chapter outlines that BESS can be utilized in regulating both voltage and frequency of the grid and mitigating the negative inertial impacts of PV generation in the grid. The proposed BESS and adaptive SOC method can be adopted and adjusted in MG or large-scale network.

From the perspective of a transmission network, BESS has enormous potential to provide various grid stability supports. In particular, BESS can be an alternative to the conventional Flexible AC Transmission System (FACTS) for improving transient stability while improving the power transfer capacity of the grid. Additionally, new types of BESS active/reactive power regulating controllers need to be explored for performance evaluation.

Chapter 6

The application of BESS in Stabilizing Simultaneous Voltage and Frequency in a Transmission Network and Enhancing Power Transfer Capacity

This chapter contains the following publication - U. Datta, A. Kalam and J. Shi, "Battery Energy Storage System to Stabilize Transient Voltage and Frequency and Enhance Power Export Capability," IEEE Transactions on Power System, vol. 34, pp. 1845-1857, 2019.

6.1 Introduction

Presently, the electric transmission network is facing with a major control and stability threats mainly due to the aged transmission network, the increasing demand for energy and the expansion of RES in the grid. The conventional vertical structure of power system is undergoing a reformation which adds more challenges in terms of the loading of the transmission and distribution lines and voltage variations. The power system with the ever-growing volume and complexity have drawn much consideration by the power

utility as the grid is vulnerable to various transient contingency events that frequently happens in the power system. Deregulated energy market and variable RES generation result in the unplanned transfer of power within the areas of the network. This may induce added pressure in the loading of certain transmission lines which can generate stability challenges in the case of network faults. Moreover, government subsidies and other initiatives for sustainable energy mobilized the growth in large-scale PV and wind generations which are usually placed at a distance from the main load center. This requires the satisfactory operation of the grid resources in order to ensure a reliable power system i.e the fulfillment of (N-1) criteria.

The power system experiences small or large oscillations following any temporary or permanent contingency events which require to be compensated for improving the stability of the system. FACTS solution have been in the power system for a while and it has been contributing in improving the oscillation damping of the grid by controlling the power flows and strengthening the power transfer capability of the grid [255]. Among various FACTS solutions, special attention is given to static compensator (STATCOM) which has already built its own footprint in the power system due to its capability to enhance power transfer capacity [256], minimize inter-area oscillations [257] and provide quicker and effortless recovery of grid voltage [258]. Moreover, STATCOM provides better oscillation damping [259] and enhanced transmission facility [260] than other FACTS devices.

Compared to STATCOM, which provides reactive power compensation, BESS basically performs a distinct role in the grid i.e. frequency regulation [261], smoothing of RES active power output [93], enhancement of transient stability [262], improvement of power oscillations damping [263] and support for improving the voltage and power quality of the grid. The study in [262] identified that BESS can enhance the transient stability of the grid whereas the study in [263] presented that BESS performs better in minimizing the electromechanical oscillations of the system compared to a PSS. In a single machine infinite bus system, it is shown that BESS outperforms STATCOM in providing oscillation damping. In RES incorporated power system, the combination of STATCOM-supercapacitor [264] or STATCOM-battery [265] is determined to achieve

improved performance compared to STATCOM only operation mode. The performance is evaluated in terms of transient stability enhancement and power oscillation damping.

From this perspective, the utilization of BESS in enhancing the stability of the grid and improving the power transmission capacity between long-distance interconnected electric grid is comparatively a new field of importance which requires thorough investigation. The proper planning and placement of BESS can not only minimize network congestion and prolong the plan for network extension but also can provide financial gain to the grid [266]. The study in [2] demonstrated that BESS stabilizes the transient frequency of the grid following a permanent contingency event and increases the amount of power export from one area to the other end of the network. An improved oscillation damping with battery integrated STATCOM is presented in [267, 268]. However, both studies do not provide any insight on improving the power transfer capacity of the interconnected power system. In addition, the comparative stability performance of STATCOM and BESS has not been given any attention in both studies in terms of concurrent voltage and frequency regulation.

Considerable research effort has been given to study voltage and frequency regulation and enhancing the oscillation damping capacity of the grid. The studies in [269–271] presented that battery integrated STATCOM improves voltage and frequency damping. Nevertheless, either battery SOC is not considered at all or weighed as constant SOC, which is an incorrect approach. In addition, traditional PI controller [270, 271] is utilized for regulating BESS active and reactive power. As no deadband is included in BESS design [269–271], this will result in continuous charging/discharging of the battery and will result in an increased cost of BESS operation. In [215], priority based active or reactive power control is proposed in order to regulate either frequency or voltage, at any given time. In another study in [272], battery integrated STATCOM is employed for reducing inter-area oscillation. Nevertheless, either active or reactive power compensation is provided, at any particular time. Nonetheless, coordinated control of voltage and frequency and battery SOC are not taken into account in the study. The earlier investigations lack the study of simultaneous voltage and frequency control and battery SOC or comparative

performance analysis of BESS and STATCOM in stabilizing voltage and frequency of the grid and increasing the volume of power transmission within interconnected systems.

In this chapter, the comparable performance analysis of STATCOM and BESS in enhancing transient voltage and frequency stability and strengthening the power transmission capability between large-scale interconnected electric systems are investigated. Multiple temporary and permanent contingency events such as line faults, short circuit faults in an equivalent 400kV transmission network are considered for performance evaluation. The transient stability performance is analyzed in terms of voltage and frequency control according to the standards of NEM policy by the Australian Energy Market Operator (AEMO) [273, 274]. The proposed BESS is outlined for simultaneous voltage and frequency control while BESS operation is constrained within the defined battery SOC which has not been discussed in the earlier literature. In addition, PI-lead and lead-lag controllers are also employed to adjust the active and reactive power output of BESS. The efficacy of the proposed controllers is investigated and compared with the traditional PI regulated BESS in maintaining the grid voltage and frequency following multiple contingency events. Through simulation studies, it is shown that when the volume of power export between two large-scale networks is 450MW, the network voltage and frequency remains stable, following the permanent line outage event. However, when the amount of power is increased by 44.44% i.e. increased to 650MW from 450MW, the grid fails to maintain stable voltage and frequency for the same line outage event. Although the integration of STATCOM can provide a decent level of voltage stability support at the initial stage of the post-fault condition, however it cannot provide any frequency support due to the lack of active power control, which causes the STATCOM to finally fail in stabilizing voltage and frequency. On the contrary, BESS with active and reactive power control capability become successful in stabilizing the grid which rationalizes the importance of this study.

6.2 BESS Layout

The basic layout of BESS control is already defined in subsection (5.3) in Chapter 5 which comprises voltage and frequency regulator that generates the reactive and active power reference for BESS regulation. The detailed discussion of voltage and frequency controllers are provided in (5.3.1.1) and (5.3.1.2) in Chapter 5. Once the reference for d and q axis are directed to PQ controller, it regulates the updated current reference based on the charge controller error and power output at BESS AC side.

6.2.1 Active/Reactive (PQ) Controller

In this research, three different categories of controllers i.e. PI, PI-lead and Lead-lag controllers are employed for regulating BESS active and reactive power. The detailed discussion on PI regulated PQ controller are presented in (4.3.2) in Chapter 4. The PQ controller with the conventional PI controller is displayed in Fig. 6.1. The modeling and associated transfer functions of lead-lag regulated PQ controller are discussed in (5.3.1.3) in Chapter 5. The PQ controller with the lead-lag controller is shown in Fig. 6.2.

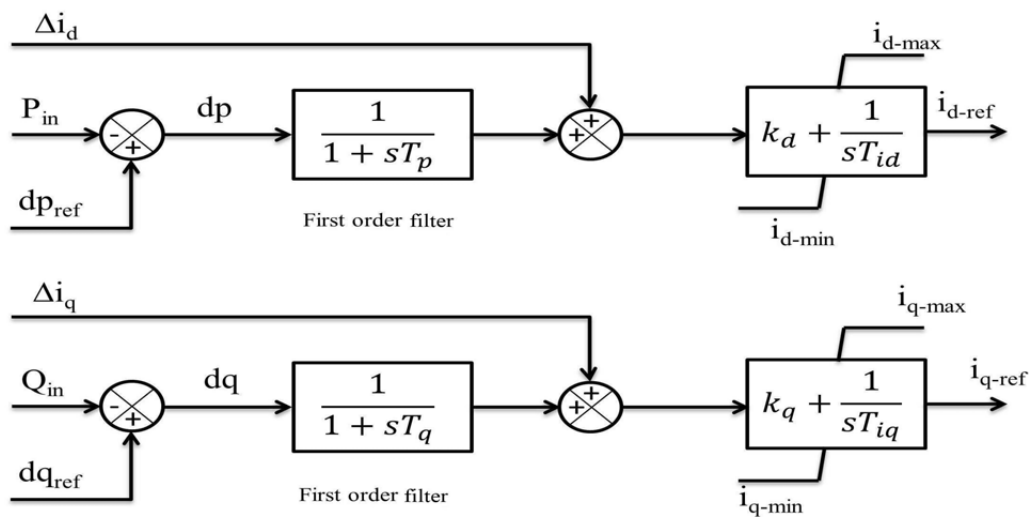


Fig. 6.1 Conventional PI regulated PQ controller [220]

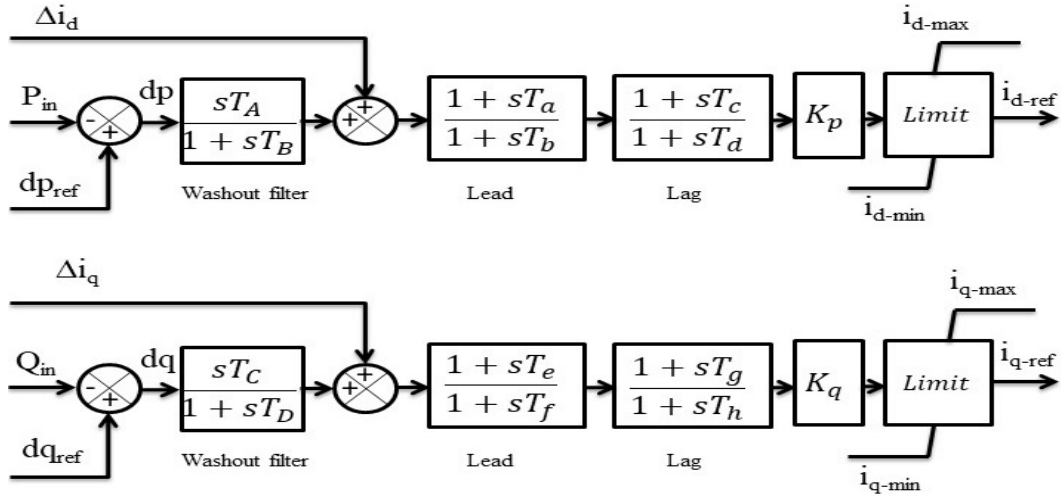


Fig. 6.2 Lead-lag regulated PQ controller [220]

6.2.1.1 PI-lead Controller

The proposed PI-lead controller is constructed by combining PI and lead controller in series as illustrated in Fig. 6.3. The purpose of cascading a lead controller with a PI controller is to achieve an improved transient outcome i.e. reduce the maximum percentage overshoot and settling time with the compensation of a positive phase angle by varying the location of closed-loop poles in the s -plane. The transfer functions of the lead controller for d and q axis can be written as:

$$K_d(s) = \frac{T_{B1} (s + 1/T_{B1})}{T_{A1} (s + 1/T_{A1})} \quad (6.1)$$

$$K_q(s) = \frac{T_{B2} (s + 1/T_{B2})}{T_{A2} (s + 1/T_{A2})} \quad (6.2)$$

DC gain = 1. $T_{B1} > T_{A1}$ and $T_{B2} > T_{A2}$.

The in-depth analysis on PI-lead controller is available in [252, 275]. The location of poles and zeros are selected based on iterative technique and the PI values are the same as in PI regulated PQ control. The associated parameters of the PI, PI-lead and lead-lag controllers are given in Appendix B1.

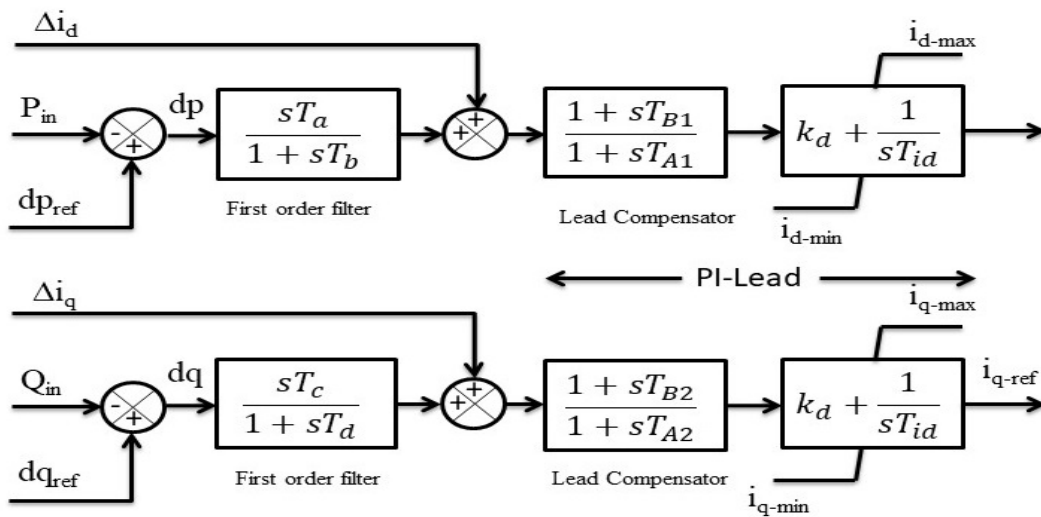


Fig. 6.3 PI-lead regulated PQ controller [220]

6.3 Studied System and Stability Criterion

The brief discussion on the studied 400kV network, STATCOM modeling and stability criteria are presented in this section.

6.3.1 System Description

In order to analyze BESS contribution in enhancing system stability as compared to STATCOM, a 400kV equivalent network of the Finnish transmission grid is selected in this work. The simplified diagram of the testing grid is illustrated in Fig. 6.4. The grid consists of the equivalent model of 15 SGs, 11 loads and 7 series capacitors. The associated parameters of capacitors, the active and reactive power output of loads and SGs are outlined in Appendix B2. The parameters of the network components such as SGs, transformers at generator and load terminal and transmission lines can be found in [276].

The electrical components of SGs at North-West (NW), North (N), North-East (NE), and Central-North (CN) are modeled with 5th order state-space models. The electrical components of SGs at Nordic N1, Nordic N2, Nordic S and Nordic C are modeled with 6th order state-space models. The mechanical components of the above-mentioned areas

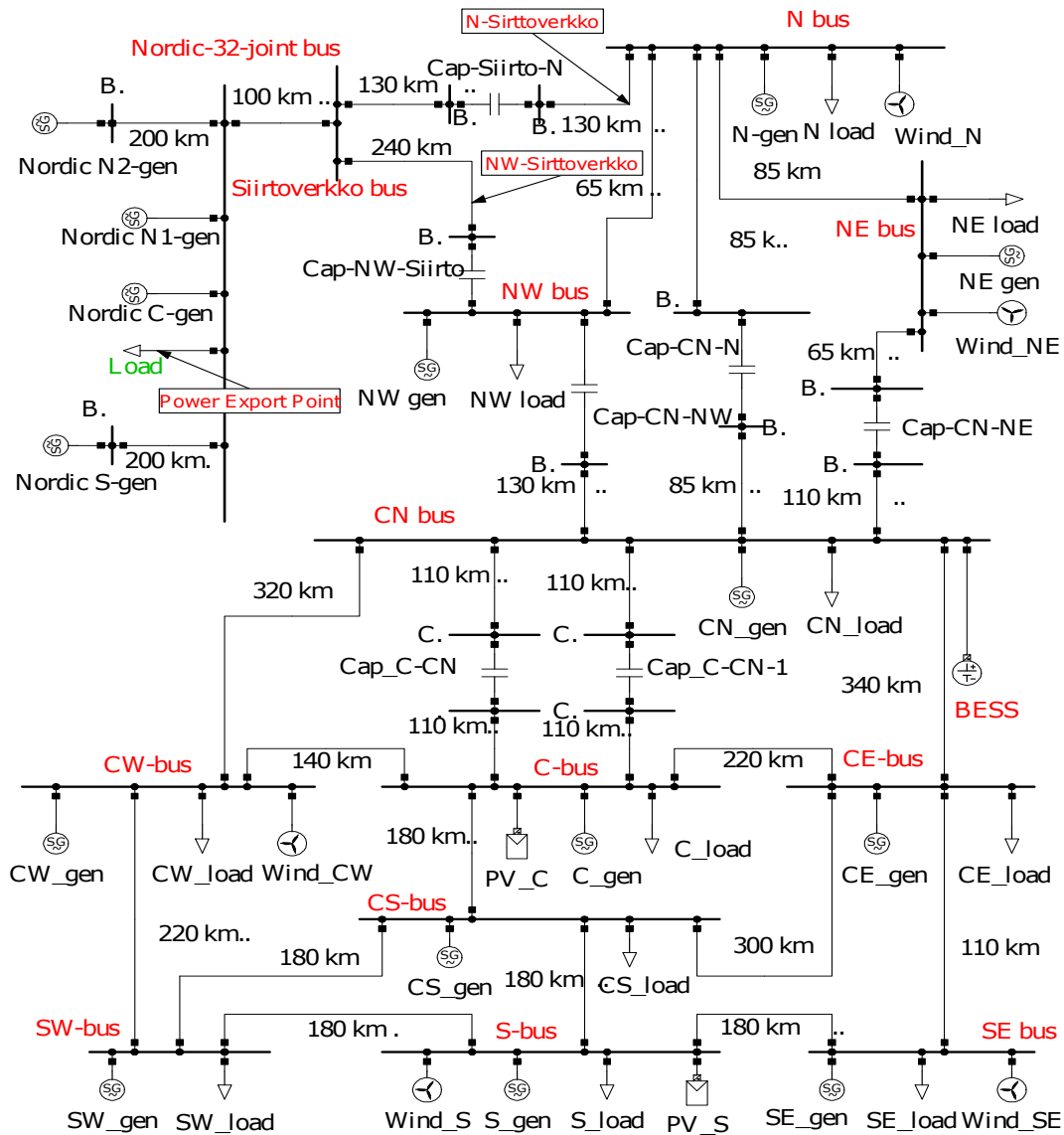


Fig. 6.4 The studied customized equivalent transmission grid [220]

are modeled with hydro turbine and governor arrangements. The electrical components of SGs at Central-West (CW), Central (C), Central-South (CS) and Central-East (CE) and south (South-West (SW), South (S) and South-East (SE)) are modeled with 6th order state-space models and no turbine and governor systems are considered i.e. they are operating with constant torque. The exciter for SW generator is an IEEE-AC5A type and the rest of the generators are equipped with ST2A type exciter.

The voltage at the generator connected terminal is 13.8kV and hence connected via a 13.8kV/400kV transformer to the high voltage grid. The generators in the Nordic transmission grid are an equivalent depiction of the entire Swedish generation network.

The SW generator is selected as the reference machine and the rest of the generators are designed as PV. No PSS is considered at the generator's terminal. The transmission lines between SW-CW, SW-S, SW-CS, S-SE, S-CS, SE-CE, CS-C and Siirtoverkko to Nordic-32-joint consists of two parallel lines and the rest of the lines are of a single line. The voltage at load connected point is 110kV and loads are modeled as balanced load.

The designed poles/zeros locations of the lead-lag controller for d-q axis can be written as:

$$K_d(s) = K_q(s) = \frac{8(s+1)(s+0.25)}{(s+2)(s+0.067)} \quad (6.3)$$

The designed poles/zeros locations of the lead controller in PI-lead for d-q axis can be written as:

$$K_d(s) = K_q(s) = \frac{1+s}{1+0.5s} = \frac{2(s+1)}{(s+2)} \quad (6.4)$$

6.3.2 STATCOM and Wind Model

The STATCOM model comprises a DC source that supplies stable voltage to the VSC. The VSC converts the DC voltage into AC which is connected to the grid connecting transformer. This transformer operates as an interface to the grid. The modeling details of the selected STATCOM model is available in [277]. The voltage at STATCOM connection point is selected as the reference for regulating STATCOM output. The wind turbine models are DFIG type. The wind farms are equipped with FRT and hence remain connected to the grid during contingencies. The wind speed is considered as a constant which results in a stable DFIG power output.

6.3.3 Stability Criterion

In order to satisfy the grid defined standards, the oscillatory responses of the grid should be constrained within limits following a single/multiple contingencies. The frequency standards define that for a network event, the frequency must be restricted within $\pm 1\%$ of the nominal frequency (0.99-1.01pu) within 1 minute of the post-fault condition and should be restored within the NOFB of 0.997-1.003pu in a period of 5 minutes as illustrated in Fig. 6.5 [273]. In the event of numerous contingencies, the frequency must be retained between 0.99-1.01pu within 2 minutes and restored to the NOFB within 10 minutes. The AEMO defined transient voltage standard varies between $\pm 10\%$ of the nominal voltage value which must be retained within 20 minutes at post-fault condition [274]. At any time of operation, the grid voltage and frequency must not violate the above-mentioned conditions. If the voltage and frequency are retained within the defined limit at post-fault condition, the system is considered as stable and secure.

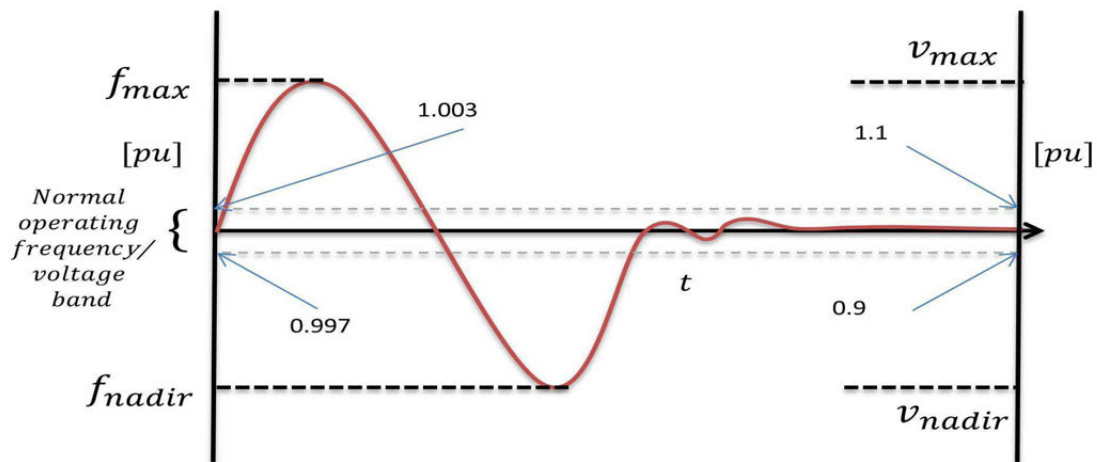


Fig. 6.5 Voltage and frequency standards by NEM [220]

The stability performance of voltage and frequency defines the limit of power transfer. This stability limit also most likely to be dependent on network operating condition. A considerable amount of AEMO study highlighted that line outage has a significant impact on the amount of power transfer and maintain the grid defined boundary [278]. Furthermore, it is found that multiple contingency events have a higher impact in restricting the volume of power transmission as compared to a single contingency event to satisfy stability limits [279]. Hence considering such phenomena,

single/multiple contingency events are considered in this study for analyzing transient stability performance of the studied grid to avoid blackout incident as described in [280].

STATCOM is one of the most commonly studied compensation devices in the power system to provide better transient oscillation damping and improving the amount of power transfer. The comparative stability enhancement of STATCOM and BESS is the main focus of this study following single/multiple contingency events. The performance will be assessed in terms of NEM criterion as illustrated in Fig. 6.5.

6.4 Results and Analysis

An equivalent depiction of an actual transmission network is selected in this work in order to analyze the comparative benefits of STATCOM and BESS in the grid. A thorough investigation of power export studies is carried out in DigSILENT Powerfactory under various transient events. In the first step, the maximum limit of power export from the south side of the network to the north side is identified following the studied transient conditions without any compensation devices integrated into the grid. Later, the volume of power export is raised so that the system becomes unstable and the support from STATCOM and BESS is analyzed in stabilizing the grid responses. The transmission lines connecting two large-scale systems are of significant importance from the perspective of grid stability. The performance of PI-lead and lead-lag regulated BESS is compared with PI regulated BESS and STATCOM.

In order to determine the performance of STATCOM and the control of BESS power output, three case studies (cases 1-3) are carried out. Furthermore, three other case studies (cases 4-6) are carried out to validate BESS competence in enhancing the stability of the grid.

- Case 1: Permanent line outage of N-Sirttoverkko line.
- Case 2: Load growth and Permanent line outage of N-Sirttoverkko line.

- Case 3: Permanent line outage of N-Sirttoverkko line and load growth.

The performance of BESS in other circumstances:

- Case 4: Momentary single-phase-to-ground fault.
- Case 5: Permanent single-phase-to-ground fault.
- Case 6: Without series capacitors between two systems.

In order to determine the secure and reliable limit of power export, various amount of power export cases are analyzed. The generators at SW provides 50MW, S and SE each provides 200MW for supplying 450MW at the power export point in the Nordic area. A 3-phase fault is triggered at $t=3s$ on N-Sirttoverkko line for the duration of 100ms. A fault simulation study indicates that 450MW is the maximum power export limit without any support from the compensation devices following the permanent loss of one of the two transmission lines. Hence, the volume of power export is raised to analyze the unstable system with the support of STATCOM and BESS.

6.4.1 Case 1: Permanent line outage of N-Sirttoverkko line

In order to validate the contribution of STATCOM/BESS in improving power transmission capacity of the grid, the amount of active power is increased to 650MW. The generator output of SW is increased to 250MW and the other two generators S and SE provides 200MW individually. The N-Sirttoverkko line is the heavily loaded line which was carrying 321MW at the steady-state condition. A similar 3-phase fault is applied on the heavily loaded line at $t=3s$ for the duration of 100ms. The simulation results of bus voltages at SW and Siirttoverkko bus and frequencies of SW and CN generators are illustrated in Figs. 6.6 (a) and (b), respectively. The Figs. 6.6 (a) and (b) show that due to insufficient damping capability of the existing generators excitation system, the grid becomes unstable when the export amount is increased by 44.44% compared to the stable operation limit and one of the lines are removed permanently from the grid after the clearance of the fault. The grid voltage and frequency fail to settle down after the fault within the defined time frame as highlighted in Fig. 6.5. Instead, the oscillations tend to increase over the time towards instability which will

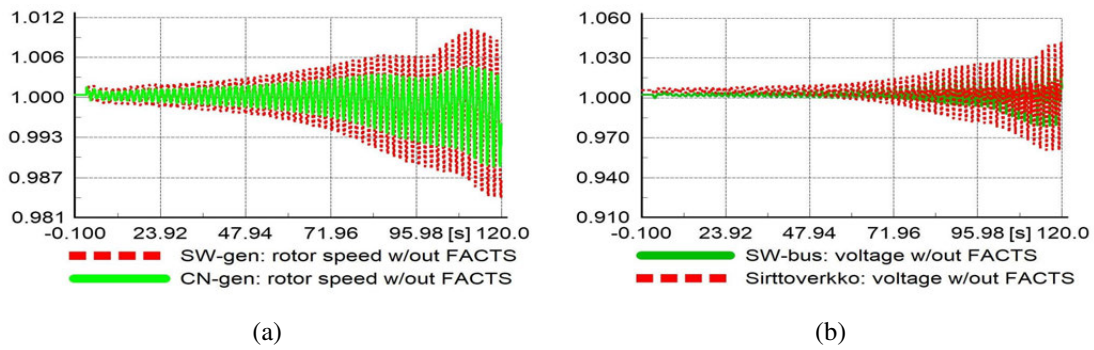


Fig. 6.6 The frequency of generators [p.u.] (a) and bus voltages [p.u.] (b) with line outage and without STATCOM/BESS [220]

lead to complete blackout of the grid. In order to stabilize the grid, these growing oscillations need to be diminished and hence supplementary damping contribution is mandatory. The STATCOM/BESS is incorporated at CN bus to supply additional system damping to diminish the enlarging oscillations that arise due to the transient event while exporting the higher amount of power and stabilize the system. The location for BESS/STATCOM installation is selected through iterative process.

STATCOM has already demonstrated its capability in enhancing power oscillation damping and increasing power transfer capability in the grid. The size of the integrated STATCOM is 80MW and the same line outage event is applied for the performance analysis of STATCOM. The frequency and voltage plots at the selected locations with the integrated STATCOM are illustrated in Figs. 6.7 (a) and (b), respectively. It can be observed that although there is a slight improvement in the grid responses, the damping support from the STATCOM is not sufficient and thus remains ineffective in stabilizing the grid. The voltage and frequency responses at the post-fault condition continue to oscillate and never reaches within the stability limits according to NEM requirements [273, 274]. It is noticed that a large size of STATCOM also remains unsuccessful in stabilizing the grid responses at the post-fault condition.

The total reactive power provide by the STATCOM is 80MVAR and there is no active power contribution as shown in Fig. 6.8. Hence, it can be said that the zero active power output of STATCOM fails to provide active power oscillation damping and causes the collapse of the system. Thus, in the case of voltage and frequency transients,

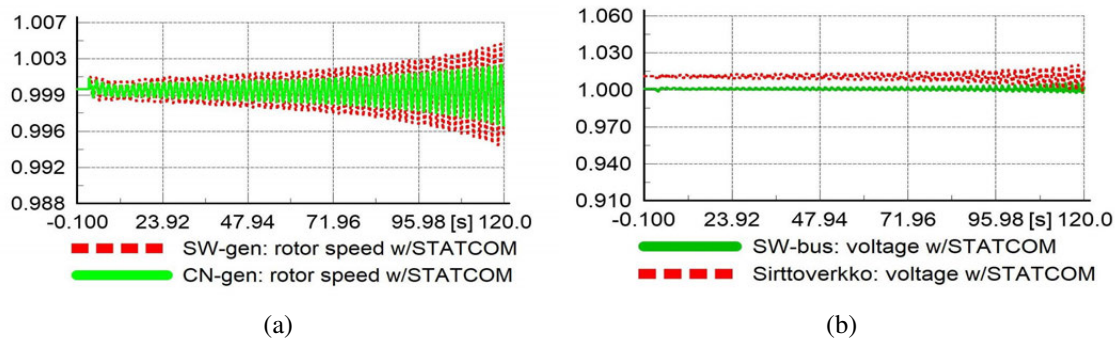


Fig. 6.7 The frequency of generators [p.u.] (a) and bus voltages [p.u.] (b) with line outage and STATCOM [220]

a STATCOM is not capable of stabilizing the grid and enhancing the power export. Considering such phenomena, a device with active and reactive power compensation is mandatory to provide ample damping into the system and sustain grid voltage and frequency.

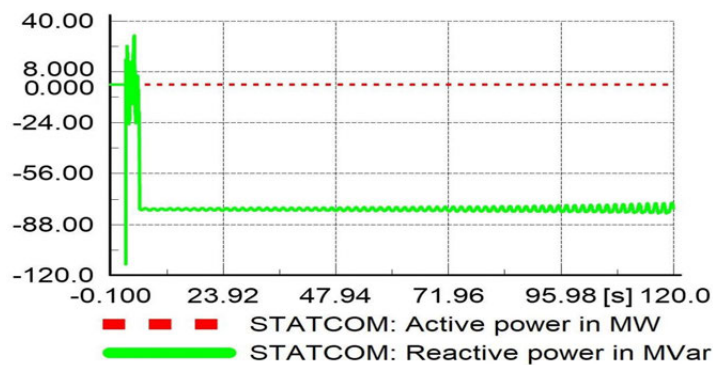


Fig. 6.8 The active and reactive power of STATCOM

The aim of BESS integration is to supply active and reactive power to improve oscillation damping. The grid responses with the incorporated BESS as illustrated in Figs. 6.9 (a) and (b) manifest that BESS provide sufficient damping support into the grid and successfully diminishes the voltage and frequency oscillations within the mandatory recovery boundary as specified in Fig. 6.5. The grid responses achieve the stability point with the incorporated BESS. Hence it can be said that BESS enhances the stability of the grid while exporting 650MW between two interconnected systems.

In order to further determine the performance of the proposed BESS control strategies, PI-lead and lead-lag regulated BESS is compared with the traditional PI

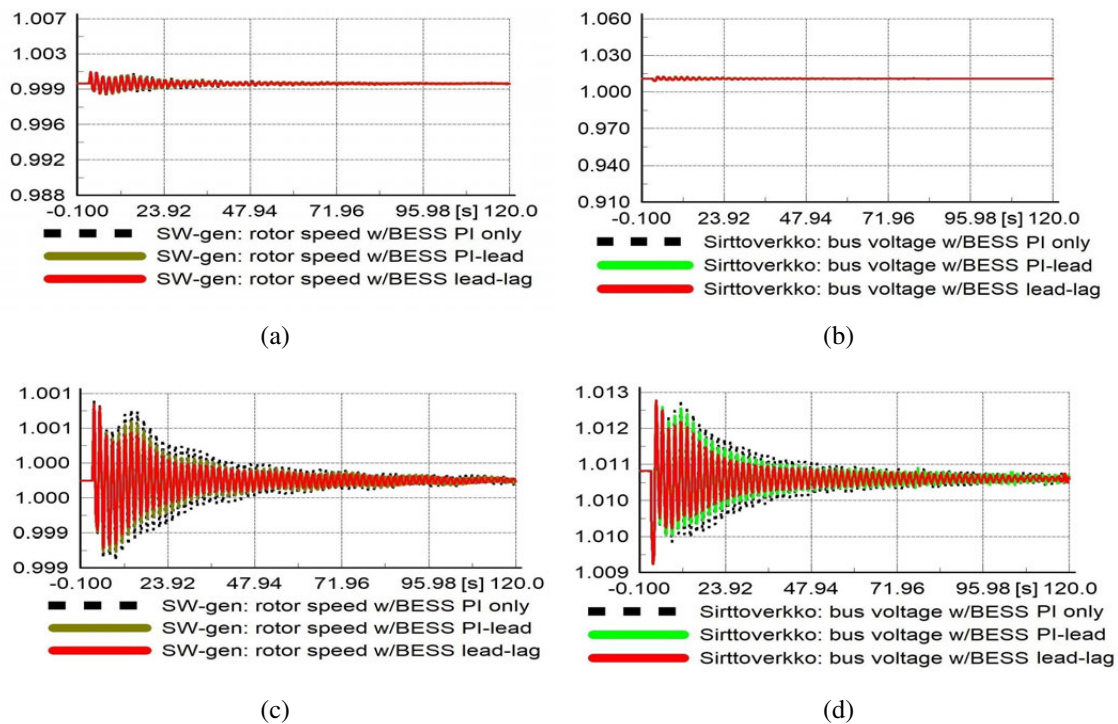


Fig. 6.9 The frequency of generator [p.u.] (a), bus voltage [p.u.] (b), the closer look of frequency (c) and voltage (d) with line outage and BESS [220]

regulated BESS. Simulation results as highlighted in Figs. 6.9 (a) and (b) indicate that regardless of the types of controllers, BESS stabilizes the grid responses and the proposed PI-lead/lead-lag regulated BESS demonstrates better responses as compared to traditional PI regulated BESS as shown in Figs. 6.9 (c) and (d).

Figs. 6.10 (a) and (b) show the power output of BESS. It is visible that the amount of BESS power is less in the case of PI and PI-lead regulated BESS compared to lead-lag regulated BESS which is reflected as a better frequency outcome. In addition, BESS power output does not reach to zero in the case of PI and PI-lead regulated BESS once the voltage and frequency stabilize. This mainly highlights the limitations of the PI controller which is highly reliant on network operating conditions and may perform unsatisfactorily with the changing environment. However, the output of lead-lag regulated BESS reaches to zero when the system is stabilized within the NOFB which further demonstrates the effectiveness and robustness of the proposed lead-lag controller regulated BESS. Since BESS operation lasts only for several seconds, the change in battery SOC is not significant as shown in Fig. 6.11. If sufficient capacity of BESS is

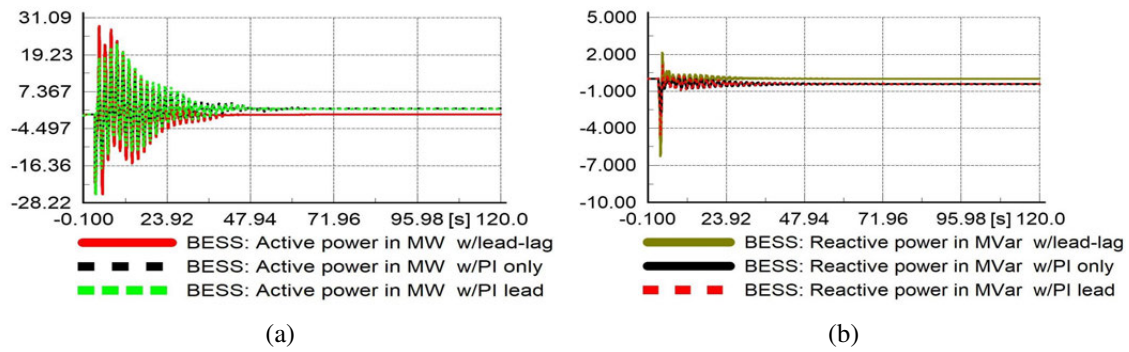


Fig. 6.10 BESS power output - active (a) and reactive (b) [220]

not available during a transient event, the existing generator and turbine should participate in oscillation damping. As system shows instability without BESS, it needs to be ensured that sufficient BESS capacity is available. Hence, a battery of large capacity is selected to ensure adequate battery capacity is available to support the transient periods for energy surplus and shortfall.

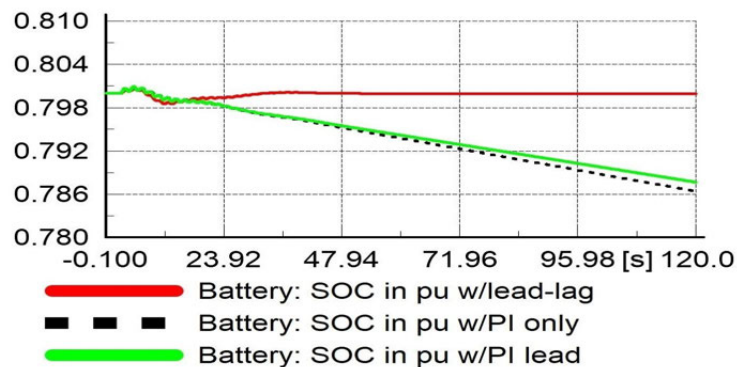


Fig. 6.11 Battery SOC for all BESS control strategies

The selected BESS converter capacity is 40MVA for all the case studies. The NOFB of BESS is selected as ± 0.0002 pu from the nominal frequency. The droop gain is 500 which determines that the total BESS power is triggered for a frequency change of ± 0.1 Hz with a grid frequency of 50Hz. The amount of reactive power is constrained within the BESS converter capacity. The reactive power is designed to be triggered beyond ± 0.004 pu of the pre-fault steady state voltage with a droop gain of 12.5 that describes the activation of total converter capacity for a change of $\pm 8\%$ from the bus voltage. The droop gain for reactive power is small in order to limit the control of BESS for reactive power as grid voltage varies from the nominal value quite often during the grid

operation. Nevertheless, the droop gains can be adjusted according to the grid codes and requirements of the grid. The associated battery values are presented in Appendix B3.

To summarize the comparative study between STATCOM and BESS with new control approaches, BESS maintains the voltage and frequency stability to regulate power flows and thus allows the system to expand the use of usable power transmission capacity. Hence, it can be said that a STATCOM is not capable of competing with BESS when the grid experiences the voltage and frequency instability and cannot support the increased amount of power export. In the case of line outage at post-fault condition, the loading of NW-Sirttoverkko line is increased to 32.4% from 15.3% which clearly validates the BESS effectiveness as compared to STATCOM in enhancing the power transfer capacity in the grid.

6.4.2 Case 2: Load growth and Permanent line outage of N-Sirttoverkko line

As explained in subsection 6.3.3, multiple contingency events have a significant impact on the stability of the grid and hence the efficacy of STATCOM and BESS are assessed following two consecutive faults while transporting power between interconnected areas. The distance between two disturbance events is 20s and the order of contingency events are altered in Case 3.

A three-phase-to-ground fault at $t=3s$ for the duration of 100ms is triggered while exporting the same amount of power. After clearing the fault, a 10% growth in active and reactive power demand at NW load is triggered at $t=23.1s$. Simulated responses of the generators for dual contingencies are presented in Figs. 6.12 (a) and (b), respectively. It can be observed that although STATCOM reduces the frequency and voltage acceleration by a slight margin (Figs. 6.12 (c) and (d) compared to without any FACTS devices (Figs. 6.12 (a) and (b)) but it fails to stabilize the grid responses within the mandatory boundary. The STATCOM is unable to provide adequate damping to the grid and thus fails to maintain voltage and frequency responses within the NEM defined

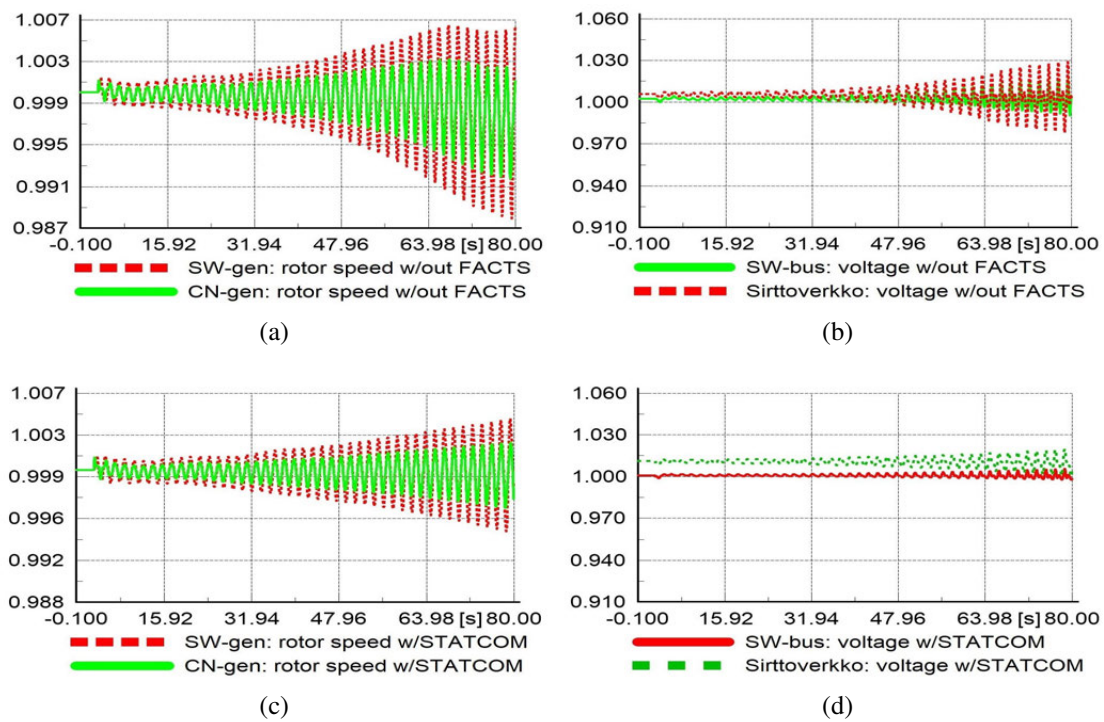


Fig. 6.12 The frequency of generators [p.u.] (a), bus voltages [p.u.] (b) without STATCOM/BESS, the frequencies [p.u.] (c) and voltages [p.u.] (d) with STATCOM [220]

stability limits.

Nevertheless, the frequency and voltage responses as presented in Figs. 6.13 (a) and (b), manifest that the integrated BESS contributes in sufficient system damping at the post-fault condition that maintains a continuous power supply and stabilizes the grid responses within the NEM defined limits. The grid responses also illustrate that BESS with all the control approaches successfully stabilizes the grid and maintains a continuous flow of power in the grid. In addition, the lead-lag controlled BESS provides slightly better frequency outcome as compared to other control approaches.

BESS active and reactive power are presented in Figs. 6.14 (a) and (b), respectively. Similar to the previous case, the post-fault steady-state values is not zero in the case of BESS with PI and PI-lead controllers. However, the lead-lag regulated BESS settles down to zero once the system reaches to the steady-state condition. Since a very small amount of active power is visible for PI and PI-lead regulated BESS controller, the final battery SOC will be lower than that of lead-lag regulated BESS. Thus, it can be said that

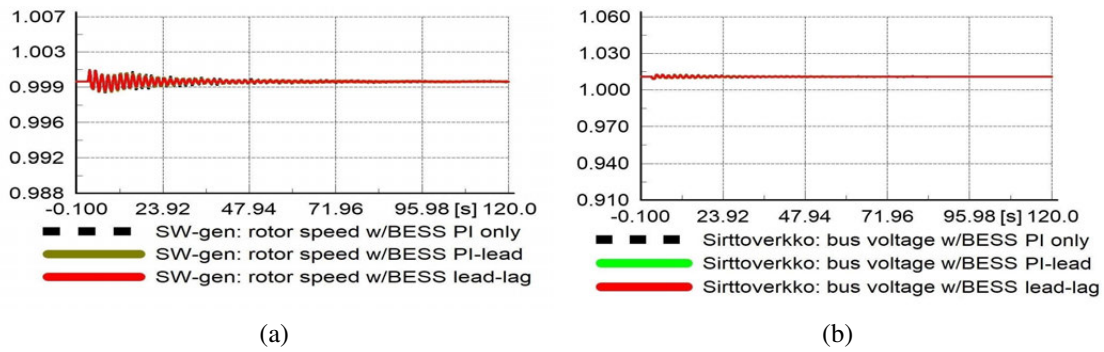


Fig. 6.13 The frequency of generator [p.u.] (a) and bus voltage [p.u.] (b) with BESS [220]

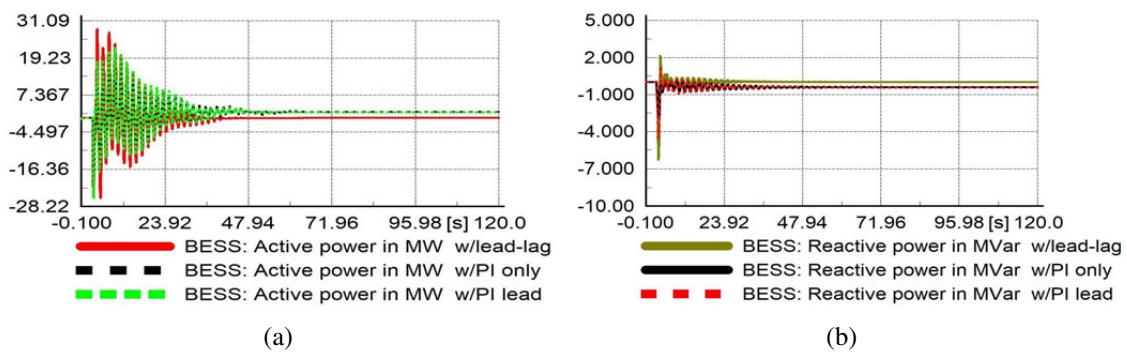


Fig. 6.14 BESS power output - active (a) and reactive (b) [220]

BESS is effective in maintaining grid stability following multiple contingency events.

6.4.3 Case 3: Permanent line outage of N-Sirttoverkko line and load growth

The order of contingency events is altered as in Case 2 to investigate the performance of BESS and STATCOM when the disturbance event occurs in reverse order. The same load amount (19%) is increased at $t=3.1$ s at NW load point and the three-phase fault is applied at $t=23$ s for the duration of 100ms. The grid responses following the consecutive load increase and three-phase fault events are shown in Figs. 6.15 (a) and (b). Similar to Case 2, the voltage and frequency of the grid manifests that without any FACTS devices, the voltage and frequency oscillations accelerate towards instability as presented in Figs. 6.15 (a) and (b). Although STATCOM marginally reduces the accelerating oscillations, as a result of inadequate damping contribution into the grid, voltage and frequency do not

settle down within the stability boundary as presented in Figs. 6.15 (c) and (d) as defined by the NEM standards.

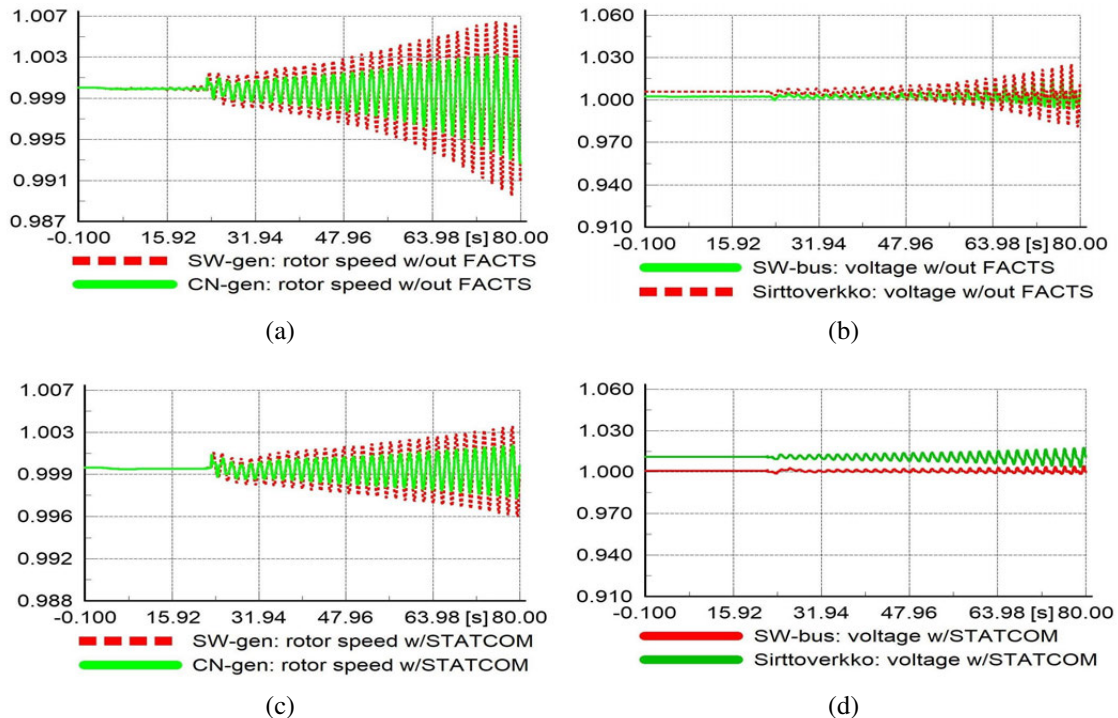


Fig. 6.15 The frequency of generators [p.u.] (a), bus voltages [p.u.] (b) without STATCOM/BESS, the frequencies [p.u.] (c) and voltages [p.u.] (d) with STATCOM [220]

On the contrary, the simulated results as shown in Figs. 6.16 (a) and (b) manifest that the installed BESS at CN provides sufficient damping into the grid that minimizes the transient oscillations and stabilizes the voltage and frequency of the grid at post-fault condition within the mandatory grid boundary. The active and reactive power output of BESS as shown in Figs. 6.17 (a) and (b) exhibit a similar level of performance as in Case 2 and the lead-lag regulated BESS demonstrates better performance compared to other BESS controllers.

The report on South-Australia (SA) blackout by AEMO mentioned that multiple line faults on transmission line increased the amount of power transfer and voltage and frequency stability arose due to line outage which eventually led to complete blackout [280]. This comparative study presents a deep insight into the applicability of BESS in voltage and frequency stability. This study presents that when the supply of

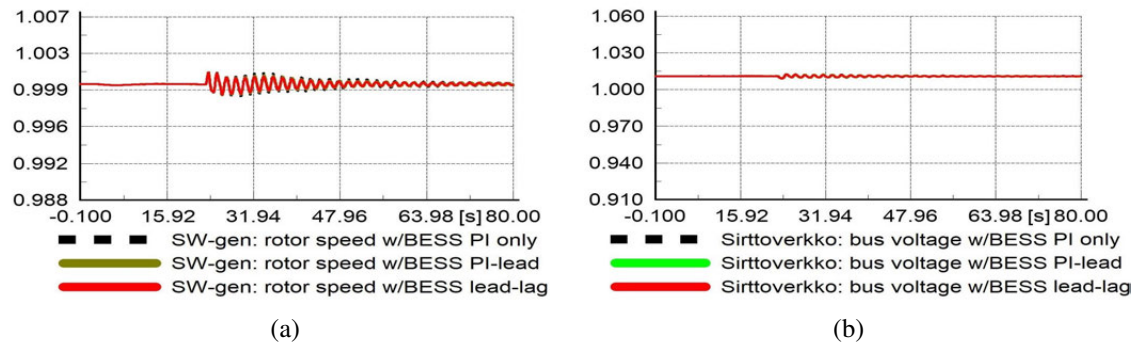


Fig. 6.16 The frequency of generator [p.u.] (a) and bus voltage [p.u.] (b) with PI, PI-lead and lead-lag controlled BESS [220]

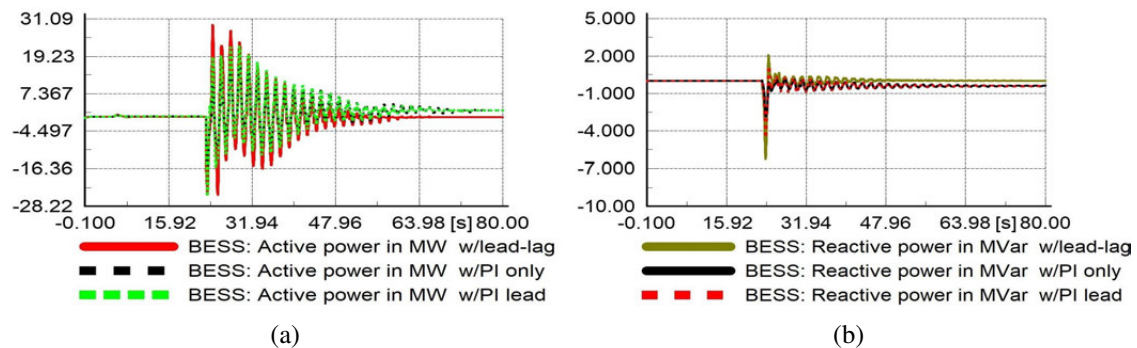


Fig. 6.17 BESS power output - active (a) and reactive (b) [220]

power export is raised by 44%, the system becomes unstable for single and multiple contingency events. The integrated STATCOM fails to contribute in enough oscillations damping and thus cannot stabilize the grid responses following the fault events. However, BESS contributes to sufficient damping into the grid at post-fault conditions and successfully stabilizes the voltage and frequency of the grid for all the studied single/multiple contingency events. This demonstrates that BESS can be an effective solution in order to avoid blackout event such as what happened in SA [280].

6.4.4 The Performance of BESS in Other Circumstances

The effectiveness of BESS for other momentary circumstances are further investigated for validating the suitability of BESS in stability improvement of the grid. Three added case studies are investigated to analyze BESS performance while exporting the same

amount of power as in Cases 1-3 and they are explained as follows:

6.4.4.1 Case 4: Momentary Single-phase-to-ground Fault

The single-phase-to-ground fault is one of the most frequently occurring fault in the power system. Therefore, a fault at phase-a is triggered at $t=1$ s at SW bus for the duration of 150ms. The frequency response at SW generator and voltage at Siirtoverkko bus as illustrated in Figs. 6.18 (a) and (b) show that BESS effectively maintains the stability of the grid at the post-fault condition. Furthermore, the lead-lag regulated BESS provides better frequency response in term of faster reduction of oscillation as compared to PI and PI-lead regulated BESS controllers. The active and reactive power output of BESS as shown in Figs. 6.19 (a) and (b) manifests that the power output of BESS reaches to zero at post-fault stabilized condition.

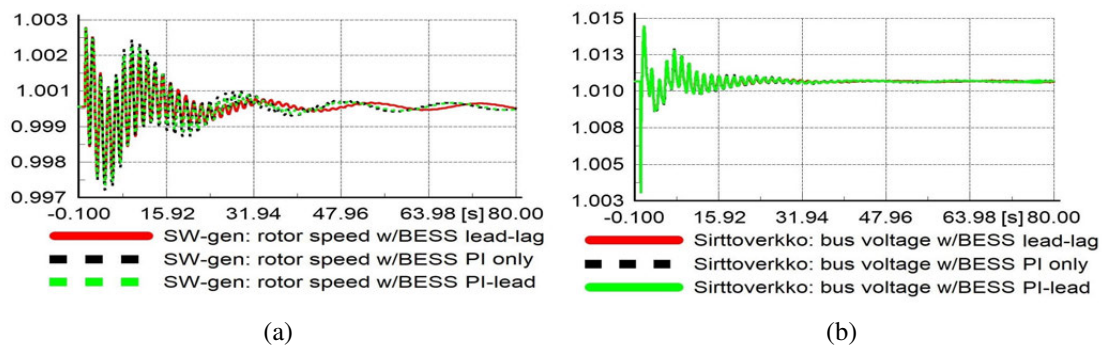


Fig. 6.18 The frequency of generator [p.u.] (a) and bus voltage [p.u.] (b) [220]

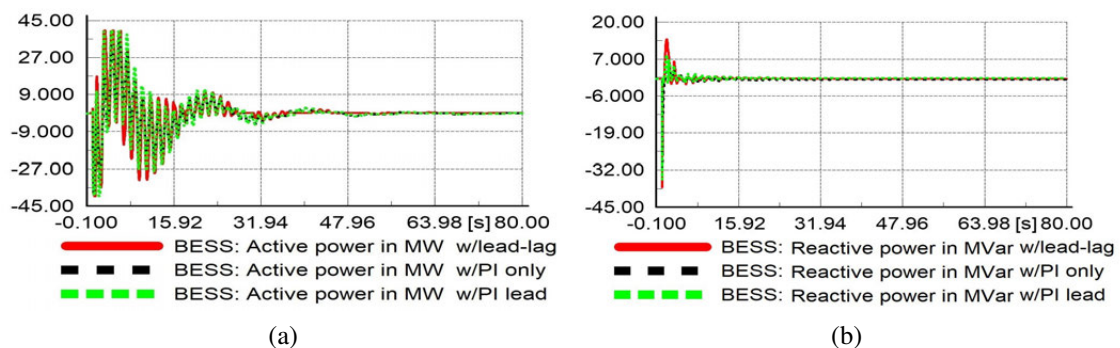


Fig. 6.19 The power output of BESS - active [MW] (a) and reactive [MVar] (b) [220]

6.4.4.2 Case 5: Permanent Single-phase-to-ground Fault

As BESS effectively stabilizes the grid following a temporary fault, the efficacy of BESS is investigated for a permanent fault. A permanent phase-a to ground fault is triggered at $t=1s$ at SW bus. It is found that the generator frequency becomes volatile following the applied permanent fault and without a BESS. However, the installed BESS effectively stabilizes the grid voltage and frequency as shown in Figs. 6.20 (a) and (b). Moreover, the PI-lead regulated BESS provides better oscillation damping compared to PI regulated BESS controllers. Nevertheless, lead-lag regulated BESS demonstrates superior performance than the PI or PI-lead regulated BESS controllers.

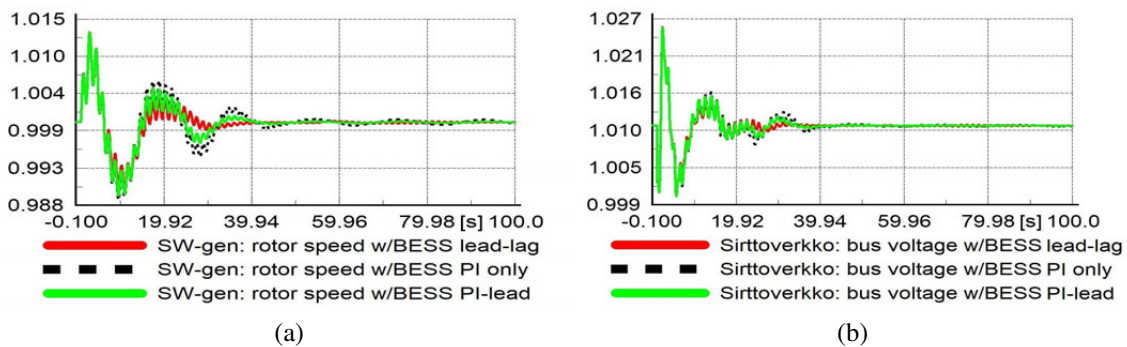


Fig. 6.20 The frequency of generator [p.u.] (a) and bus voltage [p.u.] with permanent single-phase-ground fault (b) [220]

The active and reactive power output is presented in Figs. 6.21 (a) and (b). It can be observed that the lead-lag regulated BESS provides better power regulation which supports in achieving an improved oscillation damping in the grid. It also needs to be mentioned that BESS converter size is increased to 140MVA in order to stabilize the grid voltage and frequency for the permanent single phase fault.

6.4.4.3 Case 6: Without Series Capacitors Between Two Systems

Series capacitors greatly contribute to improving the voltage stability of the grid. Since there are two capacitors in the original design, they might play a supporting role in stability enhancement of the grid at post-fault condition. Hence, these series capacitors are removed in order to investigate BESS competence without any series capacitors

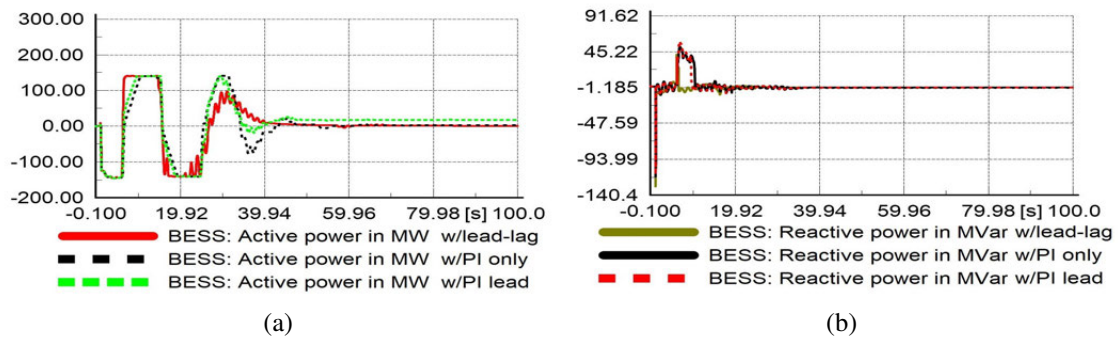


Fig. 6.21 BESS power output - active (a) and reactive (b)

between the two systems. A permanent outage of N-Sirtoverkko line while exporting 650MW is applied at $t=3.1s$. The voltage and frequency responses of the grid as shown in Figs. 6.22 (a) and (b) exhibit that BESS effectively maintains grid stability regardless of any series compensation between the two transmission lines that connects the two systems.

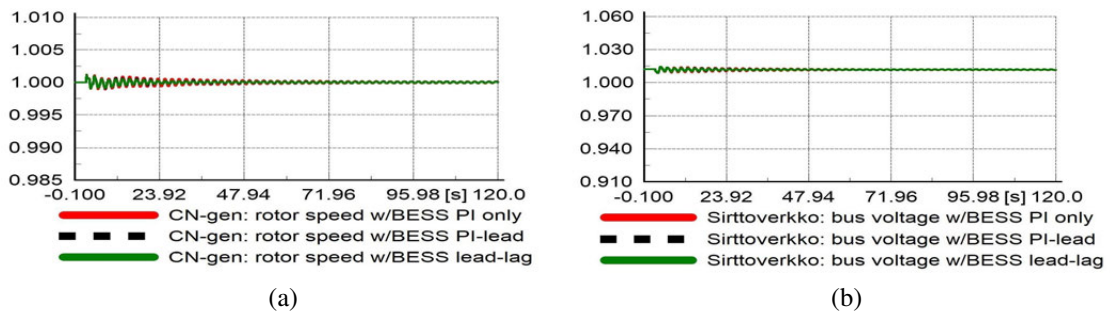


Fig. 6.22 The frequency of generator [p.u.] (a) and voltage [p.u.] (b) without series capacitors and with [220]

6.4.5 The Study of Performance Index

The comparative performance of the proposed and traditional controllers can be assessed with the use of performance index analysis. In order to evaluate controller performance, the sum of squared errors (SSE) is used as a performance indicator in following the set point as defined in (6.5).

$$SSE = \sum_{n=1}^k (x_n - y_n)^2 \quad (6.5)$$

where, x_n =initial value and y_n = actual observational n^{th} value.

The SSE estimation of grid voltage and frequency for the first three cases are outlined in Table 6.1. It can be seen that for the traditional PI regulated BESS controller, the SSE value is high compared to others. Although PI-lead regulated BESS has lower SSE value than PI regulated BESS, the lead-lag regulated BESS has the lowest SSE value which demonstrates the superiority of the controllers.

Table 6.1 The comparative performance of controllers based on SSE analysis

	PI-only	PI-lead	Lead-lag	Observation
Case I	0.001171	0.000819	0.000621	frequency
	0.002051	0.001602	0.001244	voltage
Case II	0.001127	0.000804	0.000633	frequency
	0.001904	0.001501	0.001207	voltage
Case V	0.062582	0.053704	0.050276	frequency
	0.05222	0.048938	0.048168	voltage

6.5 Conclusion

In this chapter, PI-lead and lead-lag regulated BESS controllers are presented and compared with the conventional PI regulated BESS for providing voltage and frequency support and enhancing the power export capability of the grid. BESS competence is also compared with STATCOM technology which has been widely used for enhancing power export in the grid. It is observed that a network contingency event limits the amount of power that can be exported between two interlinked systems and it may become unstable if the volume of power export exceeds that allowable limit. This defines the need for supplementary damping support in the grid.

Simulation studies illustrate that with 44% increase in the amount of power export,

the system becomes unstable. The integrated STATCOM remains unsuccessful in providing necessary damping into the grid and stabilizing the grid responses at the post-fault condition. However, the incorporated BESS at CN provides sufficient damping support to the grid and thus the grid voltage and frequency oscillation decelerates over the time and stabilizes within the NEM defined boundary. This validates BESS potential in stabilizing voltage and frequency oscillations and could prevent grid failure. It is also observed, considering the transient stability perspective, battery power plays a greater role than the energy capacity of BESS. In addition, lead-lag regulated BESS exhibits superior grid response compared to PI and PI-lead regulated BESS in regard to smaller settling time, lower oscillation and better steady-state value at the post-fault condition. The SSE based performance analysis validates the superior performance of lead-lag and PI-lead regulated BESS.

In conclusion, BESS with all three types of controllers proved that BESS is an effective technology in enhancing the stability of the grid and supporting the increased amount of power export in the grid. Also, BESS with lead-lag controller outperforms other controllers.

Apart from the transmission level application, BESS can also be utilized at a low voltage level. In EVCS aggregated with PV, BESS can be employed to minimize transformer overloading, provide numerous grid supports and thus maximizing the benefit of EVCS and BESS. To this aim, the smart control of BESS in EVCS is put forward in the next chapter to explore the potential of BESS for ensuring various services while regulating the power output at the connection point within the transformer capacity.

Chapter 7

Coordinated control of PV and BESS in a smart EVCS for reducing the overloading of grid connecting transformer, PV smoothing and V2G

This chapter contains the following publication - U. Datta, A. Kalam and J. Shi, “Smart control of PV and BESS in EV charging station for reducing transformer overloading and providing grid ancillary service,” *Journal of Energy Storage*, vol. 28, pp. 101224, 2020.

7.1 Introduction

Electric vehicles (EVs) are revolutionizing the transportation industry due to the growing supports from the government and manufacturers, advancements in battery technology such as improved battery capacity, faster charging capability and a decline in battery costs. However, the scattered distribution of EV connection in the existing electric grid results in the complexity in operation and difficulty in proper planning of the grid [281]. In order to accommodate the growing urge of EVCSs, the capacity of the existing network

needs to be upgraded that requires huge capital investment.

According to several research studies, effective planning of EV charging/discharging can minimize the adverse impact of EV. In many occasions, EVs may have a positive impact on the electric network depending on their energy management policy [282] and can minimize investment and operating cost [283] under reasonable amount of EV penetration. With the arrangement of vehicle-to-grid, EV can minimize the demand at peak time and related investment costs [284].

An incorporation of PV system in EVCS can amplify the reduction of carbon dioxide and may provide the flexibility to participate in providing ancillary services into the grid [285, 286]. The bulk of energy import from the grid can be reduced by maximizing the use of available PV energy [287]. Time of use pricing [288] and day ahead price [289] schemes are adopted so that EV owner charge their vehicle during PV production periods with lower price and can also discharge EV power for charging other EVs [290]. However, the variation of PV output is not given any consideration for such PV integrated EVCS.

To minimize the drawback of variable PV power output and EVs charging demand, several strategies for managing the charging/discharging of BESS is presented in literature [291–293]. A variable price model is discussed in [294] that promotes the storing of surplus energy in the case of lower electricity price and selling it to the grid in the case of higher electricity prices. A similar strategy is adopted in [295] for a PV-BESS integrated EVCS which demonstrates an increment in the annual profit of EVCS resulting from the efficient use of PV-BESS. In addition, authors in [296] showed that RES and storage system diminish grid impact by curtailing power absorption from the grid. Nevertheless, grid performance under EVCS uptake is neglected in the studies [291, 293–296]. Authors in [297] demonstrated various operation modes of BESS particularly for peak load minimization and demand fluctuation. A BESS connected EVCS is proposed in [298, 299] that reveals the benefit of reduced operation costs. However, in order to obtain the benefit, SOC constraints are ignored [299] and the battery is drained out fully which will affect its lifetime [298]. Few other similar studies in [300, 301] have suggested optimal operation strategies depending on the market price

which has pushed the BESS to be charged/discharged continuously throughout the day. However, no studies with PV-BESS-EV have considered overloading stress on the grid and grid-connected transformer of EVCS.

The study in [302] discussed that distribution network can be overloaded if EV load demand is managed inefficiently. Existing distribution network infrastructure needs to be upgraded in order to accommodate the rising penetration of EV and avoid failure of the network resulting from network overloading. Studies in [303,304] suggested that soaring EV penetration initiates the rise of hot-spot temperature in distribution transformer which significantly accelerates the loss of the transformer's life.

Realizing the upward trend of EV penetration and its adverse impact in the grid, numerous charging strategy of EV and PV integration in EVCS are suggested in earlier studies. In order to reduce cost and negative impact on grid connecting transformer, an interactive EV charging and grid monitoring strategy are proposed in [305]. Authors in [306] demonstrated that by using available PV power output in a PV integrated EVCS, overloading and in turn rise in hot-spot temperature can be significantly reduced. Another study in [307] suggested that adjusting EV demand as a controllable load can diminish the rise of peak demand due to EV charging. This arrangement can minimize transformer aging due to overloading and therefore existing network infrastructure would be able to sustain large EV penetration. Nonetheless, the broader application of BESS for providing other ancillary services such as Battery to Grid (B2G) within the transformer capacity limit has not given any consideration when BESS remains unused. Regulated EV charging is discussed in [308–310] by controlling EV charging at on/off-peak periods [308] and slow/fast charging strategy [309]. The charging power is limited within the transformer's rated capacity in the case of higher power demand than the rated capacity to avoid overloading [310]. A coordinated charging is presented in [311] for a PV-BESS integrated EVCS in order to minimize transformer overloading. In another study in [312], it is shown that BESS reduces the power demand for EV charging to recharge within the transformer capacity. However, the detailed modeling of BESS [311], PV adoption [312] and B2G [311,312] strategy are completely ignored in the study.

This chapter presents a coordinated charging strategy in a PV-BESS installed EVCS in order to regulate BESS operation aiming to avoid transformer overloading while fulfilling EV charging demand. Furthermore, BESS output is managed to smooth PV power output with respect to the loading condition of the transformer and available PV output for minimizing the adverse impact of intermittent PV output. In addition, B2G service is assimilated in EVCS to facilitate power export from BESS but without violating the transformer's rated capacity. It is demonstrated that with the proposed strategy, transformer overloading can be significantly reduced. Two different sizes of transformer are used in the simulation in order to validate the efficacy of the proposed BESS charging strategy. BESS for smoothing during PV output power variation and B2G are demonstrated through simulation studies. Battery recharging within the transformer capacity is further illustrated through simulation.

7.2 Studied EV Charging Station

The layout of the presented EVCS is illustrated in Fig. 7.1 with corresponding arrows defining power flow. The connection comprises several EVs which are connected to the AC bus via an aggregator, a 22kW PV module, a 200kW and a 167kW BESS and a grid connecting the transformer. PV and BESS are integrated to the AC bus via DC/AC converter. EVCS is connected to the grid via a 0.4/11kV transformer.

In order to determine the corresponding rated power of BESS, charging demand at two spots, food center and residential area, as presented in [314] are considered. The load demands are shown in Fig. 7.2. However, load demand which is more than 90kW are considered in this study and thus the capacity of the grid connecting transformer is selected as 90kW for demonstration purposes. According to Fig. 7.2, it is observed that the highest load demand for a particular period of time is 290kW in a day. This indicates the reality of overloading of a small-sized transformer or selecting a large size transformer to avoid overloading for a shorter length of time. Therefore, the technical benefit of BESS integration in a PV integrated EVCS and associated control methods are presented in this study.

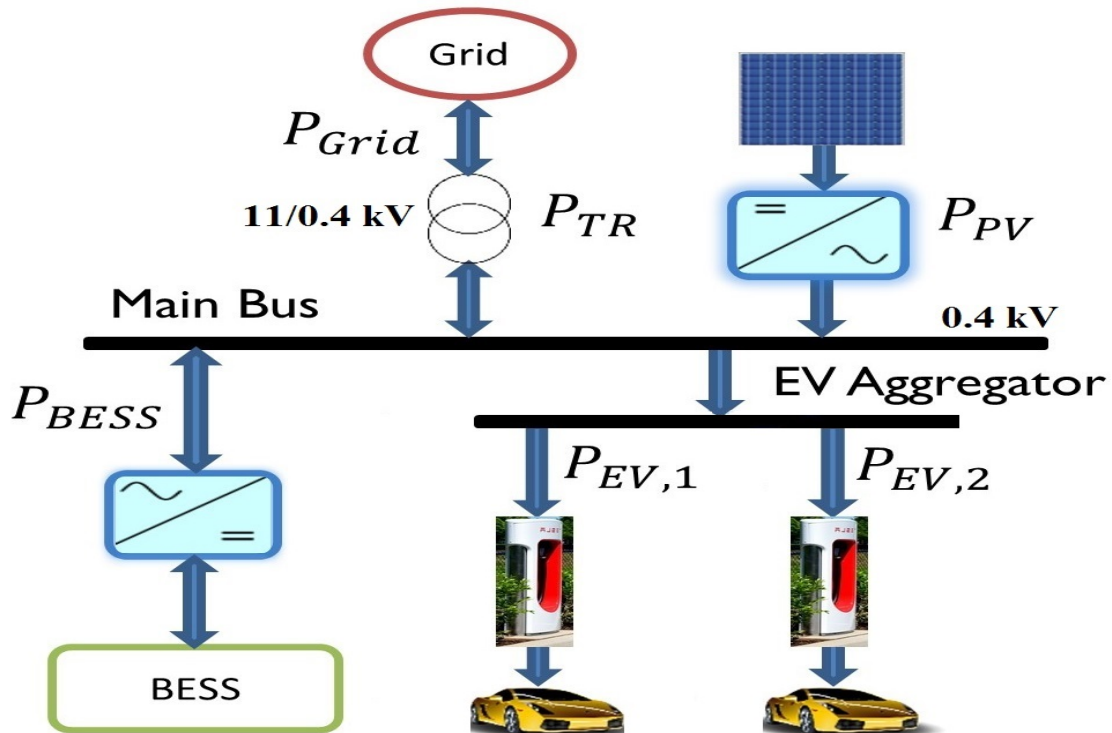


Fig. 7.1 Studied EVCS with EVs, PV and BESS [313]

EVs load demands are considered as an aggregated load instead of as an individual load demand and therefore, a detailed model for EV is not considered in the simulation study. Furthermore, it is assumed that EV operates only in charging mode as in [314] and thus EV arrival, state-of-charge of individual EV is not taken into consideration. PV output varies in real time, but in this study, PV is designed to generate 20kW during all the studied contingency events. The detailed modeling and control of BESS is discussed

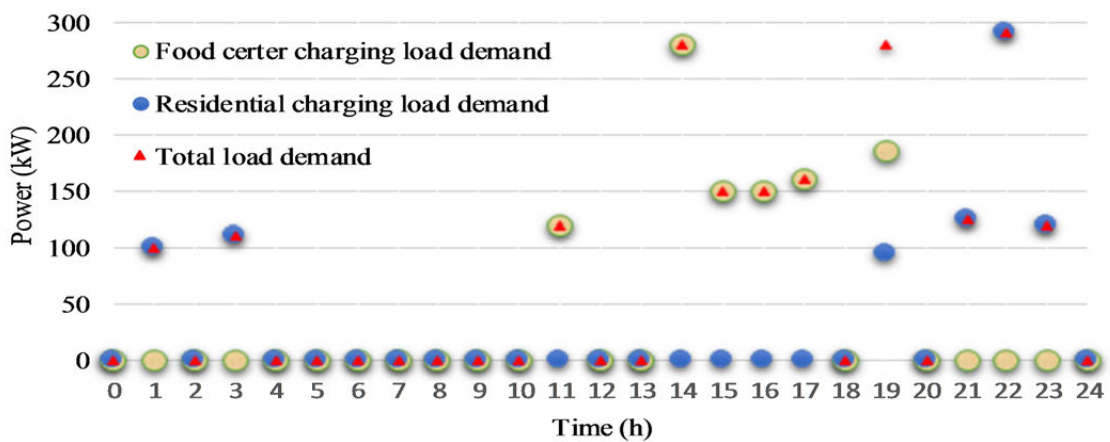


Fig. 7.2 Load profile of EVCS in food center ($P_{EV,1}$) and residential area ($P_{EV,2}$) [313]

in Sub-section 7.3.

7.3 BESS Modeling at EVCS

The presented BESS model encompasses battery bank, BESS controller and bi-directional DC/AC converter. The rated capacity of BESS converter defines the amount of active and reactive power available to participate in providing response to the control action. However, in this study, active power of BESS is the main focus and hence the reactive power control is disabled which can be extended if needed. The complete layout of BESS controller can be divided in the following sections:

1. Reference power generator P_{ref}
2. Active power (P) regulator
3. Battery charge regulator
4. d and q axis current regulator
5. Battery model and SOC estimation

7.3.1 Reference Power Generator $P_{BESS-ref}$

The reference power generator $P_{BESS-ref}$ generates active power reference for regulating BESS power output in response to the measured power ($P_{meas(s)}$). The ($P_{meas(s)}$) is taken at the point of transformer connection and according to the defined control logic as illustrated in Fig. 7.3 where BESS output power at AC terminal is defined by P_{in} . The nature of application delineates the amount and direction of BESS power flow. During transformer overloading reduction, BESS injects the amount of power deficit above the rated capacity of transformer. The thorough discussion on producing reference power generator P_{ref} is outlined in Section 7.4 for various operation conditions.

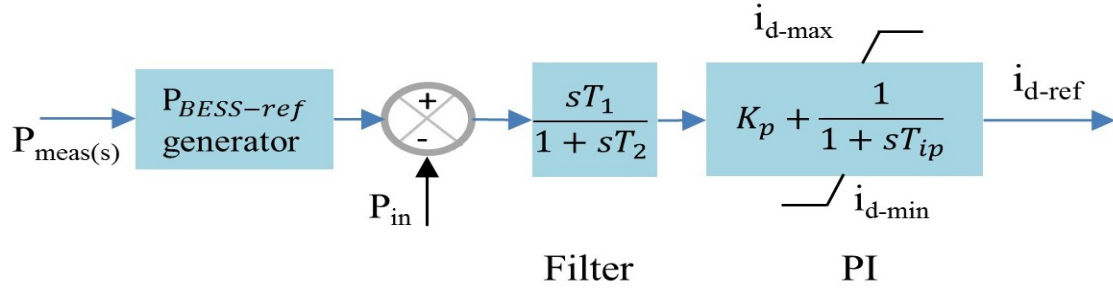


Fig. 7.3 Active power (P) regulator with $P_{BESS-ref}$ generator [313]

7.3.2 Active Power (P) Regulator

The calculated power resulting from the error between reference power generator P_{ref} and P_{in} as presented in Fig. 7.3 passes through a first order filter. The filter output is passed through a PI controller which generates active power reference in d-axis. The time constants T_1 and T_2 in the first order filter shapes the dynamic response and thus a large value of time constant results slower transient response. In order to avoid integrator windup, an anti-windup limiter is incorporated in the PI controller. The mathematical derivation of anti-windup can be expressed as in (7.1):

$$y_o = \left[y_{er} * \left(K_p + \frac{K_i}{T_i} \int_{y_{mn}}^{y_{mx}} dt \right) \right]_{y_{mn}}^{y_{mx}} \quad (7.1)$$

where, PI controller output $y_o=i_{d-ref}$, $y_{mx}=i_{d-max}$ and $y_{mn}=i_{d-min}$.

The charge control receives the generated d-axis current (i_{d-ref}) signal from the PI controller. The considered value of PI controller are as follows: $K_p=2$, $T_i=0.01$, $i_{d-max}=1$ and $i_{d-min}=-1$.

7.3.3 BESS Charge Controller and Current Controller

The set constraints for battery charging regulation is illustrated in Fig. 7.4 that delineates the control of BESS power output i.e. charging/discharging mode of battery in response to the designed event. BESS can discharge if present battery SOC is above the lowest allowable SOC and charge if lower than the minimum SOC which can be adjusted if needed. In this study, the lowest and maximum SOC limit constraints are taken as 0.2pu and 1pu. The regulation of BESS active power for various SOC constraints can be calculated as in (7.2):

$$i_{d-ref} = \begin{cases} i_{d-ref-in} & SOC \geq SOC_{min} \\ -i_{d-ref-in} & SOC \leq SOC_{max} \\ 0 & Otherwise \end{cases} \quad (7.2)$$

The battery needs to be recharged once battery SOC reaches to the minimum SOC value and recharging should continue until it reaches to the maximum SOC of 1pu as

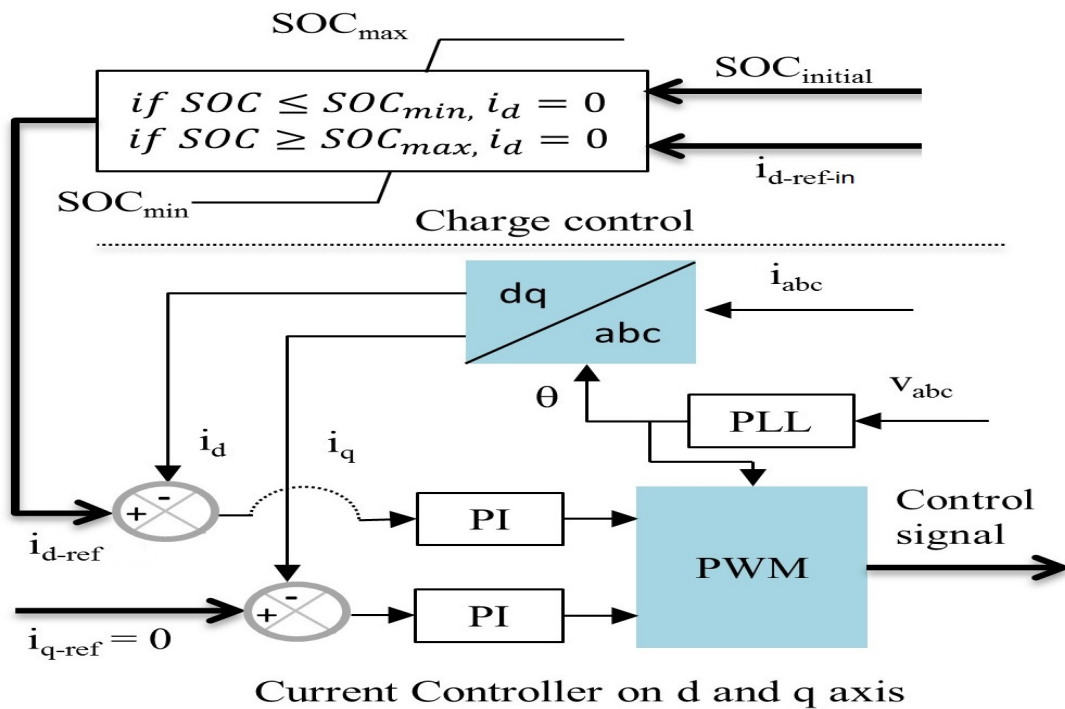


Fig. 7.4 BESS charge/discharge control and d-q axis current controller [313]

per the designed constraints. Battery should be recharged only if the transformer is not overloaded i.e. the available power for BESS recharging is the unused capacity of the transformer after feeding the EV charging demand. This will make sure that battery recharging does not result overloading of the transformer and only take actions if the constraints are satisfied. The d and q axis current controller as shown in Fig. 7.4 regulates BESS active/reactive power based on the error between the grid and the generated reference. However, as BESS is regulated for active power, reactive power reference in q-axis is set to 0.

7.4 BESS Control in PV Combined EVCS

The coordinated regulation is an indispensable part of managing various energy resources and operating modes. This coordination regulates BESS output and its direction of flow with respect to the changes in PV output and dynamic load demand. The individual control loop is regulated independently but the inputs are partially dependent on each other. This assures the action of an appropriate control operation for the designed operating condition while other control loops should not operate.

7.4.1 Control of BESS Scaling Down of Transformer Overloading

The main purpose of installing BESS is to reduce the amount of imported power in EVCS if EV power demand surpasses the transformer's nominal capacity and thus avoids transformer overloading. The mathematical calculation for determining power at transformer integration point can be expressed as in (7.3):

$$P_{TR} = \begin{cases} P_{EV} - P_{BESS} & \text{if } P_{EV} > P_{TR-nom} \\ & \text{and } SOC \geq SOC_{min} \\ P_{EV} & \text{if } P_{EV} \leq P_{TR-nom} \end{cases} \quad (7.3)$$

where the total power output at the transformer end and EV charging demand are defined by P_{TR} and P_{EV} respectively. The addition of $P_{EV,1}$ and $P_{EV,2}$ results P_{EV} that must be equal or less than the nominal capacity of transformer for avoiding overloading. The power output of BESS P_{BESS} continues to support as long as SOC constraints are maintained. The reference power output of BESS $P_{BESS-ref}$ regulation can be written as in (7.4)

$$P_{BESS-ref} = P_{EV} - P_{TR-nom} \quad (7.4)$$

where nominal capacity of transformer is defined by P_{TR-nom} . The overall process of reducing transformer overloading with BESS is illustrated in Fig 7.5. According to (7.4), BESS output response $P_{BESS-ref}$ is only available if power output for EV charging demand is greater than P_{TR-nom} i.e a positive value or else $P_{BESS-ref}$ is zero. The value of P_{ref} is then passed through a PI controller to generate d-axis current reference as illustrated in Fig 7.3.

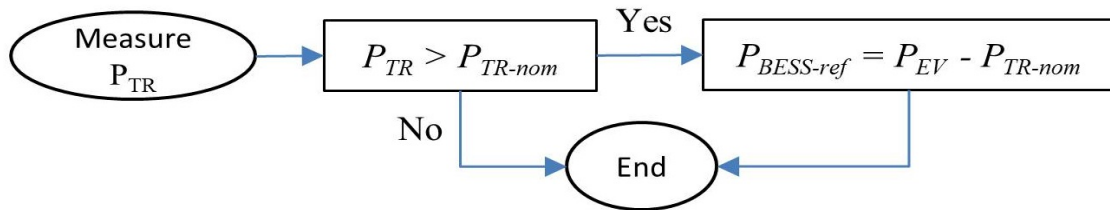


Fig. 7.5 Flow diagram for transformer overloading reduction with BESS [313]

7.4.2 PV Output Smoothing and Transformer Overloading Reduction

If PV panels are installed in the EVCS ceiling, this can lessen the amount of grid power consumption and thus transformer overloading can be reduced partially. However, due to the intermittent nature of PV, grid power is subjected to frequent oscillation. In order to support this phenomenon, BESS is designed to provide PV output smoothing when PV output drops below a certain predefined level. The regulation of BESS power output in EVCS for an aggregated PV smoothing and transformer overloading reduction is

illustrated in Fig. 7.6. It is worth mentioning that, PV smoothing, in this study, is referred to as providing the amount of power shortage other than 20kW. The amount of BESS power output for transformer overloading reduction is defined by P_{BESS1} . The amount of BESS power for PV smoothing is defined by $P_{BESS/PV}$ which is equal to the variation between PV output P_{PV} and set predefined value P_{PV-lim} as in (7.5). When P_{PV} is equal or above P_{PV-lim} , the value of $P_{BESS/PV}$ is zero.

$$P_{BESS/PV} = \begin{cases} |P_{PV} - P_{PV-lim}| & \text{if } P_{PV} < P_{PV-lim} \\ & \text{and } SOC \geq SOC_{min} \\ 0 & \text{else} \end{cases} \quad (7.5)$$

It is assumed in this study that PV generation is always less than EV charging demand and hence, BESS does not participate in charging when P_{PV} is above the P_{PV-lim} .

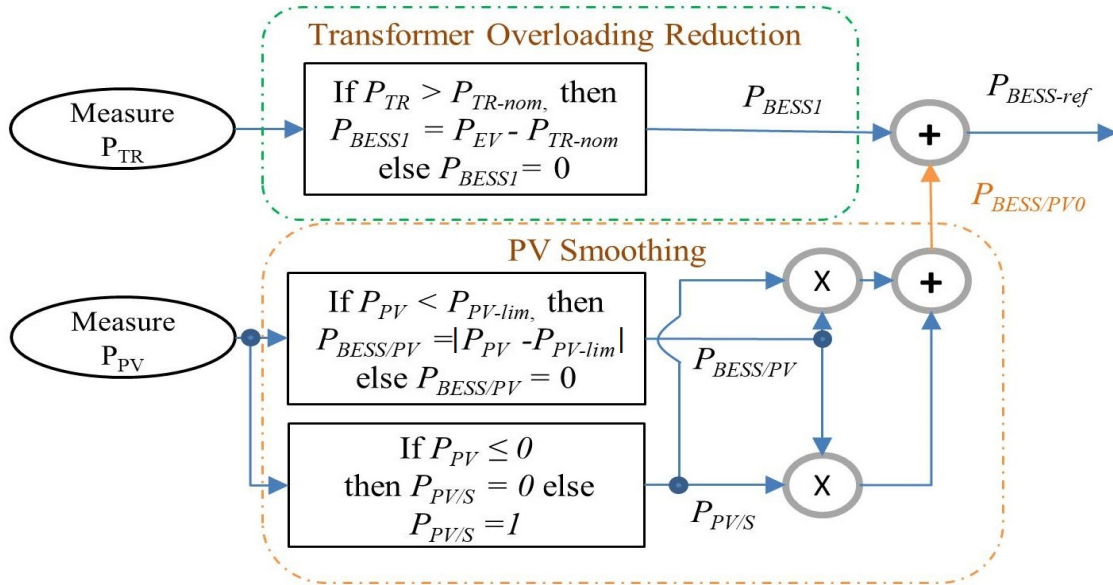


Fig. 7.6 Coordinated control of transformer overloading reduction and PV smoothing with BESS [313]

While providing PV smoothing, it needs to be assured that the control action remains inactive during the night time or on a very cloudy day. To implement this, a status signal of PV output $P_{PV/S}$ is sent to smoothing regulator (0= PV output is not available, 1=PV output is available) when $P_{PV} \leq 0$. Depending on the signal output of

$P_{PV/S}$, $P_{BESS/PV}$ is zero or a positive value. The fundamental advantage of the presented PV-BESS regulation is that PV smoothing only operates when PV output is available i.e. during the day time only. PV smoothing power reference $P_{BESS/PV0}$ is finally added with transformer overloading reduction signal P_{BESS1} to generate the combined power reference of BESS $P_{BESS-ref}$.

7.4.3 The Integrated Control for B2G and Battery Recharging

In a deregulated market where the consumer is allowed to sell energy to the grid and when electricity price is high, installed BESS can participate in B2G services. However, the main constraint is the price which needs to be economically justifiable i.e. the price for B2G P_{B2G} must be higher than that of grid-to-battery P_{G2B} . Considering a single point of power connection, only power export or import is possible at any given time of operation. BESS can be designed to participate in frequency or active power regulation if needed. The coordinated control of curtailed transformer overloading, PV smoothing, B2G and battery recharging is illustrated in Fig. 7.7 (shaded in pink). The selection of each mode defines the power flow direction. When the power flow signal directs from the grid to the EVCS, the combined overloading reduction and PV smoothing reference $P_{BESS-ref/OLS}$ defines BESS power output reference $P_{BESS-ref1}$. During B2G operation, power flow signal directs from the EVCS to the grid and hence $P_{BESS-ref/OLS}$ remains inactive. In that case, BESS power output reference $P_{BESS-ref1}$ is defined by $P_{BESS-ref/B2G}$. In order to ensure that $P_{BESS-ref/B2G}$ is regulated within the rated capacity of transformer, the boundary for B2G operation ($P_{TR-B2G-lim}$) is defined by the ratio of P_{TR-nom} and the nominal capacity of BESS ($P_{BESS-nom}$). This is particularly important for a BESS size higher than the rated capacity of transformer as illustrated in (7.6).

$$P_{TR-B2G-lim} = P_{TR-nom}/P_{BESS-nom} \quad (7.6)$$

While passing the updated power reference through a PI controller, the operating limit needs to be adapted in accordance with the operation mode of BESS. The active power controller in various operation modes are illustrated in Fig. 7.7 (on the right column).

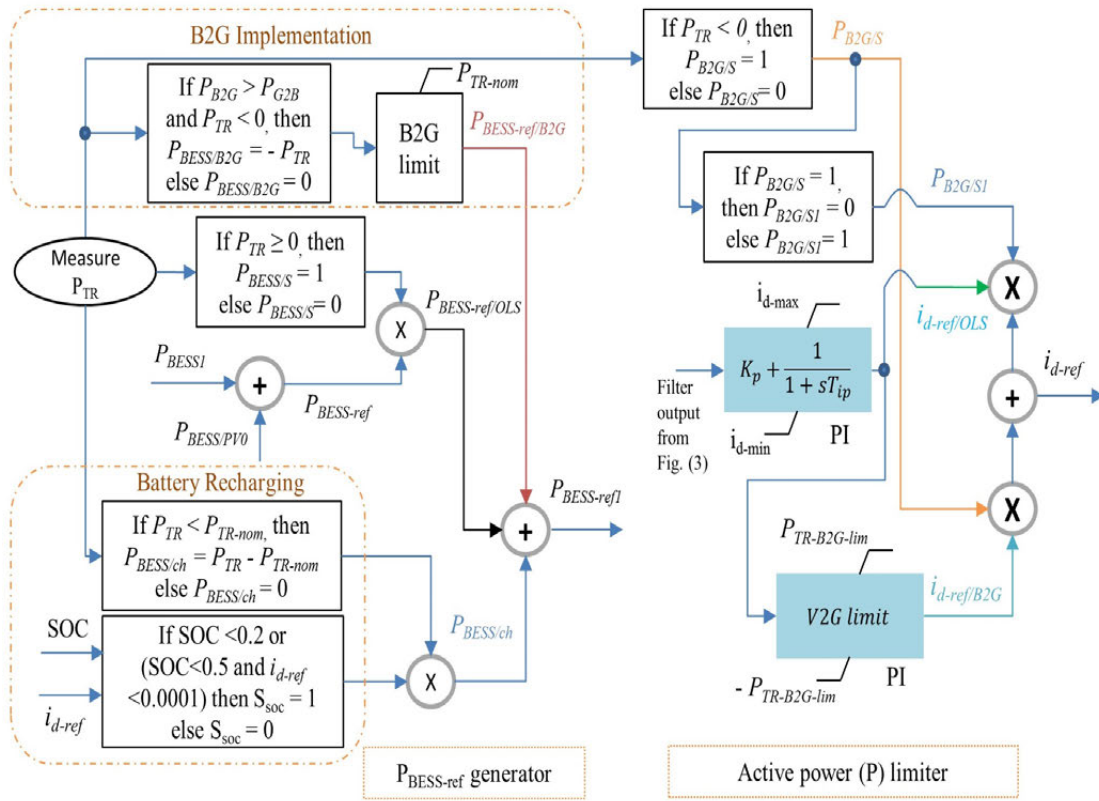


Fig. 7.7 Coordinated control of reducing transformer overloading, smoothing PV output and B2G at EVCS with BESS [313]

BESS output is controlled within the maximum value i.e. $P_{B2G/S1}$ as 1 when BESS operates in transformer overloading reduction and PV smoothing. Nevertheless, during B2G operation, the output limit is adjusted within the ratio of P_{TR-nom} and the nominal capacity of BESS ($P_{BESS-nom}$). Hence, $P_{B2G/S}$ is set to 1 and thus $P_{B2G/S1}$ becomes zero.

Battery recharging is designed for two operating scenarios: (a) SOC is below the minimum SOC (0.2pu) value, (b) SOC is below 0.5pu and i_{d-ref} is lower than 0.0001pu which ensures the avoidance of any clash between battery charging and discharging signal during $0.5pu > SOC > 0.2pu$. Furthermore, the recharging power of BESS $P_{BESS/ch}$ should be available when $P_{TR} < P_{TR-nom}$. The amount of $P_{BESS/ch}$ can be calculated as $P_{TR} - P_{TR-nom}$.

7.4.4 Determining BESS (kW) and Transformer (kVA) Capacity

To determine an appropriate size of BESS, it is crucial to decide the rated capacity of the grid connecting transformer. Referring to the load profile at the chosen location as exhibited in Fig. 7.2 demonstrates that a very high load demand is visible for a certain period of the day. In order to avoid transformer overloading between 2pm to 11pm, two various sizes of the transformer, a 121kVA and 200kVA rated transformer, (P_{TR-nom}) are chosen.

According to Fig. 7.2, peak EV charging demand (P_{EV-max}) is 288kW at approximately 10pm. To reduce the amount of power consumption from the grid and in turn curtail transformer loading, the calculation of needed BESS size ($P_{BESS-req}$) can be expressed as in (7.7).

$$P_{BESS-req} = P_{EV-max} - P_{TR-nom} \quad (7.7)$$

For the given peak EV charging demand from 2pm to 11pm and with a 200kVA transformer, a 100kW of BESS is sufficient to reduce transformer loading. Furthermore, as the BESS size is lower than the transformer's rated capacity, the transformer will not be overloaded during B2G or battery recharging. On the other hand, for a 121kVA transformer and assuming a charging/discharging efficiency of 85% [315], the required BESS size is 200kW. The overall control design is demonstrated via a flowchart as illustrated in Fig. 7.8.

7.5 Results and Analysis

The effectiveness of the presented integrated control design is substantiated through numerous case studies which are outlined as follows:

- (a) Reducing Transformer Loading with BESS and without PV

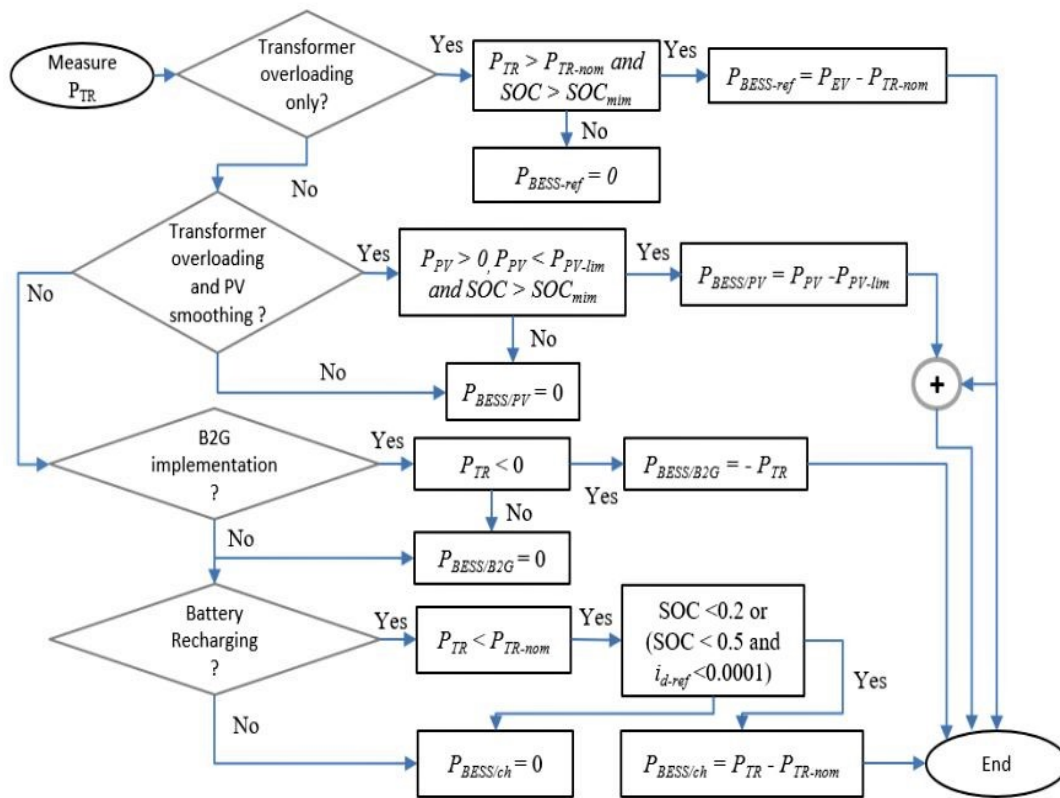


Fig. 7.8 Flowchart of the proposed energy management scheme [313]

(b) Integrated control of PV & BESS to Reduce Transformer Loading and PV Smoothing

- (1) Stable PV Output and Reducing Transformer Loading Only
- (2) PV Smoothing Only
- (3) PV Smoothing and Reducing Transformer Loading

(c) BESS for B2G Service

(d) Battery Recharging without Violating Transformer Capacity

7.5.1 Reducing Transformer Loading with BESS and without PV

The reduction of transformer overloading for various operation modes with and without a BESS is presented in Fig. 7.9. Fig. 7.9(a) depicts the variation of EV load demand between 95kW to 288kW [314]. A typical load demand of 120kW is selected for the

simulation purposes. A 87.5% load growth in EV charging demand i.e. 225kW at $t=5s$ is applied which entails the need of 104kW from the BESS when a 121kVA transformer is selected to avoid overloading. The load demand is lowered to the normal condition at $t=65s$. At $t=70s$, load demand is increased by 140% which implies 167kW demand to be met by BESS to reduce transformer overloading. On the contrary, in the case of 200kVA transformer, the required contributions of BESS power are 25kW and 88kW respectively. Transformer overloading in various operating conditions as depicts in Fig. 7.9(b) indicate that without a BESS, transformer overloading reaches upto 238% for the particular case study. However, it can be seen that with an integrated BESS, transformer overloading can be effectively reduced. A large size of transformer i.e. a 200kVA transformer requires a moderate size of BESS (100kW) to reduce stress on transformer loading. Nevertheless, an optimal size calculation of transformer and BESS can provide better insight on the techno-economic benefit of the selection which is not the focus of this thesis. The reduction in transformer overloading will reduce the hike in hot-spot temperature of transformer which can prolong transformer lifetime [309].

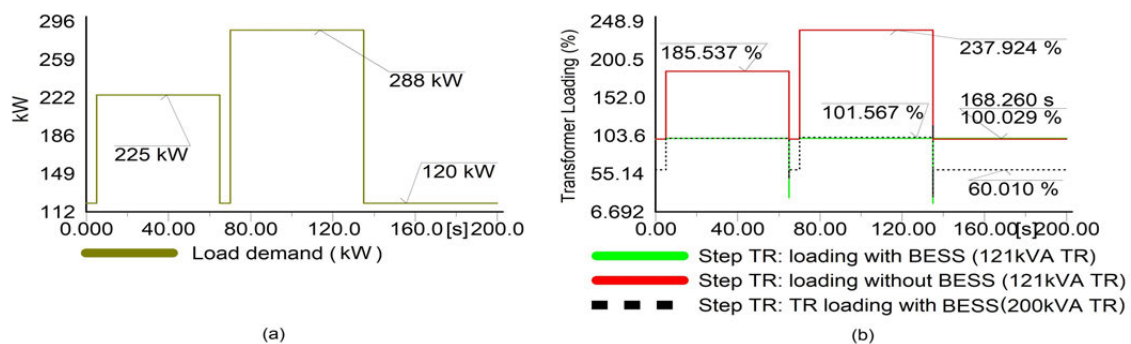


Fig. 7.9 EV charging load demand (a) and transformer overloading in different operation modes (b) [313]

The output power of BESS for transformer overloading reduction is presented in Fig. 7.10(a). It can be seen that 200kW rated BESS delivers the necessary 104kW and 167kW following the variable load demand and curtails transformer loading within the nominal capacity. With the larger size of transformer (200kVA) and smaller BESS (100kW), loading at peak demand period is maintained within the nominal capacity of transformer without making it overloaded. SOC of the Battery for both cases are illustrated in Fig. 7.10(b) that indicates that battery SOC reduces during the service and

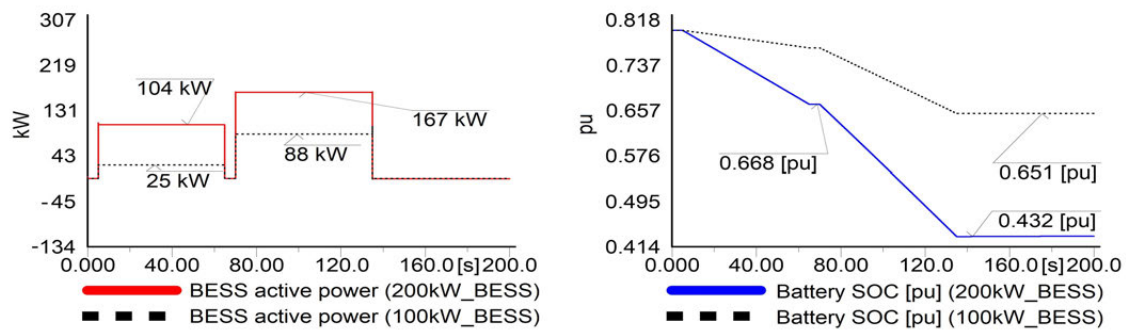


Fig. 7.10 BESS active power output (a) and battery SOC during transformer overloading period (b) [313]

hence a larger energy capacity of battery is essential to provide support for longer periods.

7.5.2 Integrated Control of PV & BESS to Reduce Transformer Loading and PV Smoothing

In this study, a 22kW rated PV system is considered in the EVCS ceiling which provides a constant 20kW output. Hence, the power consumption of EVCS reduces by 20kW. The amount of BESS power for overloading reduction, in this case, slashes to 84kW as compared to 104kW and 147kW as compared to 167kW as in Section 7.5.1. For 200kVA transformer, the needed BESS power is 5kW during $t=5s$ to $t=65s$ and 68kW for the duration of $t=60-135s$ as illustrated in Fig. 7.11 (a). For 100kVA transformer, the desired BESS power is 84kW during $t=5s$ to $t=65s$ and 147kW for the duration of $t=60-135s$ as exhibited in Fig. 7.11 (a). In both cases, transformer overloading is reduced and regulated within 100% of its rated capacity as depicted in Fig. 7.11 (b). Thus, the installed PV can maximize the use of renewable energy and reduce power consumption from the grid during the day time.

While smoothing PV output, load demand is assumed to be constant and lower than the rated capacity of the transformer. In the proposed design, BESS is allowed to regulate its output when PV output reduces to a value lower than 20kW. PV output drops to 15kW at $t=5s$ which further drops to 13kW at $t=15s$ and finally recover to its nominal

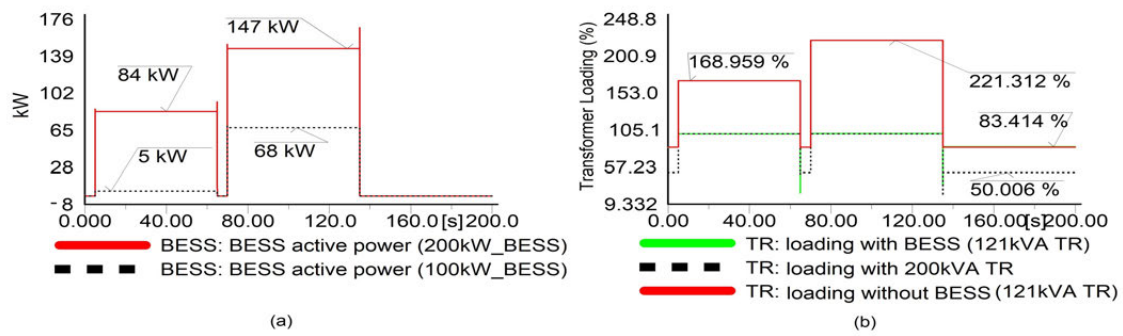


Fig. 7.11 BESS active power output (a) Transformer loading during overloading reduction with constant PV output (b) [313]

generation of 20kW as illustrated in Fig. 7.12(a). The PV output following BESS output is depicted in Fig. 7.12(b) that clearly indicates the efficacy of the proposed control design of regulating BESS power output according to the variation in PV output.

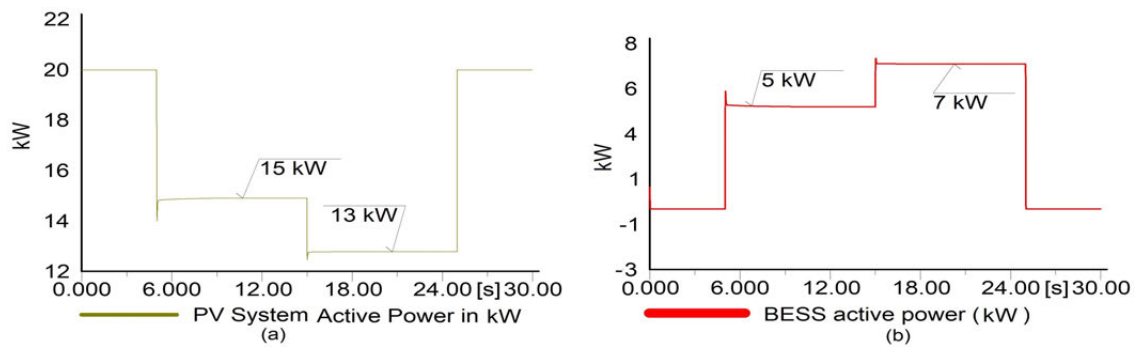


Fig. 7.12 PV output variation (a) and BESS active power output during PV smoothing with no transformer overloading action (b) [313]

To further validate the coordinated control of PV-BESS, a combined event of overloading reduction with constant output as in Fig. 7.12 and PV smoothing only as in Fig. 7.11 is carried out. At $t=5s$, the aggregated power reference for 200kW BESS is 89kW which is the resultant of 84kW from transformer overloading reduction and 5kW from PV smoothing. As PV output drops further, the power reference for BESS increases to 91kW. On the contrary, the power reference for 100kW BESS is 10kW and 12kW respectively for the same contingency events. Fig. 7.13(a) indicates that BESS efficiently regulates its output as transformer loading and PV output varies so that transformer loading stays within the nominal capacity of the transformer. This substantiates the efficacy of the proposed PV-BESS control to minimize transformer loading and PV smoothing coherently. The loading of the transformer under various

operating scenarios are illustrated in Fig. 7.13(b) that indicates BESS efficacy in avoiding transformer overloading.

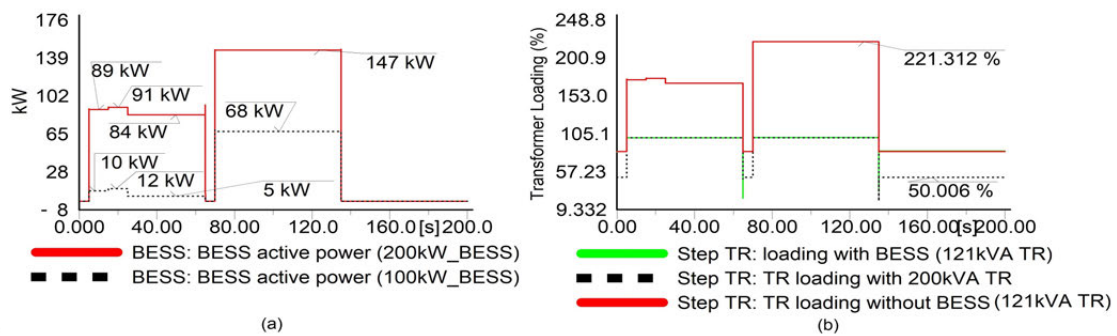


Fig. 7.13 BESS active power (a) Transformer loading and during integrated control (b) [313]

Further simulation studies are carried out to demonstrate the efficacy of the proposed control design in term of BESS providing PV smoothing service only during the day time. The variation in PV output is illustrated in Fig. 7.14(a) which indicates that PV output diminishes over the simulation time and finally reduces to zero at t=25s which replicates a night time scenario. In following the proposed control design, BESS initially delivers 5kW and 7kW respectively. However, BESS does not inject any power i.e. output power reduces to zero once there is no PV output at t=25s according to the control design as illustrated in Fig. 7.14(b).

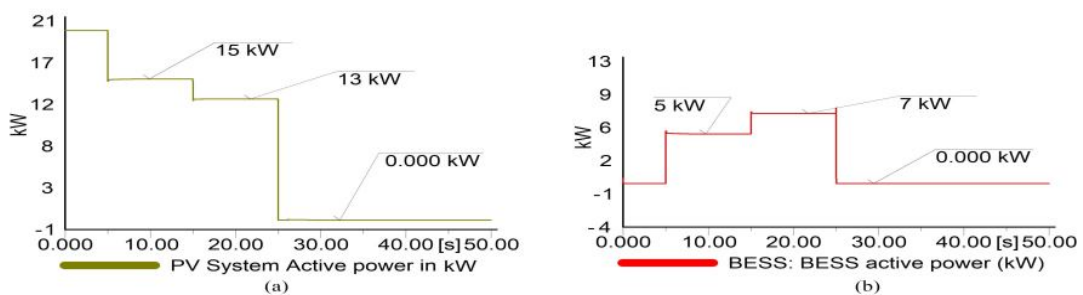


Fig. 7.14 Fluctuation of PV output (a) and BESS active power response (b) [313]

7.5.3 BESS for B2G Service

In the absence of EV charging demand, BESS can participate in B2G and BESS can sell its energy to the grid if the selling price is high. B2G service may range from energy

arbitrage to frequency control. In order to implement B2G, it is considered that electricity selling price already attractive to the EVCS owner to participate in B2G. BESS continues to support until SOC constraints are not violated. In the case of higher demand during B2G, BESS power output is regulated within the rated capacity of the transformer. The power output of BESS during B2G implementation under two operation limits are depicted in Fig. 7.15(a). At $t=4s$, a 140kW demand is enforced for the duration of 16s. With 200kW BESS, this load demand can be supplied but this will result in an undesirable overloading of the transformer. Nevertheless, with the specified operating boundary, the amount of BESS power is equal to the rated capacity of transformer i.e. 121kW which implies avoidance of transformer overloading. As predicted, Fig. 7.15(b) shows higher SOC in the case of 100kW BESS as compared to 200kW BESS.

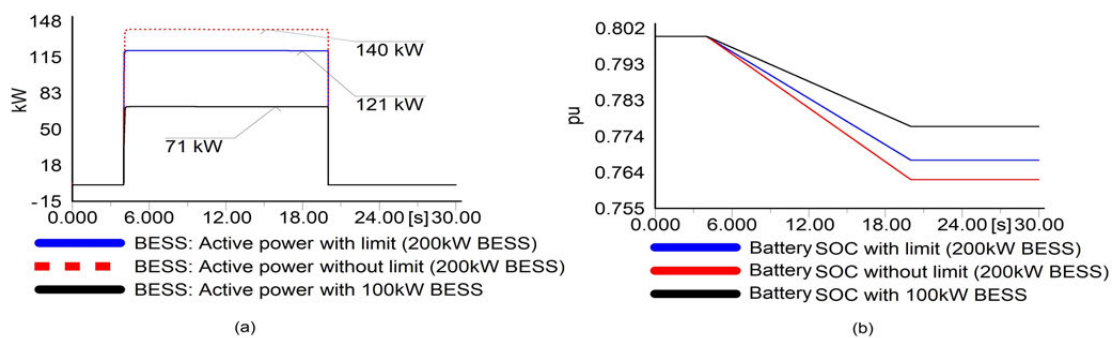


Fig. 7.15 BESS active power (a) and battery SOC (b) during B2G with and without designed constraint [313]

7.5.4 Battery Recharging without Violating Transformer Capacity

Fig. 7.16 illustrates the implementation of the proposed battery recharging method with a 121kVA transformer. Fig. 7.16(a) shows load demand and Fig. 7.16(b) shows battery SOC for various operation modes. When battery SOC is above 0.5pu, battery recharging is not required as depicted in Fig. 7.16(b). However, when the battery SOC drops to 0.46pu, battery needs to be recharged according to the control design. But as the load demand is $141-20=121$ kW which implies that the transformer is fully loaded and thus it does not have sufficient capacity (NEC) to accommodate further demand for recharging the battery. On the contrary, when load demand drops to $92-20=72$ kW, transformer has a

spare capacity of $121-72=49\text{kW}$ to recharge the battery. This substantiates the efficacy of the proposed battery recharging method without violating the loading limit of transformer.

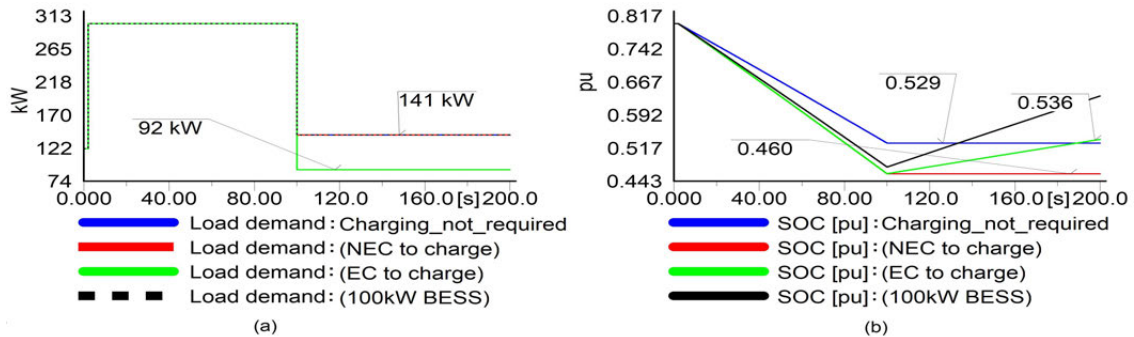


Fig. 7.16 BESS active power (a) and battery SOC (b) during battery recharging [313]

7.6 Conclusion

In this study, an amalgamated control of PV-BESS in a EVCS is proposed to reduce overloading of the grid connecting transformer. A detailed model of BESS in association with control techniques is presented to curtail grid consumption for avoiding overloading and providing PV smoothing and B2G services. The investigated summary can be encapsulated as follows:

- A BESS in EVCS can significantly lower grid power consumption and thus reduce overloading of the grid connecting transformer. It is demonstrated that a BESS can lessen an overloading of 138% than that of without a BESS scenario.
- BESS demonstrates simultaneous capability in regulating its output to reduce transformer loading and PV smoothing coherently as required by the EVCS.
- BESS engages in B2G when the energy selling price (battery discharging) is above the purchasing price of recharging the battery to ensure profit.
- During B2G implementation, a larger capacity of battery (200kW) than the transformer's rated capacity (121kVA) can result in overloading of the

transformer. The proposed constraints effectively regulates BESS power output for B2G without resulting in an overloading of the transformer.

- During battery recharging, BESS only participates in recharging, if there is a spare capacity of transformer after feeding the EVCS load demand. This ensures transformer overloading, while battery recharging occurs.

Chapter 8

General Conclusions and Future Research Works

8.1 General Conclusions

This research thesis focuses on improving voltage and frequency stability with the growing penetration of renewable energy in the power system. The study presented in this thesis contributes to new knowledge in the modeling of BESS for regulating voltage and frequency in dynamic simulation studies of power system. In addition, the design of sectional droop control in wind turbine for frequency control in a MG and BESS in reducing transformer overloading in a charging station also contributes to the current knowledge. The detailed modeling of BESS, for the regulation of frequency is the initial stage of developing BESS model which is further modified according to the applications and design requirements in later stages to carry out dynamic simulation studies of power system.

In the beginning, combined inertia and sectional droop control coordinated with FLC based pitch controller are designed to perform frequency control in a MG. This combined design provided a valuable insight into the contribution of a wind turbine in dynamic frequency regulation. For example, the presented multi-gain droop control

implied that the frequency response of MG is greatly improved compared to the conventional droop gain method. Furthermore, to avoid the speedy acceleration and deceleration of wind turbine during low wind speed, the amount of power margin is adjusted to two different values according to the corresponding wind speed. This provided the flexibility of grid frequency to be regulated by the wind turbine without compromising the stability performance of MG. However, the capability of a wind turbine for participating in frequency regulation is merely dependent on available wind speed, which is inherently variable in nature. Hence, sole dependency on a wind turbine for frequency control will expose the grid to the risk of failure, if sufficient wind speed is not available and so alternative measure of reserved energy sources is in indispensable need in terms of maintaining the stability and security of the grid.

The pivotal control technique differs, depending on the particular application of BESS i.e. if frequency/voltage or both the voltage and frequency regulation is needed. Regardless of application types, the control design of voltage, frequency and charge controller remains unchanged. The fundamental difference is in designing PQ (active/reactive power) controller which varies according to its particular application. When BESS is intended to provide frequency support only, the voltage controller is disabled and reactive power regulation in PQ controller is set to zero. Through simulation studies, it is observed that with the increased penetration of low inertial wind energy, the capability of the electric power system for oscillation damping reduces significantly and frequency responses of generators violate the mandatory grid requirements. Simulation results with the incorporated BESS demonstrated that the designed BESS model whose intent was to provide frequency support greatly improved the oscillation damping of the system and satisfied grid conditions. The advantage of integrating BESS is that it reduced frequency deviation and stabilized the frequency responses at a faster rate than without a BESS demonstrating its potentiality in grid application.

On the contrary, when BESS is designed for voltage and frequency regulation, BESS converter capacity determines the amount of active and reactive power participation in regulation services. The reactive power was calculated from the remaining BESS

capacity once the active power is estimated for frequency regulation. The simulation studies show that with zero inertial PV system, the frequency responses violate mandatory grid conditions. The PSS provided a trivial contribution in enhancing grid responses but failed to provide adequate support that could satisfy mandatory grid code conditions. Nevertheless, BESS integrated system demonstrated better oscillation damping that fulfilled the grid requirements. Moreover, the reactive power regulation of BESS contributed to better control of grid voltage, which substantiates BESS potential in regulating simultaneous voltage and frequency. Furthermore, an original SOC recovery scheme is also presented in this study. It is observed that battery SOC can be easily restored to the desired level according to the plan of BESS operator without affecting the capacity of BESS during network events. The main benefit of the proposed SOC recovery strategy was that the operational flexibility could be achieved effortlessly by changing the value of charging current that provides added mobility of BESS regulation for various network conditions, operational planning and management.

In order to further determine BESS competency in regulating and enhancing voltage and frequency stability of the grid, the comparative performance of BESS and STATCOM is investigated in a large-scale power system which is an equivalent depiction of a real power system. The aim was to maintain the grid stability under various contingencies and improve the power transmission capacity of the grid. The performance of PI-lead and lead-lag regulated BESS controller was designed and compared with the conventional PI regulated BESS. The simulation studies exhibited that due to network fault and without any FACTS device, the grid responses accelerate over the time which leads to instability and subsequent grid failure. The STATCOM contributed in oscillation damping but by a fraction only and thus it was not able to diminish the growing oscillations of grid voltage and frequency. However, unlike STATCOM, BESS provided sufficient damping into the grid that was able to stabilize the grid voltage and frequency. So, it is validated that BESS has the superior capability in grid application than that of a STATCOM in terms of maximizing the capability of available power transmission capacity without affecting the grid stability performance. In addition, BESS performed remarkably regardless of the installed series capacitors between the two interconnected transmission lines. Moreover, it is also shown through

SSE analysis that PI-lead regulated BESS performed better than the traditional PI regulated BESS. However, SSE analysis concluded that lead-lag regulated BESS demonstrated the best outcome for all the studied contingencies.

Finally, a smart coordinated BESS and PV control is designed in an EV charging station mainly to minimize the overloading of the grid coupling transformer. The output power of BESS is designed to be regulated once the demand for EV charging load exceeds the rated transformer capacity. In addition, BESS output is also regulated to smooth out PV power beyond the specified threshold. Furthermore, as the battery capacity is higher than the transformer nominal rating, the battery recharging limit is regulated within the transformer capacity to avoid overloading. Also, BESS participated in B2G without overloading the coupling transformer as it is designed to participate in B2G within the maximum transformer capacity limit. Simulation results validated the effectiveness of BESS in achieving the expected outcome according to the design.

8.2 Future Research Works

The applicability of BESS has been illustrated in terms of dynamic voltage, frequency and power regulation in various power system and network operating conditions. It is observed that the regulation techniques of BESS power output have a significant impact on its performance and hence, there are ample scopes for further advancements in BESS control techniques in future research work. The following are the scope for research work in the area:

- The optimal tuning of BESS parameter is obvious in demonstrating a better performance of BESS in dynamic network conditions. In addition, the value of sectional droop parameters have a significant influence on the damping performance of a wind turbine for frequency control. Hence, an optimal parameter tuning of BESS and adaptive droop parameters need to be given careful attention which may provide a better regulation capability of BESS and wind turbine in a changing operating conditions.

- Considering the wide application of machine learning and artificial intelligent algorithms, these methods can further be integrated for regulating BESS. In view of multiple inputs as a set of conditions, artificial processing techniques can have an outstanding privilege over the traditional methods which can be a particular interest in future study.
- The size and placement of battery carry a great importance in terms of providing the necessary services while ensuring the maximum benefit of BESS usage. Therefore, optimization approaches such as stochastic, heuristic/meta-heuristic and evolutionary computing techniques can be adopted to determine the optimal size and placement of BESS installation for maximum techno-economic benefit.
- The power regulation of wind turbine for frequency control may result in a reduction in the net power output depending on the amount of power exchanges that will affect the financial gain. Hence, the techno-economic pay off of wind turbine for frequency control and the potential use of BESS for providing the same service within the economic constraints will get further attention. This may provide an influential insight into comparative techno-economic performance between individual BESS and wind farm or coordinated control for frequency regulation.
- In consideration of EV charging demand, real-time variable EV demand can be included in the coordinated control that imitates a more realistic approach. In addition, instead of a single charging station, this can further be coordinated with other charging stations that can provide added benefit to the distribution network operation and control. The voltage and frequency control can also be added in BESS design for network stability besides power control. EV can be designed and coordinated with BESS for frequency/voltage regulation (vehicle-to-grid). The price for B2G is considered to be always high that will attract BESS to participate in B2G. However, considering a real scenario, the real-time pricing can also be further included for regulating BESS in B2G operation.
- Although BESS provides rapid response to grid abnormalities and allows further integration of RESs, the high capital cost is one of the dominant factors towards

its prevalent implementation. Furthermore, BESS undergoes rapid charging and discharging while providing grid services over the BESS lifetime and this increases the impedance of battery cells and results in battery degradation. Therefore, the comparative analysis of economic advantage and technical benefit of using BESS for various grid services such as frequency and/or voltage control, balancing mechanism, etc. requires careful attention. To this aim, techno-economic assessment through optimization during grid service will get further attention in future study.

Appendix A

Frequency controller: deadband- 0.0004, droop setting: $R=0.001$

Voltage controller: deadband- 0.1, droop setting: $R=1$ P controller: $K_p=1$, $K_i=1$,
 $T_{ip}=0.04$, $y_{min}=i_{d-min}=i_{q-min}=-0.7pu$

Q controller: $K_p=0.25$, $K_i=0.25$, $T_{iq}=1$, $y_{max}=i_{d-max}=i_{q-max}=1pu$, current controller:
 $K_d=K_q=K_{id}=K_{iq}=1$, $T_d=T_q=0.01$

Battery parameter: Initial SOC=80%, capacity/Cell (Ah)=12, no. of parallel cell=20,
nominal voltage=0.9kV, $SOC_{min}=0.2$, $SOC_{max}=1$.

Appendix B1

PI controller: $T_p=0.01$, $T_q=0.02$, $K_d=K_q=1$, $T_{id}=4$, $T_{iq}=4$, $i_{d-max}=i_{q-max}=1$,
 $i_{d-min}=i_{q-min}=-1$.

PI-lead controller: $T_p=0.01$, $T_q=0.02$, $T_{b1}=T_{b2}=1$, $T_{a1}=T_{a2}=0.5$, $K_d=K_q=1$, $T_{id}=4$,
 $T_{iq}=4$, $i_{d-max}=1$, $i_{d-min}=i_{q-min}=-1$.

Lead-lag controller: $T=6$; $T_{z1}=1$, $T_{p1}=0.5$, $T_{z2}=4$, $T_{p2}=15$, $T_{z3}=1$, $T_{p3}=0.5$, $T_{z4}=4$,
 $T_{p4}=15$, $K_P=K_Q=5$, $i_{d-max}=i_{q-max}=1$, $i_{d-min}=i_{q-min}=-1$.

Appendix B2

Capacitor parameters:

Cap-Siirto-N= Cap-CN-NW=106 μF , Cap-NW-Siirto=114.83 μF , Cap-C-CN= Cap-C-
 CN-1=62.63 μF , Cap-CN-N=81.06 μF

Parameters of Network Power Flow:

Table B2.1 Load parameter

Load	MW	MVar	Load	MW	MVar
South-West	570	250	Central-South	485	150
South, South-East	570	250	Central-North	570	250
Central	428	0	North	135	50
Central-East	285	100	North-East	135	50
Central-West	428	150	North-West	285	50

Table B2.2 Generator active and reactive power parameters:

South-West	481	-137	Central-East	285	-210
South	570	-87	Central-North	570	-170
South-East	570	30	North	85	-144
Wind-S	200	0	North-East	85	-75
Wind-SE	100	0	Wind-NE	50	0
Central	428	-336	North-West	285	-184
Wind-C	100	0	Nordic N2	0	-163
Central-West	428	-144	Nordic N1	0	0
Wind-CW	50	0	Nordic C	0	0
Central-South	285	-251	Nordic S	0	-585

Appendix B3

Capacity/Cell-30 Ah, Empty cell minimum voltage-22 V, Full cell voltage-13.85 V, Cells in parallel-60, Cells in row-65, Nominal source voltage-0.9 kV, Resistance/cell-0.001 ohm.

References

- [1] M. T. Lawder, B. Suthar, P. W. C. Northrop, S. De, C. M. Hoff, O. Leitermann, M. L. Crow, S. Santhanagopalan, and V. R. Subramanian, “Battery energy storage system (BESS) and battery management system (BMS) for grid-scale applications,” *Proceedings of the IEEE*, vol. 102, pp. 1014–30, June 2014.
- [2] U. Datta, A. Kalam, and J. Shi, “Battery energy storage system for transient frequency stability enhancement of a large-scale power system,” in *2017 Australasian Universities Power Engineering Conference (AUPEC)*, pp. 1–5, Nov 2017.
- [3] C. Liang, P. Wang, X. Han, W. Qin, Y. Jia, and T. Yuan, “Battery energy storage selection based on a novel intermittent wind speed model for improving power system dynamic reliability,” *IEEE Transactions on Smart Grid*, vol. PP, no. 99, pp. 1–1, 2017.
- [4] S. A. Abdelrazek and S. Kamalasadnan, “Integrated PV capacity firming and energy time shift battery energy storage management using energy-oriented optimization,” *IEEE Transactions on Industry Applications*, vol. 52, pp. 2607–2617, May 2016.
- [5] S. J. Chiang, K. T. Chang, and C. Y. Yen, “Residential photovoltaic energy storage system,” *IEEE Transactions on Industrial Electronics*, vol. 45, pp. 385–94, Jun 1998.

- [6] S. Pourmousavi and T. K. Saha, "Evaluation of the battery operation in ramp-rate control mode within a PV plant: A case study," *Solar Energy*, vol. 166, pp. 242 – 254, 2018.
- [7] K. A. Joshi, N. M. Pindoriya, and A. K. Srivastava, "A two-stage fuzzy multiobjective optimization for phase-sensitive day-ahead dispatch of battery energy storage system," *IEEE Systems Journal*, vol. 12, pp. 3649–3660, Dec 2018.
- [8] F. Zhang, K. Meng, Z. Xu, Z. Dong, L. Zhang, C. Wan, and J. Liang, "Battery ess planning for wind smoothing via variable-interval reference modulation and self-adaptive soc control strategy," *IEEE Transactions on Sustainable Energy*, vol. 8, pp. 695–707, April 2017.
- [9] H. Beltran, E. Bilbao, E. Belenguer, I. Etxeberria-Otadui, and P. Rodriguez, "Evaluation of storage energy requirements for constant production in PV power plants," *IEEE Transactions on Industrial Electronics*, vol. 60, pp. 1225–34, March 2013.
- [10] N. Pearre and L. Swan, "Reimagining renewable electricity grid management with dispatchable generation to stabilize energy storage," *Energy*, vol. 203, p. 117917, 2020.
- [11] S. Impram, S. Varbak Nese, and B. Oral, "Challenges of renewable energy penetration on power system flexibility: A survey," *Energy Strategy Reviews*, vol. 31, p. 100539, 2020.
- [12] S. Sukumar, M. Marsadek, K. Agileswari, and H. Mokhlis, "Ramp-rate control smoothing methods to control output power fluctuations from solar photovoltaic (pv) sources—a review," *Journal of Energy Storage*, vol. 20, pp. 218 – 229, 2018.
- [13] D. Lamsal, V. Sreeram, Y. Mishra, and D. Kumar, "Output power smoothing control approaches for wind and photovoltaic generation systems: A review," *Renewable and Sustainable Energy Reviews*, vol. 113, p. 109245, 2019.
- [14] IEEE, "IEEE standard for interconnecting distributed resources with electric power systems," *IEEE Std 1547-2003*, pp. 1–28, July 2003.

- [15] E. Troester, “New German grid codes for connecting PV systems to the medium voltage power grid,” in *2nd International Workshop Concentrating Photovoltaic Power Plants: Optimal Design, Production, Grid Connection*, pp. 1–4, 2009.
- [16] Italian Authority for the Electricity Gas & Water, “Disposizioni in materia di dispacciamento delle fonti rinnovabili non programmabili a seguito della sentenza del consiglio di stato - sezione sesta - 9 giugno 2014, n. 2936,” [Accessed on 09.08.2017]. Available From: <http://www.autorita.energia.it/it/schedetecniche/14/522-14st.htm>.
- [17] Bundesministeriums Der Justiz Und Für Verbraucherschutz , “Gesetz für den ausbau erneuerbarer energien (erneuerbare-energien-gesetz e eeg 2014),” [Accessed on 09.08.2017]. Available From: http://www.gesetze-im-internet.de/eeg_2014/EEG_2017.pdf.
- [18] OFGEM, “Renewables Obligation (RO),” [Accessed on 09.08.2017]. Available From: <https://www.ofgem.gov.uk/environmental-programmes/ro>.
- [19] Y. Sun, Z. Li, M. Shahidehpour, and B. Ai, “Battery-based energy storage transportation for enhancing power system economics and security,” *IEEE Transactions on Smart Grid*, vol. 6, no. 5, pp. 2395–2402, 2015.
- [20] A. Atif and M. Khalid, “Savitzky–golay filtering for solar power smoothing and ramp rate reduction based on controlled battery energy storage,” *IEEE Access*, vol. 8, pp. 33806–33817, 2020.
- [21] G. J. May, A. Davidson, and B. Monahov, “Lead batteries for utility energy storage: A review,” *Journal of Energy Storage*, vol. 15, pp. 145 – 157, 2018.
- [22] M. M. Rahman, A. O. Oni, E. Gemechu, and A. Kumar, “Assessment of energy storage technologies: A review,” *Energy Conversion and Management*, vol. 223, p. 113295, 2020.
- [23] M. S. Guney and Y. Tepe, “Classification and assessment of energy storage systems,” *Renewable and Sustainable Energy Reviews*, vol. 75, pp. 1187 – 1197, 2017.

- [24] A. Jaiswal, "Lithium-ion battery based renewable energy solution for off-grid electricity: A techno-economic analysis," *Renewable and Sustainable Energy Reviews*, vol. 72, pp. 922 – 934, 2017.
- [25] X. Li and S. Wang, "A review on energy management, operation control and application methods for grid battery energy storage systems," *CSEE Journal of Power and Energy Systems*, pp. 1–15, 2019.
- [26] C. A. Hill, M. C. Such, D. Chen, J. Gonzalez, and W. M. Grady, "Battery energy storage for enabling integration of distributed solar power generation," *IEEE Transactions on Smart Grid*, vol. 3, pp. 850–7, June 2012.
- [27] P. V. Subramanyam and C. Vyjayanthi, "Integration of PV and battery system to the grid with power quality improvement features using bidirectional ac-dc converter," in *2016 International Conference on Electrical Power and Energy Systems (ICEPES)*, pp. 127–32, Dec 2016.
- [28] V. Monteiro, B. Exposto, J. G. Pinto, M. J. Sepúlveda, A. A. N. Meléndez, and J. L. Afonso, "Three-phase three-level current-source converter for EVs fast battery charging systems," in *2015 IEEE International Conference on Industrial Technology (ICIT)*, pp. 1401–6, 2015.
- [29] L. Barelli, G. Bidini, D. Pelosi, D. Ciupageanu, E. Cardelli, S. Castellini, and G. Lăzăroiu, "Comparative analysis of ac and dc bus configurations for flywheel-battery hess integration in residential micro-grids," *Energy*, vol. 204, p. 117939, 2020.
- [30] V. C. Ganti, B. Singh, S. K. Aggarwal, and T. C. Kandpal, "DFIG-based wind power conversion with grid power leveling for reduced gusts," *IEEE Transactions on Sustainable Energy*, vol. 3, pp. 12–20, Jan 2012.
- [31] P. J. dos Santos Neto, T. A. Barros, J. P. Silveira, E. Ruppert Filho, J. C. Vasquez, and J. M. Guerrero, "Power management techniques for grid-connected dc microgrids: A comparative evaluation," *Applied Energy*, vol. 269, p. 115057, 2020.

- [32] A. Esmaili, B. Novakovic, A. Nasiri, and O. Abdel-Baqi, "A hybrid system of li-ion capacitors and flow battery for dynamic wind energy support," *IEEE Transactions on Industry Applications*, vol. 49, pp. 1649–57, July 2013.
- [33] D. L. Yao, S. S. Choi, K. J. Tseng, and T. T. Lie, "Determination of short-term power dispatch schedule for a wind farm incorporated with dual-battery energy storage scheme," *IEEE Transactions on Sustainable Energy*, vol. 3, pp. 74–84, Jan 2012.
- [34] T. Wen, Z. Zhang, X. Lin, Z. Li, C. Chen, and Z. Wang, "Research on modeling and the operation strategy of a hydrogen-battery hybrid energy storage system for flexible wind farm grid-connection," *IEEE Access*, vol. 8, pp. 79347–79356, 2020.
- [35] A. S. Subburaj, S. B. Bayne, M. G. Giesselmann, and M. A. Harral, "Analysis of equivalent circuit of the utility scale battery for wind integration," *IEEE Transactions on Industry Applications*, vol. 52, pp. 25–33, Jan 2016.
- [36] R. Sebastián, "Application of a battery energy storage for frequency regulation and peak shaving in a wind diesel power system," *IET Generation, Transmission Distribution*, vol. 10, no. 3, pp. 764–70, 2016.
- [37] M. Jannati, S. H. Hosseinian, B. Vahidi, and G. J. Li, "Mitigation of windfarm power fluctuation by adaptive linear neuron-based power tracking method with flexible learning rate," *IET Renewable Power Generation*, vol. 8, pp. 659–69, August 2014.
- [38] B. Wang, G. Cai, and D. Yang, "Dispatching of a wind farm incorporated with dual-battery energy storage system using model predictive control," *IEEE Access*, vol. 8, pp. 144442–144452, 2020.
- [39] A. Chersin, W. Ongsakul, and J. Mitra, "Improving of uncertain power generation of rooftop solar PV using battery storage," in *2014 International Conference and Utility Exhibition on Green Energy for Sustainable Development (ICUE)*, pp. 1–4, March 2014.

- [40] G. Oriti, A. L. Julian, and N. J. Peck, "Power-electronics-based energy management system with storage," *IEEE Transactions on Power Electronics*, vol. 31, pp. 452–60, Jan 2016.
- [41] M. R. Aghamohammadi and H. Abdolahinia, "A new approach for optimal sizing of battery energy storage system for primary frequency control of islanded microgrid," *International Journal of Electrical Power and Energy Systems*, vol. 54, pp. 325 – 333, 2014.
- [42] K. V. Iyer and N. Mohan, "Modulation and commutation of a single stage isolated asymmetrical multilevel converter for the integration of renewables and battery energy storage system in ships," *IEEE Transactions on Transportation Electrification*, vol. 2, pp. 580–596, Dec 2016.
- [43] J. D. Boles, Y. Ma, J. Wang, D. Osipov, L. M. Tolbert, and F. Wang, "Converter-based emulation of battery energy storage systems (bess) for grid applications," *IEEE Transactions on Industry Applications*, vol. 55, pp. 4020–4032, July 2019.
- [44] V. Karthikeyan and R. Gupta, "Varying phase angle control in isolated bidirectional dc–dc converter for integrating battery storage and solar PV system in standalone mode," *IET Power Electronics*, vol. 10, no. 4, pp. 471–479, 2017.
- [45] E. Chatzinikolaou and D. J. Rogers, "A comparison of grid-connected battery energy storage system designs," *IEEE Transactions on Power Electronics*, vol. 32, pp. 6913–6923, Sep. 2017.
- [46] G. Wang, G. Konstantinou, C. D. Townsend, J. Pou, S. Vazquez, G. D. Demetriades, and V. G. Agelidis, "A review of power electronics for grid connection of utility-scale battery energy storage systems," *IEEE Transactions on Sustainable Energy*, vol. 7, pp. 1778–1790, Oct 2016.
- [47] P. D. Judge and T. C. Green, "Modular multilevel converter with partially rated integrated energy storage suitable for frequency support and ancillary service provision," *IEEE Transactions on Power Delivery*, vol. 34, pp. 208–219, Feb 2019.

- [48] U. Datta, A. Kalam, and J. Shi, "Battery energy storage system control for mitigating PV penetration impact on primary frequency control and state-of-charge recovery," *IEEE Transactions on Sustainable Energy*, pp. 1–1, 2019.
- [49] M. Gholizadeh and F. R. Salmasi, "Estimation of state of charge, unknown nonlinearities, and state of health of a lithium-ion battery based on a comprehensive unobservable model," *IEEE Transactions on Industrial Electronics*, vol. 61, pp. 1335–1344, March 2014.
- [50] B. Xiao, Y. Liu, and B. Xiao, "Accurate state-of-charge estimation approach for lithium-ion batteries by gated recurrent unit with ensemble optimizer," *IEEE Access*, vol. 7, pp. 54192–54202, 2019.
- [51] X. Hu, H. Yuan, C. Zou, Z. Li, and L. Zhang, "Co-estimation of state of charge and state of health for lithium-ion batteries based on fractional-order calculus," *IEEE Transactions on Vehicular Technology*, vol. 67, pp. 10319–10329, Nov 2018.
- [52] C. Zhang, K. Li, J. Deng, and S. Song, "Improved realtime state-of-charge estimation of $LiFePO_4$ battery based on a novel thermoelectric model," *IEEE Transactions on Industrial Electronics*, vol. 64, pp. 654–663, Jan 2017.
- [53] J. Shen, J. Shen, Y. He, and Z. Ma, "Accurate state of charge estimation with model mismatch for li-ion batteries: A joint moving horizon estimation approach," *IEEE Transactions on Power Electronics*, vol. 34, pp. 4329–4342, May 2019.
- [54] S. Peng, C. Chen, H. Shi, and Z. Yao, "State of charge estimation of battery energy storage systems based on adaptive unscented kalman filter with a noise statistics estimator," *IEEE Access*, vol. 5, pp. 13202–13212, 2017.
- [55] H. Chaoui, N. Golbon, I. Hmouz, R. Souissi, and S. Tahar, "Lyapunov-based adaptive state of charge and state of health estimation for lithium-ion batteries," *IEEE Transactions on Industrial Electronics*, vol. 62, pp. 1610–1618, March 2015.
- [56] P. Shen, M. Ouyang, X. Han, X. Feng, L. Lu, and J. Li, "Error analysis of the model-based state-of-charge observer for lithium-ion batteries," *IEEE Transactions on Vehicular Technology*, vol. 67, pp. 8055–8064, Sep. 2018.

- [57] F. R. McLarnon and E. J. Cairns, “Energy storage,” *Annual Review of Energy*, vol. 14, pp. 241–71, November 1989.
- [58] J. N. Baker and A. Collinson, “Electrical energy storage at the turn of the millennium,” *Power Engineering Journal*, vol. 13, pp. 107–12, June 1999.
- [59] P. F. Ribeiro, B. K. Johnson, M. L. Crow, A. Arsoy, and Y. Liu, “Energy storage systems for advanced power applications,” *Proceedings of the IEEE*, vol. 89, pp. 1744–56, Dec 2001.
- [60] B. Dunn, H. Kamath, and J.-M. Tarascon, “Electrical energy storage for the grid: A battery of choices,” *Science*, vol. 334, no. 6058, pp. 928–35, 2011.
- [61] J. Baker, “New technology and possible advances in energy storage,” *Energy Policy*, vol. 36, no. 12, pp. 4368 – 73, 2008.
- [62] H. Chen, T. N. Cong, W. Yang, C. Tan, Y. Li, and Y. Ding, “Progress in electrical energy storage system: A critical review,” *Progress in Natural Science*, vol. 19, no. 3, pp. 291 – 312, 2009.
- [63] D. Linden and T. B. Reddy, *Handbook of Batteries*. McGraw-Hill, 3rd ed., 2001.
- [64] H. Zhao, Q. Wu, S. Hu, H. Xu, and C. N. Rasmussen, “Review of energy storage system for wind power integration support,” *Applied Energy*, vol. 137, pp. 545 – 53, 2015.
- [65] K. Divya and J. Østergaard, “Battery energy storage technology for power systems—an overview,” *Electric Power Systems Research*, vol. 79, no. 4, pp. 511 – 20, 2009.
- [66] A. Poullikkas, “A comparative overview of large-scale battery systems for electricity storage,” *Renewable and Sustainable Energy Reviews*, vol. 27, pp. 778 – 88, 2013.
- [67] J. Leadbetter and L. G. Swan, “Selection of battery technology to support grid-integrated renewable electricity,” *Journal of Power Sources*, vol. 216, pp. 376 – 86, 2012.

- [68] D. Akinyele and R. Rayudu, "Review of energy storage technologies for sustainable power networks," *Sustainable Energy Technologies and Assessments*, vol. 8, pp. 74 – 91, 2014.
- [69] D. Berndt, "Valve-regulated lead-acid batteries," *Journal of Power Sources*, vol. 100, no. 1, pp. 29 – 46, 2001.
- [70] M. S. Whittingham, "History, evolution, and future status of energy storage," *Proceedings of the IEEE*, vol. 100, pp. 1518–34, May 2012.
- [71] Energy Storage Association, "Lithium ion (li-ion) batteries," [Accessed on 06.07.2017]. Available From: <http://energystorage.org/energy-storage/technologies/lithium-ion-li-ion-batteries>.
- [72] A. Andersson and J. Thomas, "The source of first-cycle capacity loss in lifepo4," *Journal of Power Sources*, vol. 97, pp. 498 – 502, 2001.
- [73] M. Yoshio, R. J. Brodd, and A. Kozawa, *Lithium-Ion Batteries*. Springer Science+Business Media, 2009.
- [74] A. Yamada, S.-C. Chung, and K. Hinokuma, "Optimized lifepo4 for lithium battery cathodes," *Journal of the Electrochemical Society*, vol. 148, no. 3, pp. A224–9, 2001.
- [75] J. M. Tarascon and M. Armand, "Issues and challenges facing rechargeable lithium batteries," *Nature*, vol. 414, no. 6861, pp. 359–67, 2001.
- [76] M. Ceylan, T. Sarıkurt, and A. Balıkçı, "A novel lithium-ion-polymer battery model for hybrid/electric vehicles," in *2014 IEEE 23rd International Symposium on Industrial Electronics (ISIE)*, pp. 366–9, June 2014.
- [77] S. Vazquez, S. M. Lukic, E. Galvan, L. G. Franquelo, and J. M. Carrasco, "Energy storage systems for transport and grid applications," *IEEE Transactions on Industrial Electronics*, vol. 57, pp. 3881–95, Dec 2010.
- [78] W. A. Omran, M. Kazerani, and M. M. A. Salama, "Investigation of methods for reduction of power fluctuations generated from large grid-connected photovoltaic

- systems,” *IEEE Transactions on Energy Conversion*, vol. 26, pp. 318–27, March 2011.
- [79] A. K. Barnes, J. C. Balda, S. O. Geurin, and A. Escobar-Mejía, “Optimal battery chemistry, capacity selection, charge/discharge schedule, and lifetime of energy storage under time-of-use pricing,” in *2011 2nd IEEE PES International Conference and Exhibition on Innovative Smart Grid Technologies*, pp. 1–7, Dec 2011.
- [80] J. Tarabay and N. Karami, “Nickel metal hydride battery: Structure, chemical reaction, and circuit model,” in *2015 Third International Conference on Technological Advances in Electrical, Electronics and Computer Engineering (TAECE)*, pp. 22–6, April 2015.
- [81] EOS Energy Storage, “Novel znyth®(zinc hybrid cathode) battery technology,” [Accessed on 20.07.2017]. Available From: <https://eosenergystorage.com/about-eos/>.
- [82] A. Colthorpe, “Energy to test EOS zinc battery to ‘operational boundaries’ in brazil,” [Accessed on 20.07.2017]. Available From: <https://www.energy-storage.news/news/engie-to-test-eos-zinc-battery-to-operational-boundaries-in-brazil>.
- [83] J. Yan, J. Wang, H. Liu, Z. Bakenov, D. Gosselink, and P. Chen, “Rechargeable hybrid aqueous batteries,” *Journal of Power Sources*, vol. 216, pp. 222 – 226, 2012.
- [84] Energy Storage Association (ESA), “Vanadium redox (VRB) flow batteries,” [Accessed on 04.08.2017]. Available From: <http://energystorage.org/energy-storage/technologies/vanadium-redox-vrb-flow-batteries>.
- [85] A. Weber, M. M. Mench, J. P. Meyers, P. N. Ross, J. T. Gostick, and Q. Liu, “Redox flow batteries: a review,” *Journal of Applied Electrochemistry*, vol. 41, pp. 1137–64, Sep 2011.

- [86] EPRI-DOE, “Handbook of Energy Storage for Transmission & Distribution Applications, epri, Palo Alto, CA, and the U.S. Department of Energy, Washington, DC,” 2003.
- [87] H. Zhou, H. Zhang, P. Zhao, and B. Yi, “A comparative study of carbon felt and activated carbon based electrodes for sodium polysulfide/bromine redox flow battery,” *Electrochimica Acta*, vol. 51, no. 28, pp. 6304 – 6312, 2006.
- [88] H. Bayat and A. Yazdani, “A hybrid mmc-based photovoltaic and battery energy storage system,” *IEEE Power and Energy Technology Systems Journal*, vol. 6, pp. 32–40, March 2019.
- [89] M. C. Di Piazza, M. Luna, G. La Tona, and A. Di Piazza, “Improving grid integration of hybrid PV-storage systems through a suitable energy management strategy,” *IEEE Transactions on Industry Applications*, vol. 55, pp. 60–68, Jan 2019.
- [90] C. K. Nayak, M. R. Nayak, and R. Behera, “Simple moving average based capacity optimization for vrla battery in PV power smoothing application using mctlbo,” *Journal of Energy Storage*, vol. 17, pp. 20 – 28, 2018.
- [91] S. Sukumar, H. Mokhlis, S. Mekhilef, M. Karimi, and S. Raza, “Ramp-rate control approach based on dynamic smoothing parameter to mitigate solar PV output fluctuations,” *International Journal of Electrical Power & Energy Systems*, vol. 96, pp. 296 – 305, 2018.
- [92] Y. Zhou, Z. Yan, and N. Li, “A novel state of charge feedback strategy in wind power smoothing based on short-term forecast and scenario analysis,” *IEEE Transactions on Sustainable Energy*, vol. 8, pp. 870–879, April 2017.
- [93] A. V. Savkin, M. Khalid, and V. G. Agelidis, “A constrained monotonic charging/discharging strategy for optimal capacity of battery energy storage supporting wind farms,” *IEEE Transactions on Sustainable Energy*, vol. 7, pp. 1224–1231, July 2016.

- [94] D. Lamsal, V. Sreeram, Y. Mishra, and D. Kumar, "Kalman filter approach for dispatching and attenuating the power fluctuation of wind and photovoltaic power generating systems," *IET Generation, Transmission Distribution*, vol. 12, no. 7, pp. 1501–1508, 2018.
- [95] D. Lamsal, V. Sreeram, Y. Mishra, and D. Kumar, "Smoothing control strategy of wind and photovoltaic output power fluctuation by considering the state of health of battery energy storage system," *IET Renewable Power Generation*, vol. 13, no. 4, pp. 578–586, 2019.
- [96] X. Li, D. Hui, and X. Lai, "Battery energy storage station (BESS)-based smoothing control of photovoltaic (PV) and wind power generation fluctuations," *IEEE Transactions on Sustainable Energy*, vol. 4, pp. 464–73, April 2013.
- [97] S. Chapaloglou, A. Nesiadis, P. Iliadis, K. Atsonios, N. Nikolopoulos, P. Grammelis, C. Yiakopoulos, I. Antoniadis, and E. Kakaras, "Smart energy management algorithm for load smoothing and peak shaving based on load forecasting of an island's power system," *Applied Energy*, vol. 238, pp. 627 – 642, 2019.
- [98] A. J. Pimm, T. T. Cockerill, and P. G. Taylor, "The potential for peak shaving on low voltage distribution networks using electricity storage," *Journal of Energy Storage*, vol. 16, pp. 231 – 242, 2018.
- [99] E. Reihani, M. Motalleb, R. Ghorbani, and L. S. Saoud, "Load peak shaving and power smoothing of a distribution grid with high renewable energy penetration," *Renewable Energy*, vol. 86, pp. 1372 – 1379, 2016.
- [100] S. Lakshmi and S. Ganguly, "Multi-objective planning for the allocation of PV-BESS integrated open upqc for peak load shaving of radial distribution networks," *Journal of Energy Storage*, vol. 22, pp. 208 – 218, 2019.
- [101] Z. Taylor, H. Akhavan-Hejazi, E. Cortez, L. Alvarez, S. Ula, M. Barth, and H. Mohsenian-Rad, "Customer-side scada-assisted large battery operation optimization for distribution feeder peak load shaving," *IEEE Transactions on Smart Grid*, vol. 10, pp. 992–1004, Jan 2019.

- [102] Y. Shi, B. Xu, D. Wang, and B. Zhang, "Using battery storage for peak shaving and frequency regulation: Joint optimization for superlinear gains," *IEEE Transactions on Power Systems*, vol. 33, pp. 2882–2894, May 2018.
- [103] T. Aziz and N. Ketjoy, "PV penetration limits in low voltage networks and voltage variations," *IEEE Access*, vol. 5, pp. 16784–16792, 2017.
- [104] S. Alyami, Y. Wang, C. Wang, J. Zhao, and B. Zhao, "Adaptive real power capping method for fair overvoltage regulation of distribution networks with high penetration of PV systems," *IEEE Transactions on Smart Grid*, vol. 5, pp. 2729–38, Nov 2014.
- [105] A. Samadi, R. Eriksson, L. Söder, B. G. Rawn, and J. C. Boemer, "Coordinated active power-dependent voltage regulation in distribution grids with PV systems," *IEEE Transactions on Power Delivery*, vol. 29, pp. 1454–64, June 2014.
- [106] M. Chamana and B. H. Chowdhury, "Optimal voltage regulation of distribution networks with cascaded voltage regulators in the presence of high PV penetration," *IEEE Transactions on Sustainable Energy*, vol. 9, pp. 1427–1436, July 2018.
- [107] M. Todorovski, "Transformer voltage regulation-compact expression dependent on tap position and primary/secondary voltage," *IEEE Transactions on Power Delivery*, vol. 29, pp. 1516–7, June 2014.
- [108] R. A. Shayani and M. A. G. D. Oliveira, "Photovoltaic generation penetration limits in radial distribution systems," *IEEE Transactions on Power Systems*, vol. 26, pp. 1625–31, Aug 2011.
- [109] M. Zeraati, M. E. Hamedani Golshan, and J. M. Guerrero, "Distributed control of battery energy storage systems for voltage regulation in distribution networks with high PV penetration," *IEEE Transactions on Smart Grid*, vol. 9, pp. 3582–3593, July 2018.
- [110] E. L. Ratnam and S. R. Weller, "Receding horizon optimization-based approaches to managing supply voltages and power flows in a distribution grid with battery

- storage co-located with solar PV,” *Applied Energy*, vol. 210, pp. 1017 – 1026, 2018.
- [111] J. Krata and T. K. Saha, “Real-time coordinated voltage support with battery energy storage in a distribution grid equipped with medium-scale PV generation,” *IEEE Transactions on Smart Grid*, vol. 10, pp. 3486–3497, May 2019.
- [112] O. B. Adewuyi, R. Shigenobu, T. Senjyu, M. E. Lotfy, and A. M. Howlader, “Multiobjective mix generation planning considering utility-scale solar pv system and voltage stability: Nigerian case study,” *Electric Power Systems Research*, vol. 168, pp. 269 – 282, 2019.
- [113] X. Liu, A. Aichhorn, L. Liu, and H. Li, “Coordinated control of distributed energy storage system with tap changer transformers for voltage rise mitigation under high photovoltaic penetration,” *IEEE Transactions on Smart Grid*, vol. 3, pp. 897–906, June 2012.
- [114] G. M. Tina, D. Garozzo, and P. Siano, “Scheduling of pv inverter reactive power set-point and battery charge/discharge profile for voltage regulation in low voltage networks,” *International Journal of Electrical Power & Energy Systems*, vol. 107, pp. 131 – 139, 2019.
- [115] L. Wang, F. Bai, R. Yan, and T. K. Saha, “Real-time coordinated voltage control of PV inverters and energy storage for weak networks with high PV penetration,” *IEEE Transactions on Power Systems*, vol. 33, pp. 3383–3395, May 2018.
- [116] C. Wang, L. Yang, Y. Wang, Z. Meng, W. Li, and F. Han, “Circuit configuration and control of a grid-tie small-scale wind generation system for expanded wind speed range,” *IEEE Transactions on Power Electronics*, vol. 32, pp. 5227–5247, July 2017.
- [117] S. W. Mohod, S. M. Hatwar, and M. V. Aware, “Grid support with variable speed wind energy system and battery storage for power quality,” *Energy Procedia*, vol. 12, pp. 1032 – 41, 2011.

- [118] L. Wu, H. Liu, K. Bai, and Z. Cui, "A coordinated control strategy of active power and voltage for large scale wind-storage combined generation system," in *2016 International Conference on Condition Monitoring and Diagnosis (CMD)*, pp. 811–4, Sept 2016.
- [119] V. Khadkikar, R. K. Varma, and R. Seethapathy, "Grid voltage regulation utilizing storage batteries in PV solar-wind plant based distributed generation system," in *2009 IEEE Electrical Power Energy Conference (EPEC)*, pp. 1–6, Oct 2009.
- [120] K. Khalid Mehmood, S. U. Khan, S. Lee, Z. M. Haider, M. K. Rafique, and C. Kim, "Optimal sizing and allocation of battery energy storage systems with wind and solar power dgs in a distribution network for voltage regulation considering the lifespan of batteries," *IET Renewable Power Generation*, vol. 11, no. 10, pp. 1305–1315, 2017.
- [121] S. I. Nanou, A. G. Papakonstantinou, and S. A. Papathanassiou, "A generic model of two-stage grid-connected PV systems with primary frequency response and inertia emulation," *Electric Power Systems Research*, vol. 127, pp. 186 – 196, 2015.
- [122] V. A. K. Pappu, B. Chowdhury, and R. Bhatt, "Implementing frequency regulation capability in a solar photovoltaic power plant," in *North American Power Symposium 2010*, pp. 1–6, Sep 2010.
- [123] E. Bullich-Massagué, M. Aragüés-Peñalba, A. Sumper, and O. Boix-Aragones, "Active power control in a hybrid pv-storage power plant for frequency support," *Solar Energy*, vol. 144, pp. 49 – 62, 2017.
- [124] H. Mahmood and J. Jiang, "Decentralized power management of multiple PV, battery, and droop units in an islanded microgrid," *IEEE Transactions on Smart Grid*, vol. 10, pp. 1898–1906, March 2019.
- [125] J. Engels, B. Claessens, and G. Deconinck, "Combined stochastic optimization of frequency control and self-consumption with a battery," *IEEE Transactions on Smart Grid*, vol. 10, pp. 1971–1981, March 2019.

- [126] M. F. M. Arani and E. F. El-Saadany, "Implementing virtual inertia in dfig-based wind power generation," *IEEE Transactions on Power Systems*, vol. 28, pp. 1373–1384, May 2013.
- [127] F. Wilches-Bernal, J. H. Chow, and J. J. Sanchez-Gasca, "A fundamental study of applying wind turbines for power system frequency control," *IEEE Transactions on Power Systems*, vol. 31, pp. 1496–505, March 2016.
- [128] A. M. Howlader, Y. Izumi, A. Uehara, N. Urasaki, T. Senjyu, and A. Y. Saber, "A robust h_{∞} controller based frequency control approach using the wind-battery coordination strategy in a small power system," *International Journal of Electrical Power & Energy Systems*, vol. 58, pp. 190 – 8, 2014.
- [129] R. Sebastián and R. P. Alzola, "Effective active power control of a high penetration wind diesel system with a ni–cd battery energy storage," *Renewable Energy*, vol. 35, no. 5, pp. 952 – 65, 2010.
- [130] Z. Wu, D. W. Gao, H. Zhang, S. Yan, and X. Wang, "Coordinated control strategy of battery energy storage system and PMSG-WTG to enhance system frequency regulation capability," *IEEE Transactions on Sustainable Energy*, vol. 8, pp. 1330–43, July 2017.
- [131] J. Tan and Y. Zhang, "Coordinated control strategy of a battery energy storage system to support a wind power plant providing multi-timescale frequency ancillary services," *IEEE Transactions on Sustainable Energy*, vol. 8, pp. 1140–1153, July 2017.
- [132] B. Peng, F. Zhang, J. Liang, L. Ding, Z. Liang, and Q. Wu, "Coordinated control strategy for the short-term frequency response of a dfig-es system based on wind speed zone classification and fuzzy logic control," *International Journal of Electrical Power & Energy Systems*, vol. 107, pp. 363 – 378, 2019.
- [133] G. He, Q. Chen, C. Kang, Q. Xia, and K. Poolla, "Cooperation of wind power and battery storage to provide frequency regulation in power markets," *IEEE Transactions on Power Systems*, vol. 32, pp. 3559–3568, Sep. 2017.

- [134] C. Wang, Y. Mi, Y. Fu, and P. Wang, "Frequency control of an isolated microgrid using double sliding mode controllers and disturbance observer," *IEEE Transactions on Smart Grid*, vol. 9, pp. 923–930, March 2018.
- [135] S. Acharya, M. S. E. Moursi, and A. Al-Hinai, "Coordinated frequency control strategy for an islanded microgrid with demand side management capability," *IEEE Transactions on Energy Conversion*, vol. 33, pp. 639–651, June 2018.
- [136] J. W. Shim, G. Verbič, N. Zhang, and K. Hur, "Harmonious integration of faster-acting energy storage systems into frequency control reserves in power grid with high renewable generation," *IEEE Transactions on Power Systems*, vol. 33, pp. 6193–6205, Nov 2018.
- [137] R. Bhatt and B. Chowdhury, "Grid frequency and voltage support using PV systems with energy storage," in *2011 North American Power Symposium*, pp. 1–6, Aug 2011.
- [138] F. Abusief, R. Caldon, and F. Bignucolo, "Remote islanded distribution networks supplied by BESS integrated PV generation units," in *2016 IEEE 16th International Conference on Environment and Electrical Engineering (EEEIC)*, pp. 1–6, June 2016.
- [139] S. Pati, K. B. Mohanty, S. K. Kar, and D. Panda, "Voltage and frequency stabilization of a micro hydro-PV based hybrid micro grid using STATCOM equipped with battery energy storage system," in *2016 IEEE International Conference on Power Electronics, Drives and Energy Systems (PEDES)*, pp. 1–5, Dec 2016.
- [140] R. Hemmati, N. Azizi, M. Shafie-khah, and J. P. Catalão, "Decentralized frequency-voltage control and stability enhancement of standalone wind turbine-load-battery," *International Journal of Electrical Power & Energy Systems*, vol. 102, pp. 1 – 10, 2018.
- [141] K. Li, H. Xu, Q. Ma, and J. Zhao, "Hierarchy control of power quality for wind - battery energy storage system," *IET Power Electronics*, vol. 7, pp. 2123–32, August 2014.

- [142] L. K. Gan and E. J. P. E. Subiabre, "A realistic laboratory development of an isolated wind-battery system," *Renewable Energy*, vol. 136, pp. 645 – 656, 2019.
- [143] N. Mendis, K. M. Muttaqi, S. Sayeef, and S. Perera, "A control approach for voltage and frequency regulation of a wind-diesel-battery based hybrid remote area power supply system," in *IECON 2010 - 36th Annual Conference on IEEE Industrial Electronics Society*, pp. 3054–60, Nov 2010.
- [144] F. Asghar, M. Talha, and S. Kim, "Robust frequency and voltage stability control strategy for standalone AC/DC hybrid microgrid," *Energies*, vol. 10, no. 6, pp. 760–80, 2017.
- [145] Y. Kim, E. Kim, and S. Moon, "Frequency and voltage control strategy of standalone microgrids with high penetration of intermittent renewable generation systems," *IEEE Transactions on Power Systems*, vol. 31, pp. 718–728, Jan 2016.
- [146] S. A. M. Al-Barazanchi and A. M. Vural, "Modeling and intelligent control of a stand-alone PV-wind-diesel-battery hybrid system," in *2015 International Conference on Control, Instrumentation, Communication and Computational Technologies (ICCICCT)*, pp. 423–30, Dec 2015.
- [147] M. Delfanti, D. Falabretti, and M. Merlo, "Energy storage for PV power plant dispatching," *Renewable Energy*, vol. 80, pp. 61 – 72, 2015.
- [148] California Legislative information, "California assembly bill 2514," [Accessed on 04.08.2017]. Available From: http://leginfo.legislature.ca.gov/faces/billNavClient.xhtml?bill_id=200920100AB2514.
- [149] OFGEM, "California assembly bill 2514," [Accessed on 04.08.2017]. Available From: <https://www.ofgem.gov.uk/electricity/distribution-networks/network-innovation/low-carbon-networks-fund>.
- [150] Authority for the Electricity Gas Water Italian, "Resolution 288/12/r/eel. procedura e criteri di selezione dei progetti pilota relativi a sistemi di accumulo ammessi al trattamento incentivante," [Accessed on 04.08.2017]. Available From: <http://www.autorita.energia.it/it/docs/12/288-12.htm#>.

- [151] M. Brenna, F. Foiadelli, M. Longo, and D. Zaninelli, “Energy storage control for dispatching photovoltaic power,” *IEEE Transactions on Smart Grid*, vol. 9, pp. 2419–2428, July 2018.
- [152] F. Luo, K. Meng, Z. Y. Dong, Y. Zheng, Y. Chen, and K. P. Wong, “Coordinated operational planning for wind farm with battery energy storage system,” *IEEE Transactions on Sustainable Energy*, vol. 6, pp. 253–62, Jan 2015.
- [153] C. Nguyen and H. Lee, “A novel dual-battery energy storage system for wind power applications,” *IEEE Transactions on Industrial Electronics*, vol. 63, pp. 6136–6147, Oct 2016.
- [154] P. Kou, D. Liang, F. Gao, and L. Gao, “Coordinated predictive control of DFIG-based wind-battery hybrid systems: Using non-Gaussian wind power predictive distributions,” *IEEE Transactions on Energy Conversion*, vol. 30, pp. 681–95, June 2015.
- [155] X. Dui, G. Zhu, and L. Yao, “Two-stage optimization of battery energy storage capacity to decrease wind power curtailment in grid-connected wind farms,” *IEEE Transactions on Power Systems*, vol. 33, pp. 3296–3305, May 2018.
- [156] R. Zhang, T. Jiang, L. Bai, G. Li, H. Chen, X. Li, and F. Li, “Adjustable robust power dispatch with combined wind-storage system and carbon capture power plants under low-carbon economy,” *International Journal of Electrical Power & Energy Systems*, vol. 113, pp. 772 – 781, 2019.
- [157] Z. Cai, C. Bussar, P. Stöcker, L. Moraes, D. Magnor, and D. U. Sauer, “Optimal dispatch scheduling of a wind-battery-system in German power market,” *Energy Procedia*, vol. 99, pp. 137 – 46, 2016.
- [158] C. Nguyen and H. Lee, “Power management approach to minimize battery capacity in wind energy conversion systems,” *IEEE Transactions on Industry Applications*, vol. 53, pp. 4843–4854, Sep. 2017.

- [159] S. Tarca, M. Roughan, N. Ertugrul, and N. Bean, “Dispatchability of wind power with battery energy storage in south Australia,” *Energy Procedia*, vol. 110, pp. 223 – 8, 2017.
- [160] Q. Tan, S. Mei, Q. Ye, Y. Ding, and Y. Zhang, “Optimization model of a combined wind–pv–thermal dispatching system under carbon emissions trading in china,” *Journal of Cleaner Production*, vol. 225, pp. 391 – 404, 2019.
- [161] X. Wang, M. Yue, and E. Muljadi, “Modeling and control system design for an integrated solar generation and energy storage system with a ride-through capability,” in *2012 IEEE Energy Conversion Congress and Exposition (ECCE)*, pp. 3727–34, Sept 2012.
- [162] B. Manikanta, G. Kesavarao, and S. Talati, “LVRT of grid connected PV system with energy storage,” *International Science Press*, vol. 10, no. 5, pp. 75–86, 2017.
- [163] X. Fu, P. Wang, S. Zhang, X. Han, W. Qin, and Y. Jia, “Coordinated control strategy for improving fault ride-through performance of photovoltaic/battery microgrid,” in *2016 IEEE 11th Conference on Industrial Electronics and Applications (ICIEA)*, pp. 388–93, June 2016.
- [164] R. Sarrias-Mena, L. M. Fernández-Ramírez, C. A. García-Vázquez, and F. Jurado, “Improving grid integration of wind turbines by using secondary batteries,” *Renewable and Sustainable Energy Reviews*, vol. 34, pp. 194 – 207, 2014.
- [165] W. Guo, L. Xiao, and S. Dai, “Fault current limiter-battery energy storage system for the doubly-fed induction generator: analysis and experimental verification,” *IET Generation, Transmission Distribution*, vol. 10, no. 3, pp. 653–660, 2016.
- [166] R. Chen, J. Chen, J. Lei, C. Fu, K. Wang, W. Duan, X. Dong, and G. Cai, “System stability and its influencing factors analysis of the isolated wind-solar-diesel- battery hybrid micro-grid,” in *2012 China International Conference on Electricity Distribution*, pp. 1–4, Sept 2012.
- [167] GWEC, “Global Wind Report 2017, [Available Online]: <http://gwec.net/publications/global-wind-report-2/>, [Accessed on: 2018-10-25].”

- [168] Y. Li, S. S. Choi, C. Yang, and F. Wei, "Design of variable-speed dish-stirling solar-thermal power plant for maximum energy harness," *IEEE Transactions on Energy Conversion*, vol. 30, pp. 394–403, March 2015.
- [169] M. Azzouz, A. . Elshafei, and H. Emara, "Evaluation of fuzzy-based maximum power-tracking in wind energy conversion systems," *IET Renewable Power Generation*, vol. 5, pp. 422–430, November 2011.
- [170] IESO, "Market Manual 2: Market Administration; Part 2.20: Performance Validation, [Available Online]:<http://www.ieso.ca/sector%20participants/market%20operations/-/media/84d0f4687ace4588ae13022aa29e31f7.ashx>, [Accessed on: 2019-03-14]."
- [171] Energinet, "Wind turbines connected to grids with voltages below 100 kV, [Available Online]:<https://en.energinet.dk/-/media/1196ee254b854d21ad88b2dc813bfea9.pdf?la=en&hash=acf6dbc39fef7340e206e48be4845941519cae97>, [Accessed on: 2019-03-14]."
- [172] Y. Zhang, A. M. Melin, S. M. Djouadi, M. M. Olama, and K. Tomsovic, "Provision for guaranteed inertial response in diesel-wind systems via model reference control," *IEEE Transactions on Power Systems*, vol. 33, pp. 6557–6568, Nov 2018.
- [173] F. Liu, Z. Liu, S. Mei, W. Wei, and Y. Yao, "Eso-based inertia emulation and rotor speed recovery control for DFIGs," *IEEE Transactions on Energy Conversion*, vol. 32, pp. 1209–1219, Sept 2017.
- [174] V. Gevorgian, Y. Zhang, and E. Ela, "Investigating the impacts of wind generation participation in interconnection frequency response," *IEEE Transactions on Sustainable Energy*, vol. 6, pp. 1004–1012, July 2015.
- [175] J. V. de Vyver, J. D. M. D. Kooning, B. Meersman, L. Vandeveldel, and T. L. Vandoorn, "Droop control as an alternative inertial response strategy for the synthetic inertia on wind turbines," *IEEE Transactions on Power Systems*, vol. 31, pp. 1129–1138, March 2016.

- [176] I. D. Margaritis, S. A. Papathanassiou, N. D. Hatziargyriou, A. D. Hansen, and P. Sorensen, "Frequency control in autonomous power systems with high wind power penetration," *IEEE Transactions on Sustainable Energy*, vol. 3, pp. 189–199, April 2012.
- [177] Z. Wang and W. Wu, "Coordinated control method for DFIG-based wind farm to provide primary frequency regulation service," *IEEE Transactions on Power Systems*, vol. 33, pp. 2644–2659, May 2018.
- [178] D. Ochoa and S. Martinez, "Fast-frequency response provided by DFIG-wind turbines and its impact on the grid," *IEEE Transactions on Power Systems*, vol. 32, pp. 4002–4011, Sept 2017.
- [179] H. Geng, X. Xi, L. Liu, G. Yang, and J. Ma, "Hybrid modulated active damping control for DFIG-based wind farm participating in frequency response," *IEEE Transactions on Energy Conversion*, vol. 32, pp. 1220–1230, Sept 2017.
- [180] S. Baros and M. D. Ilić, "Distributed torque control of deloaded wind DFIGs for wind farm power output regulation," *IEEE Transactions on Power Systems*, vol. 32, pp. 4590–4599, Nov 2017.
- [181] H. Mahvash, S. A. Taher, M. Rahimi, and M. Shahidehpour, "Enhancement of dfig performance at high wind speed using fractional order pi controller in pitch compensation loop," *International Journal of Electrical Power & Energy Systems*, vol. 104, pp. 259 – 268, 2019.
- [182] A. O. Ibrahim, T. H. Nguyen, D. Lee, and S. Kim, "A fault ride-through technique of dfig wind turbine systems using dynamic voltage restorers," *IEEE Transactions on Energy Conversion*, vol. 26, pp. 871–882, Sept 2011.
- [183] H. Moradi and G. Vossoughi, "Robust control of the variable speed wind turbines in the presence of uncertainties: A comparison between H-infinity and PID controllers," *Energy*, vol. 90, pp. 1508 – 1521, 2015.
- [184] R. M. Kamel, A. Chaouachi, and K. Nagasaka, "Three control strategies to improve the microgrid transient dynamic response during isolated mode:

- A comparative study,” *IEEE Transactions on Industrial Electronics*, vol. 60, pp. 1314–1322, April 2013.
- [185] Z. Civelek, M. Lüy, E. Çam, and H. Mamur, “A new fuzzy logic proportional controller approach applied to individual pitch angle for wind turbine load mitigation,” *Renewable Energy*, vol. 111, pp. 708 – 717, 2017.
- [186] D. Boëda, A. Teninge, D. Roye, S. Bacha, and R. Belhomme, “Contribution of wind farms to frequency control and network stability,” in *European Wind Energy Conference (EWEC)*, pp. 1–10, May 2007.
- [187] K.-Y. Oh, J.-Y. Park, J.-S. Lee, and J. Lee, “Implementation of a torque and a collective pitch controller in a wind turbine simulator to characterize the dynamics at three control regions,” *Renewable Energy*, vol. 79, pp. 150 – 160, 2015.
- [188] H. R. Chamorro, I. Riaño, R. Gerndt, I. Zelinka, F. Gonzalez-Longatt, and V. K. Sood, “Synthetic inertia control based on fuzzy adaptive differential evolution,” *International Journal of Electrical Power & Energy Systems*, vol. 105, pp. 803 – 813, 2019.
- [189] V. Gholamrezaie, M. G. Dozein, H. Monsef, and B. Wu, “An optimal frequency control method through a dynamic load frequency control (LFC) model incorporating wind farm,” *IEEE Systems Journal*, vol. 12, pp. 392–401, March 2018.
- [190] S. Ghosh, S. Kamalasan, N. Senroy, and J. Enslin, “Doubly fed induction generator (DFIG)-based wind farm control framework for primary frequency and inertial response application,” *IEEE Transactions on Power Systems*, vol. 31, pp. 1861–1871, May 2016.
- [191] M. Hwang, E. Muljadi, J. Park, P. Sørensen, and Y. C. Kang, “Dynamic droop-based inertial control of a doubly-fed induction generator,” *IEEE Transactions on Sustainable Energy*, vol. 7, pp. 924–933, July 2016.
- [192] J. Zhao, X. Lyu, Y. Fu, X. Hu, and F. Li, “Coordinated microgrid frequency regulation based on DFIG variable coefficient using virtual inertia and primary

- frequency control,” *IEEE Transactions on Energy Conversion*, vol. 31, pp. 833–845, Sept 2016.
- [193] Y.-K. Wu, W.-H. Yang, Y.-L. Hu, and P. Q. Dzung, “Frequency regulation at a wind farm using time-varying inertia and droop controls,” *IEEE Transaction on Industry Application*, vol. 55, pp. 213–224, January 2019.
- [194] M. Garmroodi, G. Verbič, and D. J. Hill, “Frequency support from wind turbine generators with a time-variable droop characteristic,” *IEEE Transactions on Sustainable Energy*, vol. 9, pp. 676–684, April 2018.
- [195] P. Li, W. Hu, R. Hu, Q. Huang, J. Yao, and Z. Chen, “Strategy for wind power plant contribution to frequency control under variable wind speed,” *Renewable Energy*, vol. 130, pp. 1226–1236, 2019.
- [196] ENTSO, “P1 – Policy 1: Load-Frequency Control and Performance, [Available Online]:https://docstore.entsoe.eu/fileadmin/user_upload/_library/publications/entsoe/operation_handbook/policy_1_final.pdf, [Accessed on: 2018-10-01].”
- [197] U. Datta, J. Shi, and A. Kalam, “Primary frequency control of a microgrid with integrated dynamic sectional droop and fuzzy based pitch angle control,” *International Journal of Electrical Power & Energy Systems*, vol. 111, pp. 248 – 259, 2019.
- [198] X. Zhu, M. Xia, and H.-D. Chiang, “Coordinated sectional droop charging control for EV aggregator enhancing frequency stability of microgrid with high penetration of renewable energy sources,” *Applied Energy*, vol. 210, pp. 936 – 943, 2018.
- [199] K. V. Vidyanandan and N. Senroy, “Primary frequency regulation by deloaded wind turbines using variable droop,” *IEEE Transactions on Power Systems*, vol. 28, pp. 837–846, May 2013.
- [200] Y. Fu, X. Zhang, Y. Hei, and H. Wang, “Active participation of variable speed wind turbine in inertial and primary frequency regulations,” *Electric Power Systems Research*, vol. 147, pp. 174 – 184, 2017.

- [201] J. Chen, J. Chen, and C. Gong, "New overall power control strategy for variable-speed fixed-pitch wind turbines within the whole wind velocity range," *IEEE Transactions on Industrial Electronics*, vol. 60, pp. 2652–2660, July 2013.
- [202] C. Pradhan, C. N. Bhende, and A. K. Samanta, "Adaptive virtual inertia-based frequency regulation in wind power systems," *Renewable Energy*, vol. 115, pp. 558–574, 2018.
- [203] J. Lee, E. Muljadi, P. Sørensen, and Y. Kang, "Releasable kinetic energy-based inertial control of a dfig wind power plant," *IEEE Transaction Sustainable Energy*, vol. 7, no. 1, pp. 279–288, 2016.
- [204] M. F. M. Arani and Y. A. I. Mohamed, "Dynamic droop control for wind turbines participating in primary frequency regulation in microgrids," *IEEE Transaction on Smart Grid*, vol. 9, pp. 5742–5751, November 2018.
- [205] Y. Wang, J. Meng, X. Zhang, and L. Xu, "Control of pmsg-based wind turbines for system inertial response and power oscillation damping," *IEEE Transactions on Sustainable Energy*, vol. 6, pp. 565–574, April 2015.
- [206] I. Serban, R. Teodorescu, and C. Marinescu, "Energy storage systems impact on the short-term frequency stability of distributed autonomous microgrids, an analysis using aggregate models," *IET Renewable Power Generation*, vol. 7, pp. 531–539, Sep. 2013.
- [207] A. K. Srivastava, A. A. Kumar, and N. N. Schulz, "Impact of distributed generations with energy storage devices on the electric grid," *IEEE Systems Journal*, vol. 6, pp. 110–117, March 2012.
- [208] J. Fleer and P. Stenzel, "Impact analysis of different operation strategies for battery energy storage systems providing primary control reserve," *Journal of Energy Storage*, vol. 8, pp. 320 – 338, 2016.
- [209] P. Stenzel, J. C. Koj, A. Schreiber, W. Hennings, and P. Zapp, "Primary control provided by large-scale battery energy storage systems or fossil power plants in

- germany and related environmental impacts,” *Journal of Energy Storage*, vol. 8, pp. 300 – 310, 2016.
- [210] AEMC, “The Frequency Operating Standard stage one final-for-publi, [Available Online]: <https://www.aemc.gov.au/sites/default/files/content/ce48ba94-b3a9-4991-9ef9-e05814a78526/REL0065-Review-of-the-Frequency-Operating-Standard-Final-for-publi.pdf>, [Accessed on: 2018-07-15].”
- [211] M. K. Donnelly, J. E. Dagle, D. J. Trudnowski, and G. J. Rogers, “Impacts of the distributed utility on transmission system stability,” *IEEE Transactions on Power Systems*, vol. 11, pp. 741–746, May 1996.
- [212] P. Mercier, R. Cherkaoui, and A. Oudalov, “Optimizing a battery energy storage system for frequency control application in an isolated power system,” *IEEE Transactions on Power Systems*, vol. 24, pp. 1469–1477, Aug 2009.
- [213] J. Morren, J. Pierik, and S. W. de Haan, “Inertial response of variable speed wind turbines,” *Electric Power Systems Research*, vol. 76, no. 11, pp. 980 – 987, 2006.
- [214] P. V. Brogan, R. Best, D. J. Morrow, C. Bradley, M. Rafferty, and M. Kubik, “Triggering bess inertial response with synchronous machine measurements,” in *2018 IEEE Power Energy Society General Meeting (PESGM)*, pp. 1–5, Aug 2018.
- [215] X. Xu, M. Bishop, D. G. Oikarinen, and C. Hao, “Application and modeling of battery energy storage in power systems,” *CSEE Journal of Power and Energy Systems*, vol. 2, pp. 82–90, Sept 2016.
- [216] K. L. Dinh and Y. Hayashi, “Coordinated BESS control for improving voltage stability of a PV-supplied microgrid,” in *2013 48th International Universities Power Engineering Conference (UPEC)*, pp. 1–6, Sept 2013.
- [217] M. N. Kabir, Y. Mishra, G. Ledwich, Z. Y. Dong, and K. P. Wong, “Coordinated control of grid-connected photovoltaic reactive power and battery energy storage systems to improve the voltage profile of a residential distribution feeder,” *IEEE Transactions on Industrial Informatics*, vol. 10, pp. 967–77, May 2014.

- [218] C. W. Tan, T. C. Green, and C. A. Hernandez-Aramburo, "A stochastic method for battery sizing with uninterruptible-power and demand shift capabilities in PV (photovoltaic) systems," *Energy*, vol. 35, no. 12, pp. 5082 – 92, 2010.
- [219] U. Datta, A. Kalam, and J. Shi, "The relevance of large-scale battery energy storage (bes) application in providing primary frequency control with increased wind energy penetration," *Journal of Energy Storage*, vol. 23, pp. 9 – 18, 2019.
- [220] U. Datta, A. Kalam, and J. Shi, "Battery energy storage system to stabilize transient voltage and frequency and enhance power export capability," *IEEE Transactions on Power Systems*, vol. 34, pp. 1845–1857, May 2019.
- [221] M. Chen and G. A. Rincon-Mora, "Accurate electrical battery model capable of predicting runtime and I-V performance," *IEEE Transactions on Energy Conversion*, vol. 21, pp. 504–511, June 2006.
- [222] Z. M. Salameh, M. A. Casacca, and W. A. Lynch, "A mathematical model for lead-acid batteries," *IEEE Transactions on Energy Conversion*, vol. 7, pp. 93–98, Mar 1992.
- [223] N. K. Medora and A. Kusko, "Dynamic battery modeling of lead-acid batteries using manufacturers' data," in *INTELEC 05 - Twenty-Seventh International Telecommunications Conference*, pp. 227–232, Sept 2005.
- [224] Technical Marketing Staff of Gates Energy Products, *Rechargeable Batteries Applications Handbook*. Butterworth-Heinemann, USA, 1992, pp. 166-183.
- [225] Q. Xu, J. Xiao, X. Hu, P. Wang, and M. Y. Lee, "A decentralized power management strategy for hybrid energy storage system with autonomous bus voltage restoration and state-of-charge recovery," *IEEE Transactions on Industrial Electronics*, vol. 64, pp. 7098–7108, Sep. 2017.
- [226] P. Shen, M. Ouyang, L. Lu, J. Li, and X. Feng, "The co-estimation of state of charge, state of health, and state of function for lithium-ion batteries in electric vehicles," *IEEE Transactions on Vehicular Technology*, vol. 67, pp. 92–103, Jan 2018.

- [227] X. Lu, K. Sun, J. M. Guerrero, J. C. Vasquez, and L. Huang, "State-of-charge balance using adaptive droop control for distributed energy storage systems in dc microgrid applications," *IEEE Transactions on Industrial Electronics*, vol. 61, pp. 2804–2815, June 2014.
- [228] Q. Xu, J. Xiao, P. Wang, X. Pan, and C. Wen, "A decentralized control strategy for autonomous transient power sharing and state-of-charge recovery in hybrid energy storage systems," *IEEE Transactions on Sustainable Energy*, vol. 8, pp. 1443–1452, Oct 2017.
- [229] N. Mukherjee and D. De, "A new state-of-charge control derivation method for hybrid battery type integration," *IEEE Transactions on Energy Conversion*, vol. 32, pp. 866–875, Sep. 2017.
- [230] Q. Wu, R. Guan, X. Sun, Y. Wang, and X. Li, "SoC balancing strategy for multiple energy storage units with different capacities in islanded microgrids based on droop control," *IEEE Transactions on Sustainable Energy*, vol. 8, pp. 1443–1452, Oct 2017.
- [231] W. Huang and J. A. A. Qahouq, "Energy sharing control scheme for state-of-charge balancing of distributed battery energy storage system," *IEEE Transactions on Industrial Electronics*, vol. 62, pp. 2764–2776, May 2015.
- [232] C. Zhou, K. Qian, M. Allan, and W. Zhou, "Modeling of the cost of ev battery wear due to v2g application in power systems," *IEEE Transactions on Energy Conversion*, vol. 26, pp. 1041–1050, Dec 2011.
- [233] M. Murnane and A. Ghazel, "A Closer Look at State of Charge (SOC) and State of Health (SOH) Estimation Techniques for Batteries, [Available Online]:<https://www.analog.com/media/en/technical-documentation/technical-articles/a-closer-look-at-state-of-charge-and-state-health-estimation-techniques.pdf>, [Accessed on: 2018-12-11]."
- [234] H. Bitaraf, S. Rahman, and M. Pipattanasomporn, "Sizing energy storage to mitigate wind power forecast error impacts by signal processing techniques," *IEEE Transactions on Sustainable Energy*, vol. 6, pp. 1457–1465, Oct 2015.

- [235] M. Murnane and A. Ghazel, “Test Case P.M. Anderson Power System Introduction, [Available Online]:http://fglongatt.org/old/test_case_anderson.html, [Accessed on: 2018-01-16].”
- [236] PowerFactory, DIgSILENT, “DFIG Template,” 2017.
- [237] International Energy Agency, “Renewables 2017, [Available Online]: <https://www.iea.org/publications/renewables2017>, [Accessed on: 2018-07-01].”
- [238] S. Eftekharnajad, V. Vittal, G. T. Heydt, B. Keel, and J. Loehr, “Small signal stability assessment of power systems with increased penetration of photovoltaic generation: A case study,” *IEEE Transactions on Sustainable Energy*, vol. 4, pp. 960–967, Oct 2013.
- [239] R. Shah, N. Mithulananthan, and R. Bansal, “Oscillatory stability analysis with high penetrations of large-scale photovoltaic generation,” *Energy Conversion and Management*, vol. 65, pp. 420 – 429, 2013.
- [240] S. You, G. Kou, Y. Liu, X. Zhang, Y. Cui, M. J. Till, W. Yao, and Y. Liu, “Impact of high PV penetration on the inter-area oscillations in the u.s. eastern interconnection,” *IEEE Access*, vol. 5, pp. 4361–4369, 2017.
- [241] R. Shah, N. Mithulananthan, and K. Y. Lee, “Large-scale PV plant with a robust controller considering power oscillation damping,” *IEEE Transactions on Energy Conversion*, vol. 28, pp. 106–116, Mar 2013.
- [242] D. Remon, C. A. Cañizares, and P. Rodriguez, “Impact of 100-mw-scale PV plants with synchronous power controllers on power system stability in northern chile,” *IET Generation, Transmission Distribution*, vol. 11, no. 11, pp. 2958–2964, 2017.
- [243] L. Zhou, X. Yu, B. Li, C. Zheng, J. Liu, Q. Liu, and K. Guo, “Damping inter-area oscillations with large-scale PV plant by modified multiple-model adaptive control strategy,” *IEEE Transactions on Sustainable Energy*, vol. 8, pp. 1629–1636, Oct 2017.

- [244] H. Xin, Y. Liu, Z. Wang, D. Gan, and T. Yang, "A new frequency regulation strategy for photovoltaic systems without energy storage," *IEEE Transactions on Sustainable Energy*, vol. 4, pp. 985–993, Oct 2013.
- [245] Z. Jietan, Q. Linan, R. Pestana, L. Fengkui, and Y. Libin, "Dynamic frequency support by photovoltaic generation with "synthetic" inertia and frequency droop control," in *2017 IEEE Conference on Energy Internet and Energy System Integration (EI2)*, pp. 1–6, Nov 2017.
- [246] R. Shah, N. Mithulananthan, and R. Bansal, "Damping performance analysis of battery energy storage system, ultracapacitor and shunt capacitor with large-scale photovoltaic plants," *Applied Energy*, vol. 96, pp. 235 – 244, 2012.
- [247] G. Xu, L. Xu, and J. Morrow, "Power oscillation damping using wind turbines with energy storage systems," *IET Renewable Power Generation*, vol. 7, pp. 449–457, Sept 2013.
- [248] D. Zhu and Y. A. Zhang, "Optimal coordinated control of multiple battery energy storage systems for primary frequency regulation," *IEEE Transactions on Power Systems*, vol. 34, pp. 555–565, Jan 2019.
- [249] J. Xiao, P. Wang, and L. Setyawan, "Hierarchical control of hybrid energy storage system in dc microgrids," *IEEE Transactions on Industrial Electronics*, vol. 62, pp. 4915–4924, Aug 2015.
- [250] AEMO, "Generator Technical Requirements, [Available Online]: https://www.aemo.com.au/-/media/Files/Electricity/NEM/Security_and_Reliability/Reports/2017/AEMO-GTR-RCP-110817.pdf, [Accessed on: 2018-07-15]."
- [251] ControlTheoryPro, "PI-Lead Control, [Available Online]: <http://wikis.controltheorypro.com/pi-leadcontrol>, [Accessed on: 2018-06-13]."
- [252] Z. K. Jadoon, S. Shakeel, A. Saleem, A. Khaqan, S. Shuja, Q. Hasan, S. A. Malik, and R. A. Riaz., "A comparative analysis of PID, lead, lag, lead-lag, and cascaded lead controllers for a drug infusion system," *Journal of Healthcare Engineering*, vol. 2017, Jan 2017.

- [253] P. M. Anderson and A. A. Fouad, *Power System Control and Stability, 2nd Edition*. New York: IEEE Press, 2003.
- [254] DigSILENT GmbH, “PV system,” 2017.
- [255] M. Yesilbudak, S. Ermis, and R. Bayindir, “Investigation of the effects of FACTS devices on the voltage stability of power systems,” in *2017 IEEE 6th International Conference on Renewable Energy Research and Applications (ICRERA)*, pp. 1080–1085, Nov 2017.
- [256] M. Kolcun, Z. Conka, L. Beřna, M. Kanáalik, and D. Medveřd, “Improvement of transmission capacity by FACTS devices in central east europe power system,” *IFAC-PapersOnLine*, vol. 49, no. 27, pp. 376 – 381, 2016.
- [257] M. Darabian and A. Jalilvand, “Improving power system stability in the presence of wind farms using STATCOM and predictive control strategy,” *IET Renewable Power Generation*, vol. 12, no. 1, pp. 98–111, 2018.
- [258] L. M. Castro, E. Acha, and C. R. Fuerte-Esquivel, “A novel STATCOM model for dynamic power system simulations,” *IEEE Transactions on Power Systems*, vol. 28, pp. 3145–3154, Aug 2013.
- [259] G. Cakir and G. Radman, “Placement and performance analysis of STATCOM and SVC for damping oscillation,” in *2013 3rd International Conference on Electric Power and Energy Conversion Systems*, pp. 1–5, Oct 2013.
- [260] S. Bagchi, R. Bhaduri, P. N. Das, and S. Banerjee, “Analysis of power transfer capability of a long transmission line using FACTS devices,” in *2015 International Conference on Advances in Computing, Communications and Informatics (ICACCI)*, pp. 601–606, Aug 2015.
- [261] J. Servotte, E. Acha, and L. M. Castro, “Smart frequency control in power transmission systems using a BESS,” in *2015 IEEE Innovative Smart Grid Technologies - Asia (ISGT ASIA)*, pp. 1–7, Nov 2015.

- [262] K. Kawabe and A. Yokoyama, "Effective utilization of large-capacity battery systems for transient stability improvement in multi-machine power system," in *2011 IEEE Trondheim PowerTech*, pp. 1–6, June 2011.
- [263] H. Setiadi, N. Mithulananthan, and M. J. Hossain, "Impact of battery energy storage systems on electromechanical oscillations in power systems," in *2017 IEEE Power Energy Society General Meeting*, pp. 1–5, July 2017.
- [264] M. J. Hossain, H. R. Pota, and R. A. Ramos, "Improved low-voltage-ride-through capability of fixedspeed wind turbines using decentralised control of STATCOM with energy storage system," *IET Generation, Transmission Distribution*, vol. 6, pp. 719–730, August 2012.
- [265] A. Chakraborty, S. K. Musunuri, A. K. Srivastava, and A. K. Kondabathini, "Integrating STATCOM and battery energy storage system for power system transient stability: A review and application," *Advances in Power Electronics*, vol. 2012, 2012.
- [266] J. Aguado, S. de la Torre, and A. Triviño, "Battery energy storage systems in transmission network expansion planning," *Electric Power Systems Research*, vol. 145, pp. 63 – 72, 2017.
- [267] A. Kanchanaharuthai, V. Chankong, and K. A. Loparo, "Transient stability and voltage regulation in multimachine power systems vis-a'-vis STATCOM and battery energy storage," *IEEE Transactions on Power Systems*, vol. 30, pp. 2404–2416, Sept 2015.
- [268] M. Beza and M. Bongiorno, "An adaptive power oscillation damping controller by STATCOM with energy storage," *IEEE Transactions on Power Systems*, vol. 30, pp. 484–493, Jan 2015.
- [269] B. Jena and A. Choudhury, "Voltage and frequency stabilisation in a micro-hydro-PV based hybrid microgrid using FLC based STATCOM equipped with BESS," in *2017 International Conference on Circuit ,Power and Computing Technologies (ICCPCT)*, pp. 1–7, April 2017.

- [270] J. Park, J. Yu, J. Kim, M. Kim, K. Kim, and S. Han, “Frequency/Voltage regulation with STATCOM with battery in high voltage transmission system,” *IFAC-PapersOnLine*, vol. 49, no. 27, pp. 296 – 300, 2016.
- [271] B. Singh and Z. Hussain, “Application of Battery Energy Storage System (BESS) in voltage control and damping of power oscillations,” in *2010 5th International Conference on Industrial and Information Systems*, pp. 514–519, July 2010.
- [272] Y. Ge, W. Du, and T. Littler, “Applying STATCOM/BESS stabilizers in a real large-scale power system,” in *2nd IET Renewable Power Generation Conference (RPG 2013)*, pp. 1–4, Sept 2013.
- [273] NEM, “The Frequency Operating Standard-stage one final, [Available Online]:<https://www.aemc.gov.au/sites/default/files/content/c2716a96-e099-441d-9e46-8ac05d36f5a7/rel0065-the-frequency-operating-standard-stage-one-final-for-publi.pdf>, [Accessed on: 2018-06-08].”
- [274] NEM/AEMO, “Generator technical requirements, [Available Online]:https://www.aemo.com.au/-/media/files/electricity/nem/security_and_reliability/reports/2017/aemo-gtr-rcp-110817.pdf, [Accessed on: 2018-06-08].”
- [275] ControlTheoryPro, “PI-Lead Control, [Available Online]:http://wikis.controltheorypro.com/pi-lead_control, [Accessed on: 2018-06-09].”
- [276] U. Datta, “Enhanced operational performance of siirtoverkkomalli using static compensators and bess equipment,” Master’s thesis, Tampere University of Technology, Aug, 2016.
- [277] D. GmBH, “Power Equipment Models, [Available Online]:<https://www.digsilent.de/en/faq-reader-powerfactory/do-you-have-a-model-for-a-statcom-2/searchfaq/statcom.html>, [Accessed on: 2018-06-01].”
- [278] AEMO, “Victorian transfer limit advice – outages, [Available Online]:https://www.aemo.com.au/-/media/files/electricity/nem/security_and_reliability/

- congestion-information/2017/victorian-transfer-limit-advice---outages-v5.pdf, [Accessed on: 2018-06-08].”
- [279] AEMO/NEM, “Transfer limit advice – NEM oscillatory stability, [Available Online]:https://www.aemo.com.au/-/media/files/electricity/nem/security_and_reliability/congestion-information/2017/transfer-limit-advice---nem-oscillatory-stability-v3.pdf, [Accessed on: 2018-06-08].”
- [280] AEMO/SA, “Black system South Australia 28 September 2016, [Available Online]:https://www.aemo.com.au/-/media/files/electricity/nem/market_notices_and_events/power_system_incident_reports/2017/integrated-final-report-sa-black-system-28-september-2016.pdf, [Accessed on: 2018-06-08].”
- [281] J. Y. Yong, V. K. Ramachandaramurthy, K. M. Tan, and N. Mithulananthan, “Bi-directional electric vehicle fast charging station with novel reactive power compensation for voltage regulation,” *International Journal of Electrical Power & Energy Systems*, vol. 64, pp. 300 – 310, 2015.
- [282] O. Hafez and K. Bhattacharya, “Integrating ev charging stations as smart loads for demand response provisions in distribution systems,” *IEEE Transactions on Smart Grid*, vol. 9, pp. 1096–1106, March 2018.
- [283] S. Wang, Z. Y. Dong, F. Luo, K. Meng, and Y. Zhang, “Stochastic collaborative planning of electric vehicle charging stations and power distribution system,” *IEEE Transactions on Industrial Informatics*, vol. 14, pp. 321–331, Jan 2018.
- [284] M. Taljegard, L. Göransson, M. Odenberger, and F. Johnsson, “Impacts of electric vehicles on the electricity generation portfolio – a scandinavian-german case study,” *Applied Energy*, vol. 235, pp. 1637 – 1650, 2019.
- [285] G. R. Chandra Mouli, M. Kefayati, R. Baldick, and P. Bauer, “Integrated PV charging of ev fleet based on energy prices, v2g, and offer of reserves,” *IEEE Transactions on Smart Grid*, vol. 10, pp. 1313–1325, March 2019.

- [286] Q. Chen, N. Liu, C. Hu, L. Wang, and J. Zhang, "Autonomous energy management strategy for solid-state transformer to integrate PV-assisted ev charging station participating in ancillary service," *IEEE Transactions on Industrial Informatics*, vol. 13, pp. 258–269, Feb 2017.
- [287] Y. Zhang and L. Cai, "Dynamic charging scheduling for ev parking lots with photovoltaic power system," *IEEE Access*, vol. 6, pp. 56995–57005, 2018.
- [288] Q. Chen, F. Wang, B. Hodge, J. Zhang, Z. Li, M. Shafie-Khah, and J. P. S. Catalão, "Dynamic price vector formation model-based automatic demand response strategy for PV-assisted ev charging stations," *IEEE Transactions on Smart Grid*, vol. 8, pp. 2903–2915, Nov 2017.
- [289] T. Rui, C. Hu, G. Li, J. Tao, and W. Shen, "A distributed charging strategy based on day ahead price model for PV-powered electric vehicle charging station," *Applied Soft Computing*, vol. 76, pp. 638 – 648, 2019.
- [290] W. Tushar, C. Yuen, S. Huang, D. B. Smith, and H. V. Poor, "Cost minimization of charging stations with photovoltaics: An approach with ev classification," *IEEE Transactions on Intelligent Transportation Systems*, vol. 17, pp. 156–169, Jan 2016.
- [291] M. A. Quddus, O. Shahvari, M. Marufuzzaman, J. M. Usher, and R. Jaradat, "A collaborative energy sharing optimization model among electric vehicle charging stations, commercial buildings, and power grid," *Applied Energy*, vol. 229, pp. 841 – 857, 2018.
- [292] G. Hilton, M. Kiaee, T. Bryden, A. Cruden, and A. Mortimer, "The case for energy storage installations at high rate ev chargers to enable solar energy integration in the uk – an optimised approach," *Journal of Energy Storage*, vol. 21, pp. 435 – 444, 2019.
- [293] X. Han, Y. Liang, Y. Ai, and J. Li, "Economic evaluation of a PV combined energy storage charging station based on cost estimation of second-use batteries," *Energy*, vol. 165, pp. 326 – 339, 2018.

- [294] C. Luo, Y. Huang, and V. Gupta, “Stochastic dynamic pricing for ev charging stations with renewable integration and energy storage,” *IEEE Transactions on Smart Grid*, vol. 9, pp. 1494–1505, March 2018.
- [295] L. Yang and H. Ribberink, “Investigation of the potential to improve dc fast charging station economics by integrating photovoltaic power generation and/or local battery energy storage system,” *Energy*, vol. 167, pp. 246 – 259, 2019.
- [296] J. Domínguez-Navarro, R. Dufo-López, J. Yusta-Loyo, J. Artal-Sevil, and J. Bernal-Agustín, “Design of an electric vehicle fast-charging station with integration of renewable energy and storage systems,” *International Journal of Electrical Power & Energy Systems*, vol. 105, pp. 46 – 58, 2019.
- [297] L. Novoa and J. Brouwer, “Dynamics of an integrated solar photovoltaic and battery storage nanogrid for electric vehicle charging,” *Journal of Power Sources*, vol. 399, pp. 166 – 178, 2018.
- [298] Q. Yan, B. Zhang, and M. Kezunovic, “Optimized operational cost reduction for an ev charging station integrated with battery energy storage and PV generation,” *IEEE Transactions on Smart Grid*, vol. 10, pp. 2096–2106, March 2019.
- [299] H. Mehrjerdi and R. Hemmati, “Electric vehicle charging station with multilevel charging infrastructure and hybrid solar-battery-diesel generation incorporating comfort of drivers,” *Journal of Energy Storage*, vol. 26, p. 100924, 2019.
- [300] M. O. Badawy and Y. Sozer, “Power flow management of a grid tied PV-Battery system for electric vehicles charging,” *IEEE Transactions on Industry Applications*, vol. 53, pp. 1347–1357, March 2017.
- [301] P. Sarikprueck, W. Lee, A. Kulvanitchaiyanunt, V. C. P. Chen, and J. M. Rosenberger, “Bounds for optimal control of a regional plug-in electric vehicle charging station system,” *IEEE Transactions on Industry Applications*, vol. 54, pp. 977–986, March 2018.

- [302] L. González, E. Siavichay, and J. Espinoza, “Impact of ev fast charging stations on the power distribution network of a latin american intermediate city,” *Renewable and Sustainable Energy Reviews*, vol. 107, pp. 309 – 318, 2019.
- [303] K. Qian, C. Zhou, and Y. Yuan, “Impacts of high penetration level of fully electric vehicles charging loads on the thermal ageing of power transformers,” *International Journal of Electrical Power & Energy Systems*, vol. 65, pp. 102 – 112, 2015.
- [304] R. Godina, E. Rodrigues, N. Paterakis, O. Erdinc, and J. Catalão, “Innovative impact assessment of electric vehicles charging loads on distribution transformers using real data,” *Energy Conversion and Management*, vol. 120, pp. 206 – 216, 2016.
- [305] R. Abousleiman and R. Scholer, “Smart charging: System design and implementation for interaction between plug-in electric vehicles and the power grid,” *IEEE Transactions on Transportation Electrification*, vol. 1, pp. 18–25, June 2015.
- [306] S. F. Abdelsamad, W. G. Morsi, and T. S. Sidhu, “Probabilistic impact of transportation electrification on the loss-of-life of distribution transformers in the presence of rooftop solar photovoltaic,” *IEEE Transactions on Sustainable Energy*, vol. 6, pp. 1565–1573, Oct 2015.
- [307] J. Tan and L. Wang, “Adequacy assessment of power distribution network with large fleets of phevS considering condition-dependent transformer faults,” *IEEE Transactions on Smart Grid*, vol. 8, pp. 598–608, March 2017.
- [308] S. Shokrzadeh, H. Ribberink, I. Rishmawi, and E. Entchev, “A simplified control algorithm for utilities to utilize plug-in electric vehicles to reduce distribution transformer overloading,” *Energy*, vol. 133, pp. 1121 – 1131, 2017.
- [309] G. Razeghi, L. Zhang, T. Brown, and S. Samuelson, “Impacts of plug-in hybrid electric vehicles on a residential transformer using stochastic and empirical analysis,” *Journal of Power Sources*, vol. 252, pp. 277 – 285, 2014.

- [310] R. Godina, E. M. Rodrigues, J. C. Matias, and J. P. Catalão, “Smart electric vehicle charging scheduler for overloading prevention of an industry client power distribution transformer,” *Applied Energy*, vol. 178, pp. 29 – 42, 2016.
- [311] C. M. Affonso and M. Kezunovic, “Technical and economic impact of PV-BESS charging station on transformer life: A case study,” *IEEE Transactions on Smart Grid*, pp. 1–1, 2018.
- [312] H. Ding, Z. Hu, and Y. Song, “Value of the energy storage system in an electric bus fast charging station,” *Applied Energy*, vol. 157, pp. 630 – 639, 2015.
- [313] U. Datta, A. Kalam, and J. Shi, “Smart control of bess in pv integrated ev charging station for reducing transformer overloading and providing battery-to-grid service,” *Journal of Energy Storage*, vol. 28, p. 101224, 2020.
- [314] K. Chaudhari, N. K. Kandasamy, A. Krishnan, A. Ukil, and H. B. Gooi, “Agent-based aggregated behavior modeling for electric vehicle charging load,” *IEEE Transactions on Industrial Informatics*, vol. 15, pp. 856–868, Feb 2019.
- [315] V. Knap, S. K. Chaudhary, D. Stroe, M. Swierczynski, B. Craciun, and R. Teodorescu, “Sizing of an energy storage system for grid inertial response and primary frequency reserve,” *IEEE Transactions on Power Systems*, vol. 31, pp. 3447–3456, Sep. 2016.